34th Annual Meeting of the

German Crystallographic Society (DGK) e. V.

Abstract book

Table of Content

Oral presentations

Oral presentations

Plenary lectures

PL-01

Pair distribution function analysis of cement-based materials: Beyond the standard approach

C. E. White (Princeton / US)

Cement-based materials consisting of one or more amorphous phases are ideal systems for application of the pair distribution function (PDF) technique. There is a growing body of literature that utilizes total scattering and PDF analysis to uncover local atomic structural insights on various types of cements and their starting constituents, how these cements evolve over time, and their potential degradation mechanisms. However, to date these investigations have collected bulk PDF data sets and assumed isotropic scattering, two aspects that limit our ability to fully probe these heterogeneous disordered materials.

In the first part of this talk, the disordered phases present in the heterogeneous microstructure of a sustainable cement (alkali-activated slag) will be evaluated using X-ray PDF-computed tomography (PDF-CT), where voxel-dependent X-ray PDF data sets have been obtained and analyzed. This approach has been used to isolate and evaluate the extent of atomic ordering within the disordered calcium carbonate phases that form due to CO2 exposure. The advantages and current limitations of this technique will be outlined together with future developments underway at dedicated synchrotron beamlines.

In the second part of this talk the atomic-scale viscoelastic behavior of cement-based materials will be assessed using in situ directional-dependent total scattering and PDF analysis conducted on the NOMAD instrument at the Spallation Neutron Source, ORNL. By analyzing the PDF data as a function of the azimuthal angle, changes in the local atomic structure that are uniquely attributed to the imposed load have been uncovered, revealing new insight on the nanoscale rearrangements that occur within the cement matrix.

PL-02

Macromolecular Crystallography at the European Spallation Source

E. Oksanen (Lund / SE)

Macromolecular crystallography at the European Spallation Source
The European Spallation Source (ESS) is a European project to build and operate the world's most powerful neutron source in Lund, Sweden. The unique long-pulse technology and high-brilliance moderators make the ESS well suited for life science techniques such as macromolecular crystallography. The ESS is scheduled to produce first neutrons in March 2026 and open a user programme in 2027-28. The ESS instrument suite consists of 15 instruments and a test beam line. The NMX Macromolecular Diffractometer is the only instrument dedicated to life science. NMX is a time-of-flight quasi-Laue diffractometer optimised to make use of the bright long-pulse source. The 156 m length allows the use of the full pulse with an acceptable wavelength resolution of 2-4% and the chopper system allows the wavelength range to be tuned to maximise signal-to-background. The robotic endstation enables multi-axis goniometry together with variable detector distance, which removes previous limitations on unit cell axes length. The user support in protein deuteration, crystal growth optimisation and data analysis ensures an optimal scientific throughput. NMX is scheduled to be commissioned in 2026.

PL-03

Disorder in thermoelectric materials

B. Brummerstedt Iversen (Aarhus C /DK)

Keywords: Thermoelectrics, Thermal conductivity, Anharmonicity, Correlated disorder, 3D-DPDF method, Quantum crystallography

Thermoelectric (TE) materials enable direct transformation of thermal energy into electrical energy, and the energy conversion efficiency of TE devices is quantified by the dimensionless figure of merit, $zT = S2T/(\rho\kappa) = (PF/\kappa)\cdot T = PF/(\kappa L+\kappa e)\cdot T$, where S, ρ, PF, κ, κL, κe and T are the Seebeck coefficient, electrical resistivity, power factor ($PF = S2/\rho$), total thermal conductivity (κL+κe), lattice thermal conductivity, electronic thermal conductivity and absolute temperature, respectively. High performance TE materials must have a low thermal conductivity, and this can be achieved when the translational symmetry of the crystal lattice is broken be defects. The disorder introduced by defects can be random as seen e.g. in Zn4Sb3 [1] or type I clathrates M8Ga16Ge30 [2], but the actual influence of the disorder may be limited if the material contains other mechanisms for lowering of κL such as anharmonicity [3] or rattling [4]. In some cases, the defects have local order, and the field of correlated disorder attempts to decipher the true local structure of crystals based on analysis of the weak diffuse scattering using e.g. the direct space 3D-DPDF method [5, 6]. We will discuss disorder in thermoelectric materials such as Cu2Se [7], Nb1-xCoSb [8], InTe [9], Ag2Se [10] and AgGaGe3Se8 [11].

References

[1] G. J. Snyder et al., Nat. Mater. 2004, 3, 458

[2] A. Bentien et al., Phys. Rev. B. 2005, 71, 144107

[3] T. B. E. Grønbech et al., Adv. Func. Mater. 2024, 2401703

[4] M. Christensen et al., Nat. Materials 2008, 7, 811

[5] T. Weber et al., Z. Kristallogr. 2012, 227, 238

[6] K. O. R. Juul et al., Acta Crystallogr. Sect A 2025, 81, 254

[7] N. Roth et al., Acta Crystallogr. Sect. A 2019, 75, 465

[8] N. Roth et al., IUCrJ. 2021, 8, 695

[9] J. Zhang et al., Nat. Commun. 2021, 12, 6709

[10] M. V. B. Brix et al., J. Am. Chem. Soc. 2025, 147, 25858

[11] P. S. Thorup et al., Sci. Adv. 2025, 11, eadv5865

PL-04

The subtle exchange mechanism in magnetic coordination polymers at ambient and non-ambient conditions

P. Macchi (Milano/IT), S. Sarkar, E. Levinaa

We are currently witnessing a technological revolution triggered by the enormous progresses in quantum information theory. The current challenges concern the hardware limitations (limited number of qubits), the algorithm developments (migration from classical to quantum platforms is not immediate) and the error mitigation (necessary for large scale, accurate simulations). In this talk we focus on spintronics materials which are necessary for hardware components, for example coupled with qbits (the processing unit of quantum computers). Antiferromagnets are important because they can be manipulated by external fields and can store and transfer the information using the electron spin, instead of the electron charge.
In recent years, metal-organic networks have attracted attention in this field, because they can be designed as extremely tuneable antiferromagnets, manipulating the spin state of the metal ions and the stereochemical features of the organic linkers.
Despite this interest, there is a fundamental knowledge gap, because the mechanism of super-exchange through organic linkers is still poorly understood and therefore not predictable, a sever limitation for materials design.
Our work combines experimental and theoretical studies on the electron charge and spin density of crystalline magnetic networks, with the purpose of gaining insight into the mechanism of spin propagation [1-8]. Because the chemical/material problem is intrinsically multivariate, we use elastic strain to modify the crystal structures in order to detect the correlation between structure and properties in a more systematic way. For this reason, we couple X-ray/neutron diffraction experiments at ambient and non-ambient conditions, with quantum crystallographic modelling and first principle calculations. We will show how the spin delocalization and spin polarization mechanism can be detected and what are the chemical/structural features that could enhance the antiferromagnetic coupling in a magnetic network.

References

[1] Levina, E.; Sarkar, S.; Macchi, P. manuscript in preparation.

[2] Sarkar, S.; Macchi, P. manuscript in preparation.

[3] Scatena, R.; Andrzejewski, M.; Johnson, R.; Macchi, P. J. Mat. Chem. C, 2021, 9, 8051-8056.

[4] Curley, S. P. M.; Scatena, R.; Williams, R. C.; Goddard, P. A.; Macchi, P.; Hicken, T. J.; Lancaster, T. ; Xiao, F.; Blundell, S. J.; Zapf, V.; Eckert, J. C.; Krenkel, E. H.; Villa, J. A.; Rhodehouse, M. L.; Manson, J. L. Phys. Rev. Materials¸ 2021, 5, 034401.

[5] Scatena, R.; Johnson, R.D.; Manuel, P.; Macchi, P. J. Mat. Chem. C, 2020, 8, 12840-12847.

[6] Scatena, R.; Montisci, F.; Lanza, A.; Casati, N.; Macchi, P. Inorg. Chem., 2020, 59, 10091-10098.

[7] Kubus, M.; Lanza, A.; Scatena, R.; Dos Santos, L.; Wehinger, B.; Casati, N.; Fiolka, C.; Keller, L.; Macchi, P.; Ruegg, C.; Krämer, K. Inorg. Chem., 2018, 57, 4934-4943.

[8] Dos Santos, L.; Lanza, A.; Barton, A.; Brambleby, J.; Blackmore, W.; Goddard, P.; Xiao, F.; Williams, R.; Lancaster, T.; Pratt, F.; Blundell, S.; Singleton, J.; Manson, J.; Macchi, P. J. Am. Chem. Soc. 2016, 138, 2280–2291.

PL-05

Time-resolved serial crystallography: watching enzymes at work

E. C. Schulz (Hamburg/DE)

Watching enzymes at work: time-resolved serial crystallography

X-ray crystallography has long defined structural biology by revealing atomic models of biomolecules. Today, with highly accurate structure prediction widely available, the central question has shifted from what proteins look like, to how proteins work. Time-resolved serial crystallography (TRSX) addresses this challenge by capturing structural changes as macromolecules progress through catalytic cycles, thereby linking structure to kinetics, energetics, and mechanism.

Originally pioneered at X-ray free-electron lasers, TRSX has rapidly matured into an accessible methodology at modern synchrotron sources. Advances in serial data collection, high-repetition rate detectors, and flexible reaction initiation schemes such as optical excitation, rapid mixing, temperature jumps, and electric-field perturbations now enable structural snapshots across a large variety of systems and broad timescales. These developments make it possible to observe ligand binding, catalytic intermediates, and allosteric transitions directly within crystals and under controlled experimental conditions.

Equally transformative are new approaches to environmental control, allowing systematic variation of gas composition, humidity, or temperature during data acquisition. These multi-dimensional experiments not only narrow the gap to physiological environments, but they also allow to modulate turnover kinetics within the crystal. This facilitates the selective enrichment and differentiation of reaction intermediates, thereby enabling a more in-depth characterization of enzymatic mechanisms and contributing to our understanding of protein conformational dynamics.

As the experimental landscape expands, accessibility becomes critical, that is standardized and user-friendly serial data-collection workflows, sample delivery methods, and reaction initiation systems come into the focus of current beamline development. An alternative approach that reduces the entry barrier for non-specialist users is cryo-trapping. This strategy may solve many important biologically relevant questions, such as thermodynamically trapped metastable reaction intermediates. Cryo-trapping allows for the separation of sample preparation from data collection, enabling high-throughput, dynamic experiments at most beamlines, thereby democratizing access to time-resolved crystallography.

While static protein structures are increasingly solved by prediction methods, TRSX can go further as it yields population-weighted structural ensembles that can be integrated with spectroscopy, kinetics, and computation. By directly visualizing structural heterogeneity and meta-stable states, time-resolved crystallography is evolving into a quantitative tool for mechanistic enzymology. In the coming decade, this approach is poised to transform crystallography from a method that determines structures into one that measures macromolecular function in atomic detail.

PL-06

Compositionally Complex Oxides: A Modern Frontier

K. Page (Oak Ridge / US)

Compositionally complex oxides (CCOs), including high-entropy oxides (HEOs), represent a new frontier in ceramic materials design, where structural disorder and chemical diversity can be harnessed to engineer unprecedented combinations of functional and mechanical properties. In these multicomponent systems, phase stability and performance arise from the delicate balance among cation size mismatch, configurational entropy, and defect energetics. This talk will highlight our recent investigations into two model families that exemplify the opportunities and challenges of compositional complexity. In fluorite-based CCOs, we explore how tuning composition and synthesis pathways can control chemical short-range order and optimize bifunctional oxygen evolution and reduction catalysis, yielding materials with expanded electrochemical operating windows. In contrast, rare-earth titanate pyrochlores illustrate how disorder and local lattice distortion can be leveraged to suppress thermal conductivity while retaining exceptional hardness and stiffness- an unusual combination for refractory ceramics. Across these systems, we employ a suite of electron, X-ray, and neutron scattering probes to resolve both average and local atomic structure, revealing distinctions between true solid solutions and “multi-structured” materials containing nanoscale heterogeneity. Together, these studies underscore the need for coupled experimental and computational frameworks capable of resolving and ultimately controlling the complex energy landscapes that govern emergent behavior in CCOs.

MS 1: Young Crystallographers: Lightning talks

LT-01 | PP-72

PDF analysis of amorphous calcium and magnesium carbonates at high pressures

L. Wedek (Frankfurt a. M./DE), L. Bayarjargal (Frankfurt a. M./DE), C. Prescher (Freiburg i. Br./DE), C. Otzen (Freiburg i. Br./DE), K. Glazyrin (Hamburg/DE), B. Winkler (Frankfurt a. M./DE)

In the Earth"s interior, carbonatitic melts play a crucial role in carbon transport [1]. Since melts are difficult to probe we use amorphous carbonates as proxies. For crystalline carbonates changes in the coordination number of carbon and polymerization of structural units are known [2,3]. In amorphous $K_2Mg(CO_3)_2$ a conversion from sp^2 to sp^3 carbonates was found starting at 40 GPa [4]. We expect that a polymerization occurs at lower pressures. Therefore we investigated amorphous calcium carbonate (ACC), amorphous magnesium carbonate (AMC) and amorphous calcium magnesium carbonate (ACMC) up to 40 GPa with a total scattering/pair distribution function study.

We loaded the amorphous carbonates into diamond anvil cells (DACs), together with a ruby serving as pressure calibrant. Total scattering experiments were performed at beamline P02.2 at PETRA III (DESY, Hamburg), using a Soller slit setup. For each sample, we collected diffraction data at multiple pressure points during compression, the empty DACs as background and the recovered samples after decompression. We then studied the data using pair distribution function (PDF) analysis [5]. Additionally, the compression behaviour of the samples was measured by Raman spectroscopy. A preliminary data analysis shows a shortening of the Mg/Ca-O and O-O distances.

Financial support by the DFG (DFG-Wi1232, DFG-Ba4020) is thankfully acknowledged. BW is grateful for support by BIOVIA/Dassault Systemes through the "Dassault Systems Ambassador"-program. We acknowledge DESY (Hamburg, Germany), a member of the Helmholtz Association HGF, for the provision of experimental facilities. Parts of this research were carried out at beamline P02.2.

References

[1] Z. Hou et al., Sci. Rep., 2015, 5, 10231.

[2] D. Spahr et al., Inorg. Chem., 2021, 60, 19, 14504-14508.

[3] D. Spahr et al., J. Am. Chem., 2022, 144, 2899-2904.

[4] V. Cerantola et al., Commun. Earth Environ., 2023, 4, 67.

[5] Glassure Web, DOI 10.5281/zenodo.880835.

LT-02 | PP-73

$Cs_{14}Hg_{17}O_4$ – a new cesium mercuride oxide with a previously unknown [Hg_{18}] cluster

T. Xu (Munich/DE), C. Hoch (Munich/DE)

A number of alkaline metal mercuride oxides with general formula $A_xHg_yO_z$ (*A* = Cs, Rb), containing mercuride anion clusters, has been synthesized and structurally characterized. The first in this series was a cesium mercuride oxide double salt, $Cs_{18}Hg_8O_6$, which contains both isolated oxide anions and $[Hg_8]^{6-}$ cluster anions [1]. A new mercuride anionic cluster now was found in $Cs_{14}Hg_{17}O_4$, which was obtained as black air- and moisture-sensitive crystals from the reaction of tricesium suboxide (Cs_3O) with elemental mercury under argon in a Schlenk tube at temperatures between 120 and 220 °C. Upon thermolysis starting at ca. 170 °C, $Cs_{14}Hg_{12}O_4$ and finally at 250 °C $Cs_{18}Hg_8O_6$ are formed sequentially.

$Cs_{14}Hg_{17}O_4$ (orthorhombic, space group *Cmcm*. *a* = 15.369(6), *b* = 18.273(7), *c* = 17.615(6) Å, *V* = 4947.(5) Å^3, *Z* = 4) consists of a framework of [Cs_6O] octahedra incorporating chains of clusters containing 18 mercury atoms, which can be described as fragments of a face-centered cubic (fcc) packing. The mercury atoms have a partial negative charge. The crystal structure and molecular formula were determined by single-crystal X-ray diffraction. A formal ionic decomposition into 14 Cs^+ + 4 O^{2-} + 17 $Hg^{-0.35}$ indicates metallic behaviour . Pronounced maxima in the difference Fourier map suggest an (incommensurate) modulation of the Hg chains interconnecting the cluster units. The rich structural variety of mercury compounds with egatively polarized Hg atoms is illustrated by this new structure.

This work was funded by DFG under project number 513247541

Fig. 1: View along [110] on the crystal structure of $Cs_{14}Hg_{17}O_4$, Hg atoms in dark grey, Cs atoms in light grey, O atoms in black, [Cs_6O] units in transparent light grey.

Reference

[1] L. Nusser, T. Hohl, F. Tambornino, C. Hoch, *Z. Anorg. Allg. Chem.* **2022**, *648*, e202100389.

Fig. 1

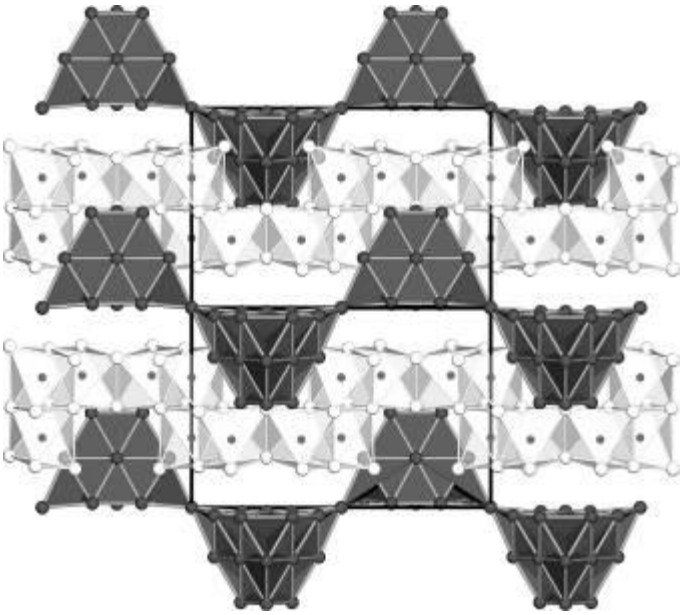

LT-03 | PP-74

Crystal structures of $Cs_{18.5}Rb_{0.5}[AlO_4]_2[Hg_4]_2$ and $Cs_{26}[Fe_2O_7]_2[Hg]_8[Hg]_6$

H. Waldmann (Munich/DE), N. Kötter (Munich/DE), L. Nusser (Munich/DE), C. Hoch (Munich/DE)

$Cs_{18.5}Rb_{0.5}Al_2O_8Hg_8$ and $Cs_{13}Fe_2O_7Hg_7$ were obtained by reacting the subvalent oxidometallates A_9MO_4 (A = Cs, Rb and M = Al, Fe) [1] with elemental mercury at 300 °C. The crystal structure of $Cs_{18.5}Rb_{0.5}Al_2O_8Hg_8$ (orthorhombic, *Cmcm*, a = 20.2217(5), b = 22.3294(5), c = 12.1989(3) Å, V = 5508.2(3) Å^3) contains structural units present in A_9MO_4: $[AlO_4]^{5-}$ anions in cuboctahedral Cs coordination and additional mixed Cs/Rb sites, not involved in the coordination of the anion. The structure is completed by square planar $[Hg_4]$ units (d(Hg-Hg) = 2.96905(6) to 3.02545(6) Å). Similar $[Hg_4]$ squares have been reported e.g. in $Rb_{15}Hg_{16}$ [2]. Formal ionic decomposition $(Cs^+/Rb^+)_{19}([AlO_4]^{5-})_2$ leaves 4.5 electrons per $[Hg_4]$ unit, suggesting metallic bonding. The crystal structure of $Cs_{13}Fe_2O_7Hg_7$ (orthorhombic, *Immm*, a = 13.3715(6) Å, b = 14.7044(6) Å, c = 19.4523(8) Å, V = 3824.7(4) Å^3) comprises $[Fe_2O_7]^{8-}$ anions. All Cs positions are part of the coordination of the $[Fe_2O_7]^{8-}$ anion. Here, mercury forms two different units: $[Hg_8]$ cubes, as known from e.g. $Rb_{15}Hg_{16}$ [2] or $Cs_{18}Hg_8O_6$ [3], and planar $[Hg_6]$ units (d(Hg-Hg) = 2.76210(13) to 3.02246(13) Å) which have not been reported yet. Formal ionic decomposition $(Cs^+_{13}[Fe_2O_7]^{8-})_2$ leaves 10 electrons. $[Hg_8]^{6-}$ was established for mercuride oxides, suggesting 4 electrons per $[Hg_6]$ unit. The bonding situation in both compounds will be further investigated by conductivity measurements and with quantum chemical calculations.

This work was funded by DFG under project number 444769550

Fig. 1: Unit cell of $Cs_{18.5}Rb_{0.5}Al_2O_8Hg_8$ (a) and $Cs_{13}Fe_2O_7Hg_7$ (b). Cs (light grey), Hg (dark grey), $[Cs_8AlO_4]$ columns (grey polyhedra), $[Fe_2O_7]$ double tetrahedra (dark grey).

References

[1] C. Hoch, J. Bender, A. Wohlfarth, A. Simon, *Z. Anorg. Allg. Chem.* **2009**, *635*, 1777–1782.

[2] H.-J. Deiseroth, A. Strunck, *Angew. Chem. Int. Ed. Engl.* **1989**, *28*, 1251-1252.

[3] L. Nusser, T. Hohl, F. Tambornino, C. Hoch, *Z. Anorg. Allg. Chem.* **2022**, *648*, e202100389.

Fig. 1

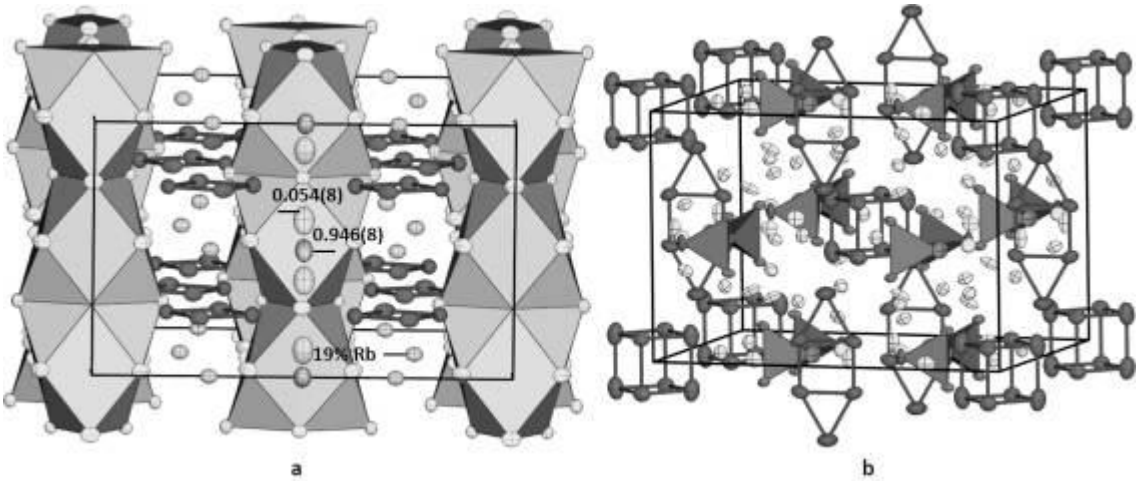

LT-04 | PP-75

Three Polymorphic Modifications of Yb(OAc)3 Co-existing in the Temperature Range 200-523K: A Relation Between Orthorhombic and Hexagonal Structures

M. Zhernakov (Gießen/DE), J. Möbs (Gießen/DE), K. Müller-Buschbaum (Gießen/DE)

Anhydrous lanthanide acetates Ln(OAc)3 show large structural variety, crystallizing in monoclinic, orthorhombic, tetragonal, and trigonal systems. This diversity of crystal structures leads to phase transitions, which are known for the acetates in the series Sm–Lu and Y. Moreover, anhydrous acetates of Sm–Lu undergo a phase transition to higher symmetry upon heating, and they were supposed to mimic the crystal structure of anhydrous Sc(OAc)3, crystallizing in the space group *P*63/*mcm*. This fact raises synthetic challenges for obtaining pure phases of these compounds. For instance, anhydrous La(OAc)3 can be obtained in H20, but anhydrous Yb(OAc)3 is obtained via solid-state reaction of metallic Yb and malonic acid.[1–3]

Herein, we present an in-depth study of anhydrous Yb(OAc)3, describing a new synthetic route and full characterization to shed light on its structural changes in a wide temperature range.

Anhydrous Yb(OAc)3 was obtained as a bulk material and analyzed using SCXRD at 100 K and 295 K, PXRD in the temperature range 200–573 K, Rietveld method, and thermal analysis.

The studied material was obtained via the reaction between Yb(OH)3 and glacial AcOH in dry EtOH at 80°C as both bulk product and single crystals. Comprehensive structure analysis of Yb(OAc)3 revealed that it crystallizes in the space group *Pna*21 at 100 K, in the space group *Cmc*21 at 295 K, and undergoes a phase transition to a high-symmetry structure at 523 K. Moreover, PXRD showed an equilibrium of both orthorhombic phases at room temperature. Upon heating the ratio is shifted to the *Cmc*21 phase, completing the transition at 323 K. Since Yb(OAc)3 crystallizes in polar space groups, its optical properties will be investigated.

References

[1] A. Lossin, G. Meyer, *Z. Anorg. Allg. Chem.* 1993, *619*, 1609.

[2] A. S. Oreshonkov, N. O. Azarapin, A. P. Tyutyunnik, D. V. Pankin, I. A. Razumkova, *Inorg. Chim. Acta* 2024, *572*, 122310.

[3] S. Takeda, H. Kataoka, S. Ikeda, K. Yamaguchi, *Phys. B.* 1996, *226*, 174.

LT-06 | PP-77

Structural Insights into the ADP Ribosyltransferase (ARR) from* Mycobacterium smegmatis *and the Implications for Inhibitor Search

L. von Soosten (Hamburg/DE)

Antibiotic resistance has become a major global health issue, causing over 1.2 million deaths in 2019, with more than 5 million associated deaths[1]. *M. smegmatis*, a type of non-tuberculosis mycobacteria, is resistant to several antibiotics, including rifampicin, a drug commonly used to treat *M. tuberculosis*. It produces an ADP ribosyltransferase (ARR) that inactivates rifampicin. Bioinformatics studies have identified ARR orthologues across various microbial genera[2], making it an interesting target for drug research.

We have used X-ray crystallography to determine the structure of the ARR protein in its apo state and compare it with the structure of the protein in complex with rifampicin. These structures help us to understand the structural changes that occur upon ligand binding, thereby providing deeper insight into the protein-substrate interaction.

They also form the basis for *in silico* docking simulations, which enable us to screen for potential new inhibitors. Furthermore, high-throughput activity assays were performed to test existing compound libraries and the most promising docking simulation hits.

References

[1] Murray, C. J. L. et al. Global burden of bacterial antimicrobial resistance in 2019:a systematic analysis. The Lancet 399, 629–655 (2022).

[2] Baysarowich, J. et al. Rifamycin antibiotic resistance by ADP-ribosylation: Structure and diversity of arr. Proceedings of the National Academy of Sciences 105, 4886–4891 (2008).

LT-07 | PP-78

$Ba_{21}N_5(MnN_3)_2$ – a new ternary subnitridometalate

L. V. Pietsch (Munich/DE), C. Hoch (Munich/DE)

Reacting barium, sodium and manganese with barium subnitride Ba_2N at 550 °C yields $Ba_{21}N_5(MnN_3)_2$, together with $NaBa_3N$, BaNa and $BaNa_2$. The crystal structure of the new nitridomanganate(III) (*R*-3*m*, *a* = 14.4876(2), *c* = 35.4855(7) Å, *V* = 6450.2(3) Å^3) was solved and refined from single crystal data with reverse/obverse twinning. $Ba_{21}N_5(MnN_3)_2$ contains both $[MnN_3]^{6-}$ and isolated $[N]^{3-}$ anions. The latter are coordinated octahedrally by Ba atoms, condensed to complex cluster units of five $[Ba_6N]$ octahedra. The $[MnN_3]^{6-}$ anions are coordinated icosahedrally by barium atoms. Unsufficient coordination leads to two disordered, equally occupied split orientations for the $[MnN_3]^{6-}$ anions, and as a consequence for the surrounding Ba atoms. The anions are embedded in a matrix of metallic barium atoms which form icosahedra, Frank-Kasper CN = 14 polyhedra, and double-capped hexagonal prisms. Trigonal planar $[MnN_3]^{6-}$ anions were recently reported in the subnitridometalate $Na_4Ba_9MnN_3$ [1] and are well know from ionic nitridomanganates(III) like Ba_3MnN_3 [2] or $Sr_8(MnN_3)_2(MnN_3)$ [3]. Condensed $[Ba_6N]$ octahedra can be found e.g. in Ba_2N [4]. In contrast to all previous reported subnitridometalates, $Ba_{21}N_5(MnN_3)_2$ is the first one with a metallic matrix consisting of barium only.

Fig. 1: a) Unit cell of $Ba_{21}N_5(MnN_3)_2$. Condensed $[Ba_6N]$ octahedra (light grey) surrounded by disordered $[MnN_3]$ anions (dark grey) and metallically bound barium (grey Frank Kasper polyhedra). b) barium coordinated by a double-capped hexagonal prism of Ba atoms. c) cluster unit of five condensed $[Ba_6N]$ octahedra.

References

[1] L.-V. Pietsch, C. Hoch, $Na_4Ba_9MnN_3$: A New Subnitridometalate with Trigonal Planar Anions $[Mn^{III}N_3]^{6-}$, *Z. Anorg. Allg. Chem.*, accepted. DOI 10.1002/zaac.202500159

[2] A. Tennstedt, C. Röhr, R. Kniep, *Z. Naturforsch.* **1993**, *48b*, 794-796.

[3] J. K. Bendyna, P. Höhn, R. Kniep, *Z. Kristallogr.* NCS **2008**, *223*, 185-186.

[4] O. Reckeweg, F. J. DiSalvo, *Solid State Sci*. **2002**, *4*, 575-584.

Fig. 1

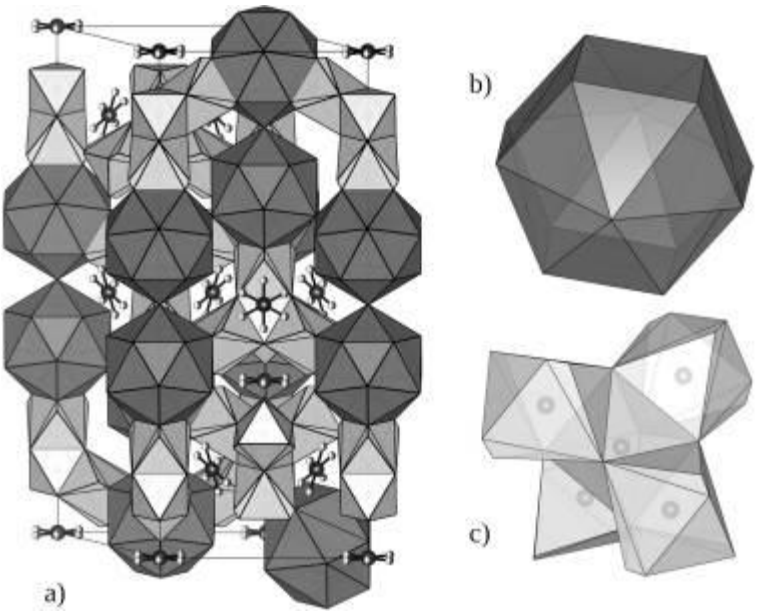

LT-08 | PP-79

Crystallographic fragment screening towards new NS2B-NS3 Zika protease inhibitors

L. S. Benz (Berlin/DE), J. Wollenhaupt (Berlin/DE), M. Oelker (Berlin/DE), A. Jirgensons (Riga/LV), T. Miletic (Berlin/DE), U. Müller (Berlin/DE), M. S. Weiss (Berlin/DE)

Fragment-based drug discovery (FBDD) in academic environments often faces challenges during fragment progression due to limited synthetic resources. To address this, the European Fragment Screening Library-96 (EFSL-96)[1] was validated against the Zika virus NS2B-NS3 protease (ZIKVpro). Currently there"s no administered vaccine or specific anti-viral drug against the Zika virus available although it is associated with severe neurological complications as Guillain-Barré syndrome and microcephaly in fetuses and newborns[2]. The library was designed to facilitate efficient fragment follow-up and streamline early-stage academic FBDD efforts.

The EFSL-96, a 96-membered subset of the European Fragment Screening Library, consists of fragments structurally related to compounds within the European Chemical Biology Library (ECBL)[3]. This design enables rapid access to over 30,000 larger analogues (an average of 311 per fragment) through EU-OPENSCREEN, significantly reducing the barrier to fragment expansion. Crystallographic screening of EFSL-96 against ZIKVpro identified eleven active-site binders, and for two of these, follow-up analogues were successfully found within the ECBL.

Screening the EFSL-96 against ZIKVpro expanded the understanding of fragment interactions within the protease active site and validated the library as an efficient, accessible tool for academic FBDD. These results highlight the EFSL-96 as a valuable resource that bridges hit identification and follow-up chemistry, accelerating early-stage, resource-efficient academic drug discovery efforts.

References

[1] L. S. Benz et al., *RSC Med. Chem.*, 2025. DOI: 10.1039/d5md00684h.

[2] Y. Feng, *Frontiers in pharmacology*, 2024, 15, 1418516.

[3] X. Jalencas et al. *RSC medicinal chemistry*, 2024, 15, 1176–1188.

LT-09 | PP-80

Low-Cost Crystallization Automation for Cationic Metallocavitands (Pillarplexes)

M. Saviak (Garching/DE), J. Zuber (Garching/DE), L. Richter (Garching/DE), A. Pöthig (Garching/DE)

Crystallization of complex supramolecular compounds, which exhibit non-covalent bonds, is crucial for obtaining their molecular structures for X-ray diffraction analysis and, consequently, their structure-property relationships. However, screening their crystallization conditions becomes increasingly challenging as the structures grow in complexity and yield more polymorphs.

Figure 1. (a) Crystallization system: schematic view. (b) Example pillraplex packing. Counterions are omitted for clarity. (c) Pillarplex molecular structure. Counterions are omitted for clarity.

Pillarplexes are a class of organometallic, supramolecular cationic cavitands composed of two NHC-pyrazolate macrocyclic ligands linearly connected by eight Cu(I)/Ag(I)/Au(I) (Figure 1c).[1] Various crystal structures of pillarplexes exhibit distinct properties, including host-guest interactions, luminescence, and solubility tuning, which are crucial for numerous applications (Figure 1b). Salts of pillarplexes yield different crystal structures and are rich in polymorphs. These structures are challenging to crystallize, particularly when they are functionalized.[2]

To efficiently obtain high-quality single crystals of pillarplexes, we automated the crystallization screening process. Nonetheless, commercially available state-of-the-art pipetting systems are expensive and offer limited customization options, making them less attractive for efficient, multifunctional use.Therefore, we assembled a crystallization system using parts from 3D printers (Figure 1a).[3]

This has already enabled several new pillarplex crystal structures, and the system is well-suited for further customization.

References

[1] P. J. Altmann, A. Pöthig, *J. Am. Chem, Soc.,* **2016**, 138, 13171

[2] Julian Zuber, Thomas Pickl, Alexandra A. Heidecker, Marco Baron, Christian Jandl, Alexander Pöthig, *Dalton Transactions* 53, **2024,** 53, 19116.

[3] Leon F. Richter, Wolfgang R.E. Büchele, Alexander Imhof, Fritz E. Kühn, *HardwareX*, **2024**, 20, e00581.

Fig. 1

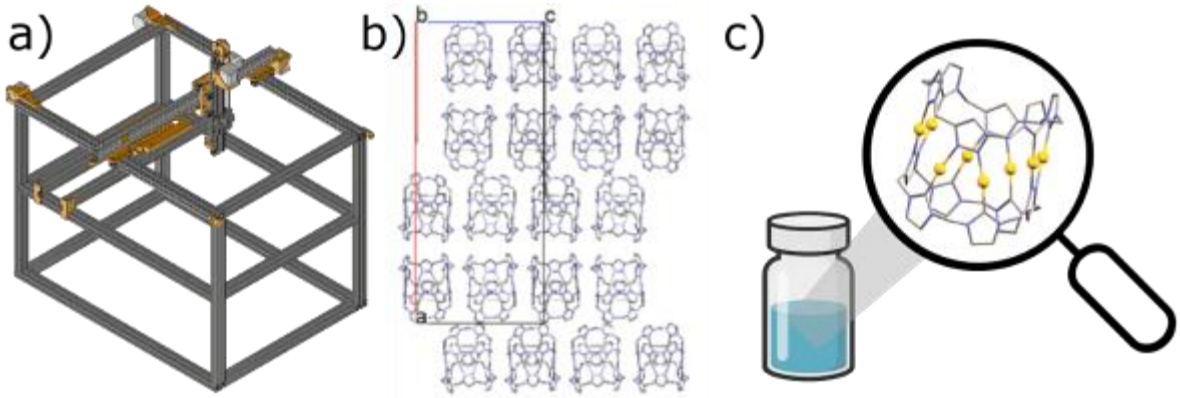

LT-10 | PP-81

Cryo and room temperature (RT) serial synchrotron crystallography (SSX) reveals binding modes of previously unexplored β-lactam antibiotics

G. Gore (Hamburg/DE), A. Prester (Hamburg/DE), D. von Stetten (Hamburg/DE), K. Bartels (Hamburg/DE), E. C. Schulz (Hamburg/DE)

One of the most common resistance mechanisms in Gram-negative bacteria is the production of β-lactamases, which hydrolyse β-lactam antibiotics. The exclusive use of broad-spectrum β-lactams since the "80s has led to the emergence of extended-spectrum β-lactamases (ESBLs) such as CTX-Ms. In this study, we demonstrate the use of both cryo and room temperature (RT) serial synchrotron crystallography (SSX) to uncover the binding modes of previously unexplored β-lactam antibiotics to class A β-lactamase through acyl-enzyme intermediates with the activity-impaired CTX-M-14 E166A. We obtained a Cryo-SSX structure of the clinically relevant cephalosporin Cefdinir and RT-SSX structures of another clinically prescribed class of β-lactam antibiotics: the Isoxazolyl Penicillins. Despite being in clinical use since the "90s, these antibiotics have no reported crystallographic structure bound to a class A β-lactamase. RT-SSX reveals the conformational heterogeneity adopted by the Isoxazolyl-Penicillins at room temperature. Cryo-SSX confirms a similar binding mode to structural homologues previously observed at cryo temperatures. In summary, the structural insights presented here could open avenues for new inhibitor and antibiotic design as well as synergy studies.

LT-11 | PP-82

High-throughput structural investigation of Cu content-dependent second phase formation in $(Mn,Fe,Co,Ni,Cu)_3O_4$ thin film materials libraries

V. Strotkötter (Bochum/DE), A. Kirsch (Bochum/DE), A. Ludwig (Bochum/DE)

Compositionally complex solid solutions (CCSS) are of great interest for several applications due to their compositional flexibility and potential for tunable functional properties.[1,2] Nevertheless, their synthesizability and the formation of secondary phases are still objects of research.[3,4] With this study, we investigate $(Mn,Fe,Co,Ni,Cu)_3O_4$ spinels and aim identifying limits for Cu dissolution for compositions between 2 and 45 at.% of Cu. Using combinatorial sputter deposition with four sputter sources, several thin-film samples with well-defined composition gradients were deposited on wafer substrates. Subsequently, these materials libraries were mapped by energy-dispersive X-ray spectroscopy for their metal contents and by X-ray diffraction (XRD) to get structural information. This approach enables efficient screening of thin films for their phase formation and the correlation of compositional and structural data in a large composition space. The results show that a single-phase spinel forms only up to 18–22 at.% Cu content. Above this, Cu segregates and forms CuO (**Fig. 1**). The systematic mapping reveals a continuous diffraction angle shift and peak shape change, with the FWHM of the spinel peaks increasing significantly with the Cu content. These findings provide insights into ion mixability and composition-dependent structural changes in CCSSs and demonstrate the efficiency of high-throughput synthesis and mapping for accelerating materials discovery.

Fig. 1: Property maps of an exemplary thin-film materials library. The element gradient maxima are marked in the corners. **a** Maximum peak intensity and **b** FWHM of spinel (311) and **c** maximum peak intensity of CuO (111). **d** Exemplary XRD pattern with spinel and CuO reflections.

References

[1] V. Strotkötter et al., Chem mater 2022, 34, 10291

[2] J. P. Barber et al., Mater Horiz 2025, 10.1039/d5mh01033k

[3] T. A. A. Batchelor et al., Angew Chem Int Ed 2021, 60, 6932

[4] M. M. Kandage et al., J Mater Sci 2024, 59, 16618

Fig. 1

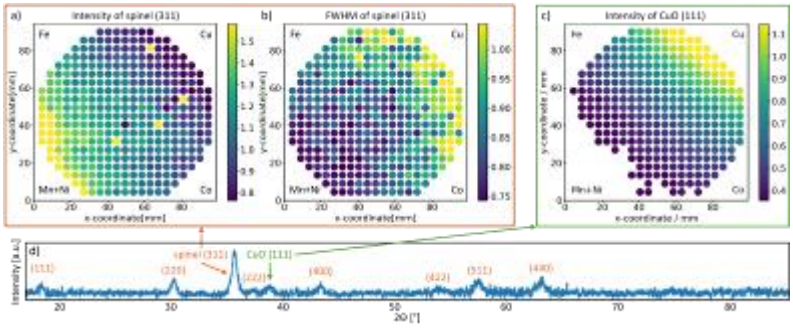

LT-12 | PP-83

Exploring compositional space in non-equimolar high entropy spinel oxides

C. F. Eugenio (Bochum/DE, Bogotá/CO), S. C. Sánchez (Bogotá/CO), A. Kirsch (Bochum/DE)

High-entropy oxides (HEOs) are a class of ceramic materials that incorporate five or more metal ions into their crystal lattice [1], combining structural stability with wide compositional flexibility. Most studies on spinel HEOs have focused on equimolar transition-metal compositions [2-4], while the structure and properties of stoichiometrically non-equimolar systems remain largely unexplored. In this work, we investigate a series of non-equimolar HEO spinel compositions containing the same principal elements as in previously reported systems (see Fig. 1). The samples were synthesized using a sol–gel method that has been shown to produce highly homogeneous HEOs [5]. Structural characterization by powder X-ray diffraction , neutron diffraction, and high-resolution transmission electron microscopy confirmed that all studied HEOs form highly crystalline, single-phase materials. These results demonstrate that the synthesis method reliably yields non-equimolar high-entropy oxides, enabling the exploration of electric and magnetic properties of a wider compositional space for future energy-related applications.

Fig. 1: (a) Unit cell of the Fd-3m cubic spinel structure. (b) Quasi-ternary phase diagram showing the synthesized HEOs marked with black, red, green, and blue dots with compositions $(Co_{0.33}Ni_{0.33}Cu_{0.33})(M1\text{-}x\ M''x)2O4$ (M = Cr, Mn, Fe).

References

[1] Solveig S. Aamlid, Mohamed Oudah, Jörg Rottler, and Alannah M. Hallas Journal of the American Chemical Society ***2023*** 145 (11), 5991-6006.

[2] Rost, C., Sachet, E., Borman, T. et al. Nature Communications ***2015*** 6, 8485.

[3] Saifei Dai, Mingya Li, Xiaoqiang Wang, Haiyang Zhu, Yihan Zhao, Zhisheng Wu, Journal of Magnetism and Magnetic Materials, ***2021***, 168123, 0304-8853.

[4] Aiqin Mao, Feng Quan, Hou-Zheng Xiang, Zhan-Guo Zhang, Koji Kuramoto, Ai-Lin Xia, Journal of Molecular Structure, ***2019***, Volume 1194, 0022-2860.

[5] Andrea Kirsch, Espen Drath Bøjesen, Niels Lefeld, Rasmus Larsen, Jette Katja Mathiesen, Susanne Linn Skjærvø, Rebecca Katharina Pittkowski, Denis Sheptyakov, and Kirsten M. Ø. Jensen Chemistry of Materials ***2023*** 35 (20), 8664-8674.

Fig. 1

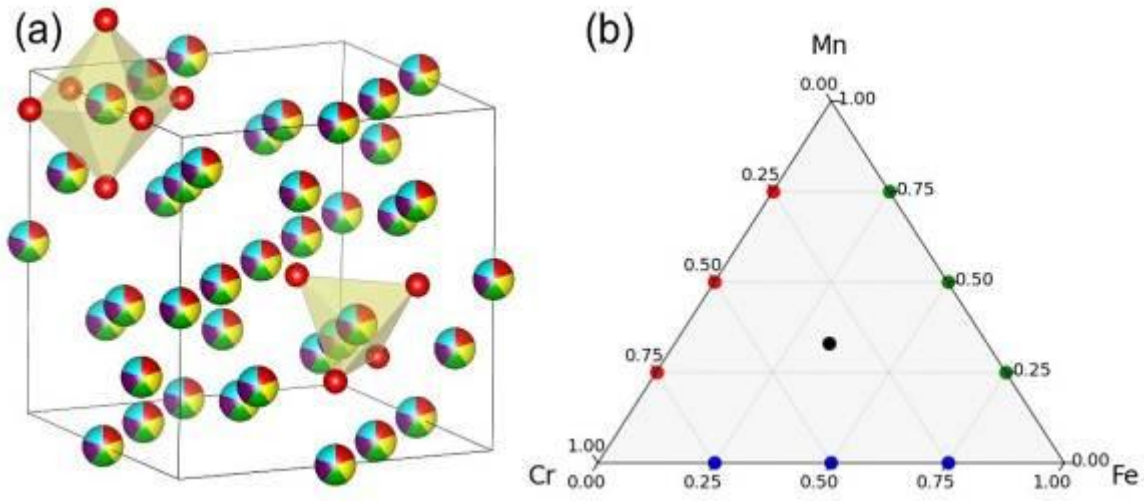

LT-13 | PP-84

Reference Database for Chemical Bonding Analysis

F. Bartley (Aachen/DE), F. Kleemiß (Aachen/DE)

The chemical bond is fundamental to understanding molecular structure, reactivity, and function, yet remains an abstract quantum-mechanical concept that is not directly observable. Quantum chemical methods such as NBO[1], QTAIM[2], ELI-D[3], and Roby-Gould Bond Indices[4] provide complementary insights into bonding, but individual limitations and computational dependencies often yield inconsistent interpretations. Experimental electron density and electrostatic potential data from high-resolution X-ray or electron diffraction in quantum crystallography[5] provide valuable references but face challenges such as reproducibility and the complexity of performing the analysis.

To overcome these challenges, we develop an integrated, user-friendly platform featuring a reference database for bonding analysis. The database currently supports an automated workflow for .xyz input files and crystallographic .cif files, facilitating direct comparison between theoretical and experimental bonding analyses. Our platform enables unbiased evaluations of bonding descriptors across chemical and conformational space, supported by statistical metrics and visualisation tools.

By providing a consistent reference tool that combines computational and diffraction-based data, this platform aims to enhance the reliability and accessibility of chemical bonding analyses. Ultimately, it will hopefully support the crystallographic community in gaining deeper insights and enable advanced bonding characterisation as a routine part of crystallographic research.

Fig.1:Current state of the database GUI.

References

[1] C. R. Landis and F. Weinhold, The NBO View of Chemical Bonding, *The Chemical Bond*, Wiley, **2014**, pp. 91-120.

[2] R. F. W. Bader, Atoms in molecules. A quantum theory, Oxford University Press **1994**.

[3] M. Kohout, *Faraday discussions* **2007**, *135*, 43-54; discussion 125-49, 503-6.

[4] K. Alhameedi, *et al. Results in Chem.* **2020***, 2*, 100053.

[5] S.Grabowsky, *et al. Chem. Sci*. ***2017****,8, 4159-4176*.

Fig. 1

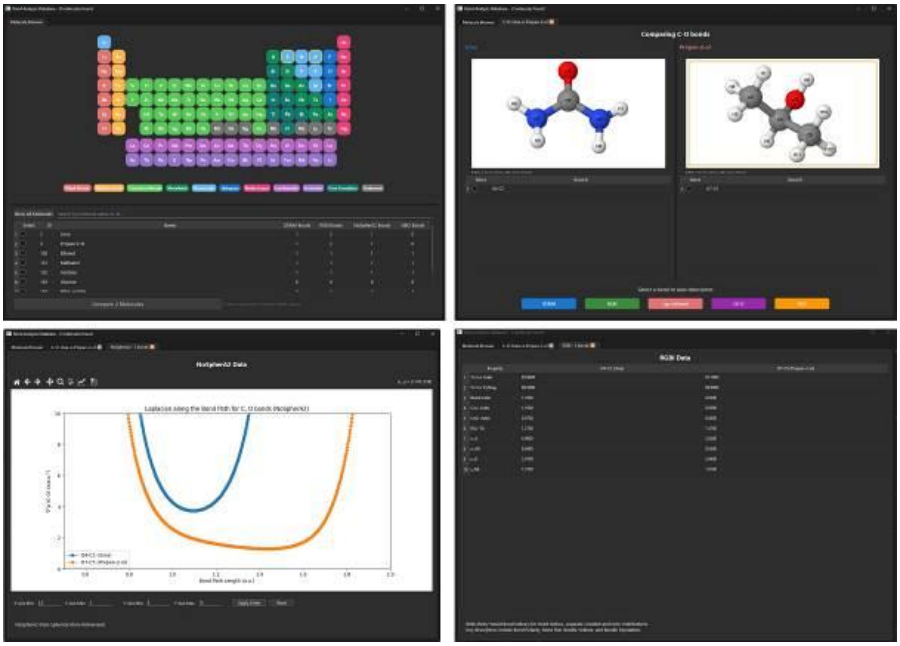

LT-14 | PP-85

Capturing Spin Transitions in Crossover Complexes* via *Quantum Crystallographic Disorder Refinement

D. Brüx (Aachen/DE), F. Kleemiß (Aachen/DE)

Spin-crossover (SCO) complexes undergo reversible transitions between low-spin (LS) and high-spin (HS) states, which are usually triggered by changes in temperature, pressure or light. These transitions, particularly in octahedral Fe(II) systems, are accompanied by significant structural and physical changes. Direct crystallographic observation of mixed spin populations within a single crystal remains challenging. [1, 2]

To address this, we employed an aspherical modelling approach from quantum crystallography. Hirshfeld Atom Refinement (HAR) [3], to distinguish between HS and LS states [4]. High-resolution data were collected on an archetypal SCO compound at multiple temperatures. The structures were refined using an aspherical disorder model that superimposes HS and LS configurations within the same crystal lattice (Fig A).

This allowed us to model each spin state with its correct geometry while refining the site occupancies as variables. This enabled the HS fraction to be quantified directly from the crystal structure alone. The results revealed a sharp change in the HS population between 175 K and 180 K, accompanied by a discontinuity in the unit cell volume (Fig B). This indicates an abrupt spin transition. Similar results were obtained for a series of additional transition-metal complexes, demonstrating the reproducibility of the method.

References

[1] V. Legrand et. al. J. Appl. Crystallogr. 2007, 40.

[2] E. Collet et. al. C. R. Chim. 2018, 21.

[3] F. Kleemiss et. al. Chem. Sci. 2021, 12.

[4] D. Brüx et. al. Chem. Eur. J. 2025, 31.

Fig 1: Crystallographic disorder model (A); Temperature dependence of the unit cell and the HS fraction (B).

Fig. 1

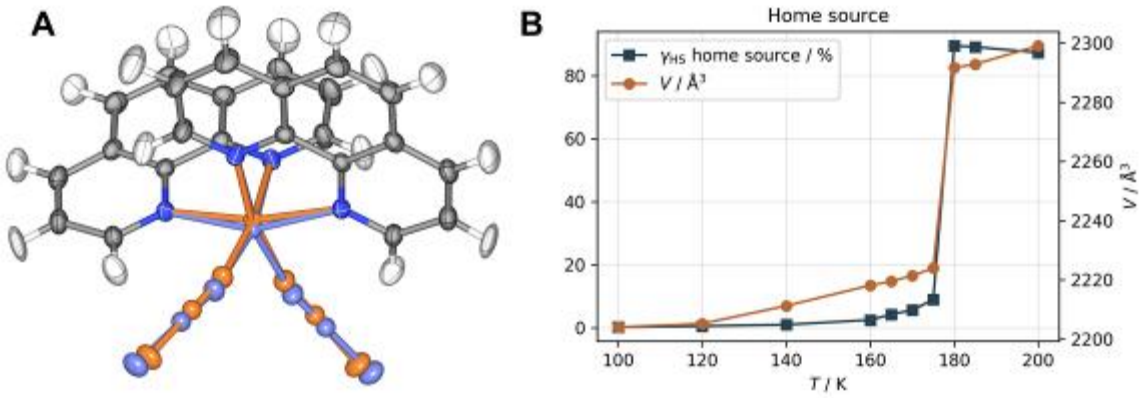

LT-15 | PP-86

Porous Pillarplex Materials: Towards Gas Adsorption in the Solid State

J. Zuber (Garching/DE), A. Heidecker (Garching/DE), A. Pöthig (Garching/DE)

Supramolecular interactions, based on non-covalent bonds, are essential for complex biological mechanisms. Various structures self-assemble from small building blocks. This natural phenomenon inspires the field of "the chemistry beyond the molecule," where scientists study and replicate these processes.[1]

A subclass of such supramolecular organometallic complexes (SOCs)[2] is depicted by pillarplexes **M8L2(X)4** (M = Ag, Au), which are octanuclear NHC complexes forming metallocavitand structures. Apart from the properties of pillarplexes, such as hosting guests in their tubular cavity, intrinsic luminescence or tunable solubilty,[3] modification of the counterion or the rim of the macrocyclic ligand entails several structural allignments and self-recognition properties.

Figure 1: Schematic representation of the tuneable solubility and shape selectivity towards linear alkanes (left) and the gas and guest uptake of the solid state depending on metal and counterion (right).

Independent of the metal and counterion, the cation can selectively encapsulate linear alkanes[3] and five-membered rings,[4] whereas larger aromatic rings cannot be accommodated. By varying the transition metal (i.e. Ag, Au) and the counterion (i.e. PF6, OAc), the solid-state packing can be systematically tuned, allowing control over pore volume and the selectivity of encapsulating different C4 hydrocarbon isomers. These isomers are not only confined within the cationic cavities but also occupy the mesopores of the material.

References

[1] J. M. Lehn, *Science* **1993**, 1762.

[2] A. Pöthig, A. Casini, *Theranostics,* 2019, **9**, 3150.

[3] P. J. Altmann, A. Pöthig, *J. Am. Chem, Soc.,* **2016**, 138, 13171.

[4] Pickl, T., Mollik, P., Anneser, M.R., Sixt, F., Geißer, K., Storcheva, O., Halter, D.P. and Pöthig, A., *Chem. Eur. J.,* **31**, 2025

Fig. 1

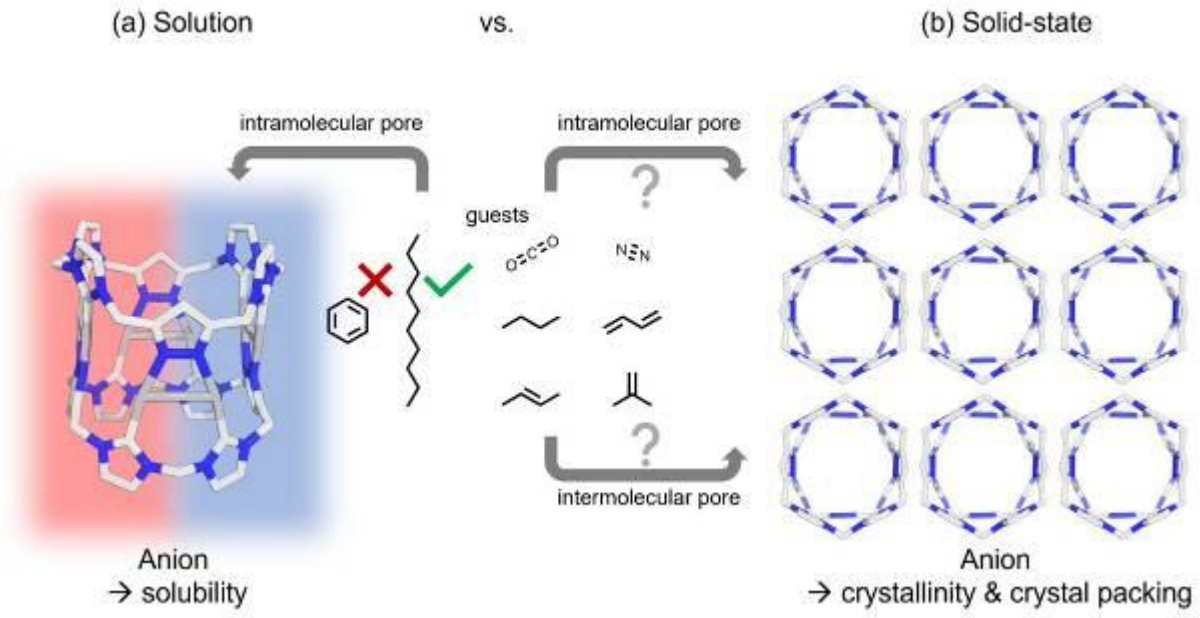

LT-16 | PP-87

Crystal architecture through energetic insights: 2,6-bis(4H-1,2,4-triazol-4-yl)pyridine hydrate

M. G. Bogdanović (Novi Sad/RS), I. S. Konovalova (Düsseldorf/DE, Kharkiv/UA), G. J. Reiss (Düsseldorf/DE), M. V. Rodić (Novi Sad/RS)

1,2,4-Triazole derivatives are particularly attractive as bridging ligands due to their versatile coordination modes. Following the synthetic procedure [1], we successfully isolated a 2,6-bis(4*H*-1,2,4-triazol-4-yl)pyridine hydrate after recrystallization from ethanol (*Fdd*2, *a* = 34.7868(8) Å, *b* = 30.5640(6) Å, *c* = 3.81450(9) Å, *V* = 4055.67(15) Å^3, *Z* = 16). The structure was refined using the Hirshfeld atom refinement (HAR) to $R_{gt}(F)$ = 0.0247, and $wR_{ref}(F^2)$ = 0.0675, with all hydrogen atom parameters freely refined. Additionally, intermolecular interaction energy calculations were performed to evaluate key interactions and their contributions to the crystal packing.

From a geometric perspective, the organic molecules (**A**) form chains propagating along the *c* axis due to π–π stacking interactions. Water molecules (**W**) connect these chains through several hydrogen bonds (O1–H1A···N6, O1–H1B···N6′, O1–H1B···N7′, C7′–H7′···O1 and C8′–H8′···O1 contacts). In addition to these interactions, the **A** molecules form a complex network of hydrogen bonds (Fig. 1a) that further obscures the identification of a clear structural motif and complicates the assessment of the true significance and strength of individual interactions. To show the true significance and individual contribution of each interaction to the overall crystal packing and to enable an unambiguous identification of the underlying structural motif, intermolecular interaction energies were calculated for all pairwise dimers within the first coordination sphere of each independent molecule using an appropriate quantum-chemical method and shown in terms of energy vector diagram [2]. This analysis revealed that the strongest interaction occurs between two organic molecules through π–π stacking interactions with an energy of interaction being –6.8 kcal mol^{-1}, and second strongest interaction (–6.7 kcal mol^{-1}) is also between two **A** molecules mediated through C6′–H6′···N3 (2.360 (18) Å, 144.3°) hydrogen bond. Third strongest interaction has energy of –6.1 kcal per mole and it arises from C2′–H2′···N4 (2.330 (19) Å, 169.6°) and C9′–H9′···N3 (2.49(2) Å, 155.3°) hydrogen bonds. Together, these strongest interactions with the weak ones lead to three-dimensional supramolecular network composed of organic molecules, within which layers of water molecules are incorporated (Fig. 1b).

Fig. 1: (a) Hydrogen bond network with asymmetric unit highlighted, and (b) crystal packing in terms of energy vector diagram, organic molecules are shown in red and water molecules in yellow.

References

[1] S. Yuan, W. Ying, *Acta Cryst. E* 2011, **67**, 1631.

[2] O.V. Shishkin, V.V. Medvediev, R.I. Zubatyuk, *CrystEngComm* 2013, **15,** 29–37.

Research was supported by the Ministry of Science, Technological Development and Innovation of the Republic of Serbia through German–Serbian joint scientific co-operation project: Application of quantum-crystallographic methods in extended routine X-ray structural analysis of small molecules (Grant No. 337-00-253/2023-05/12).

Fig. 1

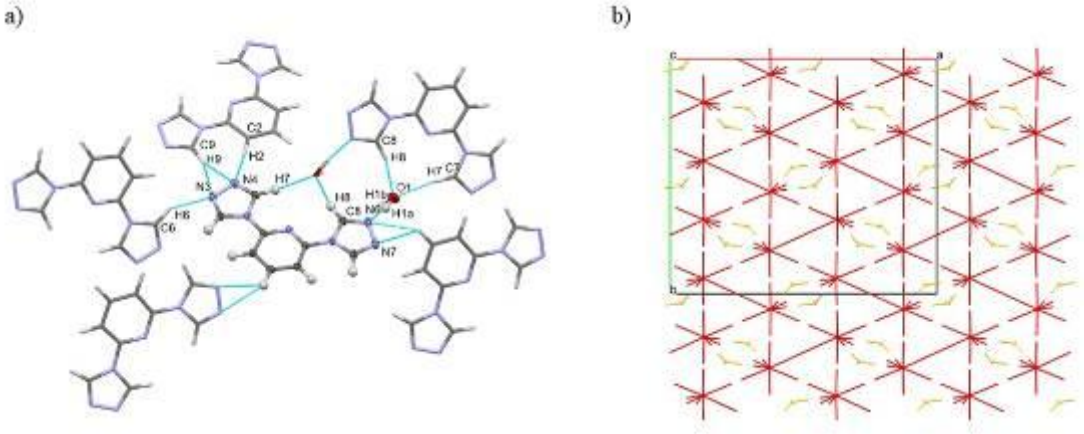

MS 2: Methods in Structural Biology

OP-01

High-throughput Macromolecular Crystallography at Beamline P11

J. Hakanpää (Hamburg/DE), S. D. Chatziefthymiou (Hamburg/DE), G. Pompidor (Hamburg/DE), A. Grebentsov (Hamburg/DE), A. Gruzinov (Hamburg/DE), O. Merkulova (Hamburg/DE)

DESY"s MX beamline P11 (1, 2) at PETRA III offers data collection as fast as 2 min per sample and the sample changer fits 23 unipucks simultaneously. The versatile focusing options, Eiger2 X 16M detector and remote operations with simple web-browser based solution make it ideal for various experiments including drug screening campaigns.

During 2025 P11 has taken into user operations MXCuBE and ISPyB for data acquisition and sample information import. We are building in further functionalities with an aim of establishing option for unattended data collections. ISPyB also now supports the sample shipments and tracking. Further upgrades will follow in 2026 when new hardware is installed, to replace the current diffractometer and sample changer. This will increase the sample capacity from 23 to 37, speed up the sample mount cycle, enable crystal reorientation and helical scans and improve the reliability of the instrument.

Serial synchrotron crystallography at P11 is enabled mainly with the CFEL tape-drive setup, also capable of time-resolved experiments by the mix-and-diffuse method (3). Real-time autoprocessing of serial data with CrystFEL (4) has been developed within a long-term proposal.

In preparation for PETRA IV, P11 is now solely accessed by the academic users via rolling access. The industrial use of the beamline has grown significantly and we further develop the features important for industrial access but also benefitting for the academic users.

References

[1] Burkhardt A., et al., Status of the crystallography beamlines at PETRA III. (2016) Eur. Phys. J. Plus131, 56

[2] Oberthür D. et al., Present and future structural biology activities at DESY and the European XFEL (2025) J. Synchrotron Rad. 32 474-485

[3] Beyerlein K. R., et al., Mix-and-diffuse serial synchrotron crystallography. (2017) IUCrJ 4, 769-777

[4] White T. A., et al., Recent developments in CrystFEL. (2016) J. Appl. Cryst. 49, 680-689

OP-02

EMBL Macromolecular Crystallography Facilities at PETRAIII

G. Bourenkov (Hamburg/DE), D. von Stetten (Hamburg/DE), M. Nikolova (Hamburg/DE), M. Agthe (Hamburg/DE), S. Panneerselvam (Hamburg/DE), D. Ruiz Carrillo (Hamburg/DE), Y. Bloch (Hamburg/DE), K. Kovalev (Hamburg/DE), T. R. Schneider (Hamburg/DE)

EMBL Hamburg operates two Macromolecular Crystallography beamlines, P13 and P14, at the PETRAIII storage ring (DESY, Hamburg).

Beamline P13 is dedicated to standardized high-throughput cryogenic single-crystal structure determination. Increasingly high fraction of P13 beam time is devoted to industrial applications. In 2025 the P13 X-Ray optics were upgraded for providing high-flux top-hat beam in the photon energy range of 6 to 18 keV. Currently, the upgrade is being completed. The ultimate goal is to provide higher quality diffraction data at lower X-Ray doses, as it was demonstrated at the P14 beamline during the last ten yeas of operation.

P14 is shared among three user programs covering standard static crystallography, time-resolved serial crystallography (TREXX) and X-Ray imaging applications (High-Throughput Tomography, HiTT [1]).

An optionally powerful microbeam, >2e13 ph/sec, at P14 is regularly used for special applications like *in-situ* and *in-vivo* crystallography (e.g. [2]). In combination with the 96 well (CrystalDirect™) format as a sample delivery system, an on-axis laser illumination system is available. It provides unique optically clear conditions for laser-driven dynamic experiments.

Energies >30 keV were made accessible at P14 in the top-hat beam regime. In conjunction with advanced data collection workflows [3] P14 provides record resolutions and spectacular data quality. This opens the door for quantum-mechanical applications on protein structures.

The TREXX end station at P14 is mostly dedicated to solid-support-based serial time-resolved crystallography. In particular, it is equipped [4] with an environment chamber and substrate delivery system for structural studies of enzyme kinetics in a multi-temperature regime.

References

[1] Albers et al.,. J. Synchrotron Rad., 31(1), 186, (2024)

[2] Schönherr et al., Nat. Commun., 15, 1709, (2024)

[3] Fogh et al., Acta Cryst. D, in press. (2025)

[4] Schulz et al., Nat. Commun. 16, 6553 (2025)

OP-03

MATTS-PDB: A Dictionary-Based Approach for Aspherical Electron Density Modeling in Macromolecules

P. Rybicka (Warsaw/PL), M. Kulik (Warsaw/PL), C. Grandgirard (Vandœuvre-lès-Nancy/FR), M. Chodkiewicz (Warsaw/PL), P. Dominiak (Warsaw/PL)

Macromolecular crystallography increasingly calls for models that go beyond the spherical approximation of electron density, and capture its true, aspherical nature. Multipole Model (MM) [1] accurately describes bonding and lone-pair deformations but depends on subatomic (<0.6 Å) data, rarely available for macromolecules. Transferable Aspherical Atom Model (TAAM) [2] with databanks such as MATTS [3,4] enables aspherical modeling at lower resolution by transferring precomputed MM parameters between chemically equivalent atoms. However, current atom-type assignment relies on atomic coordinates, a method suitable for small molecules but computationally demanding and error-prone for macromolecules.

This work extends TAAM to macromolecules by developing a dictionary-based procedure that recognizes MATTS atom types directly from standardized residue and atom names, eliminating the need for coordinate-based matching.

Over 45,000 high-quality structures from the Protein Data Bank were processed using gemmi [5] to remove disorder and add hydrogens. Atom types from MATTS were assigned via DiSCaMB [6] and used to build the MATTS-PDB dictionary.

The MATTS-PDB dictionary enables efficient, automated atom typing for amino acids, RNA and DNA nucleotides, and common ligands, including multiple protonation and terminal variants. Together with pyDiSCaMB [7] in cctbx, which supports multipolar scattering factors, makes aspherical electron density modeling in tools like Phenix [8] possible.

Funding: National Science Centre, Poland, UMO-2023/49/N/ST4/02967.

Fig. 1: MATTS atom types assigned to HIS with different protonation states.

References

[1] Hansen & Coppens, *Acta Cryst. A* (1978).

[2] Brock et al., *Acta Cryst. B* (1991).

[3] Jha et al., *J. Chem. Inf. Model.* (2022).

[4] Rybicka et al., *J. Chem. Inf. Model.* (2022).

[5] Wojdyr, *J. Open Source Softw.* (2022).

[6] Chodkiewicz et al., *J. Appl. Cryst.* (2018).

[7] *pyDiSCaMB*, GitHub (2025).

[8] Liebschner et al., *Acta Cryst. D* (2019).

Fig. 1

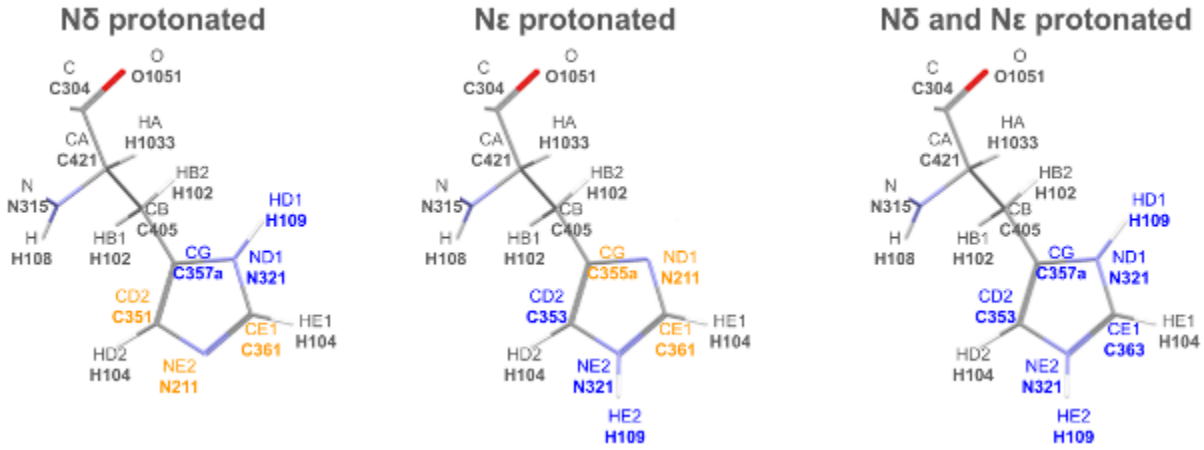
Nδ protonated
C
C304
O
O1051
HA
H1033
CA
C421
HB2
H102
N
N315
CB
C405
HD1
H109
H
H108
HB1
H102
CG
C357a
ND1
N321
CD2
C351
CE1
C361
HE1
H104
HD2
H104
NE2
N211
Nε protonated
C
C304
O
O1051
HA
H1033
CA
C421
HB2
H102
N
N315
CB
C405
H
H108
HB1
H102
CG
C355a
ND1
N211
CD2
C353
CE1
C361
HE1
H104
HD2
H104
NE2
N321
HE2
H109
Nδ and Nε protonated
C
C304
O
O1051
HA
H1033
CA
C421
HB2
H102
N
N315
CB
C405
HD1
H109
H
H108
HB1
H102
CG
C357a
ND1
N321
CD2
C353
CE1
C363
HE1
H104
HD2
H104
NE2
N321
HE2
H109

OP-04

Structural Quality and Docking Reliability of Peptide–GPCR Complexes: A Crystallographic Perspective

S. Jafari, J. Bojarska, W. Wolf (Łódź/PL)

Introduction: G protein-coupled receptors (GPCRs) are key regulators of cellular signaling and central therapeutic targets, particularly for peptide-based ligands [1,2]. Despite their importance, understanding peptide–GPCR interactions is challenging due to receptor dynamics and variability in structural quality. This study examines how structural accuracy and receptor conformational state affect the reliability of peptide docking simulations.

Methods: We analyzed three human peptide-binding GPCRs, NTSR1, CXCR4, and NK1R, using X-ray, cryo-EM, NMR, and AlphaFold2 models. Structures were assessed for resolution, R-factors, and active vs inactive states. Short model peptides were docked using AutoDock 4.6 to compare binding-site geometry, peptide orientation, and docking energetics across templates [3–5].

Results: High-resolution experimental structures, particularly active-state cryo-EM models with well-resolved peptide density, provided the most reliable docking outcomes. Inactive receptors, antagonist-bound conformations, and AlphaFold2 predictions often displayed pocket distortions or narrowing, resulting in weaker docking scores and unstable poses. Extracellular loop variability, especially ECL2 positioning, and TM6 displacement strongly influenced docking performance. Comparisons between active and inactive structures highlighted how receptor conformation shapes peptide binding [6].

Conclusions: Structural quality and receptor activation state critically determine peptide–GPCR docking reliability. Active-state cryo-EM templates offer the most consistent results, while inactive or predicted structures require caution. This framework provides practical guidance for peptide-based drug design and supports integrated use of cryo-EM, crystallography, and computational modeling in developing selective GPCR modulators [6,7].

References

[1] Sriram & Insel, Mol Pharmacol 2018.

[2] Rosenbaum et al., Nature 2009.

[3] Bojarska & Wolf, MDPI 2020.

[4] Bojarska et al., RSOS 2025.

[5] Morris et al., J Comput Chem 2009.

[6] Vilar et al., JMGM 2011.

[7] Odoemelam et al., RSC Adv 2020.

OP-05

In situ protein crystallography: a single-crystal electron diffraction pipeline for direct structure determination inside cells, _IncelluloED_

V. Polovinkin (Dolní Břežany/CZ), Š. Bílá (České Budějovice/CZ), D. Pinkas (Prague/CZ), K. Khakurel (Dolní Břežany/CZ), J. Boger (Lübeck/DE), T. Bílý (České Budějovice/CZ), J. Hajdu (Dolní Břežany/CZ, Uppsala/SE), Z. Franta (České Budějovice/CZ), I. de Diego Martinez (Schenefeld/DE), R. Tuma (České Budějovice/CZ), L. Redecke (Hamburg/DE)

Intracellular crystallisation is an emerging approach in structural biology that bypasses the need for protein purification [1]. In 2024, the *InCellCryst* pipeline was introduced for structural studies of intracellular crystals by serial X-ray crystallography [2]. Serial crystallography requires the exposure of tens of thousands of cells containing intracellular crystals, precluding high-resolution studies on proteins that crystallize only in a few cells. Here we introduce *IncelluloED*, a method that combines intracellular crystallization with *in situ* 3D electron diffraction in cells and achieves high-resolution structures from just one crystal inside one cell. Experiments on a microcrystal of the HEX-1 protein from *Magnaporthe grisea*, grown inside an insect cell, gave a structure at 1.9 Å resolution from a volume of ~1.6 µm³ as compared to 1.8 Å resolution achieved by serial X-ray crystallography from a combined volume exceeding eleven million µm³. *IncelluloED* uses widely available cryo-EM tools and brings high-resolution structural biology into home laboratories while also advancing a vision for a "single-cell structural laboratory".

Fig. 1: Schematic diagram of the *IncelluloED* experimental workflow. In panel 1, intracellular crystals are produced and detected with the *InCellCryst* pipeline [2].

References

[1] Schönherr, R., Rudolph, J. M. & Redecke, L. Protein crystallization in living cells. *Biol. Chem.* **399**, 751–772 (2018).

[2] Schönherr, R. et al. A streamlined approach to structure elucidation using *in cellulo* crystallized recombinant proteins, *InCellCryst*. *Nat. Commun.* **15**, 1709 (2024).

Fig. 1

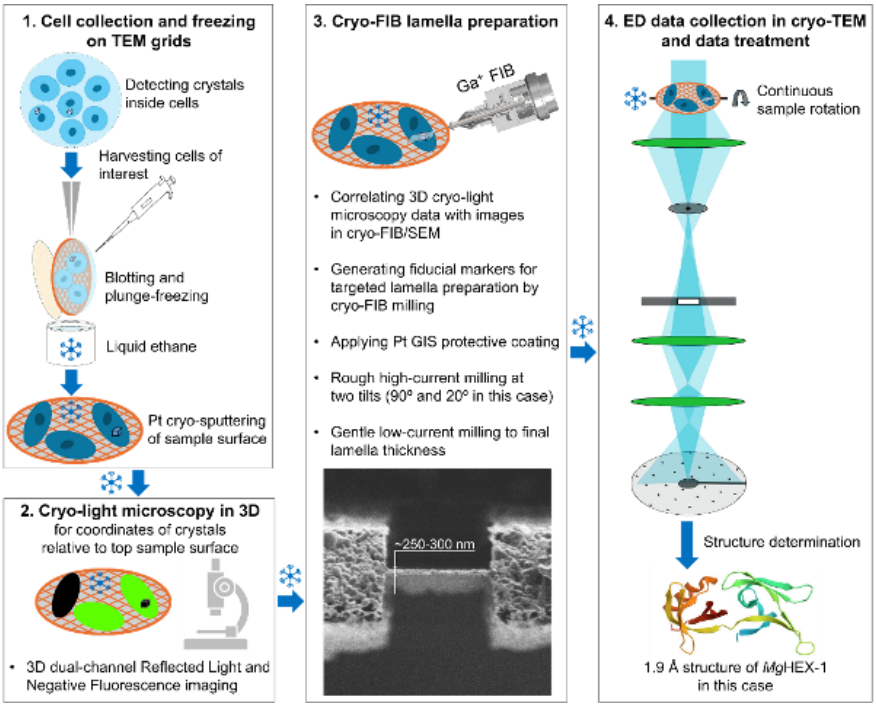

OP-06

From nanometer to millimeter: a versatile crystallization approach for electron, X-ray and neutron diffraction

A. Shaikhqasem (Halle (Saale)/DE), F. Hamdi (Halle (Saale)/DE), L. Gajdos (Grenoble/FR), M. P. Blakeley (Grenoble/FR), P. L. Kastritis (Halle (Saale)/DE), M. T. Stubbs (Halle (Saale)/DE)

While X-ray diffraction is the most applied method in bio-crystallography, neutron diffraction remains a valuable tool for determining protonation states and thus understanding enzyme mechanisms. Recent advancements in electron crystallography have demonstrated the potential for determining partial charges in macromolecules. Regardless of the method applied, crystal size has long been a critical factor in crystallography, particularly for macromolecules. While X-ray diffraction can be performed on crystals as small as a few micrometers, neutron crystallography still demands significantly larger crystals, typically in the millimeter range. On the other hand, electron crystallography ideally requires thin sub-micrometer crystals. Obtaining large crystals for neutron diffraction is particularly challenging, often limited by traditional crystallization methods where crystal growth tends to stop at a certain size. Conversely, obtaining very small crystals for electron diffraction requires specialized and expensive instrumentation, such as focused ion beam (FIB) milling. Here, we present simple and cost-effective approaches that enhance conventional crystallization methods, enabling the production of crystals within a wide size range from submicron to millimeter scale. Using the protein chorismate dehydratase MqnA as a case study, we successfully prepared crystals that are suitable for neutron, electron, and X-ray diffraction data collection.

MS 3: New Trends and Modelling of Crystal Structures and Properties

OP-07

How can we trust our crystal structure solutions?* Pseudo-*homometry and chemical reliability in single-crystal X-ray diffraction

A. Virovets (Frankfurt a. M./DE)

Single-crystal X-ray diffraction, being one of key characterization technique in synthetic chemistry, is based on a few principles that none of us places in doubt. One of them, intuitively obvious, tells that the given set of structural amplitudes, $|F|_{hkl}$, corresponds to unique structural model, the set of atomic sorts, xyz, occupancy factors and a.d.p."s. In other words, the structure solution is unique. To the best of our knowledge, there is no formal mathematical proof for this. The structures that give the same diffraction pattern can be called *homometric*.[3] Practically, $|F|_{hkl}$ are always measured within some accuracy, and the structural model from non-linear least-squares procedure features some confidence interval. Let us call the crystal structures *pseudo-homometric* if corresponding statistically different structural models give experimentally undistinguishable $|F|_{hkl}$ values. Such structures can differ in the chemical composition and constitution.

Different base scenarios are possible: models differ in the translational (**I**) or point (**II**) symmetry or both, (**III**) the symmetry is the same, but |*F*|hkl are still not sensitive to (chemically) significant changes in the model. Here factor of crystallographic disorder becomes especially important. Thus, in **I** weak overlooked reflections hide the superstructural ordering resulting in a wrong, disordered model. Enantiomerically pure structure can turn into "wrongly-disordered" if a centrosymmetric space group is chosen instead of chiral one (**II**). Elements with similar atomic scattering factor or an overlooked (chemically essential) disorder can lead to **III**, even if the symmetry is correct.

In the presentation practical examples of pseudo-homometric structures and related chemical aspects will be discussed.

Reference

[1] M. Farkas-Jahnke, K. Dornberger-Schiff, *Acta Cryst*. (1969) **A25**, 35

OP-08

Accessing new observables via nonlinear crystallography based on x-ray-optical wavemixing

D. Krebs (Hamburg/DE), C. Bömer (Hamburg/DE)

With the emergence of highly brilliant x-ray sources, the study of nonlinear phenomena in the x-ray regime has become feasible. Among the newly accessible phenomena, x-ray-optical wavemixing (XOWM) processes stand out, as they can combine diffractive imaging capabilities – similar to regular x-ray diffraction – with spectroscopic sensitivity to optical excitations.

Here, we present our theoretical approach to describe low-order XOWM as derived from non-relativistic QED. This allows us to quantitatively predict the nonlinear scattering signal and – most importantly – allows us to identify the electronic response function underlying XOWM as a newly-accessible observable. We complement the presentation with experimental results from our demonstration of x-ray-optical difference-frequency generation (DFG) in diamond. During this experiment, a pulsed optical laser (1.55 eV) drives the valence electrons of the sample while an intense x-ray FEL pulse (~ 9.7 keV) diffracts off the excited charges. Backed by our theory, we use the measured DFG signals to spatially reconstruct the diamond's valence response at sub-Angstrom resolution and, thus, give a proof-of-concept for 'nonlinear crystallography' (see Fig. 1).

As a future perspective, we propose to explore the method's scope both at FELs and synchrotron sources: From semiconductors to opto-electronics and complex correlated materials, the valence-specific nature of XOWM opens a broad range of opportunities to study electronic structure and dynamics.

Fig. 1

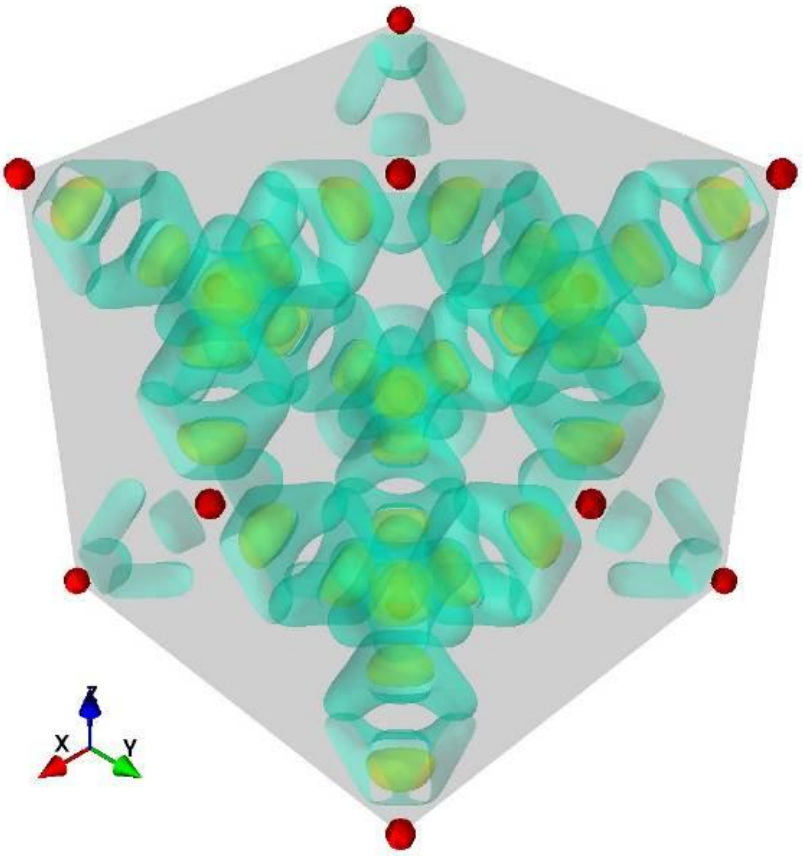

OP-09

T-BAR: Topology-Based Atom Refinement

F. Kleemiß (Aachen/DE), M. Gimferrer (Göttingen/DE)

The advantages of Hirshfeld Atom Refinement (HAR)[1] compared to spherical atom models have been reported manifold. However, recent benchmarking showed systematic discrepancies between the sophistication of the theoretical methods employed and the resulting refinement statistics.[2] Previous attempts to solve this observation, such as alternative partitioning schemes and modified versions of Hirshfeld partitioning, have not yielded conclusive results on a best practice.[3,4] Within this presentation, we propose the use of a new robust kind of partitioning scheme of Topology-Based Atoms that yields refinement statistics comparable to HAR without the need for additional fitting parameters or reference electron densities. Improved atom distances compared to neutron references can be observed for polar bonds, and the atomic displacement parameters of Hydrogen atoms show more physically plausible principal directions (see Figure 1).

References

[1] Woinska et al., Sci. Adv., 2016, e1600192.

[2] Brüx et al., Struct. Dyn., 2025, 12, 054101.

[3] Chodkiewicz et al., IUCrJ, 2020, 7, 119-1215.

[4] Chodkiewicz et al., IUCrJ, 2025, 12, 74-87.

Fig. 1

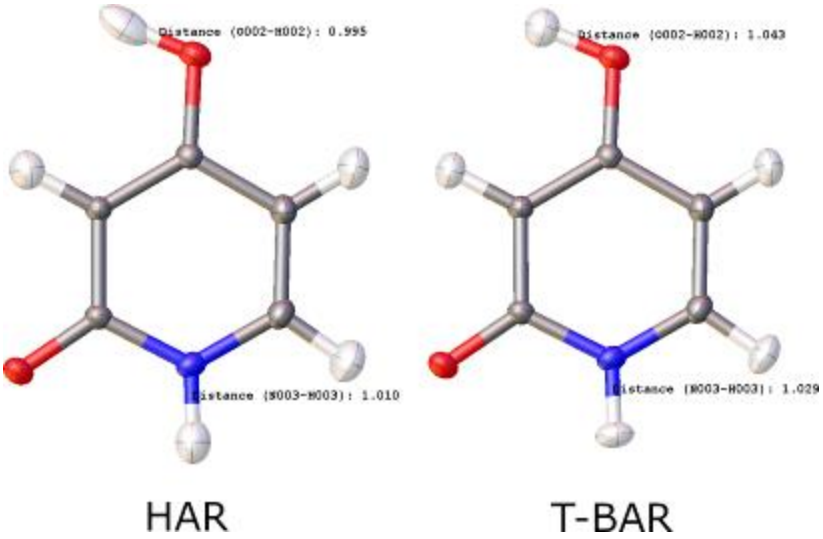

OP-10

Molecular Dynamics Simulations in Quantum Crystallography: Potentials and Challenges

M. Patzer (Mülheim an der Ruhr/DE), C. W. Lehmann (Mülheim an der Ruhr/DE)

The prediction of residual electron density in molecular crystals remains a key challenge in quantum crystallography. While static electron density is well described by Hirshfeld Atom Refinement (HAR), thermal smearing is usually approximated by ellipsoidal displacement models and guided by the Kuhs rule for anharmonic refinement (Jayatilaka & Dittrich, 2008; Hoser & Madsen, 2025). Normal Mode Refinement has linked periodic DFT with experiment by incorporating Γ-point vibrational frequencies into crystallographic refinement, thereby bridging theoretical and experimental descriptions of molecular motion (Hoser & Madsen, 2016).

Here, we introduce an alternative and conceptually direct approach employing molecular dynamics (MD, NVT, GFN2-xTB) to calculate dynamic structure factors from the time-dependent electron density. Thermal motion is inherently included within the MD trajectory, avoiding the need for convolution or partitioning schemes and allowing a natural representation of nuclear dynamics. The resulting structure factors enable refinement of Gram–Charlier coefficients and provide a theoretical framework to assess when anharmonic refinement after HAR is physically justified.

Applications to molecular crystals such as urea, thiourea, 2-mercaptopyridone, methylisothiazolinone, propionamide, oxalic acid dihydrate, and D/L-serine demonstrate that MD reproduces experimentally observed anharmonic residuals. Combined with void analysis, it further reveals preferred directions of atomic motion. This establishes a new modeling paradigm based on thermally averaged electron densities, advancing the predictive understanding of dynamic disorder and vibrational effects in diffraction data.

Jayatilaka, D. & Dittrich, B. (2008). *Acta Cryst.* **A64**, 383–393. Hoser, A. & Madsen, A. O. (2025). *IUCrJ* **12**, 421-434. Hoser, A. A. & Madsen, A. O. (2016). *Acta Cryst.* **A72**, 206–214.

Fig. 1: HAR of experimental and MD-derived diffraction data at identical resolution and temperature.

Fig. 1

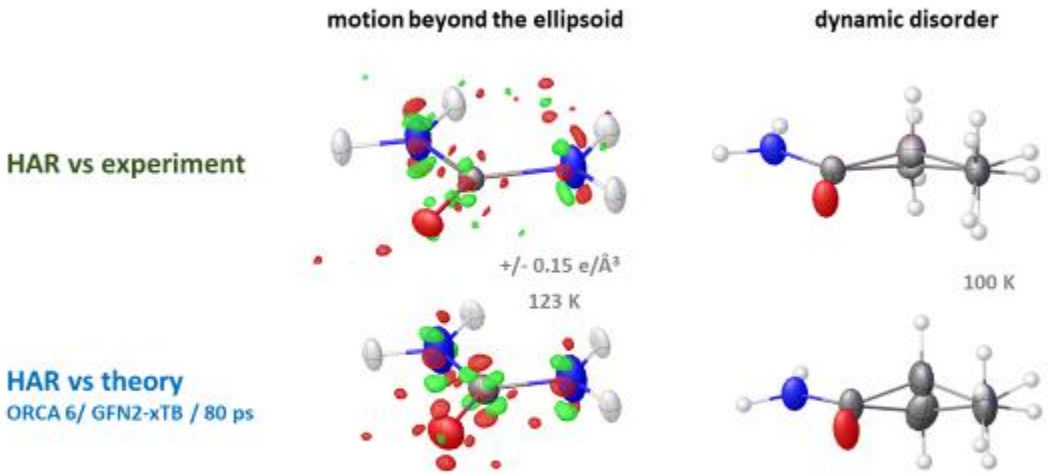

OP-11

From Static to Dynamic Polarizabilities: A Transferable Approach to Predict Optical Dispersion in Molecular Crystals

A. Krawczuk (Göttingen/DE), R. Fernandes Ligorio (Göttingen/DE)

Understanding and controlling the interaction of light with molecular materials is central to the development of next-generation photonic and optoelectronic systems. Quantities such as the refractive index and its wavelength dependence determine how efficiently light is transmitted, confined, or emitted, yet their accurate prediction remains a challenge. Conventional quantum-mechanical treatments of dynamic polarizabilities are computationally demanding and often impractical for large or complex systems.

Recent developments in the *PolaBer* software [1] extend its functionality beyond static atomic polarizabilities to include frequency-dependent (dynamic) polarizabilities, providing a direct route to estimate optical dispersion in molecular and crystalline systems. The new implementation combines *PolaBer*-derived distributed polarizabilities with the Dipole Interaction Model to capture crystal field effects and derive solid-state optical properties [2]. Through integration with the *CrysPol* module [3], dynamic electric susceptibilities and refractive indices can now be computed across the visible spectral range (400–1100 nm), enabling the prediction of refractive index dispersion in organic crystals from molecular-level input. This unified framework bridges atomic-scale polarizability analysis and macroscopic optical response, offering a computationally efficient and physically transparent approach to modeling dispersion phenomena without the need for periodic boundary conditions. Benchmark studies on chosen molecular crystals demonstrate very good agreement with experimental Sellmeier curves, highlighting the potential of the *PolaBer*–*CrysPol* workflow for rational design of optoelectronic materials.

References

[1] A. Krawczuk, D. Perez, P. Macchi *J. Appl. Cryst.* (2014) **47**, 1452-1458

[2] R.F. Ligorio, A. Krawczuk, L.H.R. Dos Santos *J. Phys. Chem. A* (2021) **125**, 19, 4152–4159

[3] R.F. Ligorio & A. Krawczuk, *manuscript in preparation*.

OP-12

Aspherical modeling: advancing x-ray scattering and sample characterization

K. García Medina (Erlangen/DE), R. Neder (Erlangen/DE)

Conventionally, scattering factors are assumed to be independent and spherically symmetric since, for typical applications, this Independent Atom Model (IAM) simplification can significantly reduce computational complexity. However, it can lead to significant discrepancies between the model and the experimental data, especially when dealing with complex organic molecular structures, since it omits the nature of chemical bonds. Commonly, the use of aspherical atomic form factors has been restricted to high-quality single crystal data sets, often aided by complementary neutron diffraction data that provide accurate nuclei positions. The DISCAMB library allows refining single crystal data with aspherical atomic form factors even if the 2Theta range is limited [1].

In this work, we implement Aspherical Atomic Model (AAM) scattering factors into a computational workflow for X-ray powder diffraction analysis and refinement, aiming to improve the accuracy of the model and the reliability of the results. The workflow, centred around the structure analysis tools suite DISCUS, has been tested on urea and other organic molecules, refining light atom nuclei to positions that better match those from neutron scattering experiments. Our research demonstrates that accurate atomic positions can be obtained with a Rietveld refinement using DISCAMB-generated aspherical atomic form factors.

Reference

[1] Chodkiewicz, M. L., Migacz, S., Rudnicki, W., Makal, A., Kalinowski, J. A., Moriarty, N. W., Grosse-Kunstleve, R. W., Afonine, P. V., Adams, P. D., & Dominiak, P. M. (2018), J. Appl. Crystallogr., 51(1), 193–199.

MS 4: Crystal Physics

OP-13

The impact of ordering phenomena on the physical properties of rare-earth oxoborates **$RCa_4O(BO_3)_3$** ***(*** **R = *Er, Y, Dy, Gd, Sm, Nd, La)***

M. Münchhalfen (Bochum/DE), J. Schreuer (Bochum/DE)

Rare-earth oxoborates $RX_2Z_2O(BO_3)_3$ have recently gathered interest regarding the application of high-temperature piezoelectric sensing applications, since they combine a high melting point at around 1770 K with no reported phase transitions, high piezoelectric sensitivity and low electric resistivity [1]. The low symmetry of monoclinic space group *Cm* results in a high number of degrees of freedom regarding the anisotropy of physical properties. $RX_2Z_2O(BO_3)_3$ offers possibilities for different cation substitution. As a consequence, depending on the ionic radius of the substituted cations, internal strain is introduced to the structure.

$RCa_4O(BO_3)_3$, crystals with *R* = Er, Y, Dy, Gd, Sm, Nd La were grown from melt using the Czochralski method and investigated regarding their thermo- and electromechanical properties between 100 K and 1473 K using dilatometry and resonant ultrasound spectroscopy. Cation ordering was investigated on ex-situ single crystal diffraction experiment were conducted on annealed and quenched samples.

Reproducible anomalies, characterized by an excess strain at high temperatures, occur, with the onset temperature depending on the type of the R^{3+} cation. Single-crystal diffraction experiments indicate that non-convergent cation ordering processes involving Ca^{2+} and R^{3+} play an essential role. The cation distribution on the specific structural sites and the evolution of disorder with temperature are mainly influenced by the size of the trivalent cation, with the minimization of internal stresses being the driving force. This in turn impacts a variety of temperature-depended physical properties.

Reference

[1] Yu, F., Hou, S., Zhao, X., Zhang, S.(2014) *IEEE Trans. Ultrason., Ferroelect., Freq. Control*,, **61**, 8.

OP-14

Phase Evolution, Phase Diagram and Annealing Effects in $V_{1-x}Fe_xO_2$ ($x \leq 1.0$ %) compounds:

D. Manousou (Jülich/DE, Athens/GR), S. B. Atata (Athens/GR), Y. J. Sohn (Jülich/DE), P. Tsipas (Magurele/RO, Athens/GR), A. Grzechnik (Jülich/DE, Aachen/DE), M. Calamiotou (Athens/GR), K. Friese (Jülich/DE, Aachen/DE), S. Gardelis (Athens/GR)

Introduction: Vanadium dioxide (VO_2) is a strongly correlated oxide exhibiting a remarkable metal–insulator transition (MIT) near 68 °C (T_{MIT}), accompanied by a monoclinic (M1)-to-rutile (R) structural phase transition (SPT) [1]. Understanding the aliovalent substitution effect in the M1 lattice remains a key challenge.

Objectives: This study investigates the impact of low-level Fe substitution ($x \leq 1.0$ %) and post-annealing on the structural evolution and phase stability of VO_2.

Materials and Methods: Polycrystalline $V_{1-x}Fe_xO_2$ ($x \leq 1.0$ %) samples were synthesized via solid-state reaction. Temperature-dependent X-ray powder diffraction (XRPD) patterns were analyzed using the Le Bail method [2]. Optical reflectance and X-ray photoelectron spectroscopy (XPS) were also performed.

Results: XRPD reveals a transition from the M1 ($P2_1/c$) to a triclinic (T) phase [3] with increasing Fe content, while a monoclinic M2 ($C2/m$) phase [3] emerges at 1.0 % Fe. The transition temperature (T_t) from T ⟶ M2 decreases with Fe doping, whereas T_{MIT} remains almost constant (Fig. 1) [4]. XPS indicates that Fe^{3+} incorporation increases V^{5+} sites, inducing lattice distortion and stabilizing T and M2 phases [4]. Post-annealing lowers V^{5+} content and reinstates the stable M1 phase. Oxygen deficiency thus acts inversely to Fe^{3+} substitution.

Conclusions: The findings provide insight into the complex phase behavior of $V_{1-x}Fe_xO_2$, highlighting the interplay among charge redistribution, vanadium valence state, and oxygen defects. Upcoming magnetometry measurements will correlate magnetic and structural changes to guide VO_2 tuning.

Fig. 1: $(011)_{M1}$ diffraction maps, $V_{1-x}Fe_xO_2$: (a) x=0, (b) 0.5%, (c) 0.75%, and (d) 1.0%. Lines: T_{MIT} (red), T_t (orange).

References

[1] F.J. Morin et al., *Phys. Rev. Lett.* **3** (1959) 34–36;

[2] V. Petříček et al., *Z. Kristallogr.* **238** (2023) 271-282;

[3] T. J. Huffman et al, *Phys. Rev. B* **95**, (2017), 075125;

[4] D. K. Manousou et al., *J. Alloys Compd* **1024** (2025) 180081.

Fig. 1

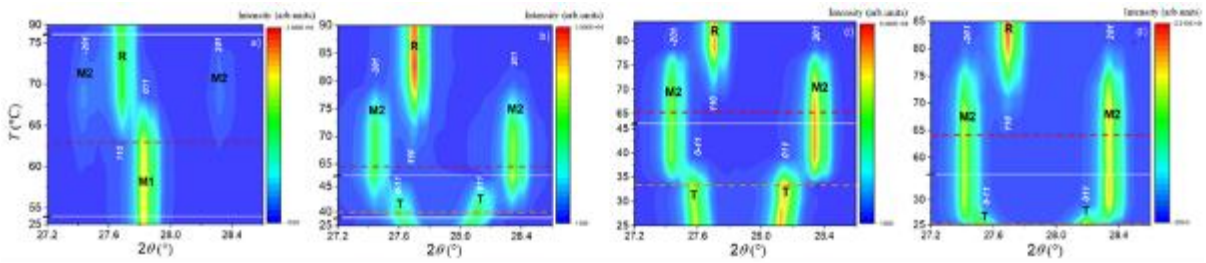

OP-15

Low-temperature anomalies in elastic properties of single-crystal $(SrAl_{0.5}Ta_{0.5}O_3)_{1-x}(LaAlO_3)_x$

M. Münchhalfen (Bochum/DE), J. Schreuer (Bochum/DE), C. Guguschev (Berlin/DE), R. Blukis (Berlin/DE), A. Dittmar (Berlin/DE), M. Brützam (Berlin/DE), S. Ganschow (Berlin/DE)

The perovskite mixed solid solution series $(SrAl_{0.5}Ta_{0.5}O_3)_{1-x}(LaAlO_3)_x$ (short LSAT) is a promising substrate material for epitaxial growth of high-temperature superconductors [1], manganese perovskites exhibiting colossal magnetoresistance [2] and GaN as a light source material for light emitting diodes and blue lasers [3]. Particular advantages of LSAT are the absence of phase transitions between melting temperature and ambient temperature [2], hence no micro twinning occurs during cooling, and the accessibility of large single crystals in the compositional range $0.23 < x < 0.41$ by the Czochralski method.

Two Czochralski grown crystals of the LSAT solid solution series with slightly different compositional parameter x were investigated for thermoelastic properties and thermal expansion in the temperature range between 103 K and 1673 K. The coefficients of thermal expansion were obtained by high-resolution dilatometry and the elastic stiffnesses by resonant ultrasound spectroscopy.

The end member $LaAlO_3$ of the solid solution series undergoes an improper ferroelastic phase transition at 800 K from cubic to trigonal symmetry [4]. The cubic LSAT samples show an elastic softening below ambient temperatures indicating precursor effects of a phase transition that likely occurs below 100 K, indicating, that the onset temperature of the phase transition depends on the parameter x in the solid solution series.

References

[1] Mateika et al., J. Cryst. Growth 109 (1991) 447–456.

[2] Berkowski et al., J. Cryst. Growth 257 (2003) 146–152.

[3] Ito et al., J. Cryst. Growth 235 (2002) 277–282.

[4] Carpenter et al., J. Phys. Condens. Matter 22 (2009) 035403.

OP-16

Determination of the Li2O – K2O – Ta2O5 phase diagram in the framework of single crystal growth of stoichiometric lithium tantalate

A. Hoffmann (Berlin/DE), R. Blukis (Berlin/DE), S. Inckemann (Berlin/DE), M. Bickermann (Berlin/DE), S. Ganschow (Berlin/DE)

A material isomorphous to the intensively investigated lithium niobate ($LiNbO_3$, LN), that has the same inherent non-stoichiometry is lithium tantalate ($LiTaO_3$, LT) [1]. Despite similar characteristics to LN, the properties of LT are significantly less studied, even though there are notable differences that favor the use of LT in certain applications. Of special interest is the investigation of stoichiometric LT (sLT) compared to congruent LT (cLT), as the lithium deficiency in cLT causes a high concentration of defects [1]. The lower defect concentration in sLT crystals results, among others, in larger electro- and nonlinear-optic coefficients [2].

Literature describes multiple methods to achieve stoichiometric LN single crystals, exemplary via the double crucible method. However, the growth method reporting a crystal composition closest to the stoichiometric ratio is the growth via the flux method [3]. Due to the similarities between LN and LT an analogous approach is the most promising, with the use of K2O as a solvent showing the best results in the case of LN [4].

In order to ensure an efficient single crystal growth in this system, knowledge about the $Li_2O–K_2O–Ta_2O_5$ phase diagram is vital [5]. As there is no literature regarding this phase diagram, this poster will present our current progress by combining DTA, PXRD and SEM measurements. Furthermore, results of our first single crystal sLT growth attempts will be presented.

References

[1] S. Kim, V. Gopalan, K. Kitamura, Y. Furukawa, *J. Appl. Phys.*, 90, 2949–2963 (2001)

[2] S. Ganesamoorthy, M. Nakamura, S. Takekawa, S. Kumaragurubaran, K. Terabe, K. Kitamura, Mater. *Sci. Eng. B*, **120**, 125–129 (2005)

[3] K. Polgár, Á. Péter, I. Földvári, *Opt. Mater*, 19, 7–11 (2002)

[4] K. Polgár, Á. Péter, L. Kovács, G. Corradi, Zs. Szaller, *J. Cryst. Growth*, 177, 211–216 (1997)

[5] M. Mühlberg, Phase Diagrams for Crystal Growth, in: Crystal Growth Technology, *John Wiley & Sons, Ltd*, 2-26 (2008)

OP-17

Pressure-Driven Depolarization in $BaTiO_3$ Probed by Second Harmonic Generation

T. H. Reuter (Frankfurt a. M./DE), L. Bayarjargal (Frankfurt a. M./DE), D. Rytz (Idar-Oberstein/DE), S. Schwung (Idar-Oberstein/DE), V. Milman (Cambridge/GB), B. Winkler (Frankfurt a. M./DE)

Ferroelectric $BaTiO_3$ (BT) and BT-based solid solutions are promising lead-free alternatives to widely used lead-bearing piezoelectrics such as $Pb(Zr,Ti)O_3$ (PZT) due to their relatively high piezoelectric coefficients starting at d_{33}^{piez} = 90 pC/N for single-crystal BT.[1] BT exhibits significant second-order nonlinear optical properties, reflecting strong ferroelectric activity in the crystal structure. In ferroelectrics, depolarization behavior is an important property for understanding the stability of spontaneous polarization and the factors influencing de- and repolarization. Temperature-dependent depolarization of BT has been extensively studied, including direct probing of the polarization using second harmonic generation (SHG). In this way, temperature-dependent occurrence of polar nanodomains (PNDs) in the otherwise paraelectric phase could be shown.[2] Pressure-dependent occurrence of PNDs has already been demonstrated using different methods, including X-ray pair distribution function analysis.[3] However, no pressure-dependent studies regarding the pressure-dependent depolarization in single-crystal BT and polycrystalline BT and BT-based solid solutions have been carried out using SHG to directly probe changes in the state of polarization. Using SHG, for single-crystal BT, the occurrence of PNDs above the Curie point could be detected. This extends the *p-T*-phase diagram of BT by a stability field of PNDs. For BT-based solid solutions, a correlation between the depolarization pressure and temperature and the solid solution formation with related paraelectric phases could be shown.[4]

We acknowledge funding from the BMBF (05K25RF3), the DFG (BA4020, WI1232) and support by the Dassault Systèmes Science Ambassador program.

References

[1] M. Acosta *et al*., Appl. Phys. Rev. **2017** 4, 041305

[2] A.M. Pugachev *et al*., Phys. Rev. Lett. **2012** 108, 247601

[3] L. Ehm *et al*., Appl. Phys. Lett. **2011** 98, 021901

[4] T.H. Reuter *et al.*, J. Phys. Chem. C **2025** 129, 35, 15914–15921

Fig. 1

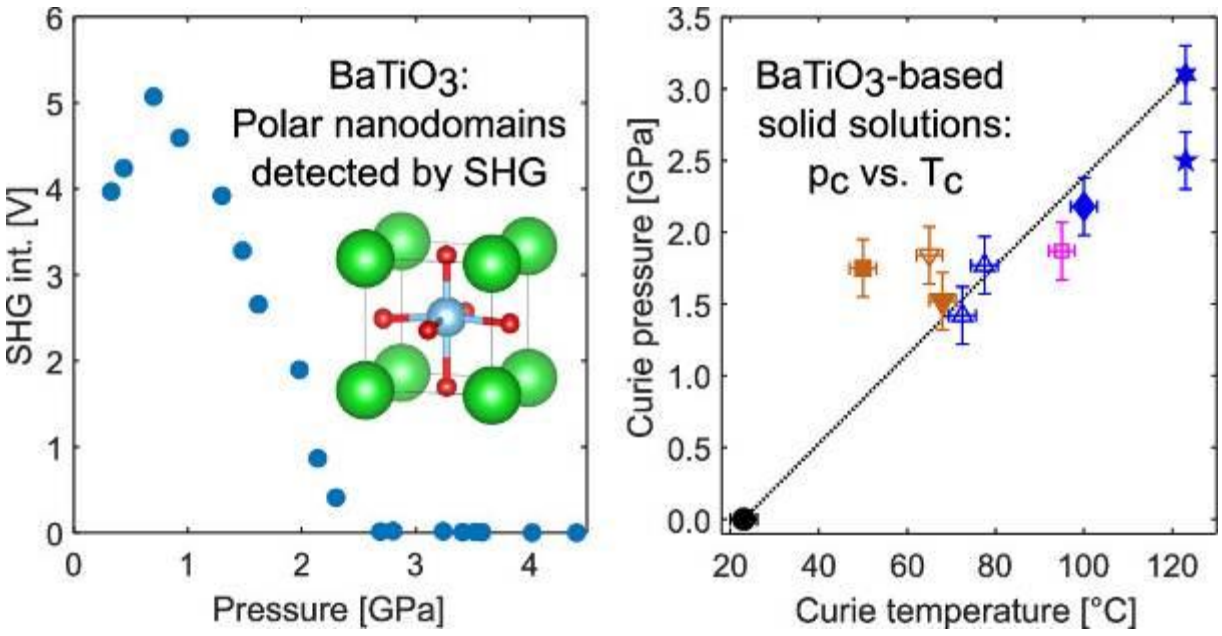

MS 5: In Situ/Operando Characterization

OP-18

Exploring the World of Carbonates: Mechanochemical Synthesis and In Situ X-ray Powder Diffraction (XRPD) Studies

H. Das (Mülheim an der Ruhr/DE), C. Weidenthaler (Mülheim an der Ruhr/DE), V. Kahlenberg (Innsbruck/AT)

Carbonates and carbonatite melts are integral to the geodynamics of the upper mantle and transition zone, influencing processes such as subduction, magma generation, diamond formation and mantle metasomatism. Alkali and alkaline-earth metal carbonates exhibit diverse crystallographic structures and variable stability conditions, often necessitating specific environmental factors for their formation. Understanding the synthesis and reaction pathways of these carbonates are essential for advancing knowledge of their stability, transformations, geological relevance and potential applications. Developing alternative synthesis strategies is essential to enable controlled carbonate formation under more feasible laboratory conditions.[1]

Mechanochemical synthesis presents a promising alternative, facilitating carbonate formation without the need for extreme pressures or temperatures. This technique utilizes high-energy ball milling to induce structural and physiochemical modifications, promoting chemical reactions through shear forces, or impact.[2] This study systematically investigates the mechanochemical synthesis of various carbonate systems, including $K_2Ca(CO_3)_2$ polymorphs[3], dolomite, and sodium-rich natrocarbonatites such as nyerereite and pirssonite. Employing a Retsch MM400 shaker mill in combination with ex-situ laboratory analysis and in situ XRPD during milling, we explore reaction pathway, phase transitions, and crystallographic transformations to understand their phase stability and polymorphic behavior.[4,5]

References

[1] Manning; C. E., et al. Carbon in Earth"s Interior. (2020).

[2] James; S. L., et. al. *Chem. Soc. Rev.* **41**, 413 (2012).

[3] Kahlenberg, V., et al. *RSC mechanochem*, **2**, 152, (2025).

[4] Rathmann;, T. et al. *Rev. Sci. Instrum*. **92**, 114102 (2021).

[5] Weidenthaler, C. *Crystals* **12**, 345 (2022).

Fig. 1

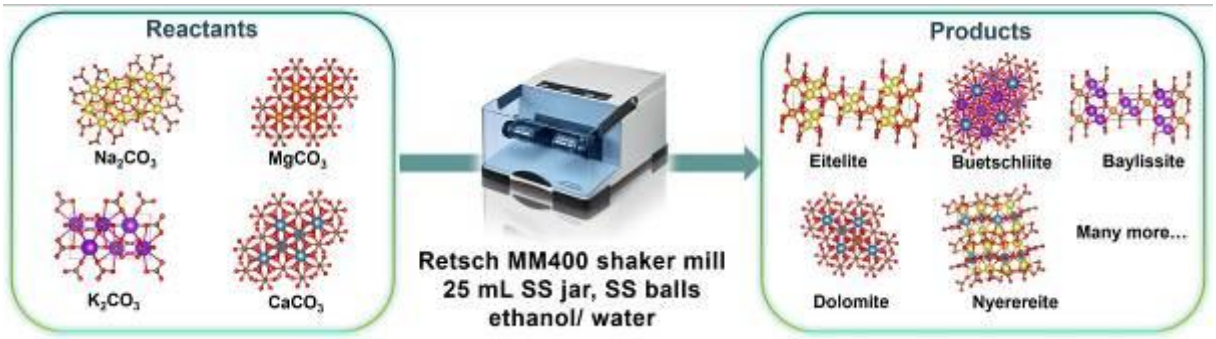

OP-19

In situ H_2/D_2 sorption study of Zinc-based CALF-20 by XRPD

A. Sleptsova (Stuttgart/DE), S. Bette (Stuttgart/DE), P. Sarkar (Stuttgart/DE), M. Hirscher (Stuttgart/DE), F. Adams (Stuttgart/DE), R. E. Dinnebier (Stuttgart/DE)

The last few decades, the efficient separation of hydrogen isotopes has become important, but is also complicated because of their identical physicochemical properties. Recently, metal-organic frameworks (MOFs) have gained attention as materials for gas storage and separation.

Thus, in this work we studied zinc-based MOF called CALF-20 as potential H_2/D_2 separator. We conducted an *in situ* variable temperature X-ray powder diffraction (XRPD) experiment using a home-built gas loading setup. Before starting the experiment, the MOF was activated under a dynamic vacuum at 130°C. Then the capillary with the sample was filled up to 1 bar with H_2, D_2, or N_2. Measurements were performed upon cooling in the temperature range from 130°C to -180°C. The fully weighted Rietveld refinements were performed to determine the lattice parameters of the MOF during gas loading, as well as the approximate amount of gas molecules and their position in the bulk pores.

On the one hand, the weak scattering power of the absorbed hydrogen molecules do not normally have a significant impact on the XRPD pattern. But on the other hand the scale of peak intensity changes upon decreasing temperature (Figure 1) shows a tangible amount of electron density in the pores. Therefore, Rietveld plots of CALF-20 measured in H_2 atmosphere at -160°C with included hydrogen molecules in the pore (a) shows better fit of the diffraction pattern compared to the model without (b) additional molecules included into refinement model.

Figure (c) shows the calculated amount of absorbed gases using the refinement model from (a). CALF-20 starts to absorb N_2 below 0°C and reaches a complete saturation at -140°C with 0.94 mol per Zn atom. At the same time H_2 loading forms a plateau below -170°C with 6.65 mol per Zn, when D_2 sorption never reaches the plateau. Presumably kinetic effects caused by D_2 and H_2 isotopes sorption/desorption are the reason for the different behavior, and thus may be used in their separation.

Fig. 1

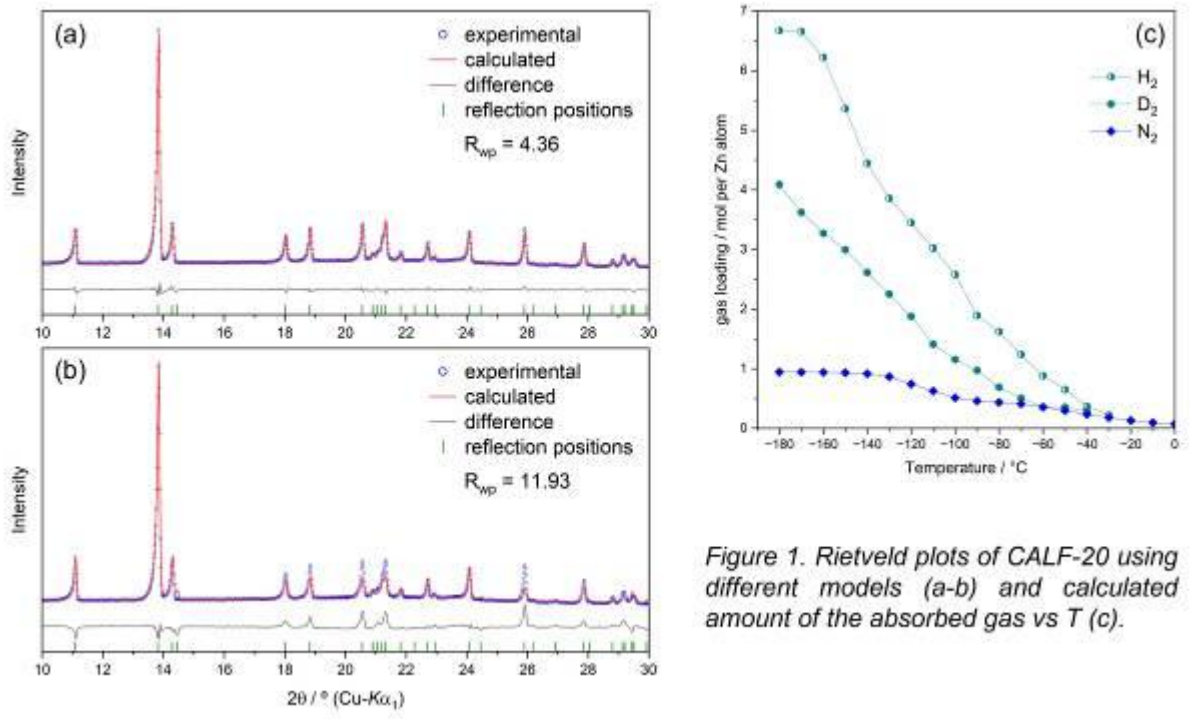

Figure 1. Rietveld plots of CALF-20 using different models (a-b) and calculated amount of the absorbed gas vs T (c).

OP-20

In Situ Investigation of Fluorination Pathways in Ruddlesden-Popper Oxyfluorides

J. Jacobs (Halle (Saale)/DE), J. Geßner (Halle (Saale)/DE), S. G. Ebbinghaus (Halle (Saale)/DE)

Ruddlesden-Popper oxyfluorides (general formula $A_{n+1}B_n(OF)_{3n+1}$) represent a versatile class of materials. Due to their structural relationship to 3D perovskites, they exhibit promising properties such as optical band gaps in the visible range (relevant for photocatalysis), high anion mobility (enabling F-ion batteries), and intriguing magnetic behavior. Their synthesis can be achieved via reactions with F_2 gas, solid-state reactions using AgF, CuF_2, or XeF_2, or by employing fluorinated polymers such as PVDF and PTFE. The redox behaviour of these fluorination routes strongly affects product composition and properties.

The pronounced metastability of these compounds complicates targeted synthesis, often necessitating extensive trial-and-error approaches, while mechanistic insights into reaction pathways and intermediate phases remain scarce. Time- and temperature-resolved *in situ* X-ray diffraction (XRD) has proven highly effective in elucidating reaction mechanisms, allowing direct observation of intermediates and thus enabling improved control over solid-state syntheses.

This work aims to deepen understanding of fluorination reactions, facilitating the tailored synthesis of new oxyfluorides, including less-fluorinated phases with unusual oxidation states. We investigate the fluorination of Ruddlesden-Popper oxides La_2NiO_4, La_2CoO_4, and $La_4Ni_3O_{10}$ using *in situ* XRD with simultaneous mass spectrometry and *in situ* neutron powder diffraction. Data analysis is performed via Rietveld refinement, complemented by ^{19}F NMR and DFT data. We observe various lower-fluorinated intermediates in all three systems. For the fluorination of La_2CoO_4 to $La_2CoO_3F_3$, we compare the effects of AgF, PVDF, and PTFE, finding pronounced differences between the oxidizing (AgF) and reducing (PVDF/PTFE) pathways.

References

[1] J.Jacobs et al., ***J. Am. Chem. Soc.*** 2025, **147**, 11, 9739–9751,

[2] J. Geßner, S. G. Ebbinghaus, and J. Jacobs, ***Dalton Trans.***, 2025,**54**, 12678-12688

Fig. 1

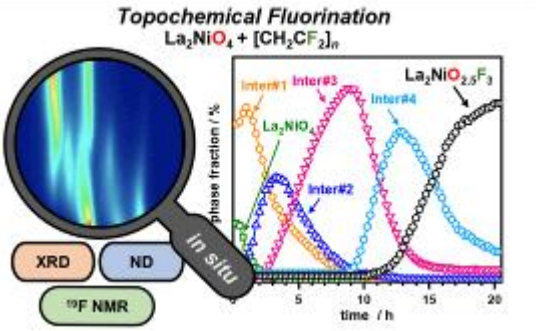

OP-21

Temperature-dependent phase transition in high-efficiency hybrid halide perovskites

A. Palacios Saura (Berlin/DE), D. M. Többens (Berlin/DE), S. Schorr (Berlin/DE)

Hybrid halide perovskites (HHPs) have shown to be promising emerging photovoltaic materials due to their high power conversion efficiency (27.0%)[1] as well as low-cost solution-based processing methods and bandgap tunability.[2,3]

The highest efficiencies of HHP-based devices are reached with mixed anion and mixed cation compositions. Devices with a triple-cation-double-anion (3C2A) HP absorber ($Cs_{0.05}(FA_xMA_{1-x})_{0.95}Pb(Br_yI_{1-y})_3$) can reach up to 24.6% in single junction and 32.6% in tandem devices[4,5]. Thus, it is crucial to understand the crystal structure of high-efficiency compositions and how it is affected by the composition.

Our study aims for a thorough understanding of structure-property relations in the chemical space important for high-efficiency HHP solar cells. Having in mind space applications discussed for HHP-based devices, the structural behaviour in dependence on temperature down to 20 K is of special interest. We used in-situ powder X-ray diffraction performed at the KMC-2 beamline[6] at BESSY II, in a temperature range from 300 K to 30 K with 20 K steps to study HHP structural phase transitions and development of phase content. We investigated not only the reported high-efficiency compositions, but also an extension of the compositional space around the champion devices to obtain the data needed for a comprehensive phase diagram elaboration. Additionally, we determined the band gap energy (at room temperature) of the studied HHPs using diffuse reflectance measured by UV-VIS spectroscopy.

We provide important insights on how the crystal structure of 3C2A HPs changes within the temperature range in which solar cells function (e.g. in space applications).

References

[1] https://www.nrel.gov/pv/cell-efficiency.html

[2] Saidaminov et al., Nat.Commun. 6, 7586 (2015)

[3] Kulkarni et al., J.Mater.Chem. A. 2, 9221 (2014)

[4] Li et al., Science. 379, 399 (2023)

[5] Mariotti et al., Science. 381, 63 (2023)

[6] Helmholtz-Zentrum Berlin für Materialien und Energie, J. large-scale Res. Facil. 2,A49 (2016)

OP-22

In situ XRPD investigations on the reduction of iron oxide and sodium chromate by hydrogen

M. Häger (Leipzig/DE), H. Kohlmann (Leipzig/DE)

Hydrogen direct reduction (HDR) is an industrially pursued green alternative to produce iron. The decrease in CO_2 emissions and the infrastructure that is created now, may be an incentive to produce other transition metals using HDR as well. For instance, the carbon-based reduction of sodium chromate (Na_2CrO_4) to chromia (Cr_2O_3) is also achievable using hydrogen.[1]

In situ X-ray powder diffraction has already been applied to the reduction of hematite (Fe_2O_3) on multiple occasions, focusing on qualitative and quantitative phase analysis.[2,3] Here we will additionally report on refined microstructural and crystal structure parameters like crystallite size, microstrain, lattice parameters, atomic positions and their evolution during the reduction process in a time or temperature resolved manner.

The before unknown crystal structure of a high temperature sodium chromate phase and the participation of this phase transition in the reduction pathway will be discussed. Like the observation of an unstable wüstite phase ($Fe_{1-x}O$) during the reduction, γ-iron was observed and could be the immediate reduction product, before transitioning to α-iron.

Fig. 1: *In situ* XRPD data during the reduction of Na2CrO4 to NaCrO2 under hydrogen flow, showing additional reflections at the reduction temperature.

Fig. 2: *In situ* XRPD data with Bragg markers of hematite (brown), magnetite (pink), and iron (green) under hydrogen flow.

References

[1] Häger M, Keilholz S, Kohlmann H. The Reduction of Group 6–8 Transition Metal Oxides with Hydrogen—From Ore Smelting to Reaction Pathways#. Eur J Inorg Chem 2025;28(30), 202500089.

[2] Jozwiak WK, Kaczmarek E, Maniecki TP, Ignaczak W, Maniukiewicz W. Reduction behavior of iron oxides in hydrogen and carbon monoxide atmospheres. Appl Catal A 2007;326(1):17–27.

[3] Nielsen MR, Moss AB, Bjørnlund AS, Liu X, Knop-Gericke A, Klyushin AY, et al. Reduction and carburization of iron oxides for Fischer-Tropsch synthesis. J Energy Chem 2020;51:48–61.

Fig. 1

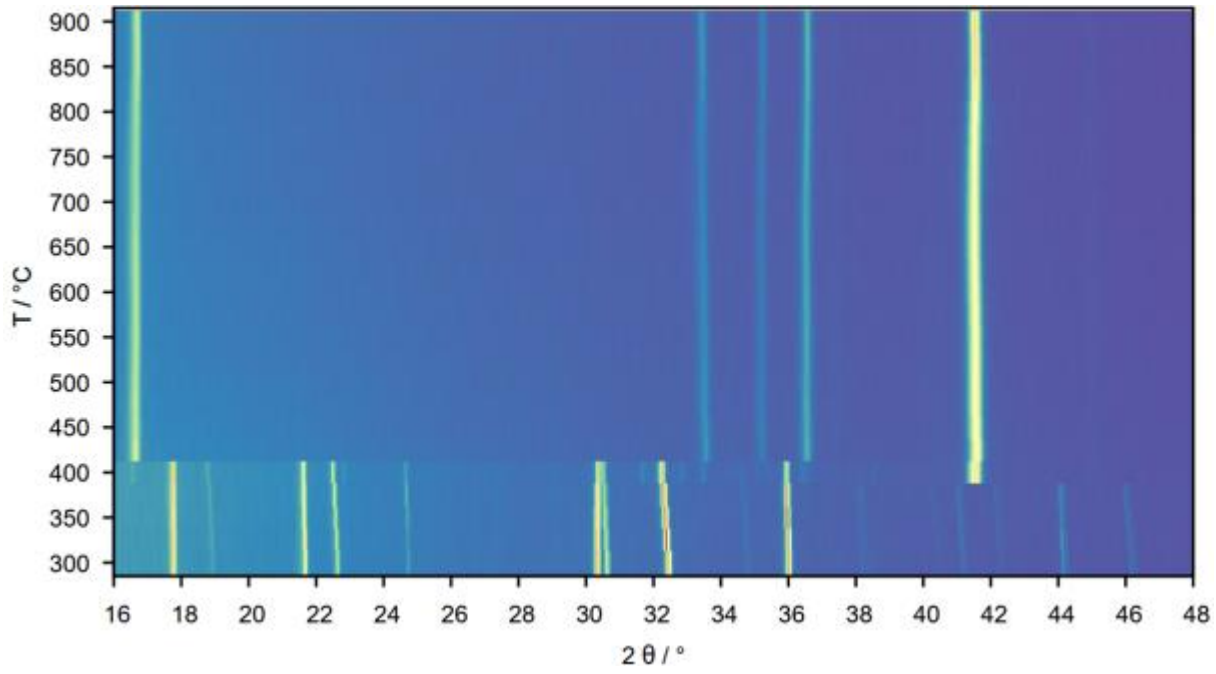
T / °C
900
850
800
750
700
650
600
550
500
450
400
350
300
16
18
20
22
24
26
28
30
32
34
36
38
40
42
44
46
48
2 θ / °

Fig. 2

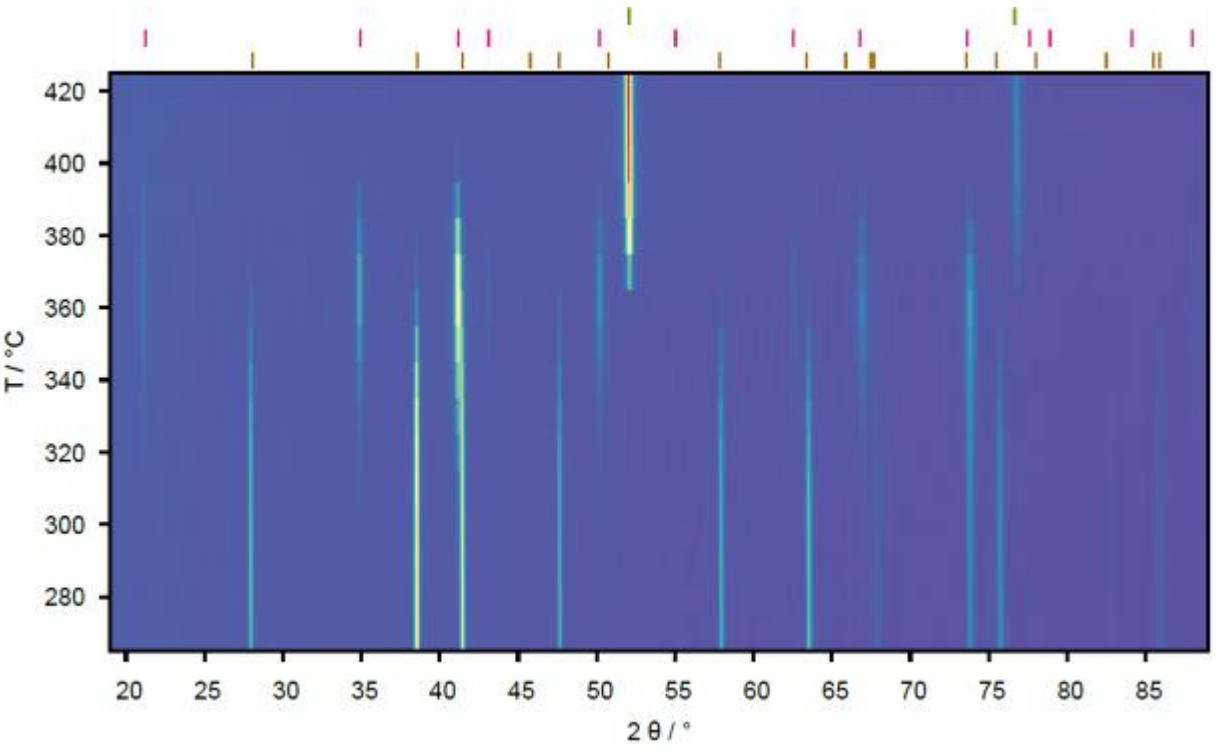
T / °C
420
400
380
360
340
320
300
280
20
25
30
35
40
45
50
55
60
65
70
75
80
85
2 θ / °

OP-23

Multimetallic nanoparticle exsolution from high-entropy spinels

G. B. Strapasson (Campinas/BR, Copenhagen/DK), K. M. Jensen (Copenhagen/DK), D. Zanchet (Campinas/BR), A. Kirsch (Bochum/DE, Copenhagen/DK)

High-entropy oxides (HEOs) are chemically complex solid solutions in which multiple elements occupy a single crystallographic site. These new materials challenge traditional design paradigms and possess exceptional chemical flexibility.[1] HEOs can show catalytic performances that far exceed those of their individual parent oxides due to synergistic effects of multiple cations, as demonstrated for the electrocatalytic oxygen evolution reaction.[2] In most catalytic systems, metallic nanoparticles (NPs) serve as the active phase, often supported on oxides. Conventionally, these NPs are impregnated onto the surface, but an emerging alternative involves exsolving them directly from an oxide solid solution under reductive conditions. This strategy offers the advantage that the resulting NPs remain strongly anchored to the host oxide, thereby suppressing sintering and preserving catalytic activity over time.[3]

In this work, we studied the exsolution of NPs from high-entropy oxide spinels by in situ X-ray diffraction and total scattering, Scanning Transmission Electron Microscopy and Energy-Dispersive X-ray Spectroscopy, and Near-Ambient Pressure X-ray Photoelectron Spectroscopy. We give mechanistic insight into the evolution of multimetallic NPs from the host oxides during heating in diluted H_2. Our results show the formation of Cu-rich NPs at 400 °C, followed by the emergence of Cu@NiCo core-shell NPs at 500 °C, and their subsequent alloying into trimetallic CuNiCo at 700 °C. Upon reoxidation in air, the metallic NPs dissolve back into the host oxide matrix, demonstrating extraordinary reversibility of the exsolution process. Furthermore, compositional changes of the HEOs tune the exsolution process. This study introduces a new material platform with significant potential for the development of new innovative catalysts.

References

[1] Aamlid et al. *J. Am. Chem. Soc.* **2023**, 145, 5991

[2] Kante et al. *ACS Nano* **2023**, 17, 5329 [3] Kousi et al. *Small* **2021**, 17, 2006479

MS 6: Crystal Chemistry

OP-24

Structures and properties of new multinary bismuth subiodides with intermetallic nanoribbons and chains

N. G. Elsner (Dresden/DE)

The emerging class of topological insulators (TIs) has attracted significant attention due to their topologically protected, chiral edge states, which enable fault-tolerant information transport – crucial for applications such as quantum computing and topological spintronics. In a pioneer work, Kane and Mele proposed that a single layer of graphene could host a two-dimensional (2D) TI state, though its experimental realization remained elusive due to the material"s weak spin–orbit coupling and resulting minimal band gap.[1] A major advancement came with the discovery of $Bi_{14}Rh_3I_9$, a heavy-element-based graphene analogue, which was shown to be a three-dimensional (3D) weak TI.[2] In this compound, the intermetallic decorated honeycomb layers, which are 2D TIs themselves, are stabilized by mainly ionic spacer layers. This system offers a promising platform to explore structure–property relationships in TIs. Subsequent studies showed that substitution of the spacer layer can preserve the TI state, as seen in compounds like $Bi_{12}Rh_3Cu_2I_5$.[3] Recently, the oxidation of this structure revealed a new heavy-element-based family of graphene nanoribbon analogues, for instance the compound $Bi_{26}Rh_5Cu_8I_{17}$ (see Fig. 1).[4] The talk will focus on the structure, as well as the electronic and physical properties of $Bi_{26}Rh_5Cu_8I_{17}$. Additionally, a related compound family, which is obtained through further oxidation of the previous phase, will be discussed.

References

[1] C. L. Kane, E. J. Mele, *Phys. Rev. Lett.* **2005**, 95, 226801.

[2] B. Rasche, A. Isaeva, M. Ruck, S. Borisenko, V. Zabolotnyy, B. Büchner, K. Koepernik, C. Ortix, M. Richter, J. Van Den Brink, *Nat. Mater.* **2013**, 12, 422–425.

[3] E. Carrillo–Aravena, K. Finzel, R. Ray, M. Richter, T. Heider, I. Cojocariu, D. Baranowski, V. Feyer, L. Plucinski, M. Gruschwitz, C. Tegenkamp, M. Ruck, *Phys. Status Solidi B* **2022**, 259, 2100447.

[4] N. Elsner, Master"s Thesis, TUD Dresden University of Technology, Germany, **2025**.

Fig. 1

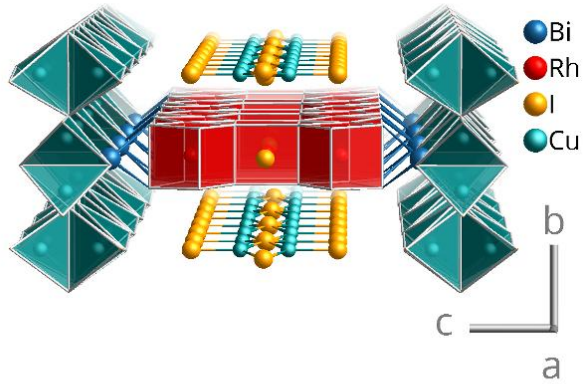

OP-25

Extending the coordination number rule – A comparison of the results for ternary fluorides, chlorides, bromides, iodides and oxides

N. Langer (Leipzig/DE), H. Kohlmann (Leipzig/DE)

The rationalization power of Beck's extended coordination number rule has already been shown on a dataset consisting of 1044 ternary fluorides as obtained from the ICSD.[1,2] Beck's coordination number rule tries to rationalize the coordination in ionic compounds.[3] The most likely coordination with regards to Beck's rule is called the simplest numerical solution (SNS). The SNS always contains the most homogenous distribution of cation-anion-contacts of all possible structures. Deviations of the experimentally determined structure from the SNS can often be explained by a better local electroneutrality in the former. Beck's rule is generally only expected to be applicable to very ionic compounds. To test this hypothesis, the investigations were extended to chlorides, bromides, iodides and oxides. The results are summarized in Fig. 1.

Fig. 1: Summary of the rationalization results obtained by automatic application of Beck's extended coordination number rule to the datasets of ternary fluorides, chlorides, bromides, iodides and oxides. The size of the respective datasets are given in parentheses. For compounds with a disagreement between the experimentally determined structure and the SNS, the explainability by the local electroneutrality is given.

The agreement within the halogenides is always higher than 60 % and does not seem to decrease with decreasing electronegativity whereas the explainability by the local electroneutrality shows a strong decrease. This behavior is expected since the compounds behave less ionic. Oxides show a relatively low agreement and a low explainability despite being very ionic. The main reason for this behavior seems to be a higher variability of cationic coordination numbers in oxides than in halogenides.

References

[1] N. Langer, H. Kohlmann, *manuscript in preparation*.

[2] D. Zagorac, H. Müller, S. Rühl, J. Zagorac, S. Rehme, *J. Appl. Cryst.* **2019**, *52*, 918.

[3] H. P. Beck, *Z. Anorg. Allg. Chem.* **2022**, *648*, e202200130.

Fig. 1

	Group	Fluorides (1044)	Chlorides (604)	Bromides (303)	Iodides (323)	Oxides (6032)
Agreement of the coordination matrices	Yes	60.1 %	67.1 %	63.0 %	65.6 %	47.4 %
	No	39.9 %	32.9 %	37.0 %	34.4 %	52.6 %
Explainable by better/equal local electroneutrality	Yes	22.0 %	14.1 %	14.9 %	9.9 %	25.1 %
	No	17.9 %	18.8 %	22.1 %	24.5 %	27.5 %

OP-26

Flexible carbodiimide and dicyanometallate frameworks – Coupling negative thermal expansion and negative linear compressibility in wine-rack-like structures

A. Corkett (Jülich/DE), K. Friese (Jülich/DE, Aachen/DE), A. Grzechnik (Jülich/DE, Aachen/DE)

The vast majority of materials are compressed in all directions by the action of hydrostatic pressure. Only a few rare examples exhibit negative linear or area compressibility (NLC/NAC), which make them highly sought after for various sensor applications. Materials featuring wine-rack-like structures have emerged as promising models for such behavior. $Ag_3[Co(CN)_6]$ (*P*-31*m*), for example, expresses such a motif in which rigid cyanide linker-ligands are coordinated to Ag hinges. This results in a framework that exhibits pronounced NLC along *c* (K_c = 76(9) TPa^{-1}) that is correlated to a colossal negative thermal expansion (NTE) response along the same direction (α_c −120 × 10^{-6} K^{-1}).[1,2]

In this work, we focus on two alternate wine-rack-like systems and explore the expansivity and compressibility of these phases. First, we examine $LaAu_3(CN)_6.3H_2O$ ($P6_3/mcm$), which like $Ag_3[Co(CN)_6]$ features extended dicyanometallate linkers (NC−Au−CN), that in this case bridge between LaN_6 trigonal prisms with face capping H_2O.[3] We then go on to explore the influence of hydration and metallophilicity (Au/Ag) on the thermomechanical response of this system. Finally, we consider hafnium carbodiimide, $Hf(NCN)_2$,[4] which, despite being derived from a close-packed [NiAs]-type crystal structure (*Pbcn*),[5] demonstrates pronounced NTE and NLC responses due to the vacancy ordering scheme over the octahedral sites.

Fig. 1: (a) Wine-rack-like LaAu3(CN)6 ($P63/mcm$) and (b) Hf(NCN)2 ($Pbcn$)

References

[1] Goodwin, A.; Calleja, M.; Conterio M. J.; Dove, M. T.; Evans, J. S. O.; Keen, D. A.; Peters, L.; Tucker, M. G. *Science* **2008**, 319, 794

[2] Goodwin, A.; Keen, D.; Tucker, M. G. *PNAS* **2023**, 105, 18708-18713

[3] Colis, J. C. F.; Larochelle, C.; Staples, R.; Herst-Irmer, R.; Patterson, H. *Dalton Trans.* **2005**, 675-679

[4] Dolabdjian, K.; Kobald, A.; Romao, C. P.; Meyer H.-J. *Dalton Trans*. **2018**, 47, 10249-10255

[5] Pöttgen, R.; Corkett, A. J.; Dronskowski, R. *Z. Kristallogr*. **2023**, 238, 95−103.

Fig. 1

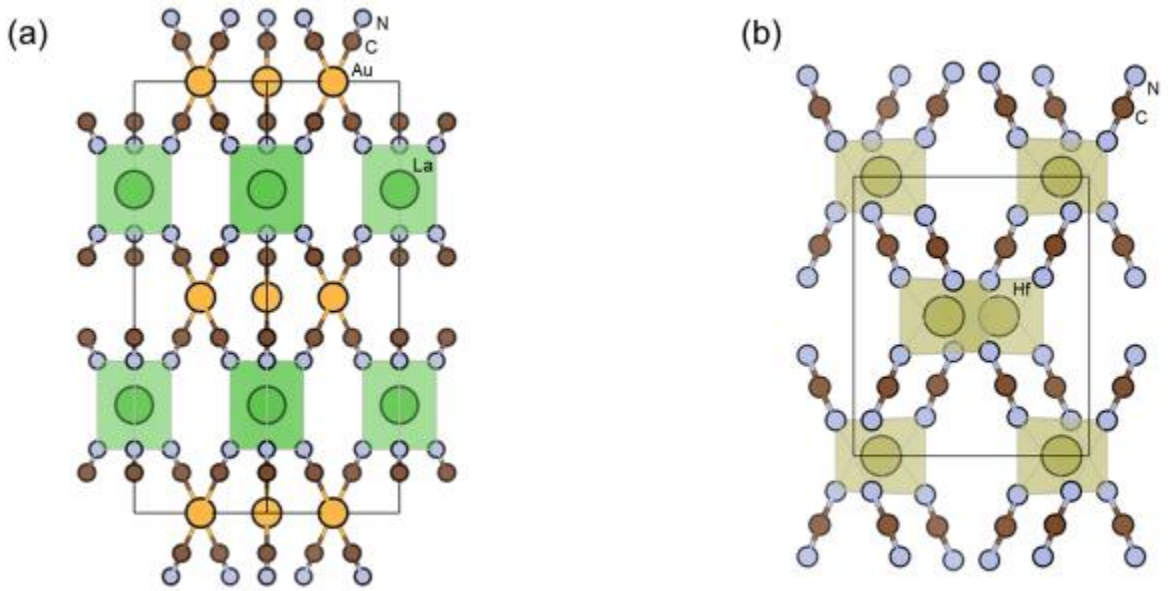

OP-27

Superstructures of Se-substituted bornite-type Cu5-xFeS4-ySey

P. Sicher (Leipzig/DE), O. Oeckler (Leipzig/DE), C. Fraunhofer (Leipzig/DE)

Bornite has attracted interest due to its potential as an environmentally friendly Cu-based thermoelectric material. Substitutions with Se aim at increasing the low electrical conductivity of the pure sulfide. From an anti-fluorite type structure (*Fm*-3*m*, *a* ≈ 5.5 Å) at high temperatures, Cu5FeS4 transforms to an intermediate structure at 235 °C, which has been described in space group *Fd*-3*m* (*a* ≈ 11 Å) [1] and as an eight-fold twin in *R*3*m*.[2]

However, new single-crystal measurements indicate that the intermediate structure of Cu5FeS4 can be convincingly described as a fourfold twin of a structure in *R*-3*m* with *a* ≈ 3.9 Å and *c* ≈ 19 Å. This twofold superstructure can be derived from the basic structure in *Fm*-3*m* with *a* ≈ 5.5 Å by the commensurate modulation vector **q1** = (0.5, 0.5, 0.5). By formally applying the modulation vectors **q2** = (0.5, -0.5, -0.5), **q3** = (-0.5, 0.5, -0.5) and **q4** = (-0.5, -0.5, 0.5) for different twin domains, pseudo-cubic symmetry is retained. Cu5FeS2.4Se1.6 shows this diffraction pattern down to room temperature. However, for Cu4.5FeS2.4Se1.6, the modulation vector becomes incommensurate with **qi** = (0.425(2), 0.425(2), 0.425(2)). For refining in the hexagonal setting, this vector transforms to **qih** = (0, 0, 1.275(3)). The resulting superspace group is *R*-3*m*(00*γ*)00 with *a* ≈ 3.9 Å and *c* ≈ 9.5 Å. Similar twinning occurs for Cu5FeS3Se; however, with a 16-fold increase of cell volume and space group *R*-3*m* (*a* ≈ 7.8 Å, *c* ≈ 38 Å). Complete ordering of the metal atoms reveals that positions with low anharmonicity of ADPs correspond to Fe sites.

Thermoelectric properties of all mentioned compounds were measured with a maximum figure of merit of ZT = 0.35 at 400 °C for Cu5FeS4. The expected increase of electrical conductivity as a consequence of Se substitution, however, cannot compensate the accompanied decrease of the Seebeck coefficient.

References

[1] Y. Kanazawa, K. Koto, N. Morimoto, *Can. Min.* **1978**, 16, 397-404.

[2] N. Morimoto, *Acta Cristallogr*. **1964**, 17, 351-360.

OP-28

High-pressure synthesis and structural studies of nitride perovskites ABN_3 (A = Pr, Nd, B = W, Re)

F. I. Akbar (Frankfurt a. M./DE), S. D. Kloß (Munich/DE), M. Bykov (Frankfurt a. M./DE)

The perovskite structure is one of the most common and most extensively studied in materials science. Replacement of oxygen (O^{2-}) by nitrogen (N^{3-}) in oxide perovskite may lead to higher polarizability and superior piezo/ferroelectric properties for use in the next-generation devices. However, in contrast to oxides, chalcogenides, and halides, pure ABN_3 nitride perovskites were almost unknown until recently, when nitride perovskites $LaWN_3$ and $LaReN_3$ were synthesized in a form of a thin film and in a bulk form in a multianvil press, respectively [1,2]. The synthesis of nitrides with metals in high oxidation states is, however, challenging owed to the low energy of nitride formation, which is a fundamental problem of nitride chemistry. Application of high pressure is a useful synthetic tool to stabilize nitrogen-rich phases. In this work, Ruddlesen-Popper nitrides Pr_2ReN_4, Nd_2ReN_4, and Pr_2WN_4, previously synthesized in a multianvil press at mild high-pressure conditions (about 8 GPa), were used as starting materials in the study of their nitridation behavior at pressures, which exceed those commonly achievable in a multianvil apparatus.

The multigrain single-crystal X-ray diffraction analysis revealed the formation of the nitride perovskite phases $PrWN_3$, $PrReN_3$, and $NdReN_3$ after laser heating at 30–40 GPa in nitrogen or argon, used as pressure-transmitting media. All compounds were found to remain stable down to ambient pressure.

The identification of these nitride perovskites as chemical reaction products formed under extreme conditions, together with their recoverability down to ambient pressure, significantly broadens the high-pressure chemistry of this class of compounds.

OP-29

Crystal structures of alkali oxidohydroxidoantimonates (Na, K, Rb, Cs) and of NaSbO2 comprising anionic chains and sheets

T. Wolflehner (Vienna/AT), M. Weil (Vienna/AT)

Condensed anions remain rare in the alkali oxidohydroxidoantimonate systems. In the context of the recently reported crystal structure of Rb[SbO(OH)4] [1] featuring the novel polymeric anion ∞1[SbO2/2(OH)4/1], we systematically investigated alkali oxidohydroxidoantimonates for Na, K, Rb and Cs. For this purpose, we particularly exploited the capacity of the hydroflux method to prepare low-hydrated phases, which promotes the formation of condensed anions.

We obtained the new phases Na2[SbO3(OH)], K3[Sb3O8(OH)2]·2H2O, K3[SbIIISbV2O7(OH)2], Rb3[SbIIISbV2O7(OH)2], Cs[SbO(OH)4] and verified the crystal structure of the oxidoantimonate(III) Na[SbO2]. Their crystal structures were determined by SCXRD and refined in monoclinic space groups. Na[SbO2] adopts the Na[BiO2] structure type [2], while Cs[SbO(OH)4] is isotypic with Rb[SbO(OH)4]. The other structures are unique with K3[SbIIISbV2O7(OH)2] and Rb3[SbIIISbV2O7(OH)2] being isotypic. Na2[SbO3(OH)], *M*3[SbIIISbV2O7(OH)2] and Cs[SbO(OH)4] feature chains made of ∞1[SbO6−x(OH)x] octahedra corner- and/or edge-sharing via O atoms. Na[SbO2] and K3[Sb3O8(OH)2]·2H2O contain ∞1[SbO4/2] chains and ∞2[Sb3O8/2O4/1(OH)2/1] sheets, respectively.

The presented crystal structure models of *M*3[SbIIISbV2O7(OH)2] phases show interesting positional disorder of SbIII. The experimental verification of the crystal structure of Na[SbO2] closes a peculiar gap in knowledge, since its alkali analogues Li[SbO2] [3], K[SbO2], Rb[SbO2] [4] and the bismuthite Na[BiO2] [2] have long been known. The Materials Project predicted a structure model of Na[SbO2] recently in 2020 using DFT calculations [5] which matches our experimental results.

References

[1] Wolflehner T. and Weil M. (2024), ZAAC vol. 651, e202400203.

[2] Schwedes B., Hoppe R. (1972), ZAAC vol. 391, p. 313-322.

[3] De Laune B.P., Bayliss R.D., Greaves C. (2011), Inorg. Chem. vol. 50, p. 7880-7885.

[4] Hirschle C., Röhr C. (2000), ZAAC vol. 626, p. 1305-1312.

[5] LBNL Materials Project (2020). Materials Data on NaSbO2 by Materials Project. doi: 10.17188/1289399.

MS 7: Structure-based Drug Discovery

OP-30

X-ray fragment screening towards the development of novel cathepsin inhibitors

S. Falke (Hamburg/DE), S. Günther (Hamburg/DE), J. Lieske (Hamburg/DE), P. Reinke (Hamburg/DE), T. Schulze (Hamburg/DE), C. Ehrt (Hamburg/DE), N. Schulz (Hamburg/DE), M. Rarey (Hamburg/DE), K. Karničar (Ljubljana/SI), D. Turk (Ljubljana/SI), A. Meents (Hamburg/DE)

Emerging pathogens continue to be a major health threat around the world and underline the need for drug development. The lysosomal cysteine protease *cathepsin L* (CatL) is involved in the cell entry of coronaviruses and has been described as an attractive drug target due to its involvement in several severe diseases and disorders.

We previously performed X-ray crystallographic compound screening targeting the SARS-CoV-2 main protease and human CatL using a repurposing approach to tackle COVID-19 [1, 2]. It was demonstrated that a few potent main protease inhibitors can be utilized for a dual-targeting strategy by additionally inhibiting CatL and related cathepsins [2, 3]. Moreover, we established high-throughput fragment screening at the HiPhaX instrument at PETRA III, DESY [4].

To intensify the structure-based development of novel CatL inhibitors we recently screened more than 1000 fragments by soaking individual CatL crystals. A hit rate higher than 10% was obtained and most of the binding fragments are located in the specificity-determining subsites of the active site. For efficient data handling and processing, a software pipeline including a database and a novel fragment hit finding tool were utilized. Selected fragment hits were subjected to a fragment growing pipeline aiming at an increase of affinity and specificity in further screening experiments. The infrastructure at PETRA III and the experiments we performed substantially contribute to the discovery of novel lead compounds and its structure-based optimization.

References

[1] Günther et al., *Science* (2021), DOI: 10.1126/science.abf7945

[2] Falke et al., *J Med Chem* (2024), DOI: 10.1021/acs.jmedchem.3c02351

[3] Reinke et al., *Comm Biology* (2023), DOI: 10.1038/s42003-023-05317-9

[4] Günther et al., *Nat Comm* (2025), DOI: 10.1038/s41467-025-64918-6

OP-31

Targeting the methylerythritol phosphate pathway (MEP), via the 1-deoxy-D-xylulose 5-phosphate reductoisomerase (DXR), using a fragment-based drug design approach

S. D. Chatziefthymiou (Hamburg/DE), F. Gerteis (Hamburg/DE, Bremen/DE), T. Szal (Hamburg/DE, Bremen/DE), J. Hakanpää (Hamburg/DE), B. Windshügel (Hamburg/DE, Bremen/DE)

In 2025, Fraunhofer ITMP and DESY joined forces and formed a strategic collaboration to promote research and innovation in drug discovery. To showcase the synergies by combining the competences of both institutions, we established a proof-of-concept (PoC) project focusing on fragment-based lead discovery. Our goal is to create an interdisciplinary platform for the rapid identification of novel therapeutics that can be accessed both by academic and industrial users.

Within this PoC study, we set up a pipeline workflow ranging from production and quality control of protein, assay development and fragment screening in solution, structural determination of the enzyme-inhibitor complexes, investigation of enzyme inhibition and microbiological assays.

In this presentation we will provide an overview of our collaboration and show the results obtained so far on a project targeting an enzyme of the methylerythritol phosphate pathway (MEP) pathway that is required for the production of isoprenoid precursors. The MEP pathway comprises several promising targets for novel antimalarial, antibacterial and herbicidal drugs since it is prevalent in most gram-negative bacteria and apicomplexan parasites but absent in humans. 1-deoxy-D-xylulose 5-phosphate reductoisomerase (DXR) is a key enzyme in the MEP pathway, catalyzing the conversion of 1-deoxy-D-xylulose-5-phosphate (DXP) into 2-C-methyl-D-erythritol 4-phosphate (MEP). We employed a biophysical method to screen a library of 1056 fragments for DXR binding. 23 compounds emerged as hits of which two fragments revealed a KD value of 145 µM and 805 µM, respectively. One of these also demonstrated DXR inhibition in a biochemical assay, the binding mode of which was revealed using X-ray crystallography.

OP-32

Room-temperature X-ray fragment screening with serial crystallography

S. Günther (Hamburg/DE), P. Fischer (Hamburg/DE), M. Galchenkova (Hamburg/DE), S. Falke (Hamburg/DE), P. Reinke (Hamburg/DE), S. Thekku Veedu (Hamburg/DE), A. C. Rodrigues (Hamburg/DE), J. Senst (Hamburg/DE), D. Elinjikkal (Hamburg/DE), L. Gumprecht (Hamburg/DE), J. Meyer (Hamburg/DE), H. Chapman (Hamburg/DE), M. Barthelmess (Hamburg/DE), A. Meents (Hamburg/DE)

Structural insights into protein-ligand interactions are essential for advancing drug development, with macromolecular X-ray crystallography being a cornerstone technique. Commonly X-ray data collection is conducted at cryogenic temperatures to mitigate radiation damage effects. However, this can introduce artifacts not only in the protein conformation but also in protein-ligand interactions. Recent studies highlight the advantages of room-temperature (RT) crystallography in capturing relevant states much closer to physiological temperatures. We have advanced fixed-target serial crystallography to enable high-throughput fragment screening at RT. Here we systematically compare RT fragment screening with conventional single crystal data collection at cryogenic temperature (cryo) of the Fosfomycin-resistance protein A from Klebsiella pneumoniae (FosAKP), an enzyme involved in antibiotic resistance. With RT serial crystallography we achieve resolutions comparable to cryogenic methods and identify a previously unobserved conformational state of the active site, offering additional starting points for drug design. For ligands identified in both screens, temperature did not have an influence on the binding mode of the ligand. But overall, we observed more binders at cryo, both at physiologically relevant and non-relevant sites. With the potential for further automation, RT screening with serial crystallography can advance drug development pipelines by making new conformations of proteins accessible.

OP-33

Accelerating Drug Discovery with Home-Lab SC-XRD

V. Smith (Karlsruhe/DE), A. Luebben (Karlsruhe/DE), T. Dunaj (Karlsruhe/DE), M. Adam (Karlsruhe/DE)

Single-crystal X-ray diffraction (SC-XRD) has long been a cornerstone of molecular structure determination in pharmaceutical research. Traditionally reliant on synchrotron facilities, the advent of high-performance home-lab SC-XRD instruments has transformed accessibility, enabling real-time structural analysis directly within research environments. This presentation explores the integration of home-lab SC-XRD systems into early-stage drug discovery workflows, highlighting their role in fragment-based screening, hit-to-lead optimisation, and solid-form characterisation.

We present case studies demonstrating how in-house SC-XRD platforms achieve resolution comparable to synchrotron facilities, enabling rapid protein-ligand structure determination[1,2,3,] efficient polymorph screening[4], and co-crystal development[5] without external scheduling delays.

Our findings underscore the strategic value of decentralised crystallographic capabilities, especially in agile research settings. By bridging the gap between structural biology and medicinal chemistry, home-lab SC-XRD empowers researchers to iterate faster, validate hypotheses sooner, and ultimately accelerate decision-making timelines in medicinal chemistry programmes.

References

[1] J. Med. Chem 2024;67,11937-11956

[2] J. Med. Chem. 2020, 63, 14805−14820

[3] Nat. Commun 2020, 11, 3717 -3722

[4] Cryst. Growth Des. 2025, 25, 4783−4794

[5] Cryst. Growth Des. 2025, 25, 3169−3185

OP-34

Crystallographic analysis of EnT-derived 3D boron heterocycles reveals covalent Ser70 binding in CTX-M-14 β-lactamase, mimicking the hydrolysis transition state and highlighting their potential as next-generation boronate inhibitors

M. Perbandt (Hamburg/DE), H. M. Kortman (Potsdam/DE), H. Fang (Potsdam/DE), K. A. C. Bastick (Potsdam/DE), C. Völkel (Potsdam/DE), D. Oberthür (Hamburg/DE), T. Beck (Hamburg/DE), P. H. Seeberger (Potsdam/DE), J. J. Molloy (Potsdam/DE)

Question:

Boron-containing frameworks offer unique opportunities for selective enzyme inhibition through covalent and hydrogen-bonding interactions. We investigated whether newly designed three-dimensional boron heterocycles can act as stable and stereochemically defined β-lactamase inhibitors, and how their binding mode can be elucidated crystallographically.

Methods:

A visible-light-driven energy transfer (EnT) catalysis approach was applied to construct fused 3D boron heterocycles via inter- and intramolecular [2+2] cycloadditions. The compounds were analysed by NMR spectroscopy, pKa profiling, and co-crystallised with the serine β-lactamase CTX-M-14. Diffraction data were collected at beamline P11 (PETRA III/DESY), and several the enzyme–inhibitor complexes were refined to high resolution.

Results:

The crystal structures revealed covalent tetrahedrals adduct between the boronate moiety and the catalytic Ser70, closely mimicking the transition state of β-lactam hydrolysis, revealing enantiospecific binding and a well-defined hydrogen bonding network. These features mirror those of the clinically relevant inhibitor Xeruborbactam, highlighting structural and mechanistic similarity and the results establish a versatile platform for the synthesis of functionalised boron heterocycles with direct translational potential in medicinal chemistry.

OP-35

***Structural and functional analysis of MqnB from* Helicobacter pylori**

S. Korn (Halle (Saale)/DE), A. Prasad (Halle (Saale)/DE), D. A. Nguyen (Halle (Saale)/DE), C. Breithaupt (Halle (Saale)/DE), M. T. Stubbs (Halle (Saale)/DE)

Helicobacter pylori is a pathogenic bacterium implicated in colon cancer [1], making the search for specific antibiotics an important topic of current research. As menaquinone is an essential molecule in the electron transport chain and thus metabolism of the bacterium, its biosynthetic route via the futalosine pathway [2] represents an attractive target for new antibiotics. In earlier studies [3, 4], it has been reported that dehypoxanthine futalosine (DHFL), an essential intermediate in the futalosine pathway, can be formed by the promiscuous enzyme methylthioadenosine nucleosidase (*Hp*MTAN) using aminofutalosine as substrate. In this work, we identify a putative *Helicobacter pylori* MqnB (*Hp*MqnB) and demonstrate that it is able to hydrolyze futalosine to produce DHFL. Although closely related, MqnBs and MTANs display crucial differences in their functionality, mechanism and structure [3], [5], [6]. We were able to crystallize and solve the structure of *Hp*MqnB in the absence of any ligands, revealing structural differences compared to the enzyme from *Thermus thermophilus Tt*MqnB and *Hp*MTAN. Soaking with the substrate futalosine revealed densities for the hydrolysis products DHFL and hypoxanthine (HPA), enabling analysis of the active site (Fig 1).

Fig. 1: (**A**) Overall structure of inactive *Hp*MqnB variant E9A in complex with HPA and DHFL (orange). (**B**) Close up view of the active site showing HPA and DHFL. Resolution: 1.9 Å, R: 0.183, Rfree: 0.225.

References

[1] Suerbaum S and Michetti P (2002). "Helicobacter pylori Infection". NEJM 347, 1175–1186. doi: 10.1056/nejmra020542.

[2] Hiratsuka T *et al.*, An Alternative Menaquinone Biosynthetic Pathway Operating in Microorganisms. *Science* 321, 1670-1673(2008). DOI: 10.1126/science.1160446

[3] Arakawa C et al. (2011). "Diversity of the early step of the Futalosine pathway". AAC 55, 913–916. doi: 10. 1128/aac.01362-10.

[4] Li X, Apel D, Gaynor E C & Tanner M E (2011). 5′-Methylthioadenosine Nucleosidase Is Implicated in Playing a Key Role in a Modified Futalosine Pathway for Menaquinone Biosynthesis in Campylobacter jejuni. *JBC*, *286*(22), 19392–19398. https://doi.org/10.1074/jbc.m111.229781

[5] Kim RQ et al. (2014). "Structural enzymology of Helicobacter pylori methylthioadenosine nucleosidase in the futalosine pathway". In: Acta Crystallographica Section D Biological Crystallography 70, 177–185. doi: 10.1107/s1399004713026655.

[6] Nguyen D A (2025). Doctoral dissertation, Martin-Luther-Universität Halle-Wittenberg.g.

Fig. 1

Fig. 2

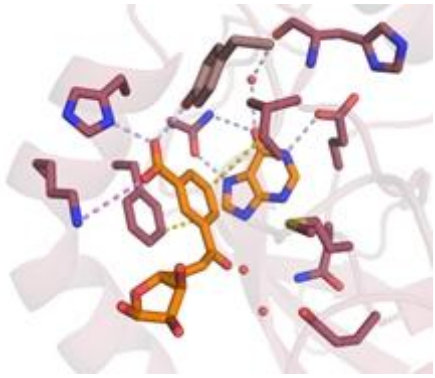

MS 8: Advances and Applications of Neutron and Synchrotron Radiation

OP-36

Structures of Ices by Quantum Crystallography and PDF

K. Wozniak (Warsaw/PL), W. Sławiński (Warsaw/PL), G. Łach (Warsaw/PL), R. Gajda (Warsaw/PL), M. Chodkiewicz (Warsaw/PL), P. Rejnhard (Warsaw/PL), M. Arhangelskis (Warsaw/PL), C. Ridley (Oak Ridge, TN/US, Chilton/GB), C. Bull (Edinburgh/GB, Chilton/GB)

Ice is the solid form of water (H_2O), a substance fundamental to life on Earth. water can crystallize into at least 21 distinct phases, unique in structure, depending on the temperature/pressure, denoted by Roman numerals (e.g., Ice Ih, II, III etc.), and have found relevance across a diverse range of different research areas, from geology and planetary science to fundamental physics.

At pressures exceeding 2–3 GPa, water molecules arrange themselves into cubic ice VII (Fig. 1a, space group Pn-3m)[1,2]. This is one of the densest ice structures (ca. 1.50g/cm3) with ices X and XI (2.51g/cm3 and >2.51g/cm3, respectively). Ice VII plays a role in the water-rich interiors of Jupiter's moon Europa and Saturn's moon Enceladus and other planetary bodies.

We will present details of structures of ices (VI[3], VII[1,2], Ih [4]) obtained with Hirshfeld Atom Refinement against single crystal X-ray and electron diffraction data. We will also present the first quantitative characterisation of disorder in D2O ice VII and VI obtained through a combination of Pair Distribution Function (PDF) analysis, Reverse Monte Carlo (RMC) modelling, and high-pressure neutron scattering. Our results provide a detailed decomposition of both the average and local atomic structures of Ice VII, revealing a previously unquantified level of structural disorder. These findings are corroborated by density functional theory (DFT) calculations, offering a comprehensive understanding of the structural behaviour of Ice VII under extreme conditions.

Fig. 1: (a) Distribution of atoms in ice VII from PDF and RMC, and (b) unique positions of water molecules in ice VII .

References

[1] Gajda et al., IUCRJ, 12(3) (2025) 288

[2] Sławiński et al., Acta Mat., (2025) submitted.

[3] Chodkiewicz et al., IUCRJ, 9 (2022) 573, IUCRJ Highlight

[4] Chodkiewicz et al., IUCRJ, 11(5) (2024) 730

Fig. 1

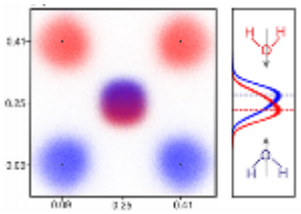

Fig. 2

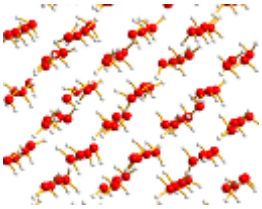

OP-38

Special effects – Verification of corrections for absorption, anomalous dispersion and polarisation

M. Bodensteiner (Regensburg/DE), C. Hennig (Dresden/DE, Grenoble/FR), F. Meurer (Regensburg/DE)

In crystallographic data processing and structure refinement, many corrections such as absorption, anomalous dispersion and polarisation are applied, both to the data and the structure model. In practice, most of these corrections are applied automatically or based on tabulated values, often without a critical examination of their validity or underlying assumptions. As a consequence, simplified or incomplete explanations are frequently passed on within the community, leading to the persistence of misconceptions and dangerous half-knowledge.

To test the impact of these effects and the validity of common correction procedures, we placed a standard single-crystal goniometer upright in a synchrotron beam (Fig.1), which is supposedly the worst possible configuration with respect to polarisation effects. Surprisingly, this setup still produced excellent structural results. The findings suggest that certain commonly accepted correction procedures may owe more to crystallographic urban legend than to experimental evidence.

By clarifying what is actually being corrected and what is merely being assumed, this talk aims to promote a more reflective and evidence-based use of standard correction procedures in crystallography.

Fig. 1

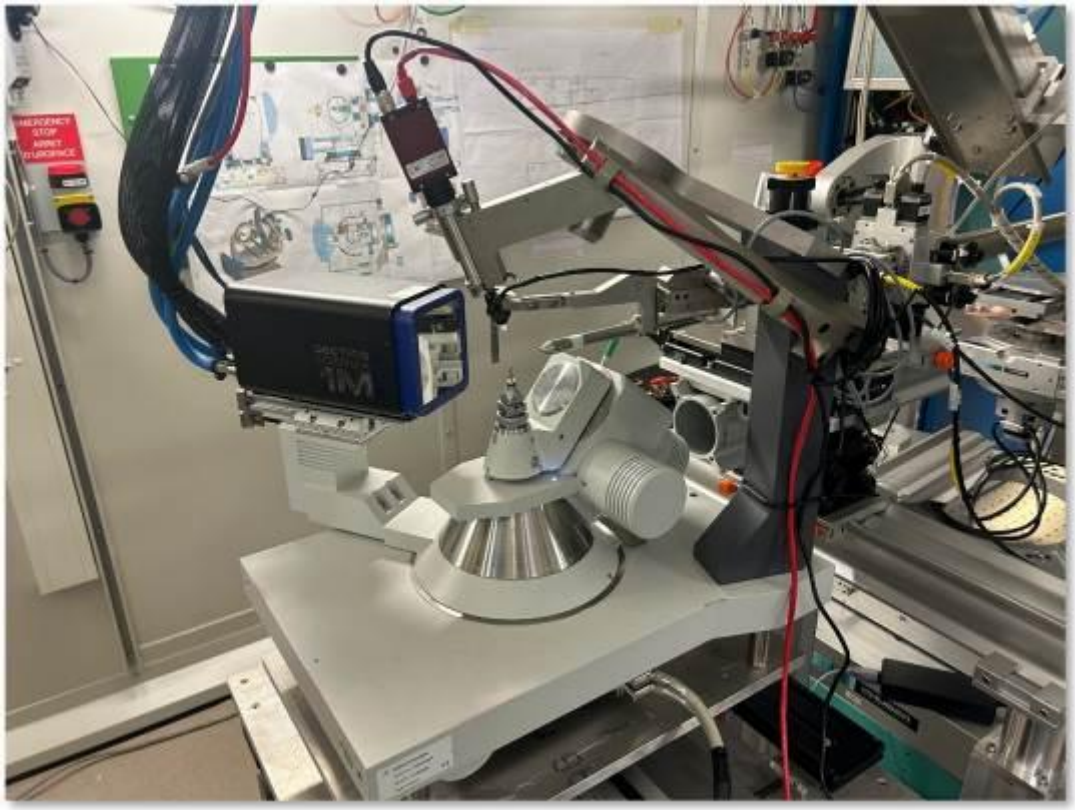

OP-39

FIREPOD: A new thermal high-throughput powder diffractometer at MLZ

C. Hauf (Garching/DE), M. Hölzel (Garching/DE), A. Senyshyn (Garching/DE), P. Wagner (Garching/DE)

The new instrument FIREPOD (FIne REsolution POwder Diffractometer) was successfully transferred from Berlin to Garching as part of a BMBF-funded project. At the MLZ,it will have a "second life" as a dedicated high-throughput instrument, ideally suited for a wide range of fast parametric studies and studies with large sample series. As such, it perfectly complements the group of three unique thermal powder diffractometers located at the SR8 beam tube of the FRM II. Due to the optimised design of the detector, even very bulky sample environments can be used. The scientific focus will be on advanced materials research, including topics with promising industrial applications such as batteries, hydrogen storage, or construction and functional materials under a wide range of conditions, particularly in situ and in operando studies. The details of the instrument design to meet these goals and its forseen capabilies will be presented in detail.

OP-40

ASAXS in Material Science and presentation of some analysis techniques with a software tool

A. Hoell (Berlin/DE), N. Huseyn-zada (Berlin/DE), S. Schorr (Berlin/DE)

Small Angle X-ray Scattering (SAXS) is a non-destructive method for the analysis of nanostructures in a wide variety of materials. This method allows determining averaged structural parameters on a length scale from just above the atomic size up to several 100 nanometres such as sizes, size distributions, volume fractions and inner surface sizes. Moreover, Anomalous Small Angle X-ray Scattering (ASAXS) exploits the anomalous dispersion of the scattering amplitudes near the X-ray absorption edges of an element contained in the sample. Therefore, ASAXS is element sensitive and can allow the calculation of a resonant scattering curve of the element on whose absorption edge the measures are done. This resonant curve identifies the spatial distribution of this element.

This contribution will elaborate on the advantages of ASAXS in the analysis of complex multicomponent materials. It will be shown how ASAXS can be applied, and which different analysis methods are possible.

While the shape and intensity of the ASAXS curves are energy dependent, two main analysis methods are existing. The set of scattering curves can be analysed as they are or can be transformed into energy independent curves [1-3]. A newly developed software tool for this transformation will be introduced.

References

[1] Stuhrmann, H. B., in Advances in Polymer Science, Vol. 67, 1985, edited by H. Kausch & H. Zachmann, pp. 123–163. Berlin: Springer-Verlag.

[2] Hoell, A., et al, J. Appl. Cryst. 2009, 42, 323

[3] Heilmann, M., et al, Adv. Eng. Mater. 2022, 2101308, 1

MS 9: Synthesis-structure / Non-crystalline/ Disordered Materials

OP-41

Revealing the Structure of Water by Variable Temperature Diffraction
J. D. Martin (Raleigh, NC/US)

Water's unique structure is thought to determine its unusual properties, properties critical to diverse natural and technological systems. Nevertheless, precise characterization and explanation of its structure has been elusive. Augmenting traditional 1-D PDF analysis, we have been developing differential techniques (d-PDF) whereby we introduce temperature as an environmental dimension to access information lost by isotropic structural averaging in liquids. Using this d-VT-PDF analysis, along with singular value decomposition (SVD) analysis of the data, we clearly identify equilibria between two types of hydrogen bonding (covalent, HBC and electrostatic, HBE) which give rise to two primary liquid structures, low- (LDL) and high-density (HDL) liquids, along with a third intermediate structure (IHDL) which is a transitional structure between fluctuating LDL and HDL regions. Furthermore, using strategies borrowed from analyzing 3-D PDFs of diffuse scattering in single crystals, we discover the at the structure of each of these liquids must be described based on principles of hierarchical intermediate range order, ranging from local crystal-like structure to isotropic fluid structure at larger distances. These structural findings are shown to account for water's anomalous properties such as its density maximum, maxima and minima in heat capacity and compressibility.

OP-42

A Peptide-Based Porous Coordination Polymer with Ultrahigh Water-Alcohol Selectivity

K. Papadopoulos (Dresden/DE), B. Mazur (Wrocław/PL), S. Ehrling (Leipzig/DE), A. Mosberger (Dresden/DE), B. Kuchta (Wrocław/PL), V. Bon (Dresden/DE), S. Kaskel (Dresden/DE)

Precise control of porosity and framework dynamics is central to advancing functional crystalline materials for selective molecular separations. Here we report the peptide-based porous coordination polymer DUT-240, a supramolecular architecture assembled from Cu–glycyl-histidine chains that crystallizes in the chiral space group $P4_32_12$.[1] Single-crystal X-ray diffraction reveals one-dimensional coordination motifs arranged into a robust three-dimensional lattice featuring ultramicroporous pockets of 3.3 Å diameter.[1] These cavities reside at the critical size threshold between water and short-chain alcohols, enabling molecular sieving governed by strong hydrogen bonding and host–guest interactions. Crystallographic studies of partially and fully hydrated phases demonstrate subtle but reversible framework adaptivity, including anisotropic unit-cell contractions and pocket merging that facilitate water diffusion while suppressing alcohol ingress. The combination of precise pore metrics and adaptive crystal chemistry results in exceptional water selectivity from both methanol/water and ethanol/water azeotropic mixtures under technologically relevant conditions. Beyond its separation performance, DUT-240 exemplifies how peptide-based motifs can be harnessed in coordination polymers to introduce chiral packing, robust hydrogen-bonding networks, and crystallographically resolvable host–guest dynamics. These findings highlight the potential of crystallographically engineered bio-inspired frameworks as a new class of sustainable, energy-efficient molecular sieves, opening pathways toward rational design of adaptive porous solids for separation and catalysis.

Fig. 1: Coordination environment (a) and packing diagram (b) of DUT-240.

Reference

[1] K. Papadopoulos et al. Chemarxiv, DOI: 10.26434/chemrxiv-2025-p3g44

Fig. 1

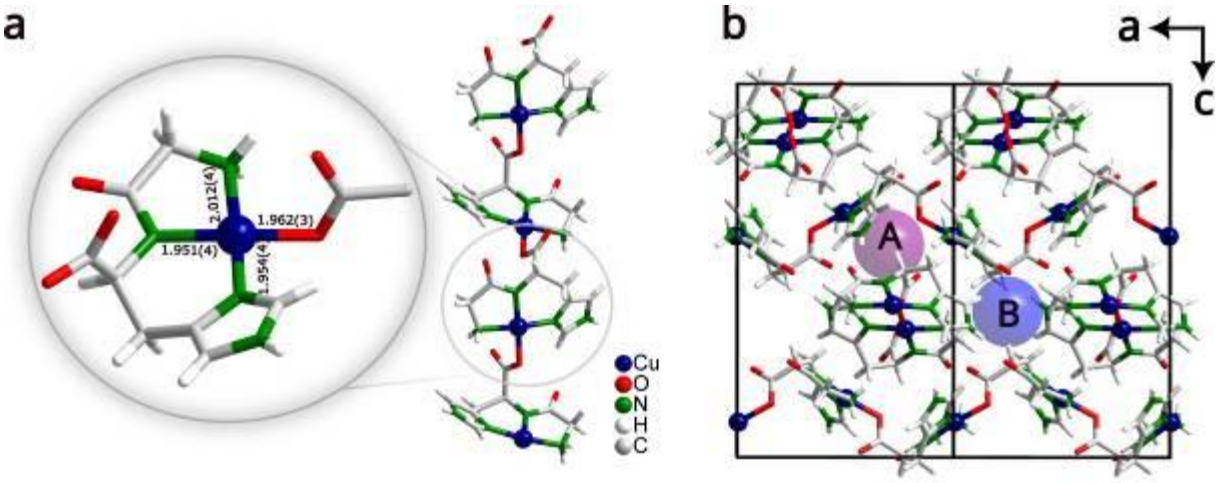

OP-43

Pressure-induced nonmetal–metal transition between SnI_4 amorphous states

K. Fuchizaki (Matsuyama/JP)

After the discovery of pressure-induced solid-state amorphization of SnI_4[1], a new amorphous state, Am-II, with a lower density, has been found [2] upon decompression from the aforementioned amorphous state, Am-I. SnI_4 thus exhibits polyamorphism. Am-I was further classified into two states, Am-IL and Am-IH; Am-IL consists of deformed SnI_4 units at room temperature below 14 GPa, whereas molecular dissociation completes in Am-IH above 18 GPa [3]. The density variation between Am-IL and Am-IH is continuous, in contrast to a jump on the Am-II—Am-I transition [3].

This study focuses on the Am-II—Am-I transition. The molecular symmetry T_d in lower-density Am-II breaks down on the transition to Am-I [3]. SnI_4 units still take molecular forms, but their symmetries are lowered to C_{3v} or C_{2v} in Am-I [3]. This deformation could be caused by a change in a molecule's electronic configuration. Indeed, the author's quantum-chemical calculation confirmed that, depending on molecular orientation, the energy lowering amounts to about 0.01 to 0.02 eV, accompanying the lowering of molecular symmetry when two SnI_4 molecules approach within ~8 Å. Although the limited computational time did not allow him to corroborate dimerization, we may reasonably assume that a metallic bond forms between two deformed SnI_4 molecules when the distance between the iodine atoms of adjacent molecules reaches the characteristic bond length of 3 Å [4] under compression. The author performed reverse Monte Carlo simulations of the structure factors during the Am-II-to-Am-I transition and found that the bonds thus defined percolate throughout the system on the transition. That is, the transition should be from nonmetallic to metallic.

References

[1] Y. Fujii et al., J. Phys. C **18**, 789 (1985).

[2] N. Hamaya et al., Phys. Rev. Lett. **79**, 4597 (1997).

[3] K. Fuchizaki et al., J. Phys. C: Condens. Matter **33**, 365401 (2021).

[4] K. Takemura et al., Phys. Rev. Lett. **45**, 1881 (1980).

OP-44

Synthesis, properties and local structure analysis of the mineral strätlingite

A. Shevchenko (Stuttgart/DE), M. W. Terban (Mannheim/DE), R. E. Dinnebier (Stuttgart/DE), S. Bette (Stuttgart/DE)

Disordered naturally occurring minerals are not a novelty, and are, in fact, known since the development of conventional crystallography and usually are treated using fractional occupancies and split atomic positions. But when it comes to quantitative phase analysis of the nanosized materials, conventional crystallography fails, and alternative structure-sensitive methods must be employed.

In this work we synthesize and characterize the mineral strätlingite ($Ca_2Al_2SiO_2(OH)_{10}{\cdot}2.25H_2O$), that, based on the crack propagation analysis, is believed to be a key component, contributing to the long-term mechanical stability of the Roman concrete.[1] Strätlingite could be classified as a phyllosilicate due to its layered structure, composed of positively charged brucite-like layers $[AlCa_2(OH)_6]^+$, and negatively charged double-tetrahedra (DT) layers $[AlSiO_2(OH)_4]^-$ (Figure 1). It exhibits a well-defined long-range order that is described by the *R-3* space group, but the occupational Si/Al disorder and vacancies within the DT-layer creates a local structure that is not fully captured by the average long-range structure coordination.

Here we focused on analysis of the defects correlation in the DT-layer using solid-state NMR spectroscopy data and PDF modelling, employing and evaluating various structural models that agree with complementary analytical methods and are chemically reasonable. Based on that, we have proposed a deformed double six-member Si rings with $Q^3(3Al)$ configuration as a representation of the local structure of the DT-layer. The additional deformation along the c-axis accounts for the variation in the interplanar d_{00l} distance, which is reflected in the observed anisotropic diffraction peak broadening and provided more realistic Si-O-Si angle in the DT-layer compared to the one in the average model.

1. M. D. Jackson et. al. *Proc. Natl. Acad. Sci. U. S. A.*, 2014, **111**, 18484–18489.

Fig. 1

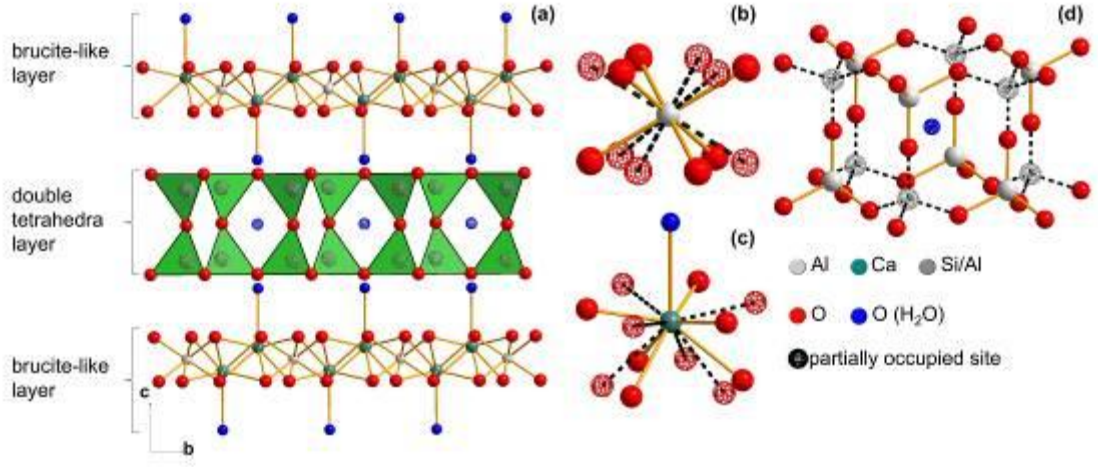

OP-45

Synthesis and performance analysis of novel nanocomposite-based Hydroxyapatite in agriculture

I. Adouar (Fez/MA), S. Herradi (Fez/MA), S. Rakib (Fez/MA), B. El Bali (Fez/MA), M. Lachkar (Fez/MA)

Agriculture is the major user of phosphorus fertilizers, accounting for 80-90% of the world demand. With the increasing population, rising demands for bioenergy crops will increase the future demand for chemical fertilizers. However, intensifying the application of these fertilizers will damage the environment, human being health and all living creatures as well. Hydroxyapatite (HAp) is a mineral, $Ca_{10}(PO_4)_6OH_2$, that is the principal storage form of calcium and phosphorus in bones. The nanoparticles of HAp are considered as one of the most important elements in agricultural applications, which can provide phosphorus nutrients. The use of HAp, however, focused on its biomedical applications because of its excellent biocompatibility and bioactivity, but the agricultural applications are recently taken into consideration. The aim of this study is to synthesize a hydroxyapatite-based nanocomposite for agricultural applications and to analyze its performance with other nanocomposite types, with the goal of enhancing crop productivity and environmental protection through the efficient and minimal use of chemical fertilizers.

References

[1] Adouar, I., Idboumlik, M., Bouhazma, S., Herradi, S., Hazm, J.E., Rakib, S., El Bali, B., Lachkar, M., 2024. Synthesis and characterization of iron and magnesium co-doped hydroxyapatite: effects on cherry tomato fertilization. Moroccan J. Chem. 12, 1731–1741.

[2] De Silva, M., Robles Hernandez, F. C., Sahin, O., Ashokkumar, M., Ajayan, P. M., Karunaratne, V., Amaratunga, G. A. J., & Kottegoda, N. (2022). A Greener Mechanochemical Approach to the Synthesis of Urea-Hydroxyapatite Nanohybrids for Slow Release of Plant Nutrients Chanaka Sandaruwan, Sri Lanka Institute of Nanotechnology.

[3] Raguraj, S., Wijayathunga, W. M. S., Gunaratne, G. P., Amali, R. K. A., Priyadarshana, G., Sandaruwan, C., Karunaratne, V., Hettiarachchi, L. S. K., & Kottegoda, N. (2020). Urea–hydroxyapatite nanohybrid as an efficient nutrient source in Camellia sinensis (L.) Kuntze (tea). Journal of Plant Nutrition, 43(15), 2383–2394

OP-46

New structural insights and unexpected developments in boron compounds

A. Piekara (Warsaw/PL), W. Slawinski (Warsaw/PL)

Ammonia borane (BH_3NH_3) is widely regarded as a promising hydrogen-storage material [1], [2]. Its structure has been the subject of debate for many years because of hydrogen disorder, which results from a mismatch between the molecular symmetry and the symmetry of the crystal lattice. The B–N bond lies along a fourfold axis, which is incompatible with the symmetry of the $-BH_3$ and $-NH_3$ groups [2]; as a consequence, the crystal exhibits pronounced plasticity. To gain deeper insight into these features, we carried out single-crystal X-ray diffraction studies on both the room-temperature and low-temperature phases. The room-temperature structure is consistent with earlier reports [1], [2], whereas the low-temperature phase displays a structural modulation, also confirmed by powder PDF analysis.

During the recrystallization of ammonia borane, we additionally observed the co-crystallization of other boron-containing species that have not been previously described in the literature. These appear to be a layered ring-type compounds of boron and oxygen atoms with additional disorderd water [3]. An interesting observation is that, as the solvent gradually evaporates from the crystallization solution, the boron–oxygen compounds lose the water bound within their structures, which ultimately leads to the formation of borax.

References

[1] M. E. Bowden, et al., Room-temperature structure of ammonia borane, Aust J Chem, 2007, doi: 10.1071/CH06442.

[2] U. B. Demirci, Ammonia borane, a material with exceptional properties for chemical hydrogen storage, 2017, Elsevier Ltd. doi: 10.1016/j.ijhydene.2017.01.154.

[3] R. Gajda, et al., Charge density studies of single and transient (single to double) boron–oxygen bonds in (NH4)2B4O5(OH)4·2H2O, Dalton Trans., 2022, The Royal Society of Chemistry, 2022, doi: 10.1039/D2DT02442J.

MS 10: Non-ambient Conditions and Electron Diffraction Methods

OP-47

Extreme Conditions, Extraordinary Insights, Safe Operation: New SC-XRD High-Temperature Device (HTD) for temperatures up to 1300 K

T. Stürzer (Karlsruhe/DE), A. Lübben (Karlsruhe/DE), C. Wolf (Karlsruhe/DE), M. Adam (Karlsruhe/DE)

A detailed understanding of structure–property relationships is fundamental for designing materials with tailored functionalities. Single crystal X-ray diffraction (SC-XRD) is a key technique for such studies, especially under non-ambient conditions. However, high-temperature SC-XRD experiments have been limited by the lack of heating devices that are both user-friendly and safe. The new Hot Temperature Device (HTD), fully integrated into the D8 VENTURE, now enables precise and convenient measurements up to 1300 K, significantly expanding experimental capabilities.

Next to usability, particular focus was placed on safety when designing the HTD. The HTD meets current safety regulations, ensuring reliable operation even at the highest temperatures. Full integration into the path finding and strategy software eliminates the risk for damaging the diffractometer or the detector.

We will demonstrate how advanced heating technology broadens the scope of structural investigations under extreme conditions investigating the temperature/structure relationship of Vanadinite ($Pb_5(VO_4)_3Cl$), an apatite mineral and the principal industrial source of vanadium. The mineral is known to undergo a phase transition at 23.1 GPa and 600 K, while its synthetic analog $Pb_5(VO_4)_3I$ decomposes at 540 K. Related phosphate and vanadate compounds exhibit phase transitions to monoclinic, pseudohexagonal structures.

The HTD not only deepens our understanding of material behavior at elevated temperatures but also paves the way for the development of new materials with application-specific properties.

References

[1] Y. Liu et al., Minerals 2021, 11, 121.

[2] Gatta et al., Physics and Chemistry of Minerals 2009, 36, 311–317.

[3] S. Redfern et al., Mineralogical Magazine (2012) 76 (4): 997–1003.

Fig. 1

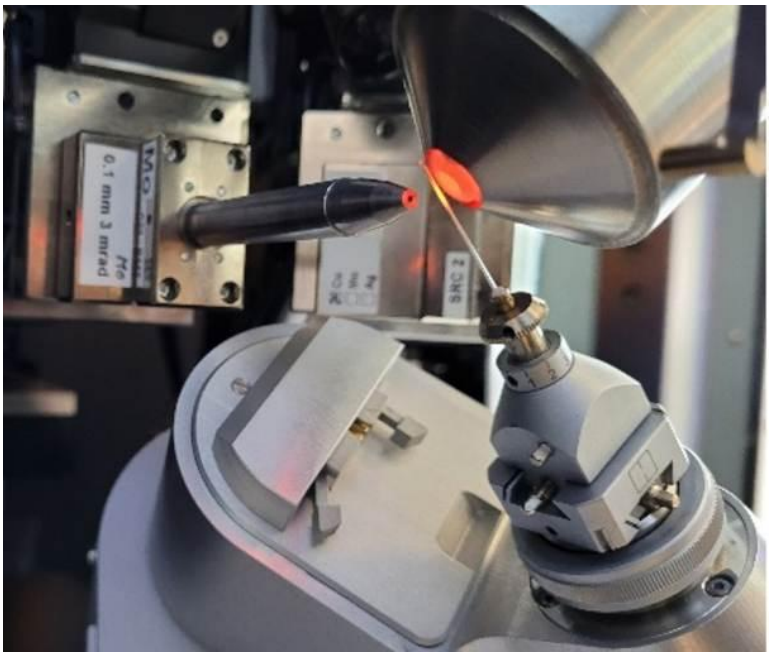

OP-48

Platform for Swift Heavy Ion Irradiation under Extreme Pressure Conditions: Design for Extending to Cryogenic and High-Temperature Regimes

T. H. Reuter (Frankfurt a. M./DE), L. Bayarjargal (Frankfurt a. M./DE), I. Tzifas (Darmstadt/DE), J. Liang (Frankfurt a. M./DE), P. Simon (Darmstadt/DE), K. O. Voss (Darmstadt/DE), C. Schröck (Frankfurt a. M./DE, Darmstadt/DE), C. Trautmann (Darmstadt/DE), M. E. Toimil-Molares (Darmstadt/DE), B. Winkler (Frankfurt a. M./DE)

Swift-heavy-ion irradiation experiments under high static pressures in diamond anvil cells (DACs) have shown that ion-induced processes can drastically influence the pressure-dependent phase behavior of materials. For example, irradiation can transform zirconia (ZrO_2) into the orthorhombic-II phase or induce the formation of the high-pressure zircon ($ZrSiO_4$) polymorph reidite at pressures far below its equilibrium transition pressures.[1,2] These findings demonstrate that irradiation under pressure enables access to otherwise inaccessible phases. Ion irradiation can also help stabilize high-pressure phases upon decompression. To improve spectroscopic access to experiments involving ion irradiation in DACs, a dedicated setup was developed in which irradiation occurs through the gasket rather than through the diamonds.[3] Building on this, a new project aims to extend the approach by enabling temperature control between 10 K and 1000 K during irradiation at pressures up to 80 GPa. This will allow systematic studies of beam-heating effects and phase stabilities. Furthermore, the deployment of diamonds with embedded electrodes will allow for in situ electrical conductivity measurements, providing real-time insights into irradiation-induced melting and defect-related electronic changes. Together, these developments will create a unique platform for investigating the coupled effects of pressure, temperature, and ion irradiation on condensed matter.

We acknowledge funding from the BMBF (05K25RF3) and the DFG (BA4020, WI1232).

References

[1] B. Schuster *et al*., Nucl. Instrum. Methods Phys. Res. B **2009**, 6, 964-968

[2] M. Lang *et al*., Earth Planet. Sci. Lett. **2008**, 269, 291-295

[3] I. Tzifas *et al*., in preparation

OP-49

iSFAC modelling: Experimental determination of partial charges with electron diffraction

T. Grüne (Vienna/AT), S. Mahmoudi (Vienna/AT), C. Schröder (Vienna/AT)

Partial charges are an important concept in chemistry. The assignment of partial charges to atoms within a molecule aids to understand their behaviour and reactivity. Quantum chemical computations provide means for a quantitative approach, but with substantial variations among different methods. Ultra-high resolution X-ray crystallography is an experimental method to determine partial charges, but many crystals are not of sufficient quality to reach the required data quality, and the measurement is time consuming. Often, partial charges are assigned only qualitatively through the labels δ^+ or δ^-.

Electrons interact with the electrostatic potential, that is, the combination between the electron cloud and the positively charged nuclei. This makes electron scattering sensitive to oxidation states, and electron diffraction seems a natural approach to probe partial charges. We developed *iSFAC modelling* (Nature, 646, 88-94 2025) in order to quantify partial charges of atoms from electron diffraction data. We found that meaningful results can be achieved with resolution data to about 0.8-0.9Å.

iSFAC modelling makes use of the SHELXL FVAR formalism and is based on a linear combination of neutral and ionic scattering factors. An unusual interpretation of the Mott-Bethe formula is used to compute the ionic scattering factors. We used XDS for data processing and SHELXL for refinement. Despite this simplified approach, ignoring dynamic scattering effects, we find striking details in our results, backed up by comparison with quantum chemical computations in several compounds like histidine, calcium tartrate from a bottle of Austrian wine, the chlorine salt of ciprofloxacin, and the zeolite ZSM-5. With future development in combination with more advanced programs specifically designed for electron diffraction, iSFAC modelling can be expected to provide unprecedented details and novel insight into the world of molecular interactions based on electron diffraction.

Fig. 1

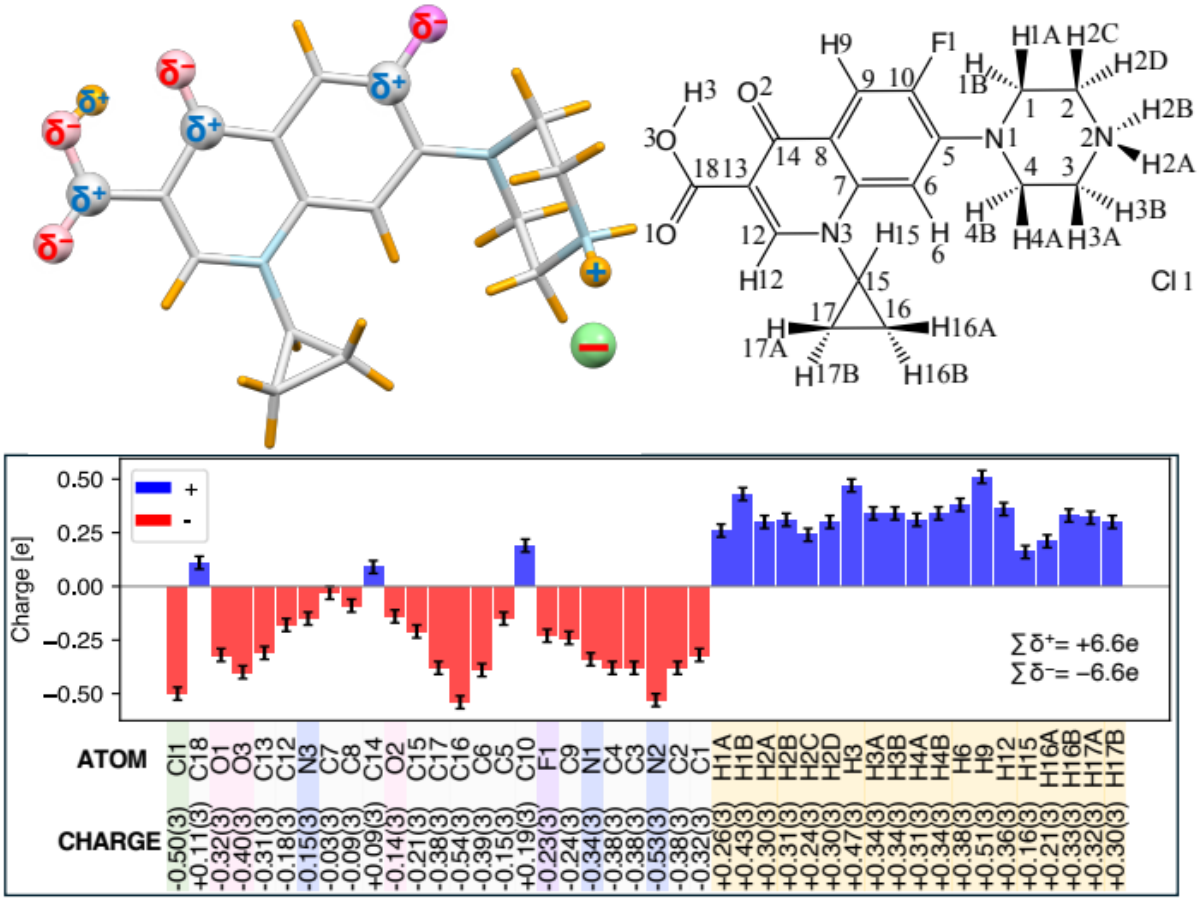

OP-50

Variable temperature diffraction and polymorph screening with the XtaLAB Synergy-ED

E. Buchsteiner (Neu-Isenburg/DE), K. N. Truong (Neu-Isenburg/DE), R. Bücker (Neu-Isenburg/DE, Tokyo/JP), C. Göb (Singapore/SG), C. J. Schürmann (Neu-Isenburg/DE), J. Wojciechowski (Neu-Isenburg/DE), M. Jasnowski (Wrocław/PL), M. Meyer (Wrocław/PL), F. White (Neu-Isenburg/DE, Tokyo/JP)

Since its launch in 2021, the XtaLAB Synergy-ED has produced many structures, with more than 100 peer-reviewed publications and over 500 unique structures from Rigaku labs alone. While many of these structures were analyzed at ambient temperature, the availability of low-temperature techniques, particularly cryo-transfer, have proven invaluable for the preservation of sensitive samples both those sensitive to vacuum and those sensitive to electron beam damage. Additionally, the instrument"s enhanced automation capabilities, such as unattended measurement queues and automatic unit cell clustering, have opened new avenues for polymorph screening.

The XtaLAB Synergy-ED"s compatibility with existing TEM instrument holders provides structural scientists with the ability to conduct various experiments traditionally performed in X-ray crystallography. Cryo-transfer and air-free transfer specimen holders protect samples prior to vacuum introduction [1], enabling the study of solvates and other vacuum- or air-sensitive species, and allowing for the investigation of phase behaviour. Examples of crucial findings made possible by cryo-transfer will be discussed.

Furthermore, a MEMS biasing/heating holder allows for the increase in temperature, facilitating the exploration of polymorphism of structures such as porous materials. Recent studies utilizing single-crystal data from electron diffraction on a MOF system, Cu(ta)2 (Hta=1*H*-1,2,3-triazole), have yielded significant insights at both room temperature and 200 °C. These findings are compared with previous studies by Grzywa et al. (2012) using SC-XRD and PXRD, demonstrating the instrument"s capability in polymorphism research.

References

[1] K.-N. Truong, S. Ito et al. (2023). *Symmetry*, **15**(8), 1555.

[2] M. Grzywa, D. Denysenkoet al. (2012). *Dalton Transactions*, **14**, 4239.

Figure 1. Overlays of the ambient and high temperature phases of Cu(ta)2 from the XtaLAB Synergy-ED (blue) and the X-ray structures by Grzywa et al. (orange).

Fig. 1

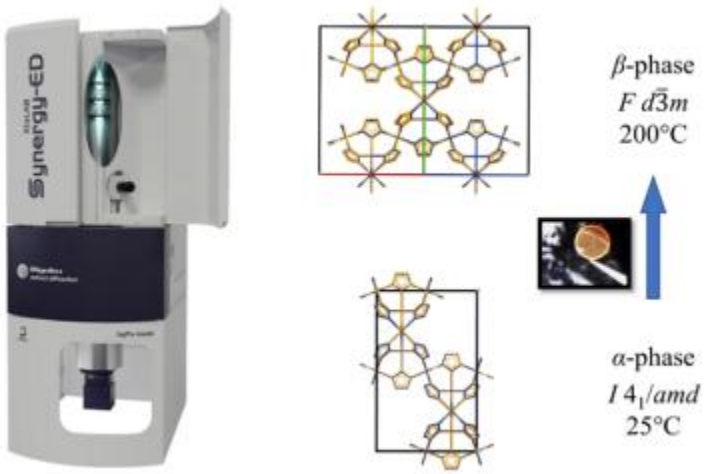

OP-51

Electron diffraction for everyone: classic and new 3DED protocols in Instamatic

D. Tchoń (Prague/CZ), L. Palatinus (Prague/CZ)

With beam characteristics and interaction cross-sections unmatched by photon sources, 3D electron diffraction (3DED) keeps extending crystallography to ever smaller and more challenging targets. While any transmission electron microscope (TEM) can record microdiffraction, the best acquisition strategy depends on the sample: a beam suitable for a mineral sample may rapidly damage an organic one. Likewise, a precise single-crystal protocol will be ill-suited to map phase distribution across many grains.

The simplest 3DED protocol involves rotating the crystal and collecting diffraction stepwise. This rotation ED (RED) can be refined by precessing the beam or acquiring data continuously, as in cRED or Fast-ADT. Each variant can be further automated. Through image recognition and clustering, serial 3DED approaches reduce beam damage by distributing the total dose over hundreds to thousands of crystals.

As the new 3DED protocols rapidly push the state of the art, they often sacrifice interoperability. In practice, modern 3DED is constrained more by implementation rather than any fundamental limitations. For the wider community, a new experimental protocol is only as valuable as it is applicable across different TEMs.

Here, I present the recent developments in Instamatic – an open-source 3DED data-collection software suite designed for interoperability. Instamatic implements all the protocols mentioned above through a generalised interface that translates commands for different TEMs at runtime. I will showcase recent improvements, including new interfaces, an improved interactive display, refined calibration, and a live emulator. I will discuss a newly developed serial precession-assisted experimental routine that minimises beam damage by replacing direct-space detection and tracking with long continuous scans over the grid.

MS 13: Mineralogical Crystallography

OP-52

Mineral–organic crystalline superstructures in biogenic glass assemblies

I. Zlotnikov (Dresden/DE)

We describe the principles of morphogenesis of glass spicules in marine sponges of the class Demospongiae. These spicules display an extraordinary diversity of highly regular, branched three-dimensional morphologies that represent a paradigmatic example of symmetry in biological systems. Our previous work revealed that the organic axial filament, which templates the shape of each spicule, is itself a perfectly ordered silica–protein composite crystal. In the present study, combining data from multiple synchrotron-based imaging and analytical methods, we demonstrate that crystallographic branching of these hybrid crystals governs the formation of the intricate and reproducible morphologies of these naturally occurring glass architectures. By comparing spicules with different levels of structural complexity from three distinct demosponges, we show that the branching directions follow specific crystallographic orientations intrinsic to the axial filament crystal lattice.

OP-53

The structure of calcium phosphate nanoparticles in comparison to biogenic and geological calcium phosphate

M. Epple (Essen/DE), K. Kostka-Wirtz (Essen/DE), K. Loza (Essen/DE), O. Prymak (Essen/DE)

Calcium phosphate constitutes the inorganic part of hard tissues like bone and teeth in many higher organisms, including humans. These compounds are also produced synthetically for biomedical use, e.g. as ceramic substitutes for bone repair or as nanoscale particles designed for drug delivery and diagnostic imaging. In geology, hydroxyapatite appears as a naturally occurring mineral that can form single crystals of several centimeters size.

Particle size, crystal phase, degree of crystallinity, and crystallite dimensions play a central role in determining the material behavior under physiological conditions, for example the dissolutionin vivo after biomedical application, e.g. in bone defects or after endocytic uptake of nanoparticles by cells.

We have carried out an in-depth examination of different forms of calcium phosphate, i.e. two biological types of nanocrystalline apatite (human dental enamel and shark enameloid), a geological single-crystal apatite, a sintered hydroxyapatite sample, and four varieties of synthetic calcium phosphate nanoparticles. Both external morphology and internal structural features were investigated. Structure-sensitive analytical methods were employed for a comprehensive picture, including electron microscopy (both scanning and transmission), X-ray powder diffraction with Rietveld refinement, and total scattering techniques for pair distribution function (PDF) analysis. Additional compositional data were obtained by elemental analysis, infrared spectroscopy, and thermogravimetry.

Fig. 1

OP-54

Demineralization and remineralization of tooth enamel from a chemical perspective

M. Epple (Essen/DE), J. Enax (Bielefeld/DE), E. Schulze zur Wiesche (Bielefeld/DE)

The surface of human teeth, i.e. the enamel, consists of calcium phosphate in the crystal structure of hydroxyapatite. In the mouth, teeth are continuously exposed to acidic challenges from foods and beverages. In the case of caries, this attack occurs by bacterial metabolic products that form beneath an ever-present biofilm. This leads to the dissolution of the enamel which lead to tooth damage and finally tooth loss.

Fortunately, tooth remineralization occurs through saliva, which is supersaturated with respect calcium phosphate. It is illustrated how both dissolution and crystallization (i.e. remineralization) of calcium phosphate take place in the oral cavity on a permanent basis, protecting the teeth from daily erosion. The chemical and crystallographic foundations of these processes that involve a number of different calcium phosphate phases are highlighted.

Fig. 1

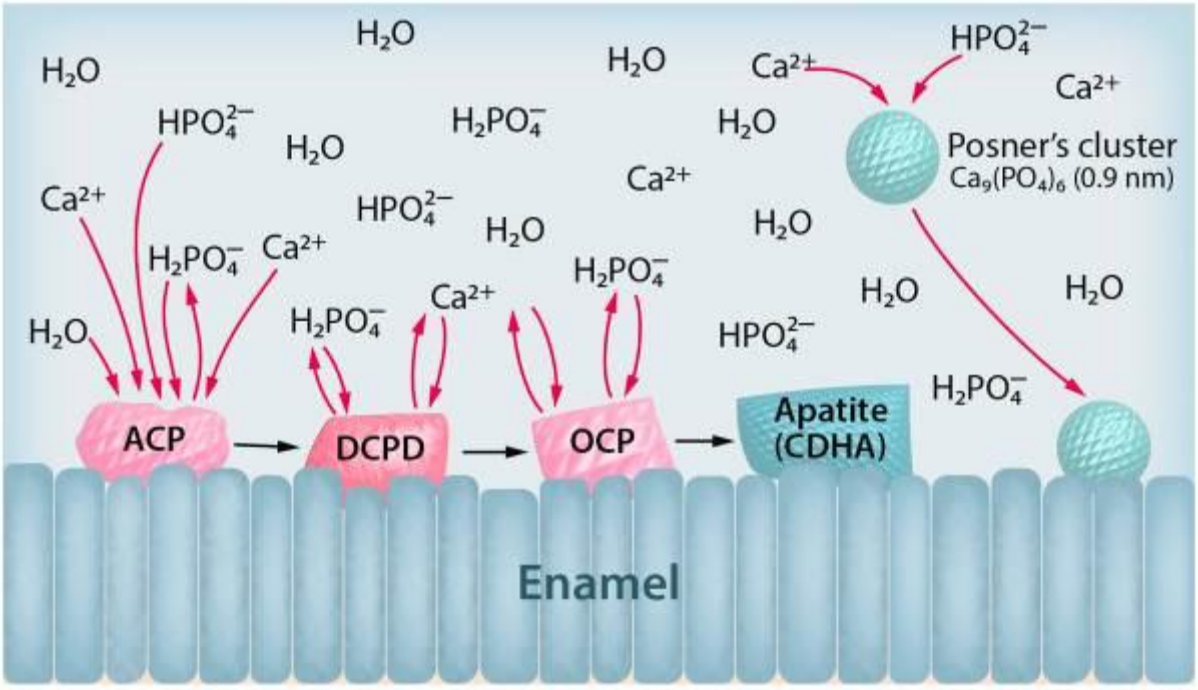

OP-55

The role of volatiles in the stabilization of iron-rich compounds at high pressures

V. Kovalev (Frankfurt a. M./DE), N. Sharapova (Frankfurt a. M./DE), X. Li (Grenoble/FR), C. Longa (Milan/IT), D. Spahr (Frankfurt a. M./DE), A. Pakhomova (Grenoble/FR), B. Winkler (Frankfurt a. M./DE), V. Cerantola (Milan/IT), E. Bykova (Frankfurt a. M./DE)

Earth's geospheres contain volatile components, such as H_2O[1] and CO_2[2], that can strongly influence geodynamic and geochemical processes. Volatiles influence the physical and chemical behavior of elements, with iron being especially sensitive due to its variable oxidation states. This highlights the need for systematic studies of iron-bearing compounds in reactive environments, rather than inert conditions typically used[3–6].

We conducted high-pressure experiments on synthetic hematite (Fe_2O_3) and siderite ($Fe[CO_3]$), using H_2O or CO_2 as both reactive agents and pressure media. Samples were compressed to 40-70 GPa in diamond anvil cells and then laser-heated. At 70 GPa and 2500-3000 K, Fe_2O_3 reacted with CO_2 to form iron sp^3-carbonates $Fe_4[CO_4]_3$[6] and $Fe_2[C_4O_{10}]$[7], while in H_2O it decomposed into $Fe_{6.33}O_9$[4] after heating to ~2800 K. Siderite exhibited similar behavior at 40-50 GPa and 2000-2200 K: in CO_2 the reaction yielded $Fe_4[CO_4]_3$[6] and $Fe_2[C_4O_{10}]$[7], whereas in the presence of H_2O, it decomposed to produce decarbonated *HP*-Fe_3O_4[3,5] and a novel anhydrous apatite-like iron oxycarbonate $Fe_5[CO_4]_3O$.

These results demonstrate that volatile components can alter reaction pathways at extreme conditions, without necessarily being incorporated into the final products. Such findings underscore the critical role of volatiles in controlling phase stability, thereby shaping deep Earth geochemical evolution.

Fig. 1: Stabilization of high-pressure phases synthesized from siderite ($FeCO_3$) and hematite (Fe_2O_3) in H_2O/CO_2 pressure media

References

[1] M. Akaogi, in *High-Pressure Silicates and Oxides*, Springer Nature, 2022.

[2] V. Stagno, *JGS*, 2019, **176**.

[3] E. Bykova et al., *Nat Commun*, 2016, **7**.

[4] E. Koemets et al., *Eur J Inorg Chem*, 2021, **30**.

[5] S. Khandarkhaeva et al., *Inorg. Chem.*, 2022, **61**.

[6] V. Cerantola et al., *Nat Commun*, 2017, **8**.

[7] V. Kovalev et al., *Commun Chem*, 2025, **8**.

Fig. 1

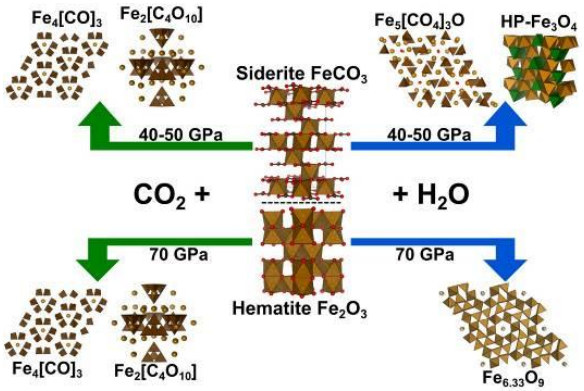

OP-56

Itelmenite-related $A^{+}_2M^{2+}_3(SO_4)_4$ sulfates: new representatives and structural classification

A. Borisov (Kiel/DE), I. Pimshin (Saint Petersburg/RU), A. Holzheid (Kiel/DE), D. Charkin (Moscow/RU)

The structural versatility of complex oxides and oxysalts of transition metals is remarkable, and they can be regarded as an excellent venue for the investigation of a variety of properties. Anhydrous sulfates hold a unique position among the listed oxysalts, and in recent years, a wide variety of structural families have been described for them. Among anhydrous sulfates, compounds with an overall composition of $A^{+}_2M^{2+}_3(SO_4)_4$ (A^{+} = Na, K, Rb, Cs; M = Mg, Cu, Mn, Fe, Co, Ni, Cd) are among the most notable representatives. The first anhydrous sulfate, $A^{+}_2M_3(SO_4)_4$, was reported approximately a decade ago as a fumarolic mineral itelmenite $Na_2CuMg_2(SO_4)_4$ [1]). Later, several synthetic compounds were reported [e.g. 2,3]. Our recent investigations [4,5, etc.] have substantially expanded and developed the "itelmenite-related" family. Representatives of this group are thought to be possible cathode [2] or nonlinear optical [6] materials.

The discussion will focus on the new representatives in the $A^{+}_2M_3(SO_4)_4$ family. The novel compounds $A^{+}_2Cu_3(SO_4)_4$, where A^{+} = Cs, (Cs,K), and Tl, are isostructural ($P2_1/c$) and are composed of corrugated Cu–SO_4 layers with large A^{+} cations located in the interlayer space. The framework architectures of the $Rb_2Cu_3(SO_4)_4$ (*Pnma*) and the Cu-Cd sulfate $K_2CuCd_2(SO_4)_4$ ($P2_1/n$) are constructed from $MO_{6\text{-}7}$ polyhedra that share edges and corners with SO_4 tetrahedra. Additionally, we will provide the structural classification of the $A^{+}_2M_3(SO_4)_4$ family.

References

[1] Nazarchuk EV, Siidra OI, Agakhanov AA, et al. (2015) Mineral. Mag., 79, 1229–1236.

[2] Gao J, Sha X, Liu X, et al. (2016) J. Mater. Chem. A., 4, 11870.

[3] Trussov IA, Male LL, Sanjuan ML, et al. (2019) J. Solid. State. Chem., 272, 157–165.

[4] Nekrasova DO, Mentré O, Siidra OI, et al. (2022) Dalton Trans., 51, 7878–7888.

[5] Borisov AS, Charkin DO, Zagidullin KA, et al. (2022) Acta Crystallogr., B78, 499–509.

[6] Wang M, Wei D, Liang L, et al. (2019) Inorg. Chem. Comm., 107, 107486.

OP-57

Structural changes in $CaSiO_3$ glass up to lower mantle pressures

C. Prescher (Freiburg i. Br./DE), C. Otzen (Freiburg i. Br./DE), G. Cocomazzi (Freiburg i. Br./DE), K. Glazyrin (Hamburg/DE), H. P. Liermann (Hamburg/DE)

The physical properties of silicate melts at temperature and pressure conditions of the Earth"s mantle have a fundamental influence on the chemical and thermal evolution of the Earth. However, direct investigations of melt structures at these conditions are experimentally very difficult or even impossible with current capabilities. To still be able to obtain an estimate of the structural behavior of melts at high pressures and temperatures, amorphous materials have been widely used as analogue materials.

Here we present the structural response of $CaSiO_3$ glass as a proxy for deep mantle melts up to 108 GPa via total X-ray scattering experiments. The measurements were carried out at beamline P02.2 at DESY, Germany, utilizing the newly commissioned Soller Slit configuration. Due to the pronounced size contrast between Ca^{2+} and Si^{4+}, the Si–O correlations are readily resolved in the pair-distribution function—something that is impossible in other three component silicate glasses, like $MgSiO_3$ where the Mg–O and Si–O peaks overlap at a larger pressure.

We observe smooth pressure-induced changes in the structure factor and pair distribution function, along with a clear increase in Si–O coordination from four-fold to six-fold within the first 50 GPa. This behavior will be examined in detail, with emphasis on mechanistic differences relative to pure SiO_2 and in comparison with other reported results for silicate glasses under similar pressure conditions.

MS 12: New Crystal Structures

OP-58

Copper bismuth iodide – a photovoltaic compound with convoluted structural classification

D. M. Többens (Berlin/DE), R. Datta (Karlsruhe/DE), A. Colsmann (Karlsruhe/DE), H. Röhm (Karlsruhe/DE), S. Schorr (Berlin/DE)

The synthesis and photovoltaic effect of $Cu_{3x}Bi_{1-x}I_3$ (CBI) thin films were studied [1]. Although CBI was originally inspired by the material class of Caswellsilverites (also known as Rudorffites), an XRD study showed that its crystal structure resembles a BiI3-cage with interstitial copper. CBI was found to demonstrate optoelectronic properties suitable for solar light harvesting, with a bandgap of 1.66 eV and thermal stability up to 333 °C. Corresponding thin-film solar cells achieved a peak power conversion efficiency of 0.65%.

The search for lead-free light absorbers has motivated extensive studies of Bi- and Sb-based perovskite-inspired compounds. Among these, Caswellsilverites form a structurally versatile family of $A_aB_bX_y$ ($y = a + 3b$) phases composed of edge-sharing octahedra, related to perovskites. While Ag–Bi–I Caswellsilverites (e.g., $AgBiI_4$, Ag_3BiI_6) are well established, copper substitution remains poorly explored, particularly at high Cu:Bi ratios. Here, we investigate $Cu_{3x}Bi_{1-x}I_3$ synthesized from Cu:Bi = 3:1 precursors. Although the nominal stoichiometry is consistent with Caswellsilverites, XRPD reveals a distinct structure (figure 1): the host lattice retains the layered topology of BiI_3, with alternate unoccupied BiI_6 octahedral layers enhancing its two-dimensional character. Copper does not occupy octahedral or tetrahedral voids but is instead located in an unusual trigonal-planar coordination. $Cu_{3x}Bi_{1-x}I_3$ is therefore best described as BiI_3 with interstitial Cu rather than as a new structural prototype. These findings expand the structural chemistry of Cu–Bi–I compounds and illustrate how unconventional cation incorporation generates novel motifs. Comparison with Ag_3BiI_6 and structural analogues demonstrates a new chapter in the already tangled history of naming these structures properly.

Fig. 1: BiI_3 with copper interstitials

Reference

[1] R. Datta *et al*., Photovoltaic properties of BiI_3 with copper interstitials. *EES Solar*, 2025, Advance Article

Fig. 1

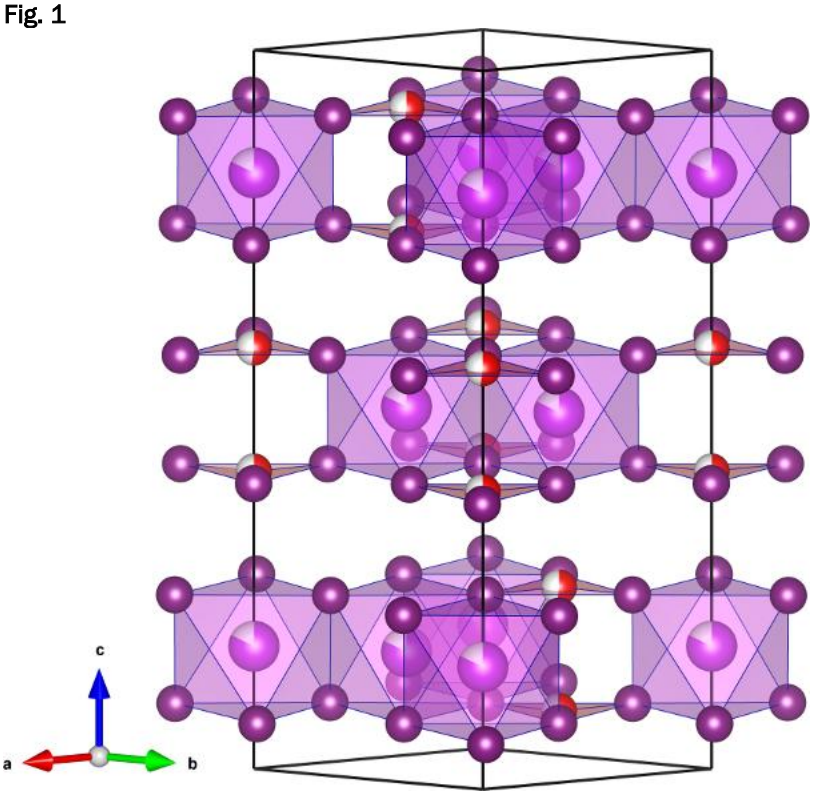

OP-59

Pressure-induced formation of compounds in the Re-S binary system

N. Sharapova (Frankfurt a. M./DE), V. Kovalev (Frankfurt a. M./DE), D. Spahr (Frankfurt a. M./DE), B. Winkler (Frankfurt a. M./DE), N. Giordano (Hamburg/DE), E. Bykova (Frankfurt a. M./DE)

Layered rhenium dichalcogenides have gained considerable attention in recent years due to their strong in-plane anisotropic optical, electrical, and phonon properties[1,2]. Compression drives rhenium disulfide (ReS_2) to transform from a 2D system into 3D phases, including a superconducting polymorph[3], and making it promising for high-pressure studies. However, for other Re-S stoichiometries, no experiments or theoretical predictions exist, which leaves the structural evolution of the Re–S system unresolved.

High-pressure studies open new pathways in chemical synthesis, enabling the formation and stabilization of compounds with previously inaccessible stoichiometries. Here, we used laser-heated diamond anvil cells to investigate the chemical reactivity of the Re–S system. At 40(5) GPa and 2200 K, we observed formation of three novel rhenium sulfides, Re2S, Re5S3 and ReS, which were characterized by single-crystal X-ray diffraction. The stability of their crystal structures was further confirmed by computational methods.

The Re_2S phase adopts a $CuZr_2$-type structure with ReS_4 tetragonal-pyramidal units, consisting of the sequential stacking of the Re and S layers along the c-axis (Fig.1b). The sequence can be expressed as follows: S–Re–Re–S–Re–Re–S. Upon the addition of one sulfur atom in ReS compound, the symmetry reduces (Fig.1c). In this case, the order of the layers is S–Re–Re–S–S–Re (Fig.1d) with isolated vertex-sharing ReS_3 trigonal pyramids. The structure of Re_5S_3 phase is more complex, comprising both ReS_3 and ReS_4 units (Fig.1e), that assemble into corrugated layers with large channels (Fig.1f). All compounds share similar building blocks and packing principles, suggesting that additional rhenium sulfides with related structural motifs may exist.

References

[1] J.Zhang et al., *PCCP*, 2018, 20.

[2] M.Hafeez et al., *Mat. Chem. Front.*, 2017, 1.

[3] D.Zhou et al., *npj Quantum Mat.*, 2017, 2.

Fig. 1. High-pressure structures of rhenium sulfides synthesized at 40(5) GPa.**Fig. 1**

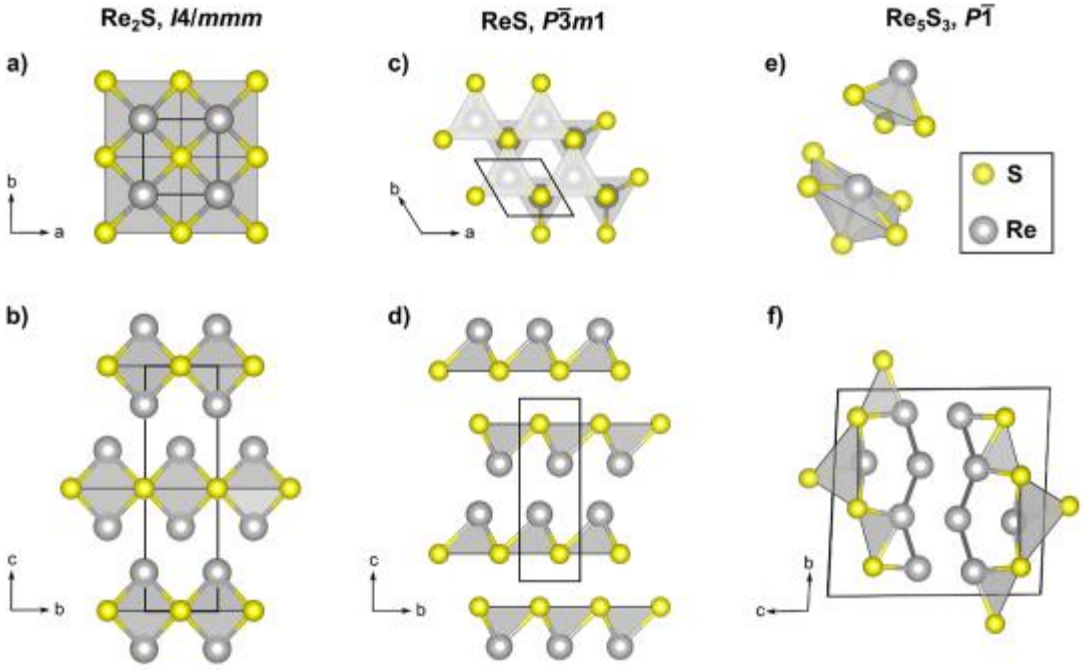

OP-60

Oxidomercurates of alkali metals – crystal structures and chemical bonding

C. Hoch (Munich/DE)

The alkali metal oxidomercurates(II) $A_xHg_yO_z$ have been described for *A* = Na–Cs and crystallize isotypically in the Na_2HgO_2 structure type (tetragonal, *I*4/*mmm*, *a* = 3.42, *c* = 13.32 Å, *Z* = 2 for Na_2HgO_2) [1,2]. The elusive Li compound erroneously was assigned to the same structure type. Phase-pure microcrystalline samples of Li_2HgO_2 were prepared from Li_2O and HgO at 500 °C, and the crystal structure was solved and refined from powder X-ray diffraction data. Li_2HgO_2 adopts a new structure type (tetragonal, *I*4/*mmm*, *a* = 3.5283(5), *c* = 11.200(3) Å, *Z* = 2) which is closely related to the Na_2HgO_2 structure type.

The first oxidomercurates(0) A_2HgO (*A* = K, Rb, Cs) have been prepared by reacting the respective alkali metals with HgO at 300 °C and crystallize as black, in thin fragments dark red transparent crystals. In the crystal structure of Cs_2HgO (monoclinic, *C*2/*m*, *a* = 14.2923(14), *b* = 4.3421(4) , *c* = 9.5830(9) Å, *β* = 108.508(5)°, *Z* = 4), the quasi-molecular $[HgO]^{2-}$ anion is coordinated by Cs^+ cations in a similar way than the $[HgO_2]^{2-}$ anions in the oxidomercurate(II): the structures can be described as a closest sphere packing of Cs together with Hg atoms, and O occupying 2/3 (Cs_2HgO_2) or 1/3 (Cs_2HgO) of the octahedral interstices. The special bonding situation in the two oxdiomercurate anions is discussed on the basis of DFT and coupled-cluster calculations.

This work was funded by DFG under project number 513247541.

Fig. 1: Crystal structures of Na_2HgO_2 [1] (left), Li_2HgO_2 (center) and Cs_2HgO (right). Na/Li/Cs atoms: light grey, Hg atoms: middle grey, O atoms: black.

References

[1] R. Hoppe, H. J. Röhrborn, *Z. Anorg. Allg. Chem.* **1964**, *329*, 110-122.

[2] R. Hoppe, R. Baier, W. Carl, H. Glaum, H. Untenecker, *Z. Anorg. Allg. Chem.* **1988**, *567*, 69-76.

Fig. 1

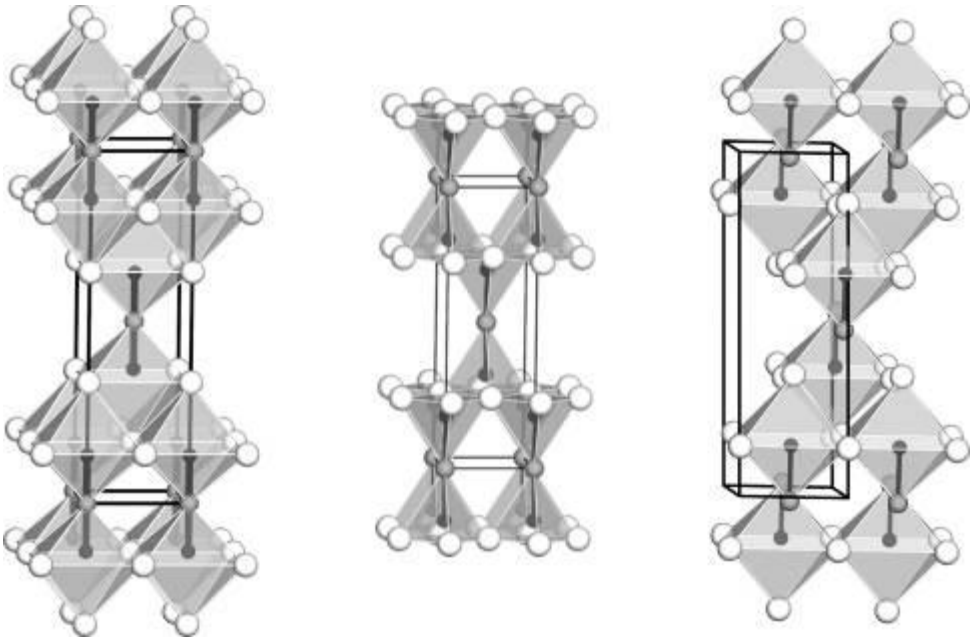

OP-61

Structure Determination from Phase Mixtures by High-Throughput Electron Diffraction

C. Jandl (Allschwil/CH), J. Merkelbach (Allschwil/CH), D. Stam (Allschwil/CH), G. Steinfeld (Allschwil/CH), G. Santiso-Quinones (Allschwil/CH)

In recent years, 3D electron diffraction (3D ED, microED, ED) has established itself as a valuable tool for structure determination of samples, from which no crystals of suitable size for single-crystal X-ray diffraction (SC-XRD) can be grown. But the method is capable of much more: The use of an electron beam typically 1 µm or lower in diameter allows to selectively illuminate individual crystallites without interference from other components. Thus, even phase mixtures can be used for structure determination.

The method becomes even more powerful when it is combined with automatic data collection protocols. We have developed a fully automated crystal mapping protocol which performs all steps from imaging the sample, recognising, selecting, and centering crystals to performing data collection in continuous rotation mode and data analysis. The protocol can collect more than 1000 datasets per day without supervision, enabling high-throughput 3D ED. Combining this with sample holders that can take up multiple TEM grids (the current standard sample support for ED) allows 24/7 operation with maximum efficiency.

The ability to determine crystal structures even from minor components in mixtures makes 3D ED the perfect tool to screen phase mixtures for by-products, impurities, decomposition products, and polymorphs. This is highly relevant for instance in the pharma sector, exemplified by the structure determination of Ritonavir polymorph 4, which was not available in pure phase.[1] Further investigations on marketed drugs that have been known for decades, like albendazole or dapsone, discovered new polymorphs in commercial samples, showing a clear benefit in using electron diffraction for solid state characterisation, because such findings can have major implications for regulations and intellectual property.

Fig. 1: Molecular structure and packing view of Ritonavir form 4.[1]

Reference

[1] L. Iuzzolino, A. W. Kelly, M. T. Chaudhry, C. Jandl, D. Stam, A. Y. Lee, submitted.

Fig. 1

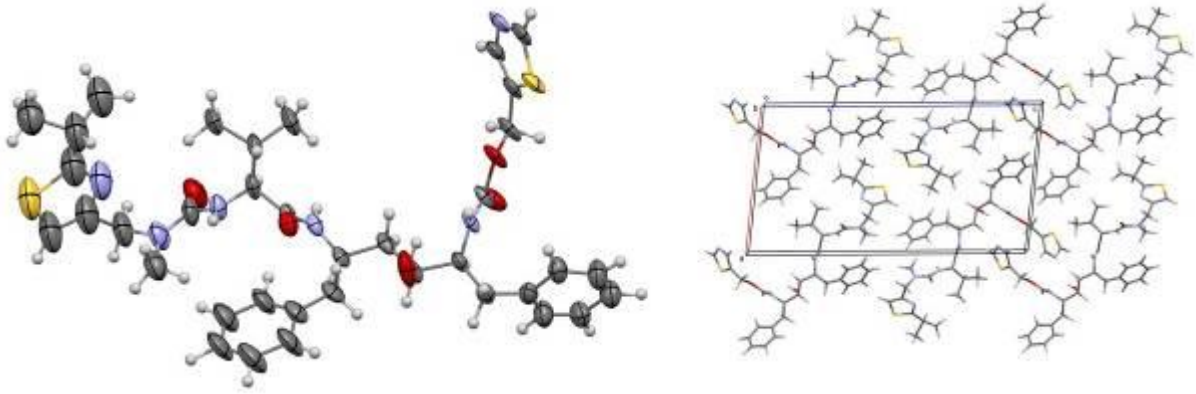

OP-62

Coordination Chemistry of Catechol-Functionalized TREN Ligand Systems

B. Ebel (Aachen/DE), G. Hempelmann (Aachen/DE), I. M. Oppel (Aachen/DE)

The coordination chemistry of catechol-functionalized TREN ligands was systematically explored to investigate their structural versatility and adaptability toward different metal centers. Single-crystal X-ray diffraction revealed three principal structural motifs: mononuclear complexes stabilized by protonated amine groups, heterobimetallic species incorporating secondary metals such as Na^{+}, Ca^{2+}, or Cd^{2+}, and μ-Ca-bridged dimers. These motifs demonstrate pronounced charge flexibility, enabling the formation of anionic, neutral, and cationic complex fragments depending on the nature of the secondary cation.

A variety of metals was successfully coordinated, including Ti(IV), Sn(IV), Al(III), Ga(III), In(III), and Fe(III). The resulting structures exhibit comparable coordination geometries despite significant differences in ionic radius and oxidation state, highlighting the intrinsic adaptability of the ligand framework. Correlating the structural insights gained from diffraction with solution-phase NMR spectroscopy and ESI-MS provides a high degree of predictability regarding the composition and geometry of the resulting complexes.

Fig. 1

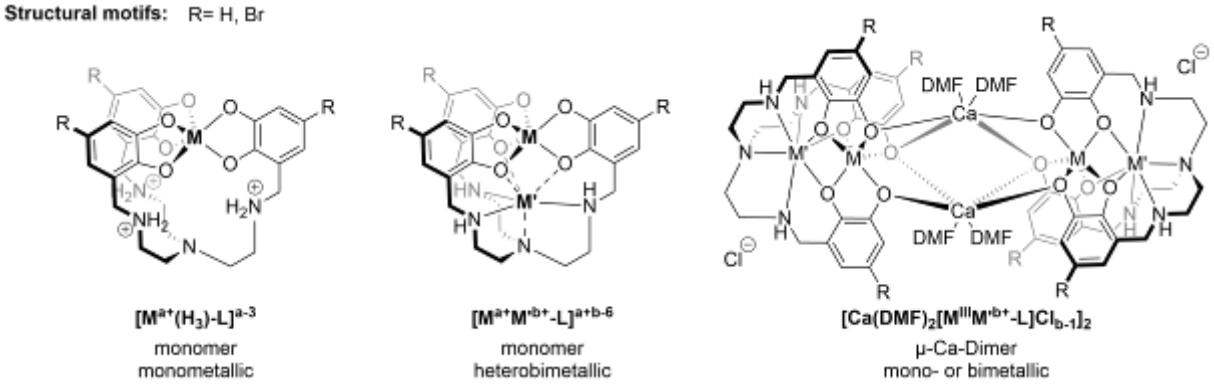

OP-63

(Poly-)Chalcogenides: From binary salts to complex Solvates

G. Thiele (Freiburg i. Br./DE)

Chalcogenide and poly-chalcogenide salts of the alkali and alkaline earth metals are becoming centerpieces of investigations again due to novel approaches in electrochemical storage technologies.[1] Such concepts, i.e., lithium-sulfur batteries, require an in-depths understanding of the fundamental redox processes and therefore the associated structural assemblies: Starting from fully reduced mono-chalcogenides, e.g., Li_2S, via intermediate polychalcogenides, e.g., Li_2S_n, to the well-known allotropes.

Despite the first representatives of such salts being crystallographically reported a century ago, many of these structures are yet to be obtained. Here, we present some approaches for the isolation of both, purely inorganic binary salts, and solvated-cation polyanionic compounds. Additionally, some unexpected reactions with supposedly inert solvents and crystallization from liquefied gasses are presented.

References

[1] W. Weng, Y. Lan, D. Tang, L. Fu, W. Tan, S. Zhong, ACS Appl. Energy Mater. 2025, 8, 18, 13139.

[2] A. Claassen, Rec. Trav. Chim. Pays-Bas 1925, 44, 790.

Fig. 1

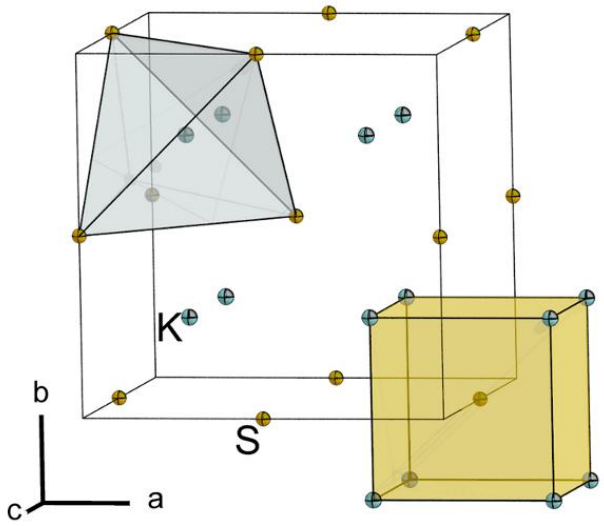

Fig. 2

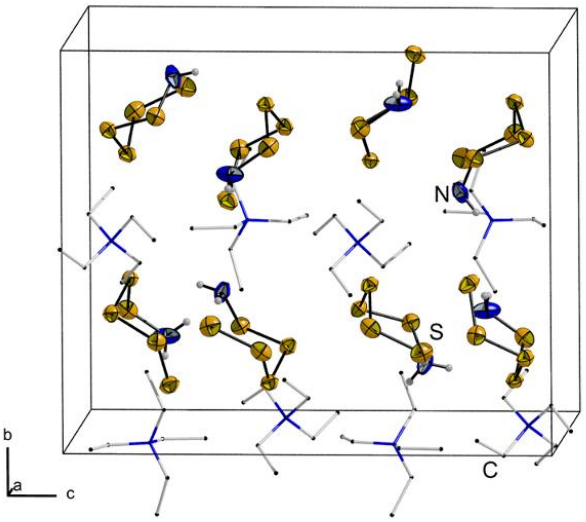
N
S
C
b
a
c

MS 11: New Biological Structures

OP-64

Racemic crystal structure of a synthetic DNA hairpin with diquinoline linker

The availability of affordable, commercial L-DNA sequences and ease to obtain diffraction-quality crystals make racemic DNA crystallography a striking alternative to conventional crystallization using D-enantiopure solutions alone [1].
The racemic DNA approach recently enabled us to obtain diffraction-quality crystals of a synthetic hairpin DNA with segments d(GT4G) and d(CA4C) conjugated with a diamide quinoline linker unit. While the D-enantiomer of this hairpin DNA yielded crystals with weak, DNA fiber-like diffraction pattern; the racemic mixture of hairpin DNA yielded crystals that diffracted to a resolution of 2.5 Å and belonged to centrosymmetric space group P-1 (Figure 1) [2].
The racemic crystal structure validated the design and synthesis of the linker unit to serve as a hairpin turn in a DNA duplex and function as an anchor point for an aromatic helical foldamer mimicking the shape and surface properties of B-DNA [3]. The crystal structure complemented with circular dichroism (CD) and molecular models demonstrated the ability of the linker to position the foldamer helix and the duplex DNA so that their rims and grooves are aligned despite their completely different chemical nature.
Figure 1: Unit cell arrangement of hairpin DNA in P-1 space group.

References

[1] Mandal, P.K.., Collie, G.W., Kauffmann, B. & Huc, I. (2014). Angew. Chem. Int. Ed. 53, 14424.

[2] Loos, M., Xu, F., Mandal, P.K., Chakrabortty, T., Douat, C., Konrad, D., Cabbar, M., Singer, J., Corvaglia, V., Carell, T. & Huc, I. (2025). Angew. Chem. Int. Ed. (in press).

[3] Ziach, K., Chollet, C., Parissi, V., Prabhakaran, P., Marchivie, M., Corvaglia, V., Bose, P.P., Laxmi-Reddy, K., Godde, F., Schmitter, J.-M., Chaignepain, S., Pourquier, P. & Huc, I. (2018). Nat. Chem. 10, 511.

Fig. 1

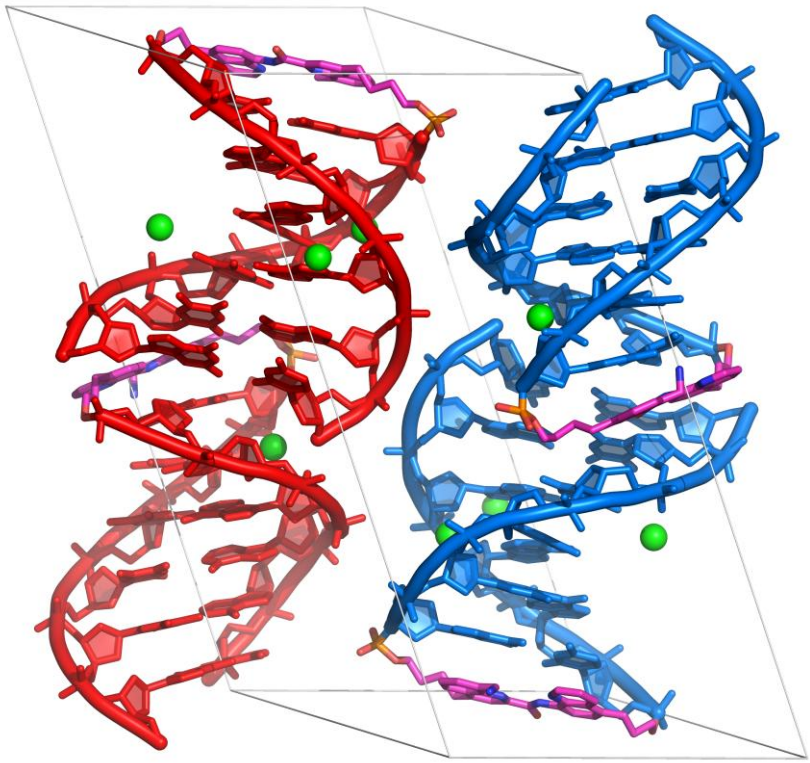

OP-65

How Nature Powers Alkane Monooxygenases: Understanding the Electron Transfer in AlkB Complexes with Different Architectures

I. Span (Erlangen/DE), R. Ganguly (Erlangen/DE), K. Parashar (Erlangen/DE), R. Austin (New York City, NY/US)

Alkanes are energy-rich carbon sources found in nature and are key targets in microbial degradation and bioremediation of oil. Alkane monooxygenases (AlkB) are membrane-bound metalloenzymes that initiate this process by converting straight-chain alkanes to alcohols. While AlkB enzymes vary in their ability to oxidize different alkane chain lengths, each typically acts on a narrow substrate range. A critical step in AlkB function is electron transfer to the diiron active site, yet the mechanisms of electron transfer across different AlkB architectures remain poorly understood. Here, we investigate the electron transfer domains from three distinct alkane-oxidizing systems, combining spectroscopy and crystallography to reveal how nature powers these enzymes. In particular, we highlight a three-domain AlkB that relies on both a ferredoxin reductase and a ferredoxin domain to shuttle electrons to the catalytic center. Our findings reveal how structural diversity in AlkB complexes shapes electron transfer pathways and substrate oxidation. These insights advance our understanding of microbial alkane metabolism and offer new perspectives for engineering AlkB systems for environmental and marine bioremediation.

Figure 1: Crystal structure of the ferredoxin reductase domain of *Polaromonas naphthalenivorans* AlkB. The protein is displayed as a ribbon diagram, highlighting the overall fold of the reductase domain. The FAD cofactor is shown as a stick model, with the $2F_O$-F_C electron density map around the cofactor (blue mesh), showing its well-defined binding within to the protein domain.

Fig. 1

OP-66

Molecular basis for azetidine-2-carboxylic acid biosynthesis

T. Klaubert (Garching/DE), J. Gellner (Garching/DE), J. Effert (Marburg/DE), V. Kaila (Stockholm/SE), H. Bode (Marburg/DE), Y. Li (Paris/FR), M. Groll (Garching/DE)

This study investigates the structural, biochemical, and phylogenetic aspects of S-adenosylmethionine (SAM) lyases, AzeJ and VioH. These enzymes catalyse the intramolecular cyclisation of SAM, yielding azetidine-2-carboxylic acid (AZE) and methylthioadenosine (MTA). The structures of AzeJ and VioH were elucidated, revealing a homodimeric form for AzeJ and a monomeric form for VioH. Both enzymes share a Rossman fold characteristic of SAM-dependent methyltransferases. The binding site analysis with S-adenosyl-L-homocysteine (SAH) uncovered structural rearrangements, suggesting a closed state during catalysis. Complex structures of AzeJ with SAM indicated the formation of AZE and MTA, shedding light on the reaction mechanism. Mutational studies highlighted key residues influencing catalytic activity, while phylogenetic analyses showed sparse distribution of AZE synthases in bacteria, mainly in Pseudomonadota and Actinomycetota. Additionally, the study explored the incorporation of AZE into pyrrolizixenamides, showcasing its potential in combinatorial biosynthesis.

Fig. 1

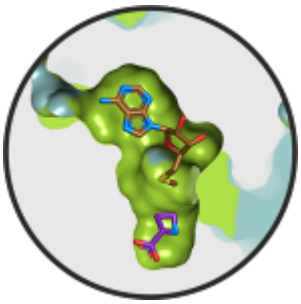

OP-67

Discovery of Arg-Cys and Gly-Cys N-O-S Linkages in Proteins via Machine-Learning and QM-Refined Structural Re-analysis

S. Bazzi (Hamburg/DE), S. Sayyad (Pullman, WA/US)

Our work [1] introduces an innovative approach at the interface of chemistry and biology, addressing the critical challenge of systematically characterizing and identifying chemical bonds and interactions in protein structures. Traditionally, new chemical bonds in proteins were discovered through serendipitous experimental observations. However, the exponential growth in experimental data and computational capabilities now necessitates the development of novel tools and methodologies essential for efficiently mining data banks and systematically uncovering chemical bonds that have been overlooked throughout the history of protein structure determination.

We have developed a framework that synergistically combines experimental data, bioinformatics tools, and machine-learning approaches. This integration fills a critical gap in the active determination of chemical bonds and interactions in proteins. As a proof of concept, we applied our algorithm to search for nitrogen-oxygen-sulfur (NOS) linkages, encompassing and extending beyond the recently uncovered lysine-cysteine linkages [2] Analyzing over 86,000 protein structures and their X-ray validation reports, our investigation led to the suggestion of two new categories of NOS linkages: between arginine and cysteine and between glycine and cysteine. In total, we identified 69 previously unrecognized NOS linkages in protein structures, along with characteristic descriptors that serve as predictive properties. Importantly, our algorithm is highly adaptable and can be easily applied to investigate chemical bonds between any desired atoms.

References

[1] Bazzi, S., Sayyad, S. Revealing arginine-cysteine and glycine-cysteine NOS linkages by a systematic re-evaluation of protein structures. *Commun Chem* 8, 146 (2025).

[2] Wensien, M., von Pappenheim, F.R., Funk, LM. *et al.* A lysine–cysteine redox switch with an NOS bridge regulates enzyme function. *Nature* 593, 460–464 (2021).

OP-68

Cryo-EM Structure of an Acyl-CoA Carboxylase Complex Essential for Mycolic Acid Synthesis in Mycobacteria

S. Geibel (Leiden/NL)

The mycolic-acid layer in the cell wall of *Mycobacterium tuberculosis* forms a permeability barrier that is critical for bacterial viability and intrinsic antibiotic resistance. Mycolic-acid biosynthesis requires several specialized enzymes, including acyl-CoA carboxylase complexes (ACCases). Among these, the long-chain acyl-CoA carboxylase (LCC) is the complex that carboxylates very long acyl-CoA substrates (C24–C26) and also acts on shorter-chain and branched acyl-CoAs. This broad specificity provides essential intermediates for fatty-acid biosynthesis, multimethyl-branched lipid formation, and the α-branch precursor for the terminal mycolate-condensation step. Despite its central role, LCC has lacked a mechanistic framework in the absence of a complete structure. Here, we present the cryo-EM structure of the endogenous LCC from *M. smegmatis*, revealing the organization of the fully assembled LCC. LCC assembles as a 868.3 kDa modular machine with a heterohexameric carboxyltransferase (CT) core (AccD4/AccD5) flexibly connected to two biotin-carboxylase (BC) tetramers (AccA3). An LCC-specific subunit, AccE5, acts as a molecular tether linking BC to the CT core, thereby explaining how it boosts catalytic activity. We captured multiple conformational states that alternate between open and closed CT active sites, outlining a trajectory for substrate binding, biotin-dependent carboxyl transfer, and product release. Together, these results define the architecture and dynamics underlying short- and long-chain acyl-CoA carboxylation by LCC in mycobacteria.

OP-69

Structural Insights into Transcription Regulation by ECF sigma factors in CRISPR Antiviral Defense

S. Binder (Bonn/DE), N. Schneberger (Bonn/DE), T. Heidler (Jülich/DE), S. Shahzad (Jülich/DE), D. Mann (Jülich/DE), M. Geyer (Bonn/DE), G. Hagelueken (Bonn/DE)

The CRISPR system provides prokaryotes with an adaptive immunity against mobile genetic elements. Type III CRISPR systems initiate complex antiviral responses by generating cyclic oligoadenylates (cOAs) that act as second messenger activating a range of downstream effector proteins which can induce viral clearance, cell dormancy or death.

Here, we elucidate the molecular details of a CRISPR signaling complex that employs an extracytoplasmic function (ECF) sigma factor/anti-sigma factor pair to regulate transcription in response to viral infection in *Sulfurihydrogenibium* spp. [1]. In this system, the protease subunit CalpL detects cyclic tetraadenylate (cA4), which triggers the release of the sigma factor CalpS and its anti-sigma factor CalpT from the complex. CalpS is subsequently freed from CalpT, likely through ClpX-mediated proteolysis [2], enabling CalpS to associate with RNA polymerase and initiate transcriptional responses.

To reveal the structural basis of this switch, we solved the crystal structure of CalpS bound to CalpT, and a cryo-EM structure of active CalpS in complex with the *E. coli* RNA polymerase core enzyme. The crystal structure of the inhibited conformation reveals an extensive interface where CalpT sequesters the RNA polymerase–binding surface of CalpS. In contrast, the cryo-EM structure shows how conformational rearrangements expose this interface, enabling an engagement of CalpS with the RNA polymerase. Together, these structures illuminate the allosteric transitions that couple cA_4 sensing to transcriptional activation, providing a mechanistic framework for how type III CRISPR systems rewire cellular transcription in response to viral infection.

References

[1] Rouillon C, Schneberger N *et al*. Antiviral signalling by a cyclic nucleotide activated CRISPR protease. doi: 10.1038/s41586-022-05571-7.

[2] Smalakyte D. Filament formation activates protease and ring nuclease activities of CRISPR Lon-SAVED. doi: 10.1016/j.molcel.2024.09.002.

MS 14: Functional Materials

OP-70

Impact of Intrinsic point defects on the performance of CZTS Monograin solar cells

H. Prell (Berlin/DE), G. Gurieva (Berlin/DE), S. Schorr (Berlin/DE)

Kesterite-type Cu2ZnSn(S,Se)4 (CZTSSe) semiconductors serve as green absorbers in the only inorganic photovoltaic technology free of critical raw materials. Conversion efficiencies of CZTSSe-based solar cells have been increasing rapidly, reaching >16% [1]. These semiconductors offer potential for low-cost, eco-friendly energy worldwide, but low open-circuit voltage and cation disorder hinder large-scale use. Employing extrinsic dopants, accurately controlling deviations from stoichiometric ratios, and precisely modulating phase evolution during synthesis are powerful strategies to manage the formation of intrinsic point defects and tailor electronic properties [2]. The Monograin technology [3] utilizes a powder of CZTS single crystals, 50-100 µm in size, embedded in a polymer matrix to form a flexible, semi-transparent solar module (MGS). CZTS absorbers with initially identical Cu-poor/Zn-rich compositions are synthesized utilizing different Alkali-salt fluxes to investigate the incorporation of Na and K and the effects on intrinsic point defects. MGS are made from these absorbers, and their performance is measured. Neutron diffraction experiments at POWGEN (BL 11A) [4] and the average neutron scattering length analysis [5] are being used to derive the cation distribution model and identify types and concentrations of intrinsic point defects in these samples. The intrinsic point defects and especially the Cu/Zn-disorder are correlated with the chemical composition, bandgap energy, and solar performance parameters to determine structure-property relationships to uncover mechanisms influencing material performance.

References

[1] Meng (June 11th, 2025) *15th European Kesterite+ and 3rd ReNewPV Workshop*

[2] Schorr et al. (2021) *Crystallography in Matrial Science*, 128

[3] Meissner et al. (2023) *Solar Energy Materials and Solar Cells*, 252, 112160

[4] Huq et al. (2019) *Applied Crystallography*, *52*(5), 1189

[5] Schorr et al. (2015) *Neutron Applications in Materials for Energy*, 83

OP-71

Structural relations in chalcogenide compound semiconductors for photovoltaic applications

S. Schorr (Berlin/DE), G. Gurieva (Berlin/DE)

Wafer-based silicon solar cells with a thickness of approximately 200 µm represent a well-established photovoltaic (PV) technology, achieving a record power conversion efficiency (PCE) of 27.8%[1] and currently accounting for 95% of the installed PV capacity in Germany [2]. Silicon crystallizes in the diamond-type structure, where each atom is tetrahedrally coordinated by four neighboring silicon atoms. As second-generation PV devices, thin-film solar cells offer significant cost reduction potential due to their thin absorber layers (1–2 µm) deposited on glass or flexible substrates. In addition to being lightweight and mechanically flexible, they utilize binary or ternary chalcogenide semiconductors such as CdTe (PCE=23.1%[1]) and $Cu(In,Ga)Se_2$ (PCE=23.6%[1]) as absorbers. These compounds adopt crystal structures derived from the diamond-type, including sphalerite, chalcopyrite, and the CuAuI-type structure. In the ongoing search for novel and more sustainable absorber materials, quaternary chalcogenides of the type $Cu_2B^{II}C^{IV}X_4^{VI}$, such as $Cu_2ZnSn(S,Se)_4$ (PCE=15.8%), have emerged as promising candidates. Substituting different cations (e.g., B^{II}=Mn,Fe,Cd; C^{IV}=Sn,Ge,Si) enables band gap tuning across a wide range (0.9–3.1eV [3]), opening access to a broad material landscape. These compounds crystallize in tetrahedrally coordinated structures derived from chalcopyrite- and CuAuI-type frameworks. Including Wurtzite-related derivatives, four main structure types are identified: kesterite, stannite, wurtz-kesterite, and wurtz-stannite. Which of these forms is realized depends largely on cation and anion size ratios. This presentation gives an overview of these complex structures based on insights gained from neutron diffraction studies showing the importance of structure-property relations when developing novel materials.

References

[1] www.nrel.gov/pv/cell-efficiency

[2] www.umweltbundesamt.de/themen/klima-energie/erneuerbare-energien

[3] Schorr, Sol.En.Mat.Sol.Cells 249 (2022) 112044

OP-72

Crystallographic Investigation of Intermediates in the Synthesis of Alkaline Earth Metals Tetrahydroborates

A. Sedykh (Leipzig/DE)

Tetrahydroborates of alkaline earth metals have several advantages over alkali metal ones for hydrogen storage: safer decomposition products and lower temperatures and enthalpies of hydrogen release. Despite $Ca(BH_4)_2$ being a compound of great interest, the complete synthetic pathway for its preparation has not been fully clarified.

In the mechanochemical reaction between $CaCl_2$ and $NaBH_4$, amorphous $Ca(BH_4)_2$ is formed. It is separated by complexation with tetrahydrofuran, yielding a well-soluble complex. Upon solvent removal, $[Ca(thf)_4(BH_4)_2]$ forms in two molecular configurations: *cis* (SG $P2_1/n$) and *trans* (SG $P2_1/c$), both previously unreported. Upon further drying, these complexes convert to $^1_\infty[Ca(thf)_2(BH_4)_2]$. Previously, the crystal structure of this compound was assigned SG $P2_1/n$[1] or $P2_1$.[2] Here, it is determined as $P2_12_12$. Additionally, β-$^1_\infty[Ca(thf)_2(BH_4)_2]$ (SG $P\bar{1}$) has been observed.

Further, $^1_\infty[Ca(thf)(BH_4)_2]$ (SG $P2_1/n$) is formed. It was previously reported as a depletion product of the calcium catalyst used in the synthesis of cyclic borazines.[3] Here, $^1_\infty[Ca(thf)(BH_4)_2]$ is directly associated with the synthesis of calcium tetrahydroborate. At higher temperature (>200 °C), the β-$Ca(BH_4)_2$ is formed. Upon cooling to room temperature, it partially transforms into other polymorphs.

The full description of the $Ca(BH_4)_2$ synthesis identified several potential pitfalls in obtaining high-purity material. Further, this knowledge could be expanded to the synthesis of other alkaline earth metals and d-block elements tetrahydroborates, with the goal to obtain double-cation tetrahydroborates $AE_xM_y(BH_4)_n$, where AE is an alkali earth metal ion (Mg, Ca) and M is an abundant lightweight d-element metal cation.

References

[1] B. Richter et al. *Inorg. Chem.* **2018**, *57*, 10768–10780.

[2] N. T. Hahn et al. *J. Mater. Chem. A* **2020**, *8*, 7235–7244.

[3] P. Bellham et al. *Organometallics* **2014**, 33, 5716–5721.

Fig. 1

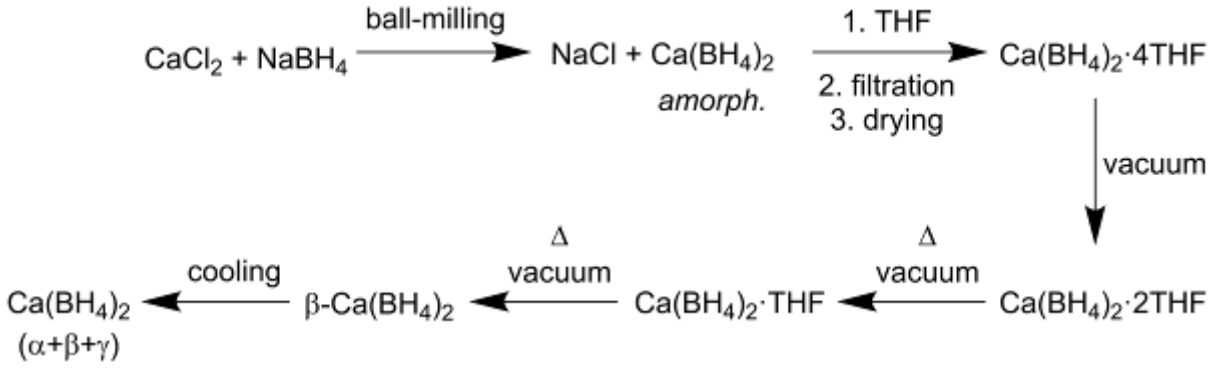

OP-73

Structural and compositional design of layered oxide cathodes for sodium batteries

D. Mikhailova (Eggenstein-Leopoldshafen/DE)

Rechargeable sodium-ion batteries are promising sustainable energy storage systems, owing to their low cost and similarities to lithium-ion batteries. Layered transition metal oxides with sodium are especially suitable for applications. However, the existing cathode chemistries exhibit restricted electrochemical performance, which hinders their practical implementation. To overcome challenges, originating from kinetically limited structural transformations, compositional and structural design can be suggested. Here, we discuss and compare three cation substitution strategies in layered sodium oxides: *i*) transition metal single-cation substitution, *ii*) transition metal multi-cation substitution, and *iii*) sodium cation substitution. Every strategy influences various material properties as structure symmetry, bulk Na-diffusivity, and phase transitions upon sodium removal and insertion. Attempts to systemize and elucidate experimental findings, also with implicating the literature data, were done.

OP-74

Fractal metal structures for battery electrodes: Morphology, microstructure, application

T. Leisegang (Freiberg/DE), S. von Bahder (Freiberg/DE), M. Momeni (Freiberg/DE), Y. M. Li (Freiberg/DE), H. Morhli (Freiberg/DE), M. Danziger (Freiberg/DE)

This work investigates metallized woven-glass-grid current collectors [1] and their application for battery electrodes. The focus is on the fractal copper top layer, which is intended to minimize local current density, "dead" lithium formation, and mechanical stress caused by active material volume expansion as well as increasing of active material adhesion. Different fractal Cu and Al current collectors were examined using scanning electron microscopy (SEM), transmission electron microscopy (TEM), X-ray diffraction (XRD), photoelectron spectroscopy (XPS) and BET analysis. The fractal dimension is determined using multifractal analysis. The relationships between the parameters are further examined in a correlation analysis. The application of fractal current collectors for different anodes is demonstrated in half and full cell geometry in coin cells of different battery chemistries.

Reference

[1] Y.-M. Li, *et al.*, Resource-Efficient Electrodes with Metallized Woven-Glass-Grid Current Collectors for Lithium-Ion Batteries. *ChemSusChem* 2025, 18, e202402233. https://doi.org/10.1002/cssc.202402233

Fig. 1

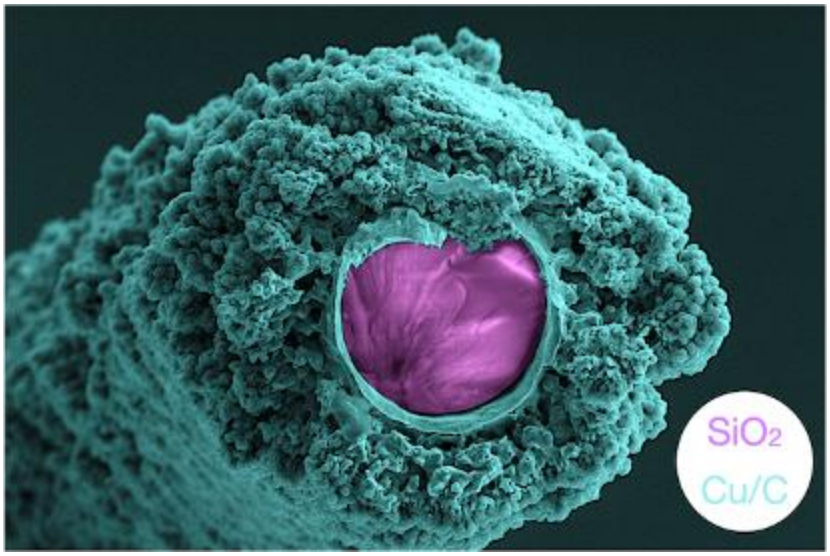

OP-75

3D electron diffraction mapping of perturbations in van der Waals gap tailored non centrosymmetric elastic molecular crystals

S. Dey (Prague/CZ), M. Jarošová (Prague/CZ), H. Chintakindi (Prague/CZ), V. Eigner (Prague/CZ), L. Palatinus (Prague/CZ)

Molecular crystals with macroscopic elastic bending property have shown tremendous potential for applications as flexible optical waveguides, fluorescent materials, piezo- and ferroelectrics, semiconductors and drug tablets in the last decade.[1] and references therein *μ*-X-ray diffraction technique has been used to understand the underlying mechanisms of deformation.[2] However, inherent disadvantages of the method preclude quantification of underlying defects under strain.

We modified the van der Waals gap/distance between acid–base synthons by crystallizing flexible single crystals isomorphous to the known elastic cocrystal solvate system of caffeine (CAF), 4-chloro-3-nitrobenzoic acid (CNB) and methanol (MeOH) in space group symmetry *Fdd*2.[3] The two new cocrystal solvates of CAF, CNB and ethanol (ETOH); and CAF, 4-bromo-3-nitrobenzoic acid and MeOH differ in van der Waals distances between the *π*-*π* stacks.

To study permanent deformation in these materials, continuous rotation 3D electron diffraction (3DED) experiments were performed using the transmission electron microscope FEI Tecnai G2 20 at T = 100 K. Several points from crystal edge lines to the central line were mapped on a micro-rod crystal (Fig. 1). At each point 3DED images were collected using conditions: -35° ≤ α ≤ 35°, Δα = 0.3°, exposure t ≤ 500 ms. The length of the c-axis ‖ π–stacking of molecules show maximum variation along the cross sections of the crystal (Fig. 1). The origin of these deformations can be due to the perturbations on the crystal shape induced during sample preparation.

Therefore, 3DED have probed the plastic regime of crystals beyond the elastic limit of these materials.

References

[1] Z. Zhou et al. (2022) Chem. Eng J. 450, 138333.

[2] A. J. Thompson et al. (2021) CrystEngComm 23, 5731.

[3] S. Ghosh et al. (2012) Angew. Chem. Int. Ed. 51, 10319.

Fig. 1: (a) Optimal image of a crystal (b) TEM image of a crystal.

The authors acknowledge P4F MSCA COFUND reg. nr: 101081515 for funding.

Fig. 1

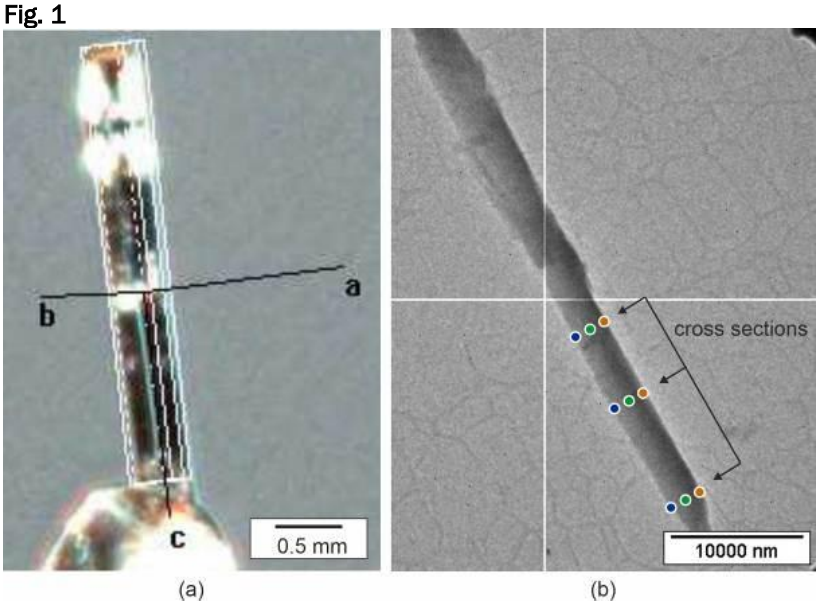

(a) (b)

MS 15: Time-resolved Crystallography and Protein Design

OP-76

Catalytic dynamics in an antibiotic resistance enzyme observed by time-resolved crystallography

R. Bosman (Hamburg/DE), E. C. Schulz (Hamburg/DE)

Antibiotic resistance is often mediated by antibiotic modifying enzymes (AMEs). Aminoglycoside Acetyltransferases (AAC) are members of the (GCN5)-related N-acetyltransferases (GNAT) family which mediate non-protein Acetyl-CoA dependent acetylation. Different AAC"s are responsible for aminoglycoside inactivation by acetylating a primary amine at a specific position on aminoglycoside sugar rings. This prevents the aminoglycoside binding to the ribosome A-site, which would disrupt protein translation. Interestingly, AAC-(6")-il is a dimeric enzyme that displays distinct temperature-dependent cooperative responses to either binding the acetyl-CoA, or aminoglycoside antibiotic substrates. Moreover, like many AAC"s, it is promiscuous to 4,5- and 4,6- linked aminoglycoside antibiotics, however unlike others, in AAC-(6")-il the aminoglycoside pocket is located between dimer subunits likely changing the interactions between dimers with different substrates.

Despite this, there is currently neither a structure for the ternary complex nor any for catalytic intermediates. We aim to understand the structural changes underpinning the allosteric communication and how it is related to acetylation. To this end we utilize our method developments in multi-temperature, time-resolved serial crystallography, and automated cryo-trapping via the spitrobot crystal plunger on the AAC-(6")-il:AcCoA complex.

These methodologies permit us to measure crystal structures in *out-of-equilibrium* conditions and determine the structure of meta-stable states. As such, we report the first aminoglycoside bound structure to AAC-(6")-il, as well as an ES complex alongside catalytic intermediates. We demonstrate that AAC adopts distinct conformations dependent on binding either its 4,5- and 4,6- linked substrates. Finally, we highlight the potential catalytic role of a previously unobserved water molecule appearing in the active-site upon aminoglycoside binding.

OP-77

Structural characterization of the BLUF photoreceptor OaPAC using time-resolved crystallography and FTIR spectroscopy

A. Chretien (Schenefeld/DE), M. Nagel (Bielefeld/DE), S. Botha (Tempe, AZ/US), D. von Stetten (Hamburg/DE), R. de Wijn (Schenefeld/DE), P. Mehrabi (Hamburg/DE), A. Mancuso (Schenefeld/DE), J. Schulz (Schenefeld/DE), A. Pearson (Hamburg/DE), T. Kottke (Bielefeld/DE), K. Lorenzen (Schenefeld/DE), R. Schubert (Schenefeld/DE)

Time-resolved crystallography (TRX) offers high spatial and temporal resolution, essential for capturing structural dynamics in light-sensitive proteins. Blue-Light sensor Using Flavin (BLUF) proteins, like the photoactivated adenylate cyclase (PAC) from Oscillatoria acuminata, are particularly useful in pump-probe experiments. PAC combines a BLUF sensor domain and an adenylate cyclase effector domain responsible for ATP-to-cAMP conversion. Complete X-ray crystallography datasets of OaPAC at cryogenic temperature and room-temperature in its dark state with ATP bound in the active site will be presented. Pump-probe time resolved crystallography using XFELs (TRSFX) and synchrotron (TRSSX) in combination with FTIR spectroscopy was performed and reveal structural changes around the FMN chromophore for several time points. The data shows the rotation of Glu48, which initiates a change in FMN hydrogen bond network and leads to a reduced distance of Glu48 to FMN O4. Notably, the observed kinetics from the TRSFX experiments differ from spectroscopy data. The obtained data suggests that the onset of the displacement of Met92 initiates signal transmission to adenylate cyclase domain. FTIR spectroscopy data revealed information about the ATP binding mode and the allosteric regulation of OaPAC. Reaction intermediates from milliseconds to seconds were captured by cryo-trapping experiments, revealing a "Tryptophan-in" conformation (W90) in the light activated state, which is known from some BLUF proteins, but was not seen for BLUF-PAC so far. The performed experiments will help to visualize and understand the entire signaling process of OaPAC, which can serve as a basis to design novel optogenetic tools.

OP-78

Implementing electric field-stimulated X-ray crystallography at EMBL P14 T-REXX using Hadamard time-resolved X-ray crystallography

M. Klureza (Hamburg/DE), J. Estengre Pérez (Hamburg/DE), E. E. Römer (Hamburg/DE), Y. Pulnova (Dolní Břežany/CZ), C. D. Gaman (Leeds/GB), F. Tellkamp (Hamburg/DE), J. P. Leimkohl (Hamburg/DE), M. Kollewe (Hamburg/DE), M. Nikolova (Hamburg/DE), H. Schikora (Hamburg/DE), G. Beddard (Leeds/GB), G. Bourenkov (Hamburg/DE), D. von Stetten (Hamburg/DE), D. Hekstra (Cambridge, MA/US), B. Yorke (Leeds/GB), A. Pearson (Hamburg/DE)

Introduction: Electric field-stimulated X-ray crystallography (EF-X) [1] offers a novel way to perturb biological macromolecules and gain insight into their dynamics. In EF-X, a strong (~1 MV/cm) electric field is established across a protein crystal, creating a pattern of applied forces localized to the charges within each protein and inducing molecular motions.

Objectives: Like many pump-probe crystallographic methods, EF-X originally relied on Laue radiation for fine time resolution. However, Laue synchrotron beamlines are rare and introduce additional complexity. We therefore sought to implement EF-X at a monochromatic synchrotron beamline.

Materials & Methods: We coupled EF-X with Hadamard time-resolved X-ray crystallography (HATRX) [2], a method that improves the time resolution for a given photon flux by summing together multiple timepoints onto a single detector image. Repeating the measurement with various combinations of timepoints, selected according to an encoding Hadamard matrix, then enables deconvolution of the underlying time-resolved data.

Results: Using this Hadamard modality, we implemented EF-X at EMBL's P14 T-REXX beamline at DESY. We successfully collected proof-of-concept EF-HATRX data in 2023; while EF-HATRX data processing is still under development, even preliminary analysis showed verifiable electron density at <500 ns (as assessed by the Perturbed Model Real-space Difference Density test [3]). We have since improved on the initial methodology and established a BAG at T-REXX to widen access to EF-HATRX.

Conclusion: Establishing EF-HATRX at P14 T-REXX both significantly improves European access to EF-X and further validates HATRX as a general approach to time-resolved crystallography.

References

[1] Hekstra, D. R. *et al.* (2016). *Nature* 540, 400-405.

[2] Yorke, B.A. *et al.* (2014). *Nature Methods* 11, 1131-1134.

[3] von Stetten, D., & Pearson, A. R. (2025). *bioRxiv* 2025-08.

OP-79

Enzymes for a sustainable plastic waste management

P. Singh (Berlin/DE), Y. Boyakova (Berlin/DE), C. Genter-Dieguez (Berlin/DE), P. Da Silva (Berlin/DE), T. Bock-Bierbaum (Berlin/DE), M. S. Weiss (Berlin/DE), F. Lennartz (Berlin/DE), G. Weber (Berlin/DE)

During the last 80 years, about 10 billion tons of plastics have been synthesized and their ongoing crude-oil derived production still makes out most products (90%) compared to bio-based (1%) and recycling (9%) alternatives. Current thermo-(mechanical) and chemical recycling technologies typically have high energy costs and lead to a material downgrade in each roundIn recent years, enzymes and microbes have become a viable option for sustainable biocatalytic re- and upcycling of plastics, paving the way towards circular economies. However, due to the complexity of different polymer types and their recalcitrance to biodegradation, these enzymes still must be improved and adapted before they qualify for industrial scales. In 2016, the discovery of a bacterium coined *I. sakaiensis* that degrades and metabolizes polyethlene terephthalate (PET) with the help of two naturally evolved key enzymes, PETase and MHETase, triggered global interest and research initiatives on this topic. We have determined the first crystal structure of MHETase bound to its substrate and enhanced the enzyme based on the structural data. Several further PET hydrolases have been structurally characterized in our group since then and improved by enzyme engineering. We obtained the first structure of urethanase SP2, an amidase that can hydrolyze the carbamate bond of polyurethanes. The structure enabled an improvement of the enzyme towards simple substrate snippets. We are currently pursuing a re-design of the enzyme with AI-based protocols to increase its activity towards larger substrates. We anticipate enzymes to play a major role in future polymer recycling processes upon their biotechnological improvement.

OP-80

From Protein Design to Crystalline Biohybrids: Building Ordered Superlattices

T. Beck (Hamburg/DE)

Self-organization of biomolecular building blocks can be harnessed for the construction of functional nanomaterials. We have recently established a novel method for the self-organization of biomolecular building blocks and nanoparticles. Here, protein cages, engineered with opposite surface charge, are used as an atomically precise ligand shell for the assembly of inorganic nanoparticles.[1] The assembly of these protein-nanoparticle composites yields highly ordered nanoparticle superlattices with unprecedented precision.[2] The biohybrid materials show interesting optical properties.[3-4]

Current work shows the assembly of two differently sized, supercharged protein nanocages to create a matrix for nanoparticle arrangement. Typically, the ordered assembly of objects with nonmatching symmetry is challenging, but our electrostatic-based approach overcomes the symmetry mismatch by exploiting electrostatic interactions between oppositely charged cages. Importantly, we refined superlattice structure data obtained from single-crystal SAXD experiments, providing conclusive evidence of the final assembly type. Our findings highlight the versatility of protein nanocages for creating distinctive types of binary superlattices.[5]

We have recently focused on using state-of-the-art protein design methods to re-engineer existing protein cages and create novel cages as templates for the assembly of nanoparticle superlattices.

References

[1] M. Künzle, T. Eckert, T. Beck, *J. Am. Chem. Soc.* **2016**, *138*, 12731-12734

[2] M. Künzle, T. Eckert, T. Beck, *Inorg. Chem.* **2018**, *57*, 13431-13436

[3] M. Lach, C. Strelow, A. Meyer, A. Mews, T. Beck, *ACS Appl. Mater. Interfaces* **2022**, *14*, 10656-10668

[4] N. O. Junker, A. Lindenau, M. Rütten, M. Lach, A. Nedilko, D. N. Chigrin, G. von Plessen, T. Beck, *Adv. Funct. Mater.* **2023**, 10.1002/adfm.202303260

[5] M. Rütten, L. Lang, H. Wagler, M. Lach, N. Mucke, U. Laugks, C. Seuring, T. F. Keller, A. Stierle, H. M. Ginn, T. Beck, *ACS Nano* **2024**, *18*, 25325-25336

OP-81

Structure based development of new E3 Ligase Ligands

S. Knapp (Frankfurt am Main/DE)

The human E3 ligase family is a large and diverse family of proteins that has not been widely explored for the development of ligands and PROTACs (PROtein Targeting Chimeras). In this talk I will discuss strategies for the identification of new ligands using DEL-ML (DNA-encoded library screening coupled to machine learning) and high throughput crystallographic fragment screening. I will also discuss strategies for the validation of E3 ligands for the development of the next generation of PROTAC degraders as well as a streamlined PROTAC synthesis platform using click chemistry in conjunction together with a "direct-to-biology" screening approach.

References

[1] Crystallographic fragment screening reveals ligand hotspots in TRIM21 PRY-SPRY domain.
Kim Y, Lučić A, Lenz C, Farges F, Schwalm MP, Saxena K, Hanke T, Marples PG, Aschenbrenner JC, Fearon D, von Delft F, Krämer A, Knapp S. Commun Chem. 2025 Jun 13;8(1):185. doi: 10.1038/s42004-025-01574-3.

[2] Workflow for E3 Ligase Ligand Validation for PROTAC Development.
Miletić N, Weckesser J, Mosler T, Rathore R, Hoffmann ME, Gehrtz P, Schlesiger S, Hartung IV, Berner N, Wilhelm S, Müller J, Adhikari B, Němec V, Sivashanmugam SA, Elson L, Holzmann H, Schwalm MP, Hoffmann L, Abdul Azeez KR, Müller S, Kuster B, Wolf E, Đikić I, Knapp S. ACS Chem Biol. 2025 Feb 21;20(2):507-521. doi: 10.1021/acschembio.4c00812. Epub 2025 Feb 11.

[3] Enantioselective Protein Affinity Selection Mass Spectrometry (EAS-MS).
Wang X, Sun J, Ahmad S, Yang D, Li F, Chan UH, Zeng H, Simoben CV, Houliston S, Dong A, Bolotokova A, Gibson E, Kutera M, Ghiabi P, Kondratov I, Matviyuk T, Chuprina A, Mavridi D, Lenz C, Joerger AC, Brown BD, Heath RB, Yue WW, Robbie LK, Beyett TS, Müller S, Knapp S, Harding R, Schapira M, Brown PJ, Santhakumar V, Ackloo S, Arrowsmith CH, Edwards AM, Peng H, Halabelian L. bioRxiv [Preprint]. 2025 Jan 22:2025.01.17.633682. doi: 10.1101/2025.01.17.633682.

[4] Functional Characterization of Pathway Inhibitors for the Ubiquitin-Proteasome System (UPS) as Tool Compounds for CRBN and VHL-Mediated Targeted Protein Degradation.
Schwalm MP, Menge A, Elson L, Greco FA, Robers MB, Müller S, Knapp S. ACS Chem Biol. 2025 Jan 17;20(1):94-104. doi: 10.1021/acschembio.4c00450. Epub 2025 Jan 3.

[5] PROTAC-mediated degradation reveals a non-catalytic function of AURORA-A kinase.
Adhikari B, Bozilovic J, Diebold M, Schwarz JD, Hofstetter J, Schröder M, Wanior M, Narain A, Vogt M, Dudvarski Stankovic N, Baluapuri A, Schönemann L, Eing L, Bhandare P, Kuster B, Schlosser A, Heinzlmeir S, Sotriffer C, Knapp S, Wolf E. Nat Chem Biol. 2020 Nov;16(11):1179-1188. doi: 10.1038/s41589-020-00652-y.

MS 16: Frontier Molecular Crystallography and Supramolecular and Framework Structures

OP-82

How many isomers hide within the disordered core of a supramolecule?

E. Peresypkina (Frankfurt a. M./DE)

Since chemical science entered the world of self-assembled molecular systems made of hundreds of components, such as giant cages in metallasupramolecular chemistry, the SC-XRD has become almost the only method for establishing the structure and composition of these compounds.[1] These molecular complexes, containing thousands of atoms, cannot be self-assembled without small deviations during the process, as their building blocks do not always have exactly one way to interact with other counterparts. Therefore, much more often than it is convenient to think, these self-assembled species have slight deviations in their molecular structure and are still able to pack in the crystal lattice due to their similar shape and size. As a result, the crystals of these compounds are intrinsically solid solutions of different forms and isomeric molecules. In the average structure established by SC-XRD, this phenomenon appears as a disordering, which can be ignored, treated formally or fully interpreted.

Our experience gained during the structural studies of pentaphosphaferrocene-based giant supramolecules (SMs) $[\{Cp^{R}Fe(\eta^5\text{-}P_5)\}_x(M)_y]$ (M = Cu, Ag, R = alkyl, CH_2Ph) shows that sometimes a barely noticeable disorder reveals that many different SMs overlap in the same crystallographic position.[2] Within this contribution, we present the way of restoring information on the initially co-crystallized molecules from SC-XRD data illustrated with two examples of average crystal structures of molecules that even have an integer number of atoms in their cores, but still are solid solutions.[3]

References

[1] A. V. Virovets, E. Peresypkina, M. Scheer (2021) *Chem. Rev.*, ***121***, 14485

[2] E. Peresypkina, A. V. Virovets, M. Scheer (2021) *Coord. Chem. Rev.*, **446**:213995

[3] S. Heinl, E. Peresypkina, W. Kremer, M. Scheer (2023) *Chem. Commun.*, **59**, 10263

Fig. 1

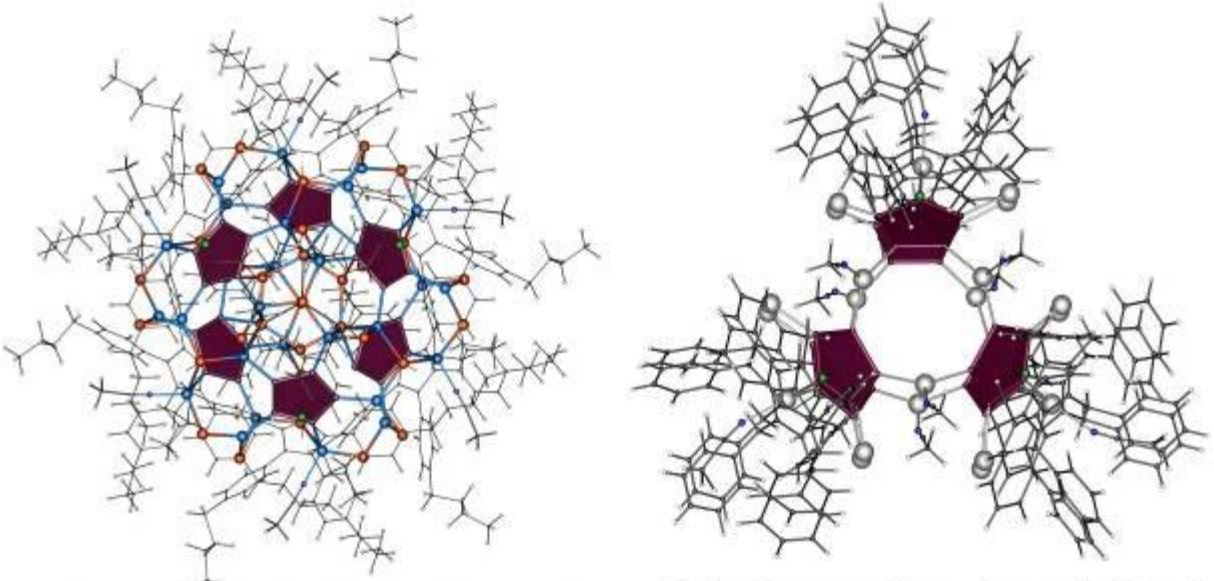

$[\{\eta^5\text{-}C_5(4\text{-}n\text{Bu}C_6H_4)_5\}_6(CuBr)_{32}(CH_3CN)_6]$ $[\{\eta^5\text{-}C_5(CH_2C_6H_5)_5\}_6Ag_9(CH_3CN)_9][SbF_6]_9$

OP-83

Photocrystallography Setup and In Crystallo Photoreaction: A Novel Approach to Study Light-Induced Chemical Processes

J. J. Holstein (Dortmund/DE)

A new design for a photocrystallography setup is presented, aimed at investigating *in crystallo* photoreactions, enabling real-time observation of light-induced chemical transformations within crystalline solids. The strainght forward integration of optical components into a single-crystal X-ray diffractometer allows for precise control over light exposure and the collection of structural data after various radiation wavelegth and doses. The applicability of this setup is demonstrated through the investigation of a reactive compound that is unstable in solution but can be effectively trapped "in crystallo" following photoreaction. Significant alterations in molecular geometry and intermolecular interactions are illustrated by the results, providing insights into reaction mechanisms that are otherwise obscured in solution-phase studies. This innovative approach not only enhances the understanding of photochemical processes at the atomic level but also opens new avenues for the design of materials with tailored photonic properties. Future applications are anticipated to include exploring of light switchable molecular motors *in crystallo.*

Fig. 1

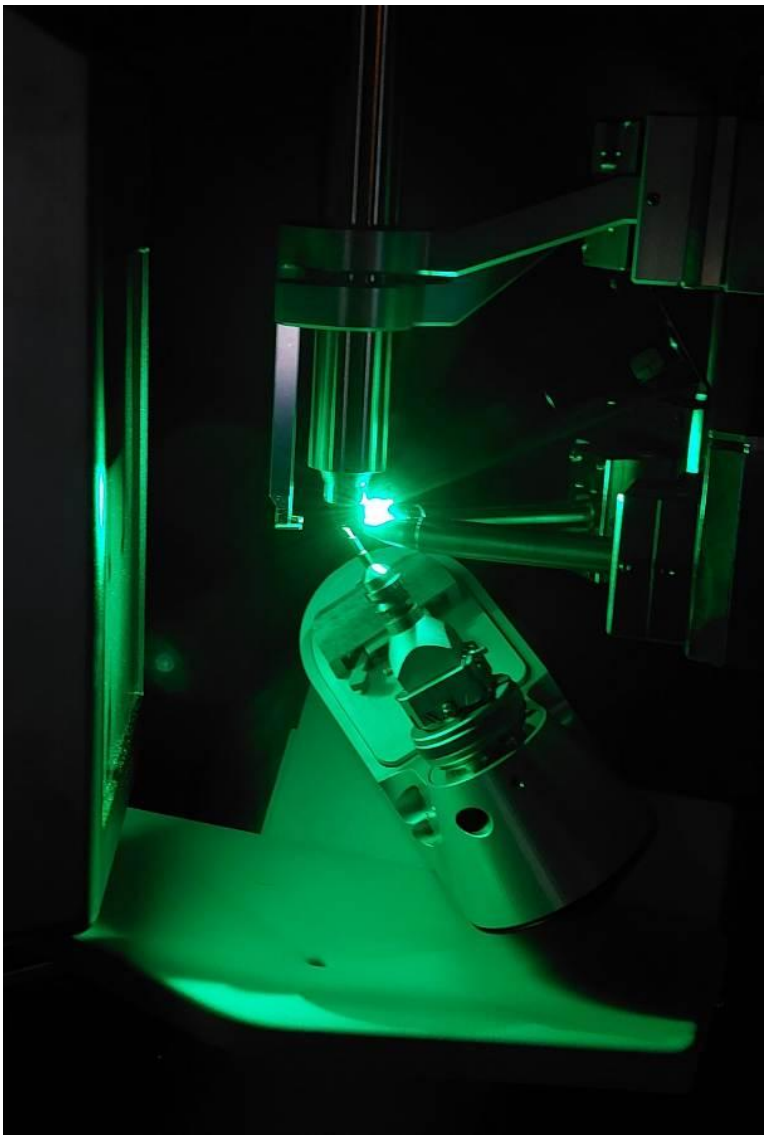

OP-84

Effect of Solvent on the Spin Crossover and Aging Process in $[Fe(NQu)_3(NCS)_2]$

P. Prakash (Jülich/DE), H. Shahed (Jülich/DE), H. Hüppe (Aachen/DE), W. Zhou (Jülich/DE, Aachen/DE), J. Qi (Jülich/DE), A. Grzechnik (Jülich/DE, Aachen/DE), J. Voigt (Jülich/DE), M. Angst (Jülich/DE), J. Perßon (Jülich/DE), B. Gasharova (Karlsruhe/DE), Y. L. Mathis (Karlsruhe/DE), D. Chernyshov (Grenoble/FR), K. Friese (Jülich/DE, Aachen/DE)

Spin crossover (SCO) compounds are molecular complexes which have a versatile nature due to their ability to switch between two spin states via temperature, pressure, light irradiation and chemical environments [1]. The transition between the spin states not only affects the magnetic properties but also couples strongly with the lattice affecting the intermolecular interactions and vibrational characteristics [2,3].

In this study we focus on a novel SCO compound $[Fe(NQu)_3(NCS)_2]$, where Qu = Quinoline and NCS^- = Thiocynate), which co-crystallizes with two solvents in its matrix namely, diethyl ether (Et2O, $(CH_3CH_2)_2O$) and methanol (MeO, CH_3OH). Magnetization measurements indicate that the fresh samples (stored in 1:1 solution of Et_2O + MeO) exhibit an abrupt and complete SCO, whereas the aged samples (exposed to atmosphere for 1 week) only exhibit incomplete SCO. The effect of aging was further investigated using infrared spectroscopy which revealed a gradual loss of MeO with time, with only trace amounts left in the aged samples. Single crystal diffraction data corroborates the solvent distribution and reveals disordered positions of the solvents. The aged crystals were further subjected to various solutions of Et_2O mixed with various polar solvents such as MeO, ethanol and acetone. The results indicate that the incorporation of MeO favors the spin state transition, establishing the compound as a potential methanol sensor.

References

[1] Kamilya et al., *Chem. Mater.* **36**, 10 (2024); P. Prakash et al., *Molecules*, **30**, 12 (2025); H. Shahed et al., *Acta. Cryst.* B**79**, (2023); K. S. Kumar *Coord. Chem. Rev.* **346**, (2017).

[2] P. Gütlich et al., *Beilstein J. Org. Chem.* **9**, (2013); E. Collet et al., *C. R. Chimie* **21**, (2018); Shatruk et al., *Coord. Chem. Rev.* **289-290**, (2015); E. Resines-Urien et al., *Chem. Soc. Rev.* **52**, (2023).

[3] J. A. Wolny et al., *C. R. Chimie* **21**, (2018); G. Molnár et al., *Ann. Phys. (Berlin)* **531**, (2019); J. Tuchagues et al., *Top. Curr. Chem.* **235**, (2004).

OP-85

Synthesis and characterization of a novel Ni-coordination polymer within the framework of a high school research project

S. Bette (Stuttgart/DE), T. Pal (Stuttgart/DE), J. Guo (Heidelberg/DE), B. V. Lotsch (Stuttgart/DE)

The HECTOR academy is promoting gifted high school students in STEM by initiating contacts between students and universities or research institutes. In a two-week research internship, a 10th grade high school student investigated the framework assembly via metal-directed organization of linear organic polymers by reacting nickel(II) acetate with phenyldiamine (PDA) and 2,5-Dihydroxyterepthaldehyde (DHTP) in a 1:1 THF-Ethanol mixture. The initial synthesis resulted into a polycrystalline powder, which could be indexed with a tetragonal unit cell, space group $I4_1/a$ (88), a = 23.1515(3) Å, c = 11.7480(2) Å and V = 6296.8(2) Å^3. As 10th grade high school students have no prior knowledge in diffraction or vibrational spectroscopy and such complex topics cannot be taught within two weeks, we decided to systematically vary the synthesis procedure in order to gain insight in the nature of the reaction product. Hence, we performed the synthesis using PDA or DHTP exclusively and, in addition, by immersing nickel(II) acetate in the THF-ethanol mixture. Interestingly, the tetragonal powder formed in all experiments. Consequently we performed the same syntheses using nickel(II) chloride as nickel source, which did not resulted in the formation of a crystalline product. This highlighted the essential role of the acetate anions in the product formation. The crystal structure solution from XRPD data using *simulated annealing* and Fourier mapping revealed a phase composition of $Ni(CH_3COO)_{1.6}(OH)_{0.4}$, which was confirmed by thermal and chemical analyses. The structure can be described as a porous, non-reticular framework (Figure 1) containing solvent molecules as guests. Further characterization was performed by sorption and SQUID measurements, as well as by vibrational spectroscopy.

Fig. 1: Crystal structure of $Ni(CH_3COO)_{1.6}(OH)_{0.4}$, (a) μ3-hydroxide ion acting as node, (b) nickel(II) acetate units as linkers, framework viewed in [00-1] (c) and [-100] (d) direction.

Fig. 1

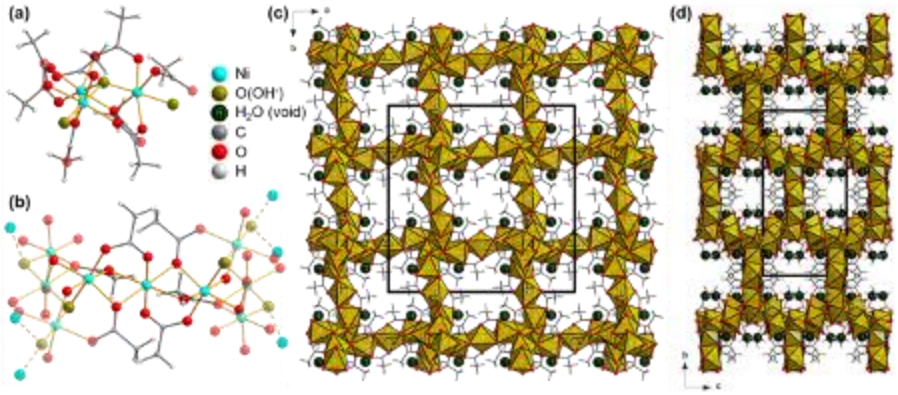

OP-86

Exploring Endohedral and Exohedral Weak Interactions of Pillarplex-Based Nanotubes

A. Pöthig (Garching/DE)

Pillarplexes M8L2(X)4 (where M = Ag, Au) are octanuclear NHC complexes that form metallocavitand architectures.[1] These supramolecular organometallic complexes (SOCs) possess notable properties such as the capacity to encapsulate linear guest molecules within their tubular cavities, inherent luminescence, and adjustable solubility. Additionally, they can be incorporated as functional units in rotaxanes.[2] Owing to their cationic charge (4+), cylindrical shape, and aromatic surfaces, these complexes readily engage in diverse non-covalent supramolecular interactions, both internally and externally. Our recent findings reveal that metal coordination enables the endohedral inclusion of non-linear guest molecules, including THF.[3] Moreover, we have shown that the electrophilic rim of the pillarplex can form CH-π interactions, which can be exploited for organocatalytic purposes.[4] Both cases are detailed here, along with structural elucidation through SC-XRD.

Figure 1. (**A**) SC-XRD structure of **[Fmoc*-Rot][Ag8L2](PF6)4** (solvatomorph B). (**B**) Perspective (partial) view of the rotaxane, highlighting the "wrapped" conformation stabilized by a combination of intramolecular CH–π interactions (green) and hydrogen bonds (red) between Fmoc* and the pillarplex rim (axle shown as capped sticks, pillarplex as spheres). (Reproduced from: reference [4]. Licensed under **CC BY 4.0**.) (**C**) SC-XRD structure of **[Cu8L2](OTf)4** and guest insertion of tetrahydrofuran (THF) into the pillarplex cation. The host–guest assembly is illustrated, with **[Cu8L2]4+** shown in capped-sticks representation and THF as *van der Waals* spheres (bronze (Cu)). (Reproduced from reference [3]. Licensed under **CC BY 4.0**.)

References

[1] P. Altmann and A. Pöthig, *J. Am. Chem. Soc.* **2016**, 138, 13171

[2] P. Altmann, A. Pöthig *Angew. Chem. Int. Ed.* **2017**, 56, 15733

[3] T. Pickl, P. Mollik, M. R. Anneser, F. Sixt, K. Geißer, O. Storcheva, D. P. Halter, A. Pöthig, *Chem. Eur. J.* **2025**, 31, e202500775

[4] T. Pickl, C. Stark, D. Briganti, M. Curcio, A. Pöthig, *J. Am. Chem. Soc.* **2025**, 147, 31, 27192

Fig. 1

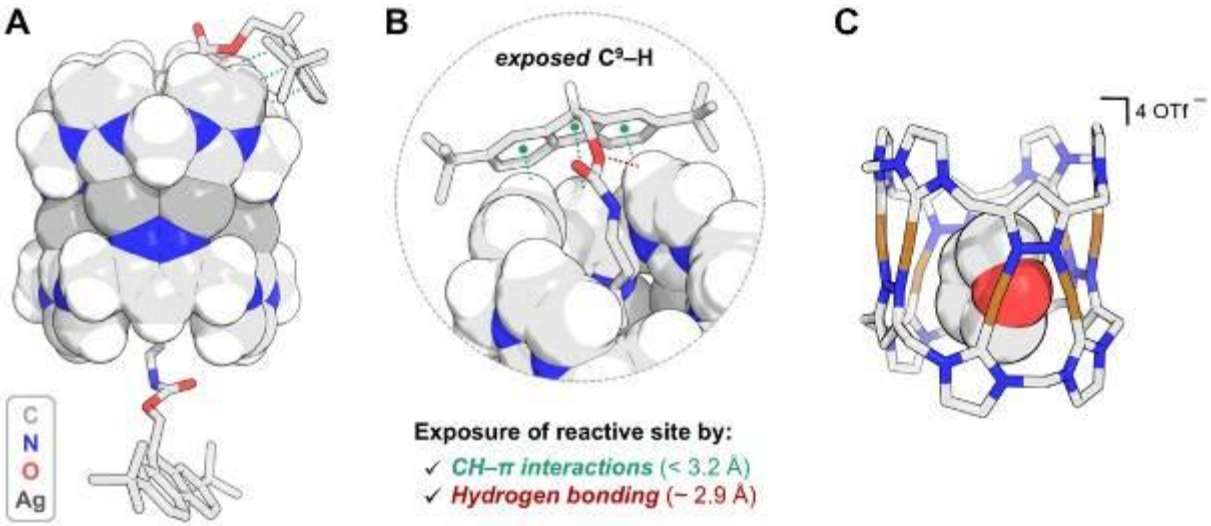

OP-87

Occupancy determination from Anomalous Dispersion Refinement

F. Luiz Alves Jardim (Regensburg/DE, Belo Horizonte/BR), J. Figueiredo (Belo Horizonte/BR), C. Pinheiro (Belo Horizonte/BR), M. Bodensteiner (Regensburg/DE)

Recent developments, both in experimental setup and in software capabilities, have created new possibilities for polymetallic structure investigation in the realm of anomalous X-ray diffraction.3 The anomalous dispersion terms, introduced to the structure factor as fj = f0j + f"j(E) + if""j(E) are usually considered as static values in single-crystal X-ray data refinement. However, chemical context can vary the absorption and resonant dispersion of X-rays, and this phenomenon carries important electronic information of the material. Correctly modeling resonant regimes not only improves refinement but also expands our knowledge of a material's electronic behavior.

This is enabled by Anomalous Dispersion Refinement (ADR) which refines the real (f") and imaginary (f"") parameters. This approach represents a major step forward in the chemical exploration of polymetallic compounds with interesting properties. It reveals how subtle changes in the local coordination sphere influence X-ray absorption and dispersion, a phenomenon fundamentally linked to electron distribution and, consequently, material properties and applications.

In the present work, ADR was used to aid in metal occupancy identification in bimetallic Metal-Organic Frameworks (MOFs). Changing the coordination metal of MOFs can affect the structure"s properties and affinities, and mixing different metals helps fine-tune those properties and improve stability in different environments. As a case study, MM-MOF-74 (M = Zn, Co, Mg) were produced by solvothermal methods and investigated by single crystal X-ray diffraction technique. It was observed that the capability of the technique to determine the metal occupation using only home-laboratory X-ray sources.

Fig. 1: Structure of MM-MOF-74: (left) the asymmetric unit and (right) crystal packing viewed along the c-axis.

Reference

[1] Juda, C. et al. J. Am. Chem. Soc. 2024, *146* (44), 30320–30331.

Fig. 1

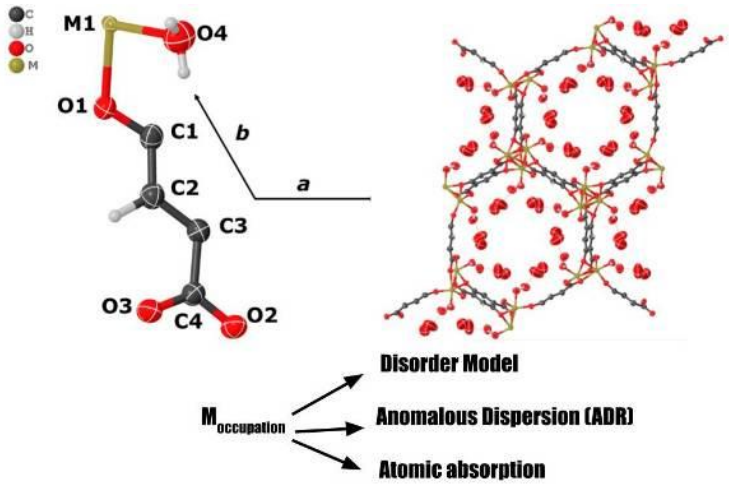

MS 17: Free Topics

OP-88

New Software Tools for Teaching Crystallography to a Broader Audience

M. Adam (Karlsruhe/DE), C. Lenczyk (Karlsruhe/DE), T. Stürzer (Karlsruhe/DE), A. Luebben (Karlsruhe/DE), J. Luebben (Karlsruhe/DE), T. Dunaj (Karlsruhe/DE)

The field of single-crystal X-ray diffraction is advancing rapidly, thanks to ongoing hardware improvements that enable comprehensive structure determination on increasingly smaller and weaker diffracting and challenging samples in less time. As the number of published structures grows, so does the interest in this method, leading to a higher demand for effective tools to explain crystallographic concepts and strategies.

Software packages like APEX and PROTEUM offer a wide range of tools to aid in teaching and understanding the often-complex aspects of crystallography. For instance, these packages provide excellent routines for visualizing reciprocal space, grasping the concept of precession photographs, selecting standard and non-standard space group settings, performing lattice transformations, and more. These routines can be invaluable for newcomers, helping them connect theoretical principles with practical applications. Additionally, both packages serve as powerful resources for comprehending concepts such as lattice indexing, twinning, and modulation.

This presentation will demonstrate how intuitive software solutions can address prominent challenges inherent in practical crystallography.

OP-89

Making chemical bonds experimentally visible – From residual electron density to bond characteristics

E. Irmer (Göttingen/DE), R. Herbst-Irmer (Göttingen/DE)

Even high school students are able to perform a simple X-ray structure refinement (Irmer 2025). At the end of the refinement process, often only the R-value is considered as a quality indicator. The residual electron density is more regarded as disturbing. However, with high quality data it can contain information about the chemical bonding in the molecule (Coppens 1977, Dunitz 1995). Various methods have been used taking this residual electron density into account using non-spherical atom formfactors.

Can these increasingly widespread methods also be taught to non-crystallographers? We would like to show how the basic principles behind a quantum crystallographic analysis according to the multipole model (Hansen & Coppens 1978) and a QTAIM analysis (Bader 1990) can be explained at a level of maximum didactical reduction so that undergraduate students, teacher students or interested school pupils can also understand the results. To illustrate this, we use multipole refinement results for simple molecules such as benzene or oxalic acid dihydrate as examples (Herbst-Irmer & Irmer 2020). Based on school mathematics knowledge of curve discussion, important terms such as Laplacian are explained and it is shown which information can be obtained about bond type, atomic charges, electrostatic potential or lone pairs.

References

[1] Bader, R. F. W. (1990). *Atoms in Molecules: A Quantum Theory*, Oxford University Press, New York.

[2] Coppens, P. (1977). *Angew. Chem. Int. Ed. Engl.* **16**/1, 32–40.

[3] Dunitz, J. D. (1995). *X-Ray Analysis and the Structure of Organic Molecules*. VCH, Basel, Weinheim.

[4] Hansen, N. K., Coppens, P. (1978). *Acta Cryst* A **34**/6, 909–921.

[5] Herbst-Irmer, R., Irmer, E. (2020). *CHEMKON* **27**/6, 275–281.

[6] Irmer, E. (2025). *J Appl Cryst* **58**/5, 1802–1809.

OP-90

From Research to Education: Teaching Crystallography with the Bilbao Crystallographic Server

G. de la Flor (Karlsruhe/DE), E. Tasci (Ankara/TR), L. Elcoro (Bilbao/ES), J. M. Perez-Mato (Bilbao/ES), G. Madariaga (Bilbao/ES), M. I. Aroyo (Bilbao/ES)

Online courses and innovative teaching methods have fostered a growing trend in education, where the integration of multimedia, online resources, and interactive tools is transforming both virtual and traditional learning environments. In crystallography, a wide range of freely available online resources (web platforms, applets, databases, and computational tools) can be incorporated into courses at different academic levels, making them more engaging and accessible. Although the *Bilbao Crystallographic Server* (www.cryst.ehu.es; hereafter BCS) [1-2] is primarily known as a research platform, this contribution highlights its additional role as a versatile teaching platform that can enrich both virtual and in-person crystallography courses [3].

The BCS is a free online server providing access to crystallographic databases and programs for solving problems in crystallography, solid-state physics, mineralogy, and materials science. It includes data from Volumes A, A1, and E of the *International Tables for Crystallography* and offers information on plane, point, space, and subperiodic groups and their symmetry relations, as well as on magnetic and double space groups and Brillouin zones. The BCS also includes a set of specialized programs for the analysis of complex problems in solid-state physics and structural chemistry, bridging the gap between theoretical concepts and their practical applications in teaching and research.

The resources available on the BCS can be effectively integrated into both introductory and advanced courses on topics such as Raman spectroscopy, magnetic symmetry, phase transitions, and group-theoretical applications. Several illustrative examples will be presented to demonstrate how BCS resources can support and enrich the teaching of crystallography and related disciplines.

References

[1] M. I. Aroyo *et al.* (2006) Acta Cryst. A**62**, 115-128.

[2] M. I Aroyo *et al.* (2011) *Bulg. Chem. Commun.* **43**, 183-197.

[3] de la Flor *et al.* (2024) *J. Appl. Cryst.* **57**, 1618-1639.

OP-91

Crystallography is more than X-ray diffraction - 2 years of teaching fundamental crystallography to chemical engineering students

J. Breternitz (Steinfurt/DE)

Sadly often, crystal structure determination (especially with X-rays) is seen as the only essential part of crystallography and teaching is limited to this aspect, rather than fundamental crystallography. This often impedes the understanding of symmetry and its consequences in crystal chemistry and crystal physics, which are so essential for modern materials sciences. I strongly believe that the knowledge of crystallography as a bridge between chemistry, physics and materials science is, however, so important that it is fundamental to start with the basics in the education of chemical engineers at FH Münster. While meeting initial scepticism of some of my colleagues, I introduced an elective module "Crystallography and Technology of Solids" for 3rd year Bachelor students, which is now running in its second year and concentrates on the basics of crystallography as well as selected crystal chemistry and crystal physics effects.

Herein, I will discuss the curriculum I discuss with my students as well as the practical examples and exercises that have proven useful to help the students understand the different symmetry operations and their relation to each other. This module also contains a lab work, in which we use a set of different experiments and techniques to demonstrate the practical aspects of classical crystallography. One such experiment, for instance, is the determination of crystal shapes with the help of a 3D scanner (fig. 1), which allows the students to create 3D models of their crystals and to determine the crystal shape using a virtual goniometer.

Fig. 1: Picture of a hematite crystal with octahedral shape on a 3D scanner. Talcum is dusted on the crystal to increase the contrast and hence scan the shape more reliably.

Fig. 1

OP-93

The thermodynamic limit as criterion to derive a crystal structure model

A. Leineweber (Freiberg/DE)

Crystal structure determination based on different diffraction methods has become apparent routine nowadays. Nevertheless, repeatedly there are new works revising long-established structure models based on new experiments or reinterpretation of old ones. In many cases diffraction data often obtained with modern techniques reveal higher level of detail than possible previously.

This new level of detail may, indeed, give an appropriate, more detailed or even corrected view of the crystal structure. However, in some cases it gets questionable in how far the new structure model, often with reduced symmetry, is representative for phase/compound studied. The point will be made that presence of inherently non-equilibrium microstructure in the studied specimen can modify diffraction data in a way, which indeed suggests modification of the crystal structure model. It is, however, proposed not to do so, but to derive structure models which represent a true time- and translation-average of the atomic structure in the thermodynamic limit, i.e., under controlled temperature, pressure and composition (locally minimizing Gibbs energy). This requires proper partitioning between diffraction effects due to the intrinsic crystal structure and due to extrinsic effects as microstructure non-hydrostatic stress.

Example cases from own work and literature will be presented related with (i) presence of microstrain broadening, which might alternatively be interpreted in terms of distortion of the unit cell, and with (ii) presence of planar faulting which yields diffraction features, which might be misinterpreted as additional Bragg reflections. The point is made that in some cases analysis of the temperature- and pressure-dependent energy landscape is helpful to arrive at an appropriate interpretation of diffraction data under specific temperature/pressure conditions.

OP-94

Energy as the architect: Decoding the supramolecular design of pyrazinamide polymorphs

I. S. Konovalova, G. J. Reiss (Düsseldorf/DE)

Pyrazinamide is a well-known antituberculosis drug, classified as an active pharmaceutical ingredient (API) and included by the World Health Organization in the Model List of Essential Medicines (Fig. 1). Despite its importance and extensive study, the literature mainly reports on its physicochemical properties, synthesis, crystallization, thermodynamics, and electrostatics. However, there remains a lack of information on its supramolecular architecture from an energetic perspective, even though pyrazinamide exists in four polymorphic modifications. Since the molecule is conformationally rigid, only orientational polymorphism can be considered. Therefore, a thorough analysis and comparison of intermolecular interactions across all polymorphs is essential.

Modern approaches to molecular crystal structure analysis typically rely on comparing geometric characteristics of intermolecular interactions. Yet these methods often prove insufficient, especially when numerous weak interactions coexist or when specific directional interactions are absent. In pyrazinamide, the coexistence of strong classical interactions (N–H-O/N hydrogen bonds, π–π stacking) and weaker interactions (N/C–H-π, non-specific) complicates the description of its crystal structures. It is difficult to identify the dominant structural motif in the solid state based solely on geometric considerations, and the energetically prevailing interaction remains unclear.

Analyzing crystal packing from an energetic viewpoint provides deeper insight into the organization of these structures. The results suggest that even very small differences in weak interactions can lead to the formation of distinct polymorphic modifications.

Fig. 1. Molecular structure of pyrazinamide according to X-ray diffraction data.

Fig. 1

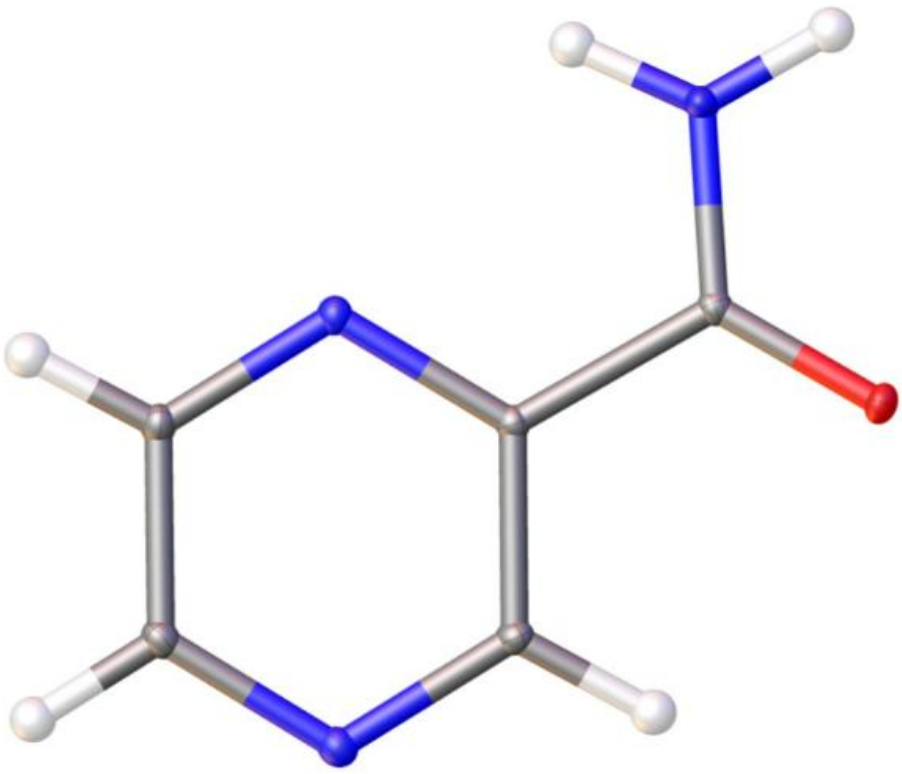

MS 18: Theory and Software, Data Infrastructure, Big Data, and Artifical Intelligence

OP-95

Analytic Scattering Factor Calculation by Direct Partitioning using Density Fitting

L. M. Seifert (Aachen/DE), F. Kleemiß (Aachen/DE)

The atomic scattering factor is central to modelling in single-crystal X-ray and electron diffraction. Traditionally, the Independent Atom Model (IAM) with precalculated factors has been used as a low-cost approximation.[1] While effective for initial structure refinement, IAM fails to capture electron density deformation at high resolutions, achievable with modern diffractometers (dmin ≤ 0.5 Å), where the differences between spherical and chemically deformed densities become significant. More advanced approaches, such as multipole models [2], maximum entropy reconstructions [3], *ab-initio* density refinements [4], and database-driven methods [5], offer higher accuracy but remain restricted to specialized working groups due to their complexity, steep learning curves, and computational demands.[6]

Working towards a fast universally applicable method, we propose a technique for *ab-initio* quantum crystallographic refinement. Using the Density Fitting (DF/RI) technique, we compute atom-centred electron densities expressed as Gaussian functions.[7] This representation allows an analytical solution of the scattering factor equation, eliminating the need for numerical integration grids. Integration into *Olex2* [8] makes this approach readily available to a broader community of crystallographers.

References

[1] R. F. Stewart, *J. Chem. Phys.* **1969**, *51*, 4569–4577.

[2] N. K. Hansen, P. Coppens, *Acta Cryst.* **1978**, *A34*, 909–921.

[3] M. Sakata, M. Sato, *Acta Crystallographica Section A* **1990**, *46*, 263–270.

[4] S. C. Capelli, H.-B. Bürgi, B. Dittrich, S. Grabowsky, D. Jayatilaka, *IUCrJ* **2014**, *1*, 361–379.

[5] S. Domagała, B. Fournier, D. Liebschner, B. Guillot, C. Jelsch, *Acta Cryst.* **2012**, *A68*, 337–351.

[6] A. Krawczuk, A. Genoni, *Acta Cryst B* **2024**, *80*, 249–274.

[7] F. P. Billingsley II, J. E. Bloor, *J. Chem. Phys.* **1971**, *55*, 5178–5190.

[8] O. V. Dolomanov, L. J. Bourhis, R. J. Gildea, J. A. K. Howard, H. Puschmann, *J. Appl. Cryst.* **2009**, *42*, 339–341.

Fig. 1

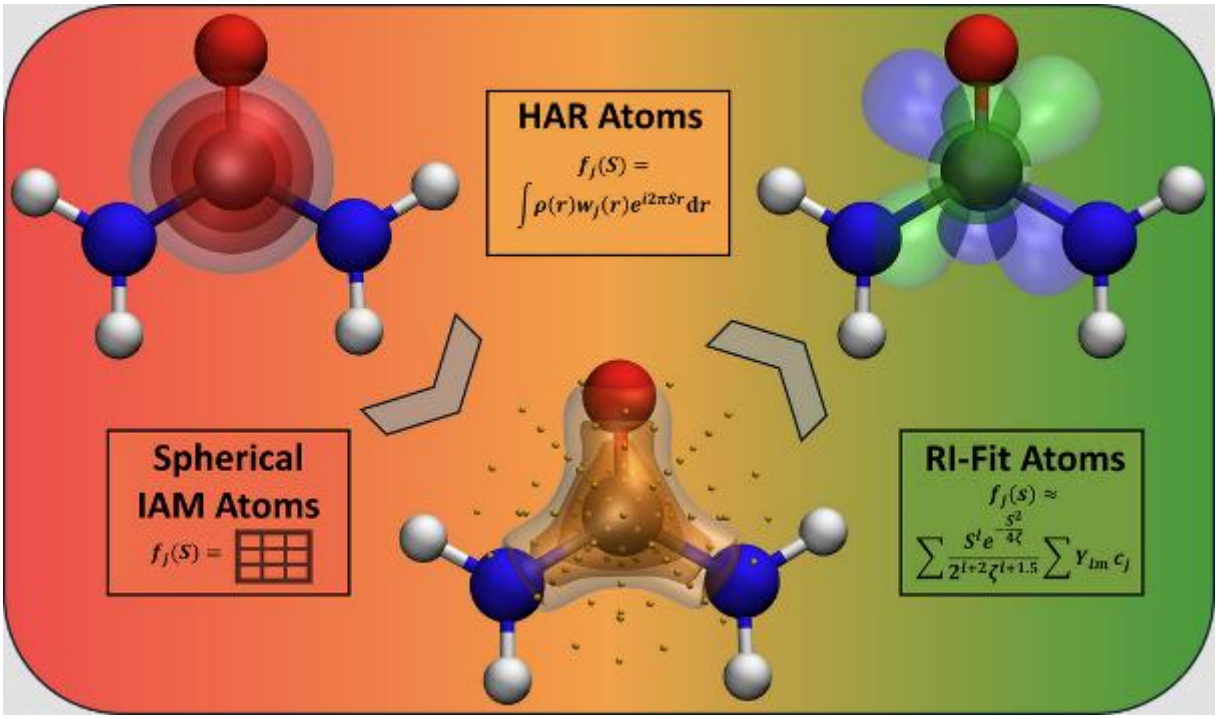
HAR Atoms
$f_j(S) = \int \rho(r) w_j(r) e^{i2\pi Sr} dr$
Spherical IAM Atoms
$f_j(S) =$
RI-Fit Atoms
$f_j(s) \approx \sum \frac{S^l e^{-\frac{S^2}{4\zeta}}}{2^{l+2}\zeta^{l+1.5}} \sum Y_{lm} c_j$

OP-96

Closed-form expressions of one-dimensional diffuse scattering and what we can learn from them

B. Stöger (Vienna/AT)

The modelling of diffuse scattering in disordered crystal structures is often considered as difficult and opaque. From a mathematical point of view, however, diffuse intensities are distinctly better behaved than discrete diffraction patterns, with "nice" convergence behavior of the employed function series.

For reasonably simple cases of layer-stacking disorder, diffuse intensities can be described as closed-form expressions in terms of simple elementary functions. [1] Such expressions provide significantly more insight than numerical simulations. For example, it can be analytically shown which pairs of distinct models possess the same diffraction pattern (are homometric) and whether such pairs exist. Moreover, the diffuse scattering can be separated into distinct components.

Using two distinct examples of disordered layer structures (one with translationally equivalent layers, one with layers of different orientations), it is demonstrated how closed-form expressions can be derived. Moreover, the expressions are analyzed with respect to homometry, pseudo-homometry and how diffraction patterns of distinct structures can be interconverted by continuous transformations (Figure 1).

Fig. 1: Left: a simple two-parameter growth model of a layer structure where adjacent layers are related by either *c* or *n* glide-reflections. Right: The *h* = 0, *k* = 1 rod for fixed parameter *A* = 0.05 and varying *B*-parameter showing a continuous transformation from one polytype to a twin of a different polytype.

Reference

[1] J. Hendricks & E. Teller. *J. Chem. Phys.* **10**, 147–167 (1942).

Fig. 1

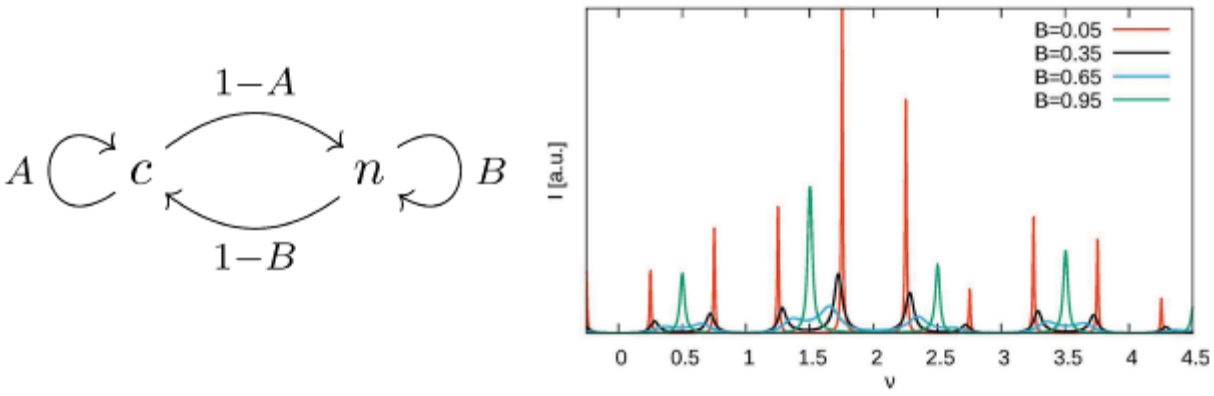

OP-97

D3A: Direct DOI Dataset Access – Streamlining Data Discovery in the OSCARS Project

M. Nentwich (Hamburg/DE), I. Akhundov (Bremen/DE), P. Fuhrmann (Hamburg/DE), A. P. Millar (Hamburg/DE)

Within the OSCARS project, we recognize that associating datasets with persistent identifiers (a globally unique ID) is crucial for ensuring that research outputs are available for open science and comply with the FAIR principles (Findable, Accessible, Interoperable, and Reusable). This enhances the value of the data and it also allows other people to recreate existing work, or to use the data in new and novel research.

Currently, several platforms and institutes offer the possibility to store data with a DOI, a type of persistent identifier. However, no standard exists that allows a machine to access or download the data from a DOI. Repositories typically either have no way to download data automatically, or have adopted some proprietary solution. With no widely deployed standard, any support for accessing or downloading data from a DOI can only be incomplete.

We have successfully developed a proof-of-concept code based on existing approaches in other contexts (HTTP content-negotiation and metalink) that demonstrates the applicability of our approach. This involves a mixture of modifying existing production software, like the fsspec python module, and developing new code to build a demonstration of the benefits of this approach.

Given our code's foundation in the fsspec Python module, its potential applications are vast and evident. It can be seamlessly integrated into various Python applications, such as Jupyter Notebooks, and is particularly well-suited for use cases where the pandas module is already employed, as pandas imports fsspec by default. Furthermore, our code has significant potential for integration within the European Open Science Cloud (EOSC), where it can facilitate dataset access and reuse across disciplines and borders, thereby enhancing the EOSC's mission to provide a unified and seamless environment for data-driven research.

OP-98

CRYSTRACT: CIF File Batch Processing for Structural Analysis

D. Ngo (Washigton, D.C./US), S. M. Morrison (Piscataway, NJ/US), A. Prabhu (Washigton, D.C./US), J. M. Hübner (Dresden/DE)

The new, freely available R package CRYSTRACT provides a comprehensive toolbox for the structural analysis of one to hundreds of CIF files simultaneously. Its core functionality begins with reading key parameters from each CIF file, including file name, database code, chemical formula, structure type, space group name and number, unit cell parameters, symmetry operators, and fractional atomic coordinates. Based on this information, CRYSTRACT automatically constructs the first coordination sphere around each symmetry-independent atom. The coordination number for each site can then be determined, and interatomic distances and bond angles, including full error propagation, can be calculated.

In addition, the package offers a range of filtering functions. These allow users to filter interatomic distances based on atom types, Wyckoff sites, or distance thresholds. Distances can be flagged or excluded if they fall outside an expected range derived from, e.g., covalent radii plus a user-defined tolerance margin, with the option to provide a custom list of radii to better match the compounds under investigation. This functionality is particularly valuable for handling structures affected by substitutional or positional disorder. Such disorder can artificially generate non-physical ("ghost") interatomic distances when symmetry operations are applied. The filtering process helps detect and remove these artifacts.

After applying the desired filters, weighted average distances can be computed for all symmetry-independent sites or for a user-defined subset, while accounting for both partial site occupancies and Wyckoff multiplicity.

The capabilities of CRYSTRACT will be demonstrated through two case studies: one from materials science and another from mineralogy.

OP-99

Quantum crystallography and anomalous dispersion refinement of actinide compounds

F. Meurer (Regensburg/DE), S. T. Liddle (Manchester/GB), M. Bodensteiner (Regensburg/DE)

Question: New and stronger X-ray sources as well as single-photon counting detectors yield reflection intensities and thus electron density descriptions of unprecedented quality. In contrast, both the elastic and inelastic atomic form factors employed in small-molecule crystallographic structure modelling are based on tabulated atomic calculations, that are half a century old. Both are generalized for isolated atoms and therefore neglect the structure-specific electron density distribution, as described by Density Functional Theory, and the resonant photon-matter interactions, as measured in X-ray absorption spectroscopy. While quantum crystallography can accurately describe the non-spherical, electron density distribution, ADR can help to model resonant effects in diffraction experiments. In this work, we summarize our current efforts to employ quantum crystallography in form of the Hirshfeld-Atom-Refinement (HAR) and ADR at the end of the practically available periodic table of elements.

Results: Figure 1 A-C shows the results of HAR of novel organometallic tri-thorium compounds, helping to visualize the 3c-2e bonding and 3c-1e bonding in two anionic, chloride-bridged Th_3 clusters.[1] Quantities such as the electron delocalisation index (A), the dynamic deformation density (B) and difference residual density map (C) can be used to visualize the electronic interaction at the Th_3 center. The results of anomalous dispersion parameters of two different uranium solid-state compounds are shown in Figure 1 D and E. Generally, the absorption spectra of these compounds is in good agreement with refined anomalous dispersion parameters. Different temperatures as well as charged atomic form factors have only little influence on the ADR.[2]

Fig. 1: Exemplary findings from two applications of HAR and ADR to actinide compounds.

References

[1] J. A. Seed *et al. Nat. Chem.* **2025**, 17, 1035-1041.

[2] F. Meurer *et al. Inorg. Chemistry* **2024**, 63, 15784-15790.

Fig. 1

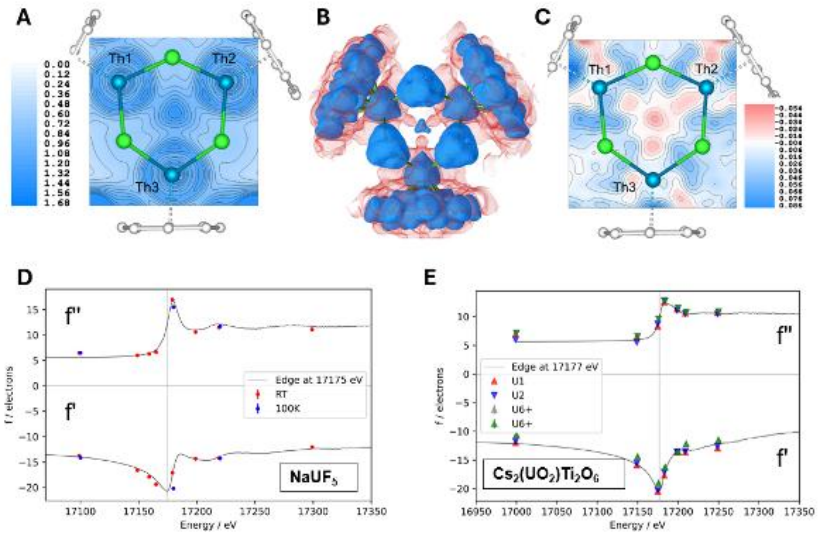

OP-100

Linearization Routines for the Parameter Space Concept to determine Crystal Structures without Fourier Inversion

M. Vallinayagam (Dresden/DE, Freiberg/DE), M. Nentwich (Hamburg/DE), D. C. Meyer (Freiberg/DE), M. Zschornak (Dresden/DE, Freiberg/DE)

Advanced computational resources have enabled practical applications of the Parameter Space Concept (PSC), proposed by Fischer *et al.* to solve crystal structures [1-2]. The presented work enhances the capability of PSC for realistic X-ray data analysis to determine the structure of multiple independent scatterers via one-dimensional projection as alternative to the Fourier inversion technique, offering a more flexible, holistic structure analysis. Our approach utilizes structure factor amplitudes or intensities (as of the experimental observations) represented by piece-wise analytic hyper-surfaces in parameter space (PS), allowing for the comprehensive examination of all structure parameter combinations consistent with available diffraction data. A concrete workflow has been developed to linearize the hyper-surfaces, span the entire PS with polytopes, intersect them, and identify solutions either under Equal Point Atom (EPA) or non-EPA schemes. Monte Carlo simulations are carried out in *P2* and *P3* to generate artificial atomic structures, to analyze different combinations of scattering factors and to validate the developed PSC routines. With limited reflections, the homometric solution space is determined with respective PS volume, and errors in structural degrees of freedom are computed to be as small as 10−6 and 10−4, respectively. The results indicate that with a limited number of reflections, our method can resolve structural details with a high degree of precision, presenting a solution space with minimal volume. Additionally, the PSC method inherently reveals all possible structure solutions, including symmetrically relatable homometries, and non-homometries aligning well with the diffraction data. This capability provides a comprehensive view of the structure analysis, which is an advantage over traditional methods

Georg-Sheldrick-Symposium 1

KL-01

George Sheldrick - the man behind SHELX

R. Herbst-Irmer (Göttingen/DE)

George Sheldrick is well known in the crystallographic community as the author of the program system SHELX. Most of the small molecule structures are nowadays solved by SHELXT [1] and refined with SHELXL [2]. In a *Nature* analysis of the most-cited papers published this century, his paper "A short history of SHELX" [3] is ranked as number 5. [4]

Who was the man behind all these great programs? I will show that he was not only a great researcher but an ideal collaborator, mentor and professor, with a wonderful sense of humour and deep humanity. [5]

References

[1] Sheldrick, G. M. (2015). *Acta Cryst.* A**71**, 3–8.

[2] Sheldrick, G. M. (2015). *Acta Cryst*. C**71**, 3–8.

[3] Sheldrick, G.M. (2008). *Acta Cryst*. A**64**, 112–122.

[4] Pearson, H.; Ledford, H.; Hutson, M.& Van Noorden, R. (2025). *Nature*. **640**, 588-592.

[5] Usón, I. & Herbst-Irmer, R. (2025). *Acta Cryst.* A**81**, 167–174.

KL-02

In Honour of George Sheldrick. Small Molecule Software: SHELX and the passing of the torch

L. Bourhis (Marne-la-Vallée/FR)

George Sheldrick's program suite SHELX [1,2] has been the de facto standards to solve and refine small molecules from Bragg's peak intensities since its inception in the 70's. George's success came from a fine balance between pragmatism and theory, combined with an approach to software development which could be characterised as minimalistic. He was particularly adept at both developing new theoretical tools, and tweaking existing ones to his goals. In this talk, I will try to convey all these aspects, rooted in examples from his very work.

In the early 2000's, David Watkin (Oxford) and Judith Howard (Durham) came to the realisation that it was not healthy for the small crystal community to be so dependent on one suite of programs. This lead to a British grant, affectionately named "Age Concern", to fund the development of new programs, on the model of the macromolecular suite PHENIX which used the open-source Computational Crystallography Toolbox (cctbx) [3] as its foundation. This lead to the development of the Small Molecule Toolbox (smtbx) inside the cctbx, and of the graphical font-end Olex2 at Durham University. [4] This work would not have been possible without extensive discussions with George. The influence of Ralf Grosse-Kunstleve, the lead author of the cctbx, was also decisive. I will try to give the big picture of those developments, and particularly of the articulation between George's work and our new developments, as well as the new opportunities that the smtbx opened for small molecule refinement using quantum computations.

References

[1] Sheldrick (2008). Acta Cryst. A, 64:112–122

[2] Sheldrick (2015). Acta Cryst. A, 71(1):3–8

[3] Grosse-Kunstleve, Sauter, Moriarty, and Adams (2002). J. of Applied Cryst., 35:126–136.

[4] Bourhis, Dolomanov, Gildea, Howard, and Puschmann (2015). Acta Cryst. A, 71(1):59–75

KL-03

In Honour of George Sheldrick. Methods Development in Crystallography

A. Thorn (Berlin/DE)

George Sheldrick was one of the most influential computational methods developers in our field. His programs and ideas have profoundly shaped how crystallographers understand and think of the three-dimensional structures of molecules, both large and small. In this talk, I will shed light on some of his strategies to do so, on the design features and quirks of his programs and what can be learned from them for future development.

Beyond their technical brilliance, Sheldrick"s approaches exemplify a rare combination of empirical trail & error, crystallographic intuition, and pragmatic coding. I will discuss how these principles resonate in current challenges: integrating machine learning with established refinement methods, balancing automation with expert control, and ensuring reproducibility and accessibility in crystallographic software.

Georg-Sheldrick-Symposium 2

KL-04

From crystallography to school – and back

E. Irmer (Göttinge/DE)

Georg-August-University Göttingen, XLAB – Göttingen experimental laboratory for young people
George Sheldrick was not only one of the most recognised crystallographers of the past decades, with an enormous impact on the development of methods for structure determination, but he also influenced the careers of many former students, PhDs and postdocs. I would like to show how my crystallographic education almost 40 years ago shaped my personal and professional path as a chemistry teacher; a path that led me back to crystallography after many years in the teaching profession. I would like to show how I incorporated structural chemistry aspects into school chemistry lessons, especially the use of crystallographic databases. And how, finally, we enable students from high school at the XLAB experimental laboratory in Göttingen to solve and refine crystal structures of simple organic compounds.

Reference

[1] Irmer, E. (2025). J Appl Cryst 58, 1802–1809.

KL-05

Core Facility run by a SHELXL power user

T. Grüne (Vienna/AT)

Tutorials on crystallography tend to start with an introduction to the command prompt and the powershell. While toddlers are observed wiping Instagram with their thumb, the fact that computers can actually do useful things when operated with ten fingers, seems to be facing oblivion. Manufacturers of single crystal diffractometers have been producing excellent software that greatly facilitates measurement and processing of diffraction data, and the refinement of crystal structures. Sometimes, however, one wishes to take a different route. The Core Facility Crystal Structure Analysis at the University of Vienna runs a STOE Stadivari and a Bruker D8, both equipped with a EIGER2 R500 detector by DECTRIS Ltd. For both instruments, the standard work-flow has been intercepted in order to be able to process data with XDS [1]. XDS is a very robust data processing program. It is particularly strong in indexing difficult cases. It is controlled through plain text files and comes with excellent documentation. This puts the user into power of the program, making XDS a versatile tool installed abundantly at a great many different sites, including inhouse SXRD, electron diffractometers, and synchrotrons. It is purely command line driven, making it suitable for background processing and pipelining. XDS was one of the first parallelised processing programs, and it is extremely fast. Prefetching of data even reduces the bottleneck of network attached storage. With the STOE Stadivari, adjusting the workflow was straightforward, since STOE provides the tools to convert the XI-image format to CBF. The program XITOOLS was written to convert the geometry description into the input file XDS.INP for every run, and data can be processed with a simple BASH script. Bruker has refused the implementation of the EIGER2 R500 into their workflow. Here, the shutter signal is buffered by an Arduino nano and passed to the detector. The detector is programmed by interpretation of the APEX runs description. The same script as with STOE is used to integrate the data. For both instruments, XDS data are converted with XDS2SAD to enable scaling with SADABS [2], entering the SHELXT/SHELXL/SHELXLE [3-5] many crystallographers are familiar with. The details of this workflow, and the situations, when the routine routes are left behind, will be presented during the DGK conference 2026.

References

[1] W. Kabsch, "XDS", Acta Crystallogr. D66 (2010), 125-132

[2] L. Krause et al., "Comparison of silver and molybdenum microfocus X-ray sources for single-crystal structure determination", J. Appl. Crystallogr. 48 (2015), 3-10

[3] G. M. Sheldrick, "SHELXT - Integrated space-group and crystal-structure determination", Acta Crystallogr. A71 (2015), 3-8

[4] G. M. Sheldrick, "Crystal structure refinement with SHELXL", Acta Crystallogr. C71 (2015), 3-8

[5] C. B. Huebschle et al, "ShelXle: a Qt graphical user interface for SHELXL", J. Appl. Crystallogr. 44 (2011), 1281-1284

KL-06

The magic triangle and beyond: Insights from doing a PhD with George Sheldrick

T. Beck (Hamburg/DE)

Universität Hamburg, Institut für Physikalische Chemie

George Sheldrick supervised many PhD students and postdoctoral researchers. In this contribution, I will share insights from my own experience as a PhD student in his lab. For example, I will discuss how the project using triangular compounds as phasing tools in protein crystallography was originally initiated. I will also describe how this PhD project and my time in George's lab shaped my subsequent academic career.

KL-07

Refining Large and Complex Molecular Structures with SHELXL

J. J. Holstein (Dortmund/DE)

After completing my PhD in 2012 at the Georg-August University of Göttingen under Professor George M. Sheldrick, he recommended me to Gérard Bricogne for a postdoctoral position at Global Phasing Ltd., the industrial partner of a Marie Curie Initial Training Network hosted at the University of Cambridge. This opportunity led to collaborations with Jonathan Nitschke (Cambridge) and Kai Severin (EPFL), marking one of the most formative chapters of my scientific career.

Coming from experimental charge-density studies, I encountered X-ray structure determination of large supramolecular assemblies characterized by low-resolution data and complex disorder. The experience gained in George's Advanced Structure Refinement Seminar proved invaluable in addressing these challenges. Equipped with beta test versions of SHELXT [1] and multi-CPU implementation of SHELXL [2], I refined demanding structures using Global Phasing GRADE2 restraint dictionaries [3] integrated into SHELXL, combined with semi-automatic modeling via DSR [4, 5]. Regular discussions with George continued throughout this time—always insightful and often accompanied by his characteristic humor. Several program improvements resulted from these exchanges, including implementation of the ACTA TABS command to suppress CHECKCIF alerts when refining multiple PARTs using identical atomic labeling schemes.

References

[1] Sheldrick, G. M. (2015a). Acta Cryst. A71, 3–8. doi:10.1107/S2053273314026370

[2] Sheldrick, G. M. (2015b). Acta Cryst. C71, 3–8. doi:10.1107/S2053229614024218

[3] Smart, O.S., Sharff A., Holstein, J., Womack, T.O., Flensburg, C., Keller, P., Paciorek, W., Vonrhein, C. and Bricogne G. (2021) Grade2 version 1.7.1. Cambridge, United Kingdom: Global Phasing Ltd. Available at: https://grade.globalphasing.org

[4] Kratzert, D., Holstein, J.J. & Krossing, I. (2015). J. Appl. Cryst. 48, 933–938. doi:10.1107/S1600576715005580

[5] Kratzert, D., & Krossing, I. (2018). J. Appl. Cryst. 51, 928–934. doi:10.1107/S1600576718004508

Rolf-Hilgenfeld-Symposium 1

KL-08

Introductory: A bird's-eye-view outline of Rolf's scientific career and milestones

J. R. Mesters (Lübeck/DE)

"a life in the fast lane, devoted entirely to science, in which he absorbed a wealth of knowledge, conscientiously created new knowledge and passionately passed it on to his students"

German teacher, Goethe-Institute, Finland (1972)

Chemistry studies (1973-80) (Wolfram Saenger), Freiburg + Göttingen
>> crown-ether compounds <<

Institute of Crystallography (Wolfram Saenger), Doctorate (1982-1996), Berlin
>> X-ray structure elucidation of the plant cysteine protease Calotropin D1 <<

Laboratory Chief (1986-1987), Hoechst AG, Hoechst / Frankfurt am Main
Biozentrum Basel, Switzerland

Group leader Structural Biology and Drug Design, Hoechst AG, Hoechst, Frankfurt am Main
Local, national and international "cooperations" with universities (Leiden, Praha, ...)
>> Insulin glARGin << >> Structure of active EF-Tu (Nature 1993) <<

Full professor of Structural Biochemistry and head of department at IMB (1995-2002), Jena
Scientific Director of the IMB (1998-2000)
Chairman of the European Structural Biology Forum (ESBF) (2001–2005)
Visiting professorship in biophysics (2003) and doctor honoris causa (2009), USB, Budweis
Visiting Fellowship from the Japan Society for the Promotion of Science (2004)
1. Heart of Europe bio-crystallography 1998; DGK-DGKK 2002 / CC 2001 / FEBS crystallization courses
HIV initiative, 5th Framework Programme, European Commission
ICCBM-9 conference in Jena in 2002; birth of the IOBCr
X-tal Controller by Xtal Concepts; EMBL X13 PX beamline
Bronze sculpture SARS Inhibited (by Mara G. Haseltine) (2006), Biopolis, Singapore
Tofo Advanced Study Weeks (TASW), Mozambique

Full professor of Biochemistry and Director (2003-2020), Lübeck
Visiting Professorships Beijing Genomics Institute (2007) + Shanghai Institute of Materia Medica (2010-2012)
Ge Hong Medal of the Institute of Virology in Wuhan (2015)
And then there was the fight against the dissolution of the University of Lübeck (2010)
Volunteered to travel to China during the SARS CoV-1 epidemic outbreak
Cited more than 1000 times, which made him one of the world most influential researchers in his field:
>> X-ray structure of inhibited SARS CoV-1 main protease (Science 2003) <<
>> α-ketoamide inhibited SARS CoV-2 protease (Science 2020) <<

Senior professor, independent research group (2020-2025), Lübeck
Carl-Hermann-Medal of the German Crystallographic Society (2023)
Thomas-Fredenhagen-Prize of the Lübeck Merchants' Association (2023)

"protease research and drug development have dominated his entire scientific career"

References

[1] https://journals.iucr.org/d/issues/2025/08/00/me6342/me6342.pdf (Obituary)

[2] https://dgk-home.de/wp-content/uploads/2023/11/Heft53.pdf (Laudatio, German language)

KL-10

"Rolf and his Crystal Contact Engineering Vision" leading to the blockbuster drug insulin glargine

H. Berchtold (Frankfurt am Main/DE)

Rolf Hilgenfeld built up an industry R&D focused protein crystallographic unit at Hoechst AG, Frankfurt am Main in 1986/89. After publication of the so-called 2 Zn Phenol monoclinic 3D-structure of human insulin by U. Derewenda et al. Nature 338, 594-596 (in March 1989) he provided me (Harald Berchtold) with a PhD theme starting in May 1989 to study several Hoechst insulin derivatives to be crystallized in this new crystal form. This was the beginning of a Crystal Contact Engineering Endeavour which finally led to a new long-acting basal insulin: Insulin glargine (A21-Gly-B31,32-DiArg-human insulin) the drug substance of current marked products Lantus® U100 and Toujeo® U300. Aspects of this highly encouraging time moving the impact of protein crystallography studies to next level at Hoechst R&D will be presented to remember and honour Rolf's incomparable impact and his sharp visionary scientific view to overcome drawbacks guiding a project secure and fast to success.

Reference

[1] Hilgenfeld R, Seipke G, Berchtold H, Owens DR. The evolution of insulin glargine and its continuing contribution to diabetes care. Drugs. 2014 Jun;74(8):911-27. doi: 10.1007/s40265-014-0226-4.

KL-11

From ssDNA Binding to Cryo-Techniques: Remembering Prof. Rolf Hilgenfeld Through SSB Structures

S. Panjikar (Melbourne/AU)

Single-stranded DNA-binding proteins (SSBs) are central to genome maintenance, protecting and organising transient ssDNA during replication, recombination, and repair. In this memorial talk, I will reflect on work carried out during my PhD under Prof. Rolf Hilgenfeld, focused on the structural biology of bacterial SSBs. X-ray crystallographic studies of SSBs from E. coli, Brucella abortus, Proteus mirabilis, and Serratia marcescens revealed a conserved overall architecture alongside species-dependent differences concentrated in loop regions. I will also briefly highlight two cryo-cooling approaches developed during this work that proved effective for SSBs and other proteins. Together, these studies illustrate Prof. Hilgenfeld's enduring influence through rigorous structural insight, methodological innovation, and mentorship that shaped both the science and the scientist.

KL-12

Impact of Rolf's drug discovery seminar on protease inhibitor research

A. Hillisch (Monheim am Rhein/DE)

Prof. Rolf Hilgenfeld's seminar series at the University of Jena left a profound and lasting impact on my scientific journey. I will never forget our sessions in the dark room shooting photos of the latest X-ray complexes directly from the screen to teach our students. We rushed to the Jena city center in a completely crowed car to get the negatives developed. We hardly made it on time to our own seminar. In the first year (must have been 1996) there were probably more colleagues teaching than actual students. I vividly remember the deep, lively discussions we had on protease drug discovery, with HIV protease serving as an especially instructive example. Rolf's ability to combine 3D-structural insights, mechanistic thinking, and medicinal chemistry relevance transformed these sessions into formative milestones in my training. The conceptual clarity and scientific rigor I gained during those seminars became foundational in my later work and directly impacted the discovery of several clinical candidates and beyond. Rolf's mentorship exemplified the rare combination of intellectual generosity, scientific depth, and human warmth. His influence continues to resonate in my work and in the many molecules, ideas, and people shaped by his remarkable contributions to drug discovery. The talk will summarize some published recent examples of protease inhibitor research.

KL-13

A Vision Realized in Budweis: International Training Born from Collaboration with Rolf Hilgenfeld

I. Kutá -Smatanová (Nové Hrady/CZ)

This lecture presents a successful example of internationalization at the University of South Bohemia in České Budějovice, illustrating how long-term collaboration with European scientific societies can strengthen education and research through specialized training programs. The initiative originated from a collaboration with Rolf Hilgenfeld, whose idea to establish advanced international courses in Budweis laid the foundation for sustained scientific collaboration.

Since 2004, the University of South Bohemia has hosted the biennial FEBS Advanced Course on Macromolecular Crystallization, supported by the Federation of European Biochemical Societies (FEBS). Over two decades, the course has brought together students, postdoctoral researchers, and leading experts for an intensive program combining lectures with hands-on training. The close interaction between participants and instructors fosters skill development, international networking, and lasting scientific impact, reflected in a global alumni network applying the acquired expertise in their home institutions.

Rolf-Hilgenfeld-Symposium 2

KL-14

Crystallographic fragment screening at SARS-CoV-2 Mpro

M. S. Weiss, T. Barthel, L. S. Benz, F. Lennartz, H. Taberman, J. Wollenhaupt, U. Mueller (Berlin/DE)

Shortly after the discovery of a new lung disease in Wuhan (China), it became clear that the causative agent was a coronavirus related to the SARS virus, which surfaced about 15 years earlier. As soon as the genome sequence of the new (later named SARS-CoV-2) virus was published on the web, several groups around the world began to produce the viral proteins for structural analysis. The Hilgenfeld group in Lübeck was among the first to crystallize the main protease (Mpro) and in February 2020 the structure of the protease was solved [1] based on data collected on beamline BL14.2 at BESSY II [2]. Shortly after that the first screening experiments began more or less parallel at DIAMOND in the UK [3], at PETRA III in Hamburg [4] and at BESSY II in Berlin. In the talk, I will highlight some of the initial hurdles as well as some early results.

References

[1] L. Zhang, et al. (2020). Crystal structure of SARS-CoV-2 main protease provides a basis for design of improved α-ketoamide inhibitors. Science 368, 409-412.

[2] U. Mueller et al. (2025). The Macromolecular Crystallography Beamlines of the Helmholtz-Zentrum Berlin at the BESSY II Storage Ring: History, Current Status and Future Directions. J. Synch. Rad. 32, 766-778.

[3] M. L. Boby et al. (2023). Open science discovery of potent noncovalent SARS-CoV-2 main protease inhibitors. Science 382, eabo7201.
[4] S. Günther et al. (2020). X-ray screening identifies active site and allosteric inhibitors of SARS-CoV-2 main protease. Science 372, 642-646.

KL-15

Rational design of protease-targeting antivirals: Working with Rolf Hilgenfeld 2018 - 2025

M. Brönstrup (Brunswick/DE), H. El Kilani (Lübeck/DE)

Viral proteases are prime targets for developing direct-acting antivirals by rational design and treating related infections. Rolf Hilgenfeld has been a pioneer and pacemaker in this area of research, and I would like to highlight two unpublished studies arising from a close and delightful collaboration of our labs.
First, we examined co-crystal structures of SARS-CoV-2's Mpro with peptidomimetic inhibitors,1 noting the close proximity of sidechains in the S1' and S2 pockets as well as S3 and S1 pockets. To improve molecular rigidity and optimize active site interactions, we used macrocyclization to fix these proximal residues. We synthesized endocyclic α-ketoamides linking P1' and P2 residues, then characterized their binding modes and biological properties with multiple co-crystal structures. A 17-membered macrocycle inhibited Mpro with an IC_{50} of 370 nM and SARS-CoV-2 with an EC_{50} of 1.9 µM. Exploring structural similarities between Mpro and enterovirus D68's 3Cpro, we found that the compound also inhibited enteroviral proteases and showed potent antiviral activity even in the low nM range. The study demonstrates how structure-guided design enabled target- and pathogen-hopping for direct-acting antivirals.
Secondly, we expanded peptidomimetic Mpro inhibitors to Proteolysis Targeting Chimeras (PROTACs), small, bifunctional molecules that induce a proteasomal degradation of target proteins. The PROTAC BT153 formed ternary complexes and exerted antiviral effects against SARS-CoV-2. Surprisingly, we found that also lysosomal degradation of monoubiquitinated targets contributed to its mechanism of action.

References

[1] Structure-based optimization of pyridone α-ketoamides as inhibitors of the SARS-CoV-2 main protease. Akula, Ravikumar; El Kilani, Haifa; Metzen, Alina; Roeske, Judith; Zhang, Kaixuan; Göhl, Matthias; Arisetti, Nanaji; Marsh, Graham; Maple, Hannah; Cooper, Mark; Karadogan, Burhan; Jochmans, Dirk; Neyts, Johan; Rox, Katharina; Hilgenfeld, Rolf; Brönstrup, Mark. Journal of Medicinal Chemistry (2025), 68, 2920−2941. doi: 10.1021/acs.jmedchem.4c02172.

[2] From repurposing to redesign: Optimization of boceprevir to highly potent inhibitors of the SARS-CoV-2 main protease. Matthias Göhl, Linlin Zhang, Haifa El Kilani, Xinyuanyuan Sun, Kaixuan Zhang, Mark Brönstrup, Rolf Hilgenfeld. Molecules (2022), 27, 4292. doi: 10.3390/molecules27134292

KL-16

Massive X-ray Screening Against the SARS-CoV-2 Main Protease: A Collaborative Response

S. Günther (Hamburg/DE)

In March 2020, faced with the onset of the global pandemic, we initiated a rapid-response collaboration eventually involving over 100 researchers from 30 institutions, primarily from Northern Germany and centered at DESY. Our aim was to bundle regional expertise in structural biology, virology, and bioinformatics to identify therapeutic starting points against SARS-CoV-2.
Central to this effort was the pioneering work of Rolf Hilgenfeld, whose laboratory provided the foundational structural understanding of the SARS-CoV-2 main protease (Mpro). With the Hilgenfeld lab's essential support, we could immediately utilize the PETRA III synchrotron to conduct a high-throughput X-ray crystallographic screen of approximately 6,000 compounds from drug-repurposing libraries. This talk will detail the evolution of these initial screening efforts, the identification of key hits, and the follow-up studies that ensued—all of which were jump-started by Rolf Hilgenfeld's lifelong dedication to coronavirus research.

KL-17

Structure-Guided Discovery of Novel Inhibitors of Enteroviral Proteases

B. Kaščáková (České Budějovice/CZ)

During my postdoctoral research, I had the privilege to work under the supervision of Prof. Rolf Hilgenfeld on the production, biochemical characterization, and structural analysis of enteroviral proteases, with a focus on EV-A71 and EV-D68 3Cpro. Our work combined recombinant protein expression, enzymatic assays, and structure-guided approaches to elucidate the molecular basis of protease function and inhibition. We established robust protein production and assay platforms, enabling detailed biochemical and structural characterization and supporting the discovery and functional validation of potent small-molecule inhibitors. In this presentation, I will summarize the key outcomes of this collaborative effort and highlight how Prof. Hilgenfeld's scientific vision and mentorship profoundly shaped the direction and impact of my subsequent research.

KL-18

M^{pro}TAC - New approach for development of SARS-CoV-2 antiviral drugs

K. Zhang (Lübeck/DE), J. Röske (Lübeck/DE), H. Maple (Lübeck/DE), A. Moloney (Lübeck/DE), G. Marsh (Lübeck/DE), Y. Chen (Brunswick/DE, Lübeck/DE), K. Rox (Lübeck/DE), M. Brönstrup (Lübeck/DE), L. Redecke (Lübeck/DE), R. Hilgenfeld (Lübeck/DE)

Following the outbreak of COVID-19, many direct-acting antiviral therapies have been developed [1] and a number of drugs (e.g. nirmatrelvir, ensitrelvir) have been approved as inhibitors of the SARS-CoV-2 main protease (Mpro). An alternative approach has recently been introduced with the Proteolysis-Targeting Chimeras (PROTACs). PROTACs are heterobifunctional molecules composed of the protein of interest (POI) ligand and an E3 ligase recruiting ligand connected by a chemical linker [2]. Different from the competitive and occupancy-driven mode of action (MOA) of inhibitors, PROTACs recruit the E3 ligase to the POI and induce the ubiquitin-proteasome-system via the 26S proteasome, resulting in the degradation of the POI [3]. Due to the catalytic event-driven MOA, degraders could achieve efficacy in lower doses as compared to conventional inhibitors, thus minimizing potential toxicity and side-effects. We developed the lead MproTAC (Mpro-targeting PROTACs), BT153, which recruits SARS-CoV-2 Mpro to DDB1-CRBN (E3 ligase), thereby resulting in targeted degradation through ternary complex formation. To determine the formation of the binary and ternary complex involving Mpro, BT153 and DDB1-CRBN or CRBN midi [4] (a stable protein, excluding the DDB1 component, which can be expressed in E. coli and used as a substitute for DDB1-CRBN), we employed biochemical, biophysical, and crystallography techniques.

References

[1] G. Li, R. Hilgenfeld, R. Whitley & E. De Clercq. Nat. Rev. Drug. Discov. 2023, 22, 449-475.

[2] D. L. Buckley, C. M. Crews, Angew. Chem. Int. Ed. 2014, 53, 2312-2330.

[3] A. Ciechanover, A. L. Schwartz. Proc Natl. Acad. Sci. 1998, 95, 2727-2730.

[4] A. Kroupova. et al. Nat. Commu. 2024, 15, 8885.

Fig. 1

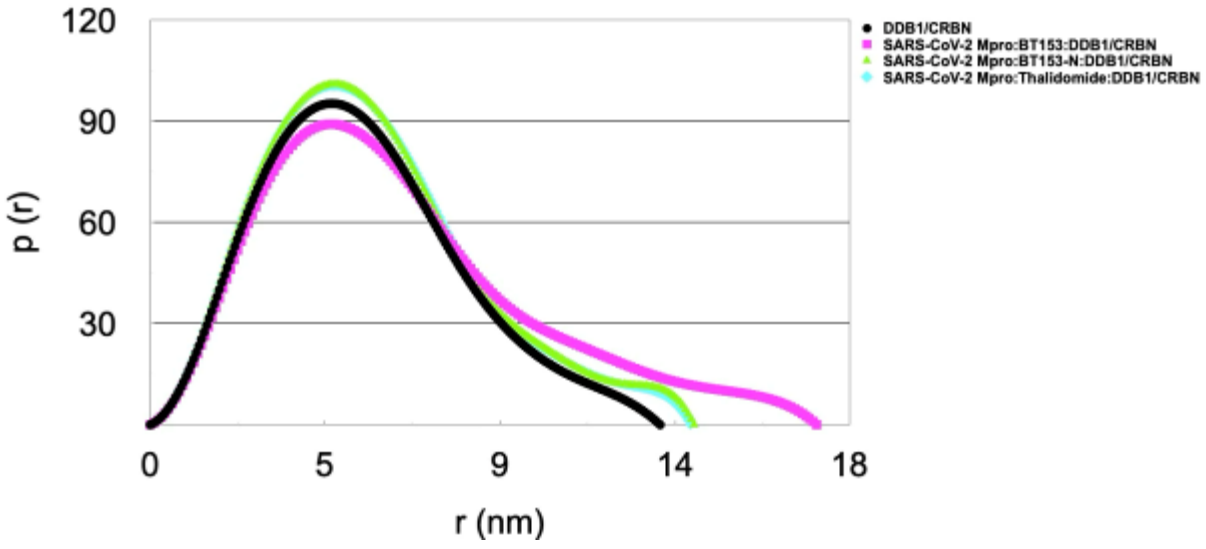

Fig. 2

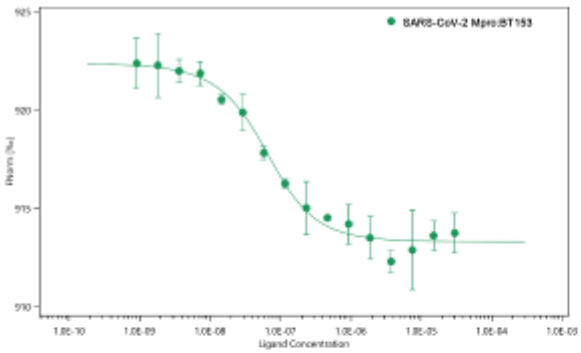
SARS-CoV-2 MproBT153
Rnorm [‰]
Ligand Concentration

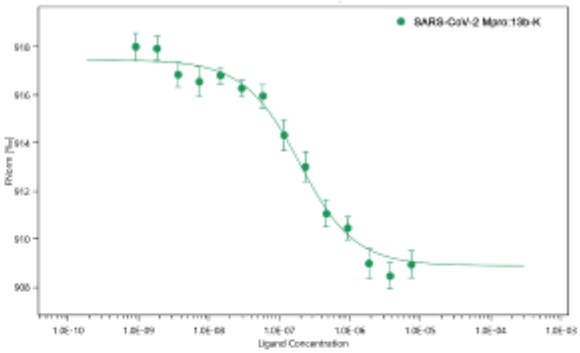
SARS-CoV-2 Mpro:13b-K
Rnorm [‰]
Ligand Concentration

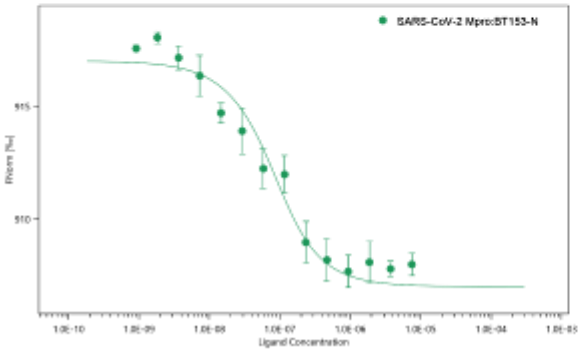
SARS-CoV-2 MproBT153-N
Rnorm [‰]
Ligand Concentration

KL-19

Structural Characterization of SARS-CoV-2 Main Protease Nirmatrelvir-Resistance Mutants

X. Sun (Lübeck/DE), H. El Kilan (Lübeck/DE), M. Ibrahim (Lübeck/DE), L. Redecke (Hamburg/DE, Lübeck/DE), R. Hilgenfeld (Lübeck/DE)

The SARS-CoV-2 main protease (Mpro) is a well-established target for antiviral drug development [1]. The inhibitor Paxlovid, a combination of nirmatrelvir and ritonavir [2], remains one of the most effective treatments for COVID-19. However, as SARS-CoV-2 is an RNA virus, the emergence of resistance mutations is expected. Several nirmatrelvir resistance-associated Mpro mutations, including E166A/V and L167F, have been identified in SARS-CoV-2 passage experiments [3-4]. In addition, some mutations such as L50F, which can co-occur with these resistance mutations, have been reported to restore viral replication fitness and enhance the cleavage efficiency of the nsp5/6 substrate [4-5]. We have recombinantly produced Mpro containing the single mutants E166A/V and L167F, the double mutants L50F+E166A/V and L50F+L167F, as well as the triple mutant L50F+E166V+L167F. These variants were characterized using X-ray crystallography, enzymology, and biophysical approaches. The potential of each mutant to lead to a wide-spread nirmatrelvir-resistance scenario will be discussed. Furthermore, we demonstrate that our inhibitor 13b-K [6], despite some cross-resistance with nirmatrelvir, exhibits significantly higher inhibitory activity against Mpro carrying the E166V mutation.

References

[1] Zhang L, Lin D, Sun X, Curth U, Drosten C, Sauerhering L, Becker S, Rox K, Hilgenfeld, R.: *Science* **368**, 409-412 (2020).

[2] Owen DR, et al.: *Science* **374**, 1586-1593 (2021).

[3] Jochmans D, Liu C, Donckers K, et al.: *MBio* **14**, 2815-2822 (2023).

[4] Zhou Y, Gammeltoft KA, Ryberg LA, et al.: *Science Advances* **8**, eadd7197 (2022).

[5] Lewandowski EM, Zhang X, Tan H, et al.: *Nature Communications* **16**, 1266 (2025).

[6] Cooper MS, Zhang L, Ibrahim M, Zhang K, Sun X, Röske J, Göhl M, Brönstrup M, Cowell JK, Sauerhering L, Becker S, Vangeel L, Jochmans D, Neyts J, Rox K, Marsh GP, Maple HJ, Hilgenfeld R.: *J. Med. Chem*. **65**, 13328-13342 (2022).

Lectures by the award winners

Max von Laue Award

Weak, Noisy and Uninteresting: Realised and unrealised opportunities from ever-increasing experimental throughput.
N. Pearce (Linköping / SE)

Data generation in experimental structure determination continues its inexorable growth in scope and complexity. Automation at experimental beamlines now enables us to carry out traditional experiments trivially, and to routinely perform historically unwieldy screening experiments comprising thousands of single-crystal data sets. This is even before we consider serial experiments, where the already-challenging integration and management of data are compounded by non-isomorphism in the crystal population; then, as the time-resolved component is added, we must sensitively identify differences between timepoints and attempt to model small structural changes that are nonetheless crucial to biological function.

We have only just begun to develop methods specifically designed to natively analyse large volumes of data. I will present an overview of my own contributions in this area, focussing on fragment screening experiments, including the identification of partial-occupancy fragments with PanDDA, and the consensus refinement of multiple data sets with MRDR. I will also try to highlight some of the unrealised opportunities to overcome long-standing obstacles in macromolecular crystallography, which are especially significant in the era of AlphaFold and Cryo-EM.

In situ X-ray Powder Diffraction Study of the Hydrogen Reduction of WO3 and V2O5
J. Bantol (Jülich /DE)

Industrially relevant materials are commonly found in nature as metal oxides or ores. To produce their elemental forms, many industries rely on reduction processes that typically involve high carbon emissions. A more promising and sustainable alternative is the use of hydrogen as a reducing agent.

In this study, the hydrogen reduction of tungsten trioxide (WO3) and vanadium(V) oxide (V2O5) was investigated using in situ X-ray powder diffraction (XRPD). For WO3, the reduction sequence WO3→H0.23WO3→W10O29→WO2→β-W→α-W was observed, with earlier formation of β-W at high hydrogen flow rates. The crystal structure of β-W remains unclear in literature and is often associated with W3O. However, this assignment is inaccurate. Attempts to isolate β-W revealed lattice contraction of WO2 at high hydrogen flow. Further investigations into the precise crystal structure of β-W are therefore recommended.

For V2O5, the reduction sequence was: V2O5→V4O9→V6O13→VO2(R/B)→V3O5→V2O3, with phase transformations strongly dependent on temperature and hydrogen flow. Isothermal measurements highlighted the challenges of isolating pure phases due to coexistence of mixed phases, but revealed the temperature-dependent stability of V6O13 and V3O5. Moreover, the lattice parameters of WO2 and V2O3 increased with temperature due to thermal expansion, and their coefficients were determined.

Overall, these findings confirmed the formation of previously unreported phases, β-W and V3O5. Rietveld refinement also enabled a detailed understanding on the structural evolution of WO2 and V2O3. The findings further demonstrate the capability of in situ XRPD to resolve complex reduction pathways and provide detailed insights into phase transformation and phase evolution. It emphasizes the critical role of temperature and hydrogen flow in stabilizing intermediate phases.

Coordination Chemistry of Metal Radionuclides using TREN-based Ligands

G. Hempelmann, B. Ebel, I. Oppela (Aachen/DE)

New coordination compounds have been synthesized to stabilize the radionuclides TiIV and SnIV for biomedical applications. Radioactive 45Ti is utilized as a PET scan metal for diagnostics, while 117mSn serves therapeutic purposes, which makes it a theragnostic approach.
Initial investigations focused on established symmetric catechol ligands with a TREN backbone—specifically, (CAm)3-TREN and (5-Br-CAm)3-TREN—as model systems for SnIV coordination. Experiments were conducted to explore the incorporation of additional metal cations into the ligand's TREN-pocket. Four species were analyzed via NMR spectroscopy, including 119Sn-NMR, and ESI-MS. There is a monometallic SnIV complex and a bimetallic SnIV complex containing CaII within the TREN-pocket for each ligand. The monometallic SnIV complex and the bimetallic SnIV complex with (CAm)3-TREN and the monometallic SnIV complex with (5-Br-CAm)3-TREN were confirmed by single crystal diffraction. Furthermore, a novel synthetic pathway for an asymmetric ligand (5-Br-CAm)(CAm)2-TREN was developed, which features bromine functionality on one catechol arm. This functionality enables subsequent organic reactions with linkers to incorporate PSMA fragments via e.g. click reactions.
Coordination experiments involving the asymmetric ligand with TiIV, SnIV, and CaII were conducted and shifts of the aromatic protons in the 1H-NMR spectra suggest successful coordination. Corresponding signals in the HSQC spectra (which point towards CaII incorporation) as well as 119Sn-NMR-spectra and ESI-MS also support the existence of these species.
Unlike the symmetric ligand systems, the crystallization of the asymmetric TiIV- and SnIV complexes proved to be more challenging. Nevertheless, a FeIII complex was successfully synthesized to provide definitive structural evidence for the existence of the asymmetric ligand. Furthermore, it confirms that the asymmetric ligand behaves similarly to its symmetric counterparts in terms of coordination ability.

Implementation of SALTED Models for Predicting Electron Densities in Single Crystal Structure Refinement

L- M- Seifert (Aachen /DE)

Accurate electron density modelling is essential for precise single-crystal refinement in crystallography. The SALTED (Symmetry Adapted Learning of Three-Dimensional Electron Densities)[1] model offers a promising alternative by predicting electron densities as coefficients within the Resolution of Identity (RI) ansatz[2], eliminating both the need for cumbersome ab initio calculations and numerical scattering factor calculation.[3]
The SALTED model was trained on multiple small molecule structures and conformers generated via metadynamics.[4] Both SALTED and analytical integration were incorporated into NoSpherA2[5]. The accuracy and computational efficiency were benchmarked against traditional ab initio Hirschfeld Atom Refinement[6] (HAR).
SALTED accurately predicted electron density coefficients, yielding scattering factors closely matching traditional methods. In combination with analytical Fourier transform it was possible to reduce computational time by an order of magnitude compared to HAR. Implementing SALTED in single-crystal refinement significantly advances computational efficiency without compromising accuracy. By enabling analytical integration through predicted coefficients, this approach has potential for widespread application in crystallography, especially larger systems, accelerating research and reducing computational resources.

References

[1] A. M. Lewis, A. Grisafi, M. Ceriotti, and M. Rossi, J. Chem. Theory Comput., vol. 17, no. 11, pp. 7203–7214, Nov. 2021

[2] F. E. Harris and R. Rein, Theor. Chim. Acta, vol. 6, no. 1, pp. 73–82, Jan. 1966

[3] J. Avery and K. J. Watson, Acta Crystallogr. Sect. A, vol. A33, no. 4, pp. 679–680, Jul. 1977

[4] S. Grimme, C. Bannwarth, and P. Shushkov, J. Chem. Theory Comput., vol. 13, no. 5, pp. 1989–2009, May 2017

[5] F. Kleemiss et al., Chem. Sci., vol. 12, no. 5, pp. 1675–1692, 2021

[6] S. C. Capelli, H.-B. Bürgi, B. Dittrich, S. Grabowsky, and D. Jayatilaka, IUCrJ, vol. 1, no. 5, pp. 361–379, Sep. 2014

Poster Session 1: Advances and applications of Neutron and Synchrotron Radiation

PP-01

Pressure-induced breakdown of the defect superstructure of $GdTe_{1.8}$

T. Doert (Dresden/DE), R. Loriga Jr. (Miami, FL/US), E. Carvajal (Miami, FL/US), G. S. Nolas (Tampa, FL/US), S. Chariton (Chicago, IL/US), V. Prakapenka (Chicago, IL/US), I. Chuvashova (Miami, FL/US)

$GdTe_{1.8}$ is a stoichiometric rare-earth metal chalcogenide which adopts a 10-fold superstructure of the ZrSi type in space group *P*4/*n* and lattice parameters of *a* = 9.661(1) Å and *c* = 17.942(1) Å under ambient conditions.[1] The structure consists an alternating stacking of puckered [GdTe] double slabs and planar [Te] layers comprising Te_2^{2-} and linear Te_3^{4-} anions, Figure 1 (left/centre). The formation of the superstructure is caused by the Te deficiency with respect to the aristotype and the resulting vacancy-ordering.

Recent high-pressure X-ray diffraction and Raman spectroscopy experiments in a diamond anvil cell reveal at least two structural phase transitions, Figure 1 (right). At 2.1(4) GPa, the vacancy-ordered-superstructure breaks down and the compound crystallizes in the cell of the aristotype in space group *P*4/*nmm* with a statistical distribution of vacancies. At higher pressures of about 20(1) GPa, a second structural transition is observed which is associated with an atomic rearrangement of the [GdTe] slabs. The space group symmetry change from *P*4/*nmm* to *I*4/*mmm* is accompanied by a significant enlargement of the *c*/*a* lattice parameter ratio. As expected, the Te–Te and the Gd–Te distances show a higher compressibility as compared to the Gd–Gd distances. However, the compression of the Te–Te distances is limited to values close to that of a covalent Te–Te bond of approximately 2.80 Å.

Reference

[1] H. Poddig, T. Donath, P. Gebauer, K. Finzel, M. Kohout, Y. Wu, P. Schmidt, T. Doert, *Z. Anorg. Allg. Chem.* 2018, 644, 1886–1896.

Fig. 1: Crystal structure of GdTe1.8 at ambient conditions, unit cell (left) and ordered Te layer (centre); change of the lattice parameters under pressure (right).

Fig. 1

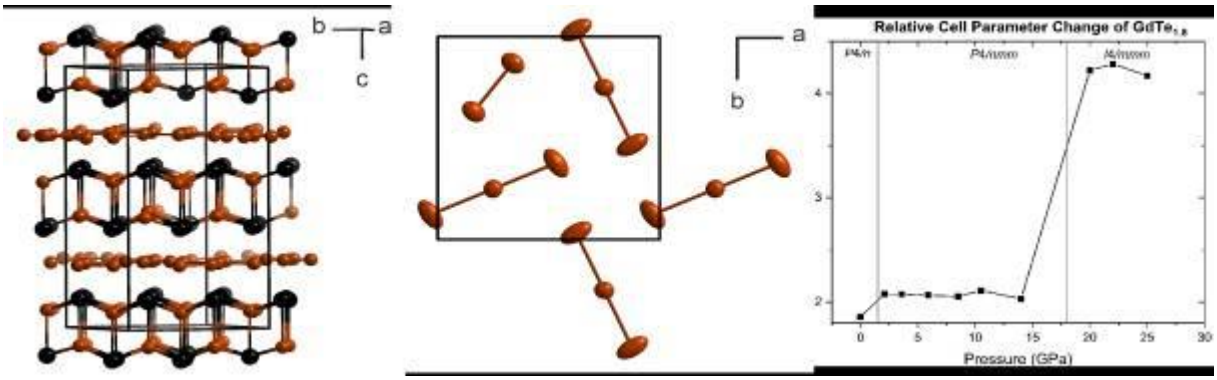

PP-02

Bridging Quantum Crystallography and Experimental Charge Density Analysis through an Iterative Multipole Refinement Scheme

M. Patzer (Mülheim an der Ruhr/DE), C. W. Lehmann (Mülheim an der Ruhr/DE)

The accurate description of weak intermolecular interactions remains a central challenge in charge density analysis, where the use of periodic boundary conditions in quantum-chemical calculations ensures a physically consistent description of the crystal environment. In this work, we present an iterative refinement framework that bridges experimental charge density analysis with periodic quantum crystallography. The approach integrates electron densities from periodic density functional theory (DFT) directly into a multipole refinement scheme, allowing for consistent treatment of both experimental and theoretical electron densities within the same refinement cycle. By iteratively updating the multipole parameters with quantum-mechanically derived densities, deviations between model and experiment can be systematically reduced, leading to an improved representation of subtle intermolecular features such as hydrogen bonding and dispersion-dominated contacts. The approach is realized within *ReCrystal*, an independent Python3 GUI designed to connect multipole refinement in XD with periodic DFT computations carried out in CRYSTAL17. The results demonstrate that the combined quantum-experimental refinement procedure not only improves the accuracy of electron density modeling, but also ensures convergence towards the physically meaningful minimum, thereby revealing systematic errors originating from experimental data or model assumptions.

Reference

[1] Patzer, M. & Lehmann, C. W. (2025). *IUCrJ*, **12**, 322–333.

Fig. 1

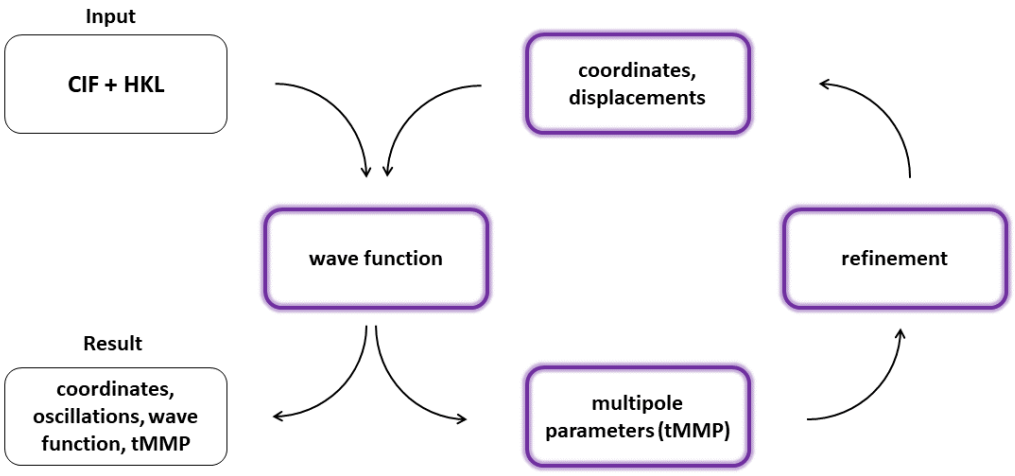

PP-04

X-Area, Integrate3D and ViewSpace: Better Views, Outstanding Data Quality, Same Reliable Software

L. C. Folkers-Karlsson (Darmstadt/DE), P. Celani (Darmstadt/DE)

X-ray data processing often begins with a look into the collected data. Usually, the 2D reconstructed slices of reciprocal space will not contain any surprises. However, once a sample is not well behaved, a look into the reconstruction of reciprocal space can improve understanding the difficulties at hand. Sometimes though, 2D reconstructions are not quite enough and therefore STOE"s new and improved ViewSpace offers 3D reconstructions of reciprocal space including a plethora of tools to investigate specific areas and effects.

To be able to include weak effects found in the 3D reconstructions, a powerful integration software is required which is able to distinguish even the smallest reflections from the background.

STOE"s new integration software, INTEGRATE3D, introduces adaptive integration profiles which adjust their shape and size dynamically around each reflection across consecutive frames, with no or minimal user intervention. This is combined with a robust description of the background [1] and integration of weak reflections via ab initio 3D profile fitting [2,3], rather than relying on learned profiles. Together these features result in variable integration areas yielding more accurate estimates of intensities (I) and improved I/σ(I). The approach particularly benefits data with weak reflections and even improves the results in average data.

The synergy between the new ViewSpace and Integrate3D allow for easier access to understanding X-ray diffraction data and higher quality results in subsequent data processing.

Fig. 1: Graphic showing the change of integration box size over consecutive frames.

References

[1] Parkhurst, J. M., Winter, G., Waterman, D. G., Fuentes-Montero, L., Gildea, R. J., Murshudov, G. N., Evans, G., *J. Appl. Cryst*., **49**, 2016, *1912–1921.*

[2] Duisenberg, A. J. M., Kroon-Batenburg, L. M. J., Schreurs, A. M. M., J. *Appl. Cryst*., **36**, 2003, *220-229.*

[3] Schreurs, A. M. M., Xian, X., Kroon-Batenburg, L. M. J., *J. Appl. Cryst.*, **43**, 2010, *70–82.*

Fig. 1

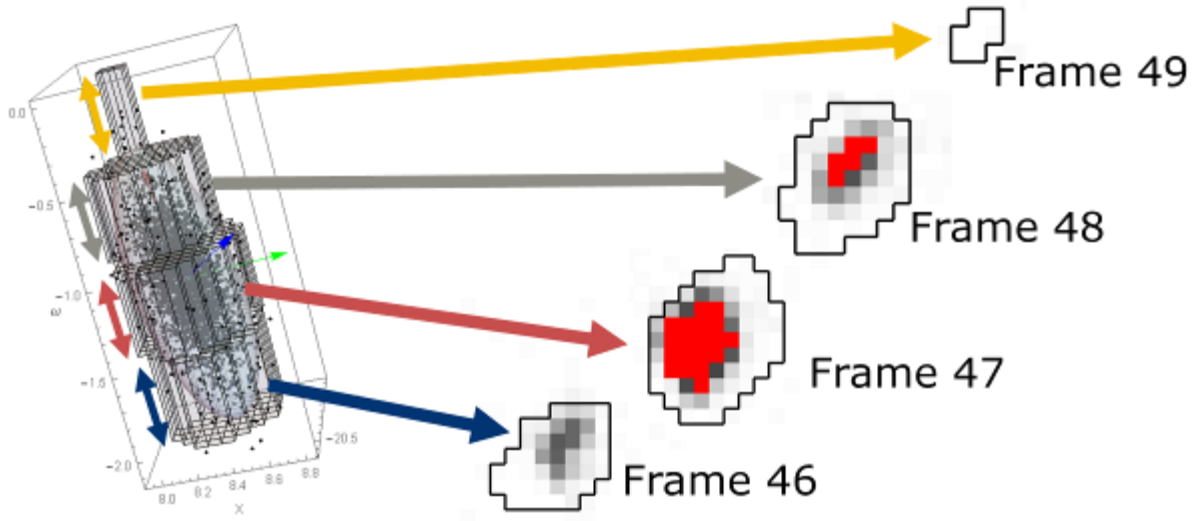

PP-05

On the artificial crystal structure generation for solving the phase problem with deep learning

D. M. Melgalvis (Riga/LV), T. Rekis (Riga/LV, Frankfurt a. M./DE)

We discuss and present approaches for generating artificial crystal structures for training neural networks to solve the phase problem. Structure generation is considered as a two-step process involving sampling unit cell parameters and filling the unit cell with atoms. The former step includes generating lattice basis vectors from randomly sampled unit cell volume. Apart from randomly placing atoms we use database data to guide fast and scalable generation of molecule-like fragments. Recently developed neural network PhAI [1] is then used as a benchmark and retrained with various sets of training data to assess how the corresponding models perform on experimental crystal structure data. We found a significant improvement of PhAI retrained on new kind of artificial data to generalize the phase problem solution for larger unit cell structures (Fig. 1).

Fig. 1: Correlation coefficient *r* versus unit cell volume (*N* = 5000) for PhAI models trained: 1) on the original PhAI training set; 2) on structures generated by sampling the volume uniformly and randomly placing the atoms but respecting minimum interatomic distance; 3) on structures generated by sampling the volume log-normally and filling the unit cell with artificial molecules. The test structures are segregated by compound classes.

Reference

[1] Larsen, A. S., Rekis, T. & Madsen, A. (2024). *Science*, **385**(6708), 522–528.

Fig. 1

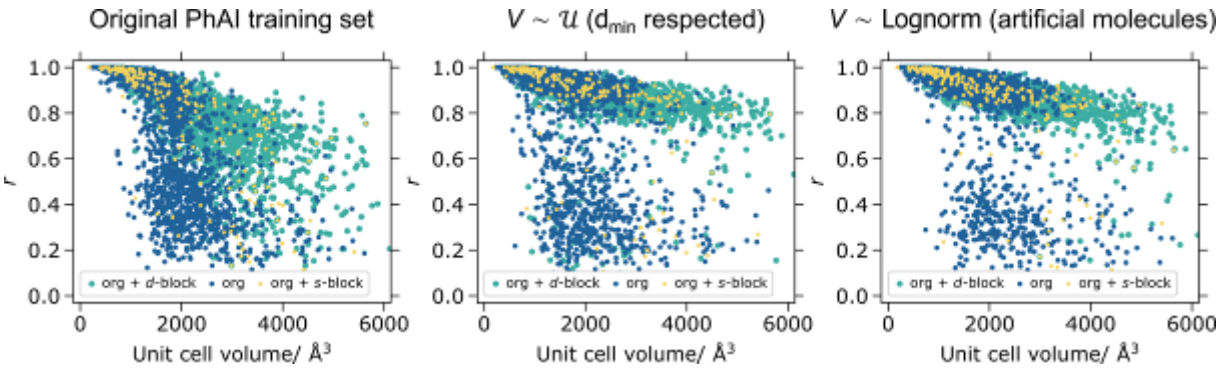

PP-06

Streamlined Structure Determination using PROTEUM and CCP4

A. Lübben (Karlsruhe/DE), J. Luebben (Karlsruhe/DE), T. Dunaj (Karlsruhe/DE)

PROTEUM is a comprehensive set of programs for protein crystallography enabling crystal characterization, data collection, reduction, analysis and structure solution (figure 1) [1].

The software suite takes advantage of automated AI technologies for crystal centering and offers project handling with multiple samples. The PROTEUM software is designed for in-house data collection on Bruker D8 VENTURE single crystal diffractometers for easy and intuitive protein crystal structure determination. The resulting output files are seamlessly input into the CCP4 suite of programs [2] for structure solution and finalization.

Fig. 1: From crystal to structure workflow in PROTEUM.

References

[1] APEX/PROTEUM software suite, Bruker AXS, Madison, 2015.

[2] J. Agirre et al. *Acta. Cryst.* **D79**, 449-461 (2023) "The CCP4 suite: integrative software for macromolecular crystallography" [doi:10.1107/S2059798323003595].

Fig. 1

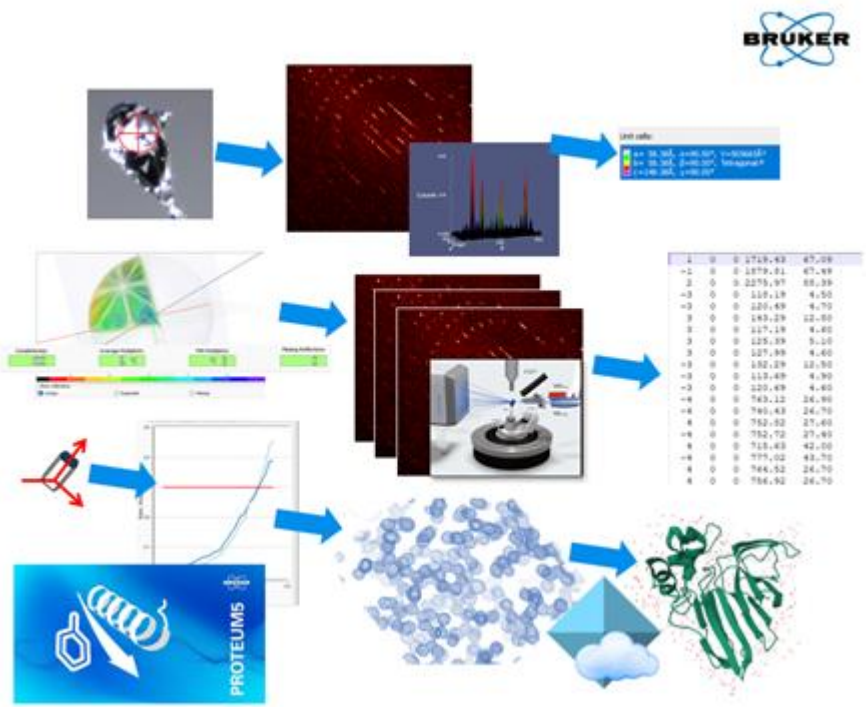

PP-07

Data analysis and gap reconstruction: an application to powder diffraction data

K. García Medina (Erlangen/DE), R. Neder (Erlangen/DE), E. Estévez Rams (La Habana/CU)

There are several cases and setups where technical limitations cause the sampling to be far from ideal. Such is the case, for example, when several line or area detectors are combined for the sake of improving time resolution. The gaps between the combined detectors can cause the collected data to have systematically missing values.

When faced with incomplete experimental powder data, Rietveld refinements can still be done against partial patterns, still allowing for the extraction of relevant long-range order information. However, for amorphous or nano-crystalline materials, is the Pair Distribution Function (PDF) analysis that provides information on short-range order. The proper procedure would be to repeat the experiment, filling in the missing data points, but requiring extra time. An alternative procedure is to exploit reconstruction techniques to recover the missing data.

In this contribution, a procedure is proposed for the reconstruction of missing data in powder diffraction patterns, based in a modified Papoulis – Gerchberg algorithm [1,2]. The method has been applied to both simulated and experimental patterns, including data collected at the European X-FEL with a single shot in 100 fs [3]. The method allowed for the reconstruction of gaps to obtain the PDF of ZnO nanoparticles at this extreme time resolution. Furthermore, some performance metrics are proposed to choose locally optimal solutions in a highly pathological space.

References

[1] Gerchberg, R. W. (1974). Opt. Acta, 21, 709–720.

[2] Papoulis, A. (1975). IEEE Tram. Circuits Syst. CAS-22, 735–742.

[3] Sapnik, A. F., … , Medina, K. G., … & Keen, D. A. (2025). IUCrJ, 12(5).

PP-08

Facilities for Macromolecular Crystallography at the HZB

U. Müller (Berlin/DE), M. S. Weiss (Berlin/DE)

The Macromolecular Crystallography (MX) group at the Helmholtz-Zentrum Berlin (HZB) has been in operation since 2003. Since then, three state-of-the-art synchrotron beam lines (BL14.1-3) for MX have been built up on a 7T-wavelength shifter X-ray source [1,2]. Currently, the three beam lines are among the most productive MX-stations in Germany, with more than 4600 PDB depositions (Status 10/2025). BLs14.1 and 14.2 are energy tunable in the range 5.5-15.5 keV, while beam line 14.3 is a fixed-energy side station operated at 13.8 keV. All three beam lines are equipped with state-of-the-art detectors: BL14.1 with a PILATUS3X 6M detector, BL14.2 with a PILATUS3S 2M and BL14.3 with a PILATUS3S 6M detector. BL14.1 and BL14.2 are in regular user operation providing close to 200 beam days per year and about 600 user shifts to approximately 100 research groups across Europe. Remote beamline operation has been established successfully at BL14.1 and BL14.2. BL14.3 is equipped with a MD2 micro-diffractometer, a HC1 crystal dehydration device and a REX nozzle changer making it suitable for room temperature experiments. Additional user facilities include office space adjacent to the beam lines, a sample preparation laboratory, a biology laboratory (safety level 1) and high-end computing resources. Within this presentation/poster a summary on the experimental possibilities of the beam lines, the ancillary equipment provided to the user community will be given as well as future upgrade project towards a new BESSY III storage ring facility.

References

[1] U. Heinemann, K. Büssow, U. Mueller & P. Umbach (2003). Acc. Chem. Res. 36, 157-163.

[2] Mueller, U., Barthel, T., Benz, L.S., Bon, V., Crosskey, T., Genter Dieguez, C., Förster, R., Gless, C., Hauß, T., Heinemann, U., Hellmig, M., James, D., Lennartz, F., Oelker, M., Ovsyannikov, R., Singh, P., Wahl, M.C., Weber, G. and Weiss, M.S. (2025), J. Synchrotron Rad. 32, 766-778

PP-09

Mass Spectrometry Platform as Sample Delivery System for Gas-phase Small-angle X-ray scattering (SAXS) Experiments

J. C. K. Kung (Hamburg/DE, Lübeck/DE), T. Kierspel (Hamburg/DE), T. Damjanovic (Hamburg/DE, Lübeck/DE), S. Mishra (Hamburg/DE, Lübeck/DE), C. Uetrecht (Hamburg/DE, Lübeck/DE)

The Mass Spectrometry for Single Particle Imaging of Dipole Oriented Complexes (MS SPIDOC) consortium has designed and constructed a MS platform for single particle imaging and related experiments at X-ray light sources [1].

MS and other well-developed gas-phase techniques are beneficial for sample delivery in X-ray structural biology experiments. Major advantages include the reduction of background scattering in the solvent-free environment, and separation and isolation of analytes by their masses and conformations. The MS SPIDOC instrument prototype is a MS platform that exploit these advantages. An additional instrument component provides the capability of dipole orientation of the particles, which enable structural reconstruction from much smaller scattering datasets.

The benefits of MS and the MS SPIDOC prototype have been explored in gas-phase small-angle X-ray scattering (SAXS) experiments. All experiments were performed at the PETRA III X-ray source at the EMBL BioSAXS Beamline. Using our prototype and GroEL as a model, scattered X-ray photons signal from the protein complex was confirmed to be above background. Simulation of X-ray scattering of GroEL was performed using the same parameters as the X-ray of the beamline. Comparing the simulation with the experimental results indicate that photon scattering from GroEL ions was indeed present. With further experiments at different light sources, the MS SPIDOC platform promises to be a valuable sample delivery system for X-ray enabled experiments.

Reference

[1] Kadek, A.; Lorenzen, K.; Uetrecht, C. In a Flash of Light: X-Ray Free Electron Lasers Meet Native Mass Spectrometry. Drug Discov. Today Technol. 2021, 39, 89–99. https://doi.org/10.1016/j.ddtec.2021.07.001.

PP-11

Structural and Dynamic Characterisation of Phloem-Mobile Protein-RNA condensates

S. Smitha (Hamburg/DE), D. P. Triandafillidis (Hamburg/DE), S. Ostendorp (Hamburg/DE), A. Pearson (Hamburg/DE), J. Kehr (Hamburg/DE), A. Madsen (Hamburg/DE)

Phloem, a vascular tissue found in higher plants, transports photosynthates and signalling molecules like RNAs. Emerging studies have shown that under stress, RNAs move through the phloem as protein-RNA condensates. These condensates are highly dynamic and responsive to their surroundings [1]. Biophysical measurements indicate that these condensates exhibit liquid like behaviour, leading to the assumption that they lack internal structure. However, advances in X-ray scattering methods allow the detection of local order in globally disordered systems like in water [2]. Whether similar internal order exists within protein-RNA condensates remains untested.

Our main objectives are to follow condensate formation from the earliest stages *in vitro*, determine the extent and time scales of internal ordering in mature condensates, and resolve time dependent internal structure at room temperature.

Biomolecular condensates produced *in vitro* will be characterised using dynamic light scattering (DLS), small angle X-ray scattering (SAXS), and X-ray cross-correlation analysis (XCCA). Condensate growth and kinetics will be analysed using DLS. The size and shape will be probed by SAXS. XCCA will be used to identify local spatial correlations.

Preliminary DLS measurements show diffusion coefficients between 10^{-7} to 10^{-9} cm^2/s and have given insights about the time scales that need to be probed to catch earliest stages of formation. Early SAXS data has revealed weak yet reproducible scattering profiles and evolution of condensate structure with differing initial conditions. This work will establish an integrated framework for structural and dynamical characterization of protein-RNA condensates using light scattering. Understanding how molecular composition governs internal order will shed light on the physical basis of long-distance RNA transport and plant stress responses.

References

[1] Ostendorp et al., J Biol Chem. 2022

[2] Kurta, Chesnokov et al., IOP Publishing, 2013

PP-88

Time-resolved electron diffraction: a method for imaging membrane proteins in action

J. Estengre Pérez (Hamburg/DE), P. Christian (Hamburg/DE), A. Pearson (Hamburg/DE), I. Fernandez-Cuesta (Hamburg/DE), N. Pranzner (Hamburg/DE), J. Teuber (Hamburg/DE)

Understanding membrane protein structural dynamics is crucial for understanding how cells communicate with each other and the outside world. To achieve this, we require time-resolved structural data showing not just the intermediate states of membrane proteins as they move between conformations, but a multi-frame "film" of exactly how the protein moves between them. Traditional approaches such as cryoEM or 3D x-ray crystallography with cryo-trapping can yield interesting time-resolved structures but these fail to capture the membrane proteins in conditions close to their native states in the cell. We present here our work towards development of a technology platform for the use of time-resolved serial electron diffraction at room temperature. We are using nanoimprinting to build liquid cells and our self-designed flow-through atomic layer deposition setup to obtain a suspended inorganic black membrane which will act as an electron window. Crystals can be precisely positioned within the cell using optical tweezers.

Poster Session 1: Structure-based Drug Discovery

PP-12

An X-ray based fragment screening approach to develop new antibacterial drugs

A. M. Herzog (Stuttgart/DE), M. Zeno (Stuttgart/DE), D. Stegmann (Stuttgart/DE, Villigen/CH), T. Barthel (Stuttgart/DE), M. S. Weiss (Stuttgart/DE), J. Steuber (Stuttgart/DE), G. Fritz (Stuttgart/DE)

Crystallography-based fragment screening is a versatile technique in structure-based drug discovery [1-4]. Applying fragment screening we aim at new antibiotics against multidrug-resistant pathogens. Among those *Pseudomonas aeruginosa* and *Klebsiella pneumoniae* are listed by the WHO as most urgent candidates for new antibiotics. We are targeting the Na^+-NQR, a membrane protein complex and have determined the structure by X-ray crystallography and cryo-EM [5,6] and used subunit NqrF for fragment-screening. A total of >2000 crystals yielded more than 150 unique fragments. The analysis of the large number of datasets has been facilitated by an in-house script that performs automatic refinement, ligand fitting and evaluation of bound ligands and provides a comprehensive and graphical output. Based on the 3D structural information and by *in silico* modifications using the software package OpenEye Scientific [7] we currently develop these fragments into new high-affinity antibacterial inhibitors.

References

[1] Wollenhaupt J, Barthel T, Lima GMA, Metz A, Wallacher D, Jagudin E, Huschmann FU, Hauß T, Feiler CG, Gerlach M, Hellmig M, Förster R, Steffien M, Heine A, Klebe G, Müller U, Weiss MS. J Vis Experiments 169, 62208 (2021).

[2] Douangamath A, Powell A, Fearon D, Collins PM, Talon R, Krojer T, Skyner R, Brandao-Neto J, Dunnett L, Dias A, Aimon A, Pearce NM, Wild C, Gorrie-Stone T, von Delft F. J Vis Experiments 171, 62414 (2021)

[3] Stegmann DP, Steuber J, Fritz G, Wojdyla JA, Sharpe ME. Methods Enzymol. 690, 235-284. (2023)

[4] Lima GMA, Talibov VO, Jagudin E, Sele C, Nyblom M, Knecht W, Logan DT, Sjögren T, & Müller U. Acta Cryst D76, 771–777 (2020)

[5] Steuber J, Vohl G, Casutt MS, Vorburger T, Diederichs K, Fritz G. Nature 516, 62–67 (2014)

[6] Hau JL, Kaltwasser S, Muras V, Casutt MS, Vohl G, Claußen B, Steffen W, Leitner A, Bill E, Cutsail GE, DeBeer S, Vonck J, Steuber J, Fritz G. Nat Struct Mol Biol. 30:1686-1694 (2023)

[7] OpenEye Scientific Software, Santa Fe, NM

PP-13

Structural and functional features of a conserved DNA-binding domain in herpesviral proteins as a basis for innovative targeted therapies

F. A. Sornaly (Lübeck/DE), M. M. Brinkmann (Brunswick/DE), T. F. Schulz (Hanover/DE), L. Redecke (Lübeck/DE)

Human herpesviruses establish lifelong persistence, which plays a key role in tumorigenesis, providing the basis for severe disease resulting from viral reactivation. Herpesviral proteins interacting with viral DNA (vDBPs) are key players in latency establishment, maintenance, and regulation. The vDBPs can be classified as latent or immediate-early (IE) lytic proteins. Latent proteins such as KSHV LANA-1 and EBV EBNA-1 of the γ-herpesvirus subfamily mediate the replication of latent viral episomes and their partitioning to daughter cells during mitosis. In contrast, lytic proteins such as HHV-6A IE2 and HCMV IE2 of the β-herpesvirus subfamily act as transcriptional activators of early or late viral promoters.

Based on the crystal structures, the DNA-binding domains (DBDs) of LANA-1, EBNA-1, and HHV-6A IE2 share significant structural homology. AlphaFold models of HCMV IE2 predict a similar structure to LANA-1, EBNA-1, and HHV-6A IE2, indicating the DBD is conserved among herpesvirus families. The project aims to develop an innovative targeted therapy through the structural and functional characterization of LANA-1 DBD and HCMV IE2 CTD in complex with viral DNA or small molecular inhibitors (SMIs). We plan to employ X-ray crystallography, *in cellulo* crystallization techniques, and cryo-EM for structure elucidation.

The HCMV IE2 CTD forms a stable dimer, indicating secondary structure formation validated by SEC-MALS and CD. MS analysis identified the protein corresponding to IE2 CTD. Crystallization screens led to crystal formation, which diffracted up to 1.5 Å; data processing and optimization are underway. For LANA-1 DBD, docking & molecular dynamics data have identified potential binding sites of the SMIs and areas of optimization, which will be validated via site-directed mutagenesis of key residues involved in interactions. In parallel, co-crystallization will be performed with viral DNA or SMIs to optimize the inhibitors and develop a novel antiviral therapy.

PP-14

Targeting Flavin Transferase with Fragment-Based Drug Discovery to Address Antimicrobial Resistance

M. Zeno (Stuttgart/DE), J. Vering (Stuttgart/DE), T. Barthel (Berlin/DE), M. S. Weiss (Berlin/DE), J. Steuber (Stuttgart/DE), G. Fritz (Stuttgart/DE)

Covalent linkage of flavin mononucleotide (FMN) is a posttranslational modification (FMNylation) that occurs in most bacterial species. This reaction is catalyzed by the enzyme ApbE that is essential for the maturation of several proteins of the bacterial energy metabolism, like the Na+-translocating NADH: ubiquinone oxidoreductase [2], the Rhodobacter nitrogen fixation (RNF) complex [3], or fumarate reductase and urocanate reductase [4]. ApbE binds FAD and transfers the FMN moiety to specific threonine residue within the target proteins and releases the residual AMP. The FMN is then bound to the threonine via a phosphoester bond [1]. Interestingly, the reaction occurs in the periplasm and ApbE has no homologue in human. Given its unique and essential function in many pathogenic bacteria, ApbE represents a promising target for new types of antibacterial drugs. We have targeted ApbE from multidrug-resistant pathogens using X-ray crystallography based fragment-screening, a medium throughput approach to identify, develop, and validate chemical scaffolds and lead compounds. We crystallized ApbE from *Klebsiella pneumoniae* and a pathogenic *Escherichia coli* strain and identified several fragments binding in active site. These findings serve now as a starting point for the development of a new class of antibiotics and demonstrate the potential of fragment based drug discovery in tackling antimicrobial resistance through targeting bioenergetic pathways.

References

[1] Bogachev, A. V., Baykov, A. A., and Bertsova, Y. V. (2018). Biochemical Society transactions 46, 5, 1161–1169.

[2] Steuber J, Fritz G, (2024): Biochim Biophys Acta Bioenerg, 1865(4):149485

[3] Vitt, Prinz, Eisinger, Ermler, and Buckel. (2022). Nature Communications 13, 6315.

[4] Méheust, Raphaël; Huang, Shuo; Rivera-Lugo, Rafael; Banfield, Jillian F.; Light, Samuel H. (2021): eLife 10. DOI: 10.7554/eLife.66878

PP-15

Structural investigation of UL3 from herpes simplex virus type 1: A structural homolog of a conserved DNA-binding protein domain in herpesviral proteins?

A. Weißenburg (Lübeck/DE), T. F. Schulz (Hanover/DE, Hanover/DE), M. M. Brinkmann (Brunswick/DE, Brunswick/DE), L. Redecke (Lübeck/DE, Hamburg/DE)

The herpes simplex virus 1 (HSV-1) belongs to the family of Orthoherpesviridae, being a widespread member of the subfamily of Alphaherpesvirinae, with a prevalence of 64 % in people under age 50. HSV-1 infection typically manifests as cold sores and genital herpes, while particularly in immunocompromised individuals and neonates it can also include severe complications such as herpes stromal keratitis, meningitis and herpes simplex encephalitis. After primary infection, HSV-1 can establish a lifelong latency in ganglionic neurons with the potential to reactivate.

Recent AI-based homology studies within the Orthoherpesviridae family using the HerpesFold algorithm have discovered structural homology in the viral DNA binding domain of important key players in the latency establishment, maintenance and regulation. These homolog structures include the Ebstein-Barr nuclear antigen 1 (EBNA1) of the Ebstein-Barr virus (EBV), the latency associated nuclear antigen (LANA) of the Kaposi's sarcoma associated herpesvirus (KSHV), and the unique long protein 3 (UL3) of HSV-1. This makes UL3 an interesting target when discussing a potential structure-function relationship.

The aim of this study is to investigate the structure of UL3 with a focus on the DNA binding domain in comparison with predicted homolog structures in other herpesviruses. The recombinant expression of the full-length UL3 as well as the C-terminal domain of UL3 in *Escherichia coli* (*E.coli*) cells and the purification of the proteins by affinity chromatography are currently in progress, followed by robot-assisted high-throughput protein crystallization screening. In parallel, an alternative expression system in insect cells is advancing, providing the opportunity for *in cellulo* crystallization approaches. A crystallographically determined structure of UL3 could be used for future structure-based identification and development of small molecule inhibitors as well as functional characterization.

PP-16

Crystallographic analysis of the human FTase β-subunit isoforms will complete kinetic and structural characterization

D. C. Rittmann (Witten/DE), M. C. Kehrenberg (Witten/DE), A. Hagemann (Witten/DE), H. Bachmann (Witten/DE)

Introduction: Farnesylation is a posttranslational modification essential for protein functionality and the progression of different diseases like cancer, progeria and hepatitis D. FTase inhibitors (FTIs) are under clinical investigation showing discrepant results. FTase is a heterodimer composed of an α- (FTα) and a β-subunit (FTβ).We identified new transcriptional variants of FTβ interacting with FTα, called F1, F2, F3, CF1, CF2. Four of the five variants form an active isoenzyme performing FTase activity (F1, F2, CF1 and CF2) but differ in their catalytic properties. Crystallizing these isoenzymes could reveal their structural and functional differences, potentially improving FTIs.

Objective: Our aim is the determination of the structures of the FTase isoenzymes and its impact on the pharmacological role of the FTIs and their future design.

Methods: Michaelis constant (Km) as well as inhibition constants (Ki) of four FTIs were determined by a continuous fluorescence assay and molecular dynamics (MD) modelling of F1, F2 and F3 and FTα has been performed. The consistency between the catalytic data and the structural models indicate that crystallization of the isoenzymes will enable direct structural analysis. A purification protocol to achieve high-grade purity has been established.

Results: Significant differences in the kinetic parameters could be observed for the isoenzymes. Additionally, the MD modelling confirmed this discrepancy. So, purification and crystallization of the isoenzymes is needed. A sequential purification protocol combining manual and automated chromatography has been established.

Conclusion: The results show a need for further investigations based on structural data. The FTase role in various diseases underlines the importance to uncover structural features causing significant catalytic differences. Resolving structural differences of the isoenzymes can be used as a basis for the development of putative new FTIs and therapeutic approaches.

PP-17

MTAN as an anti-virulence drug target – first insights via crystallographic fragment screening

L. Schenkmann (Berlin/DE), M. Oelker (Berlin/DE), T. Barthel (Berlin/DE), F. Lennartz (Berlin/DE), L. S. Benz (Berlin/DE), M. S. Weiss (Berlin/DE)

In recent years, the rise of drug-resistant infections has intensified the search for alternatives to conventional antimicrobials. So-called anti-virulence therapies aim to disrupt pathogenic processes rather than kill bacteria directly, thereby exerting reduced selection pressure.

A potential target is 5-methylthioadenosine/S-adenosylhomocysteine nucleosidase (MTAN), a bacterial hydrolase involved in the biosynthesis of autoinducers (AIs). These small, hormone-like molecules mediate quorum sensing, a key mechanism in bacterial communication and virulence [1]. Inhibition of MTAN has been shown to reduce AI production and biofilm formation in *Vibrio cholerae* [2].

Based on high-throughput fragment-screening data generated at the F2X facility at BESSY II, we aimed to develop and validate first-generation lead candidates for *Staphylococcus aureus* MTAN (saMTAN).

Screening of three fragment libraries comprising 288 compounds resulted in 36 initial hits. Structural analysis identified key active-site residues mediating fragment binding, giving us a clear direction for the following hit-to-lead process. Ligand design focused on enhancing interactions with these critical residues. Additionally, biochemical assays were established to validate future compounds.

Here we present lead candidates which provide a strong foundation for advancing MTAN inhibitors toward potent anti-virulence therapeutics.

Fig.1: Overview of all initial hits from three screened fragment libraries. F2X Entry (deep teal), EUopen (magenta) and Kit Library (lime green). Bound fragments are predominantly situated in and around the active center. 0.94 Å structure solved via molecular replacement.

References

[1] Antunes LCM, et al. (2010). Quorum sensing in bacterial virulence. Microbiology, 156(8), 2271-2282.

[2] Gutierrez JA, et al. (2009). Transition state analogs of 5′-methylthioadenosine nucleosidase disrupt quorum sensing. Nature chemical biology, 5(4), 251-257.

Fig. 1

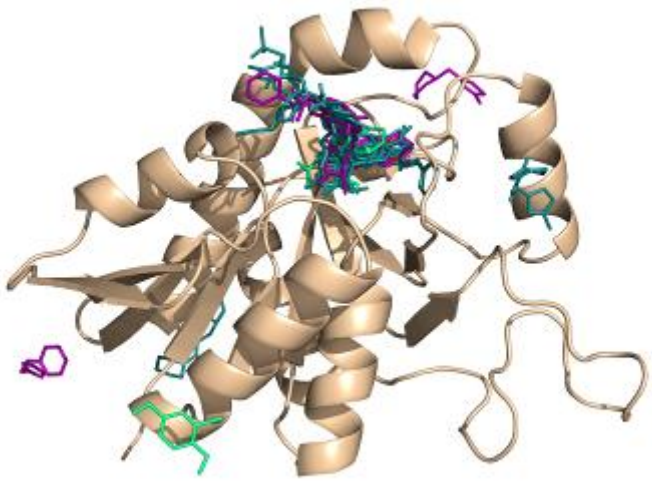

PP-92

Structural and Biophysical Characterization of Complement Control Protein of Kaposi´s Sarcoma Associated Herpes Virus

Hera Fatima, George Ssebyatika, Nina Plückebaum, Carina Jürgens, Bushra Husain, Lucas Mendes Monteiro, Nadia Martinez-Martin, Abel Viejo-Borbolla, Thomas Krey

Kaposi's Sarcoma-Associated Herpesvirus (KSHV) is an oncogenic γ-Herpesvirus that is linked to several malignancies, including Kaposi's sarcoma, Primary Effusion Lymphoma, and Multicentric Castleman's Disease, representing a major global health burden, particularly among immunocompromised individuals. Lifelong infection involves viral latency in B cells and endothelial cells. The lack of specific antiviral inhibitors and suitable small animal models for preclinical research renders the development of novel therapeutic options for the treatment of KSHV-associated diseases difficult. Targeting viral immune evasion proteins, such as the KSHV complement control protein (KCP), a glycoprotein encoded by ORF4 that inhibits the complement pathway and aids the virus in evading the host immune system, represents a promising antiviral strategy.

KCP interacts with different partners including complement proteins and proteoglycans. A recent miniature AVEXIS screening identified KCP to also interact with fibronectin leucine-rich transmembrane proteins (FLRTs), key regulators of endothelial cell migration, angiogenesis, and vascular development whose upregulation is associated with metastasis.

This study aims to comprehensively characterize the KCP interactions via biochemical and structural approaches and we present the first crystal structures of KCP alone and in complex with interaction partners and discuss implications resulting from a thorough structural analysis of these structures.

Our results provide insights into the mechanism underlying viral immune evasion, paving the way for targeted therapeutic interventions.

PP-18

Structural and spectroscopic characterisation of AlkB domains involved in electron transfer during alkane oxidation

R. Ganguly (Erlangen/DE), K. Parashar (Erlangen/DE), I. Span (Erlangen/DE)

Biological alkane oxidation plays a critical role in the global carbon cycle by enabling microorganisms to metabolise up to 800 million tons of hydrocarbons that enter the environment annually. However, alkanes are chemically inert and challenging to functionalise selectively. Nature has evolved alkane-oxidising systems (AlkBGT) that can selectively hydroxylate terminal C–H bonds across a broad range of alkane chain lengths. The objective of the work is to characterise the distinct electron transfer systems associated with AlkB enzymes, each with diverse protein architectures to get insights about their distinct roles in nature. Electronic absorption spectroscopy and X-ray crystallography were employed to investigate the structural and electronic properties of the electron-transfer systems. Spectroscopy of the electron transfer domains shows that rubredoxin-type centres are typically employed; however, we unexpectedly discovered that a ferredoxin-type [2Fe-2S] cluster can also mediate electron transfer. Additionally, we solved the crystal structure of an NADH-dependent reductase domain, providing insight into the initial electron transfer step. In summary, our results advance the structural understanding of these systems and their electron transfer strategies. The presence of different forms of AlkB in these organisms suggests evolutionary ways to improve electron-transfer strategies to AlkB. The knowledge of structural and functional properties of these domains allows us to understand why there exist differences between their Fe-S binding sites as well as overall domain architecture, and enables us to engineer more efficient biocatalysts.

Fig. 1: **A)** Alpha-fold predicted model three-domain AlkB from *Polaromonas naphthalenivorans*. **B)** High-resolution X-ray structure of the ferredoxin reductase domain. **C)** Schematic representation of the three-domain AlkB. **D)** A simplified diagram showing the electron transfer pathway in the oxidation of alkane to alcohol.

Fig. 1

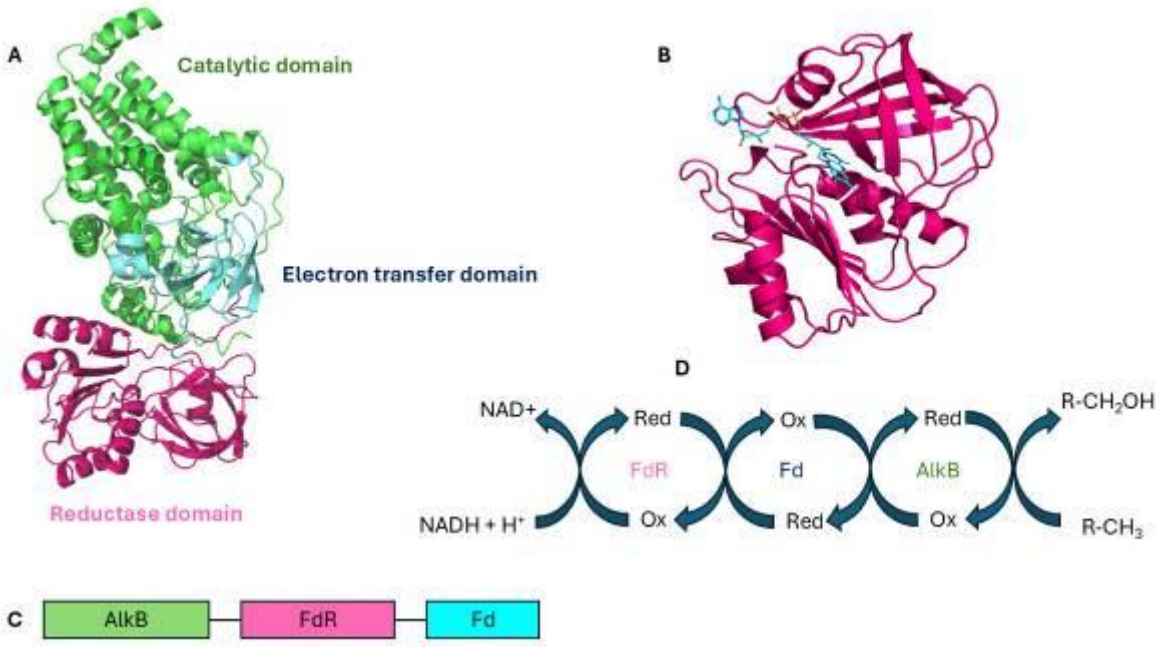

PP-19

Interplay of Proton-Coupled Electron Transfer and Enzyme Dynamics in Pyruvate Oxidase

F. Rabe von Pappenheim (Göttingen/DE), S. Bartel (Göttingen/DE), K. Tittmann (Göttingen/DE)

Pyruvate oxidases (POXs) are key enzymes in the aerobic energy metabolism of bacteria that lack a respiratory chain. These homotetrameric, dual-cofactor enzymes utilize thiamine diphosphate (ThDP) and flavin adenine dinucleotide (FAD) to catalyze the oxidative decarboxylation of pyruvate, employing molecular oxygen as the terminal electron acceptor and generating hydrogen peroxide. In the presence of inorganic phosphate, the reaction yields acetyl phosphate, which is used for ATP generation. During catalysis, two electrons and at least one proton are transferred from ThDP to FAD across a distance of over 10 Å—an energetically demanding process due to solvent reorganization and the associated energetic penalty.

To elucidate how this long-range electron transfer is facilitated, crystallographic analysis using a stable substrate-ThDP analog revealed that previously unresolved C-terminal residues bind to the active site, displacing numerous solvent molecules while also potentially serving as an electron-transfer way station.

Using X-ray crystallography, cryo-electron microscopy, and kinetic steady-state and pre-steady-state analyses, we define the structural basis for the dynamic nature of the C-terminus and its role in proton-coupled electron transfer during the catalytic cycle of pyruvate oxidase.

PP-20

Structural and biochemical characterization of regulation and function of the Rab23 GTPase

N. Elagouri (Münster/DE), S. Wilmes (Münster/DE), D. Kümmel (Münster/DE)

The Rab family of small GTPases plays an important role in the regulation of intracellular trafficking and membrane organization. They are activated by guanine nucleotide exchange factors (GEFs). Rab23 was previously shown to be required for the membrane trafficking at mature cilia during ciliogenesis and for planar cell polarity (PCP), which are important in embryonic development. Mutations in the Rab23 and its GEF genes can lead to human birth defects. Thus, a mechanistic understanding will help to provide valuable insight into understanding the development of human disease. We have recently reported the cryo-EM structure of the human Rab23 in complex with its cognate tri longin domain (TLD) GEF Fuzzy-Inturned and investigated the *Hs*Rab23 activation by Fuzzy-Inturned, revealing molecular adaptations in the catalytic mechanism and recruitment of the complex.

In addition, Fuzzy-Inturned was previously shown to regulate the localization of the atypical formin-related protein multiple wing hairs (Mwh) during PCP, which in turn regulates the actin polymerization in *Drosophila* wing cells. We hypothesize that Mwh localization may be mediated via Rab23, and indeed, we observe a transient interaction of *Dm*Rab23 with Mwh in interaction studies. As a first step towards understanding the molecular basis of Rab23-Mwh interplay, we determined the crystal structure of the formin homology domain (FH3) of Mwh and now work towards the reconstitution of a Rab23-Mwh complex.

PP-22

Two new Ba/Li gallides with [Ga_2] dumbbells: $Ba_2Li_2[Ga_2]$ and $BaLi_8[Ga_4][Ga_2]$

M. Otteny (Freiburg i. Br./DE), Q. Da Cruz (Freiburg i. Br./DE), M. Wendorff (Freiburg i. Br./DE), C. Röhr (Freiburg i. Br./DE)

The structures of the new mixed Ba/Li gallides $Ba_2Li_2[Ga_2]$ and $BaLi_8[Ga_4][Ga_2]$, yielded from stoichiometric melts of the elements (T_{max}=1100 °C), both contain [Ga_2] dumbbells with short Ga-Ga bonds, which are oriented along the long *c* axes. The tetragonal structure of $Ba_2Li_2[Ga_2]$ (new str. type, *I*4/*mmm*, *a*=489.93(6), *c*=1467.1(2) pm, *R*1=0.0194) contains such [Ga_2] units as sole anions. They are surrounded by double-capped square prisms of 10 Ba cations, with the remaining four faces of the prisms centered by four additional Li cations (Fig. 1a: gray polyhedra [$(Ga_2)\_Li_4Ba_{10}$]). Hightlighting the overall polar Li/Ga polyanion, the structure can alternatively be considered as a defect $K_2[NiF_4]$-type derivative, $Ba_2[\_Li_2Ga_2]$, containing layers of flat edge-sharing octahedra [$Ga_2Li_{4/2}$] with a central [Ga_2] unit. The hexagonal structure of the second title phase, $BaLi_8[Ga_4][Ga_2]$ (again new type, *P*6/*mmm*, *a*=441.970(10), *c*=1590.34(4) pm, *R*1=0.0179) likewise exhibits [Ga_2] dumbbells ($d^a_{Ga(1)-Ga(1)}$=253.3 pm), which are again oriented along the *c* axis. Here, the coordination polyhedron around [Ga_2] are elongated capped hexagonal prims with six extra Li^+ centering the prism's edges (Fig. 1b: polyhedra [$(Ga_2)Li_{20}$]). The blocks of [Ga_2] dumbbells around *z*=½ alter with $BaGa_2$-like (AlB_2-type, $d^b_{Ga(2)-Ga(2)}$=255.2 pm) blocks of identically oriented graphite-like nets (*z*≈0). Similar to Ga(2), Li(1) as well as Li(3) also form graphite-analogous 6^3 layers among each other, so that the overall structure can alternatively be described as an i5 symmetry reduced Ba[Ga2]-type variant, $BaLi(2)_2Ga(1)_2[Li(1,3)_6Ga(2)_4]$. The chemical bonding within the gallide anions (i.e. Zintl's concept, Ga-Ga bond length/bond order) as well as within the polar Li/Ga polyanion (i.e. tetrahedra packing) is discussed on the basis of the results of FP-APW band structure calculations (cf. Fig. 2).

Fig. 1: Crystal structure of $Ba_2Li_2[Ga_2]$ (a) and $BaLi_8[Ga_4][Ga_2]$ (b).

Fig. 2: Calculated DOS of the title compounds.

Fig. 1

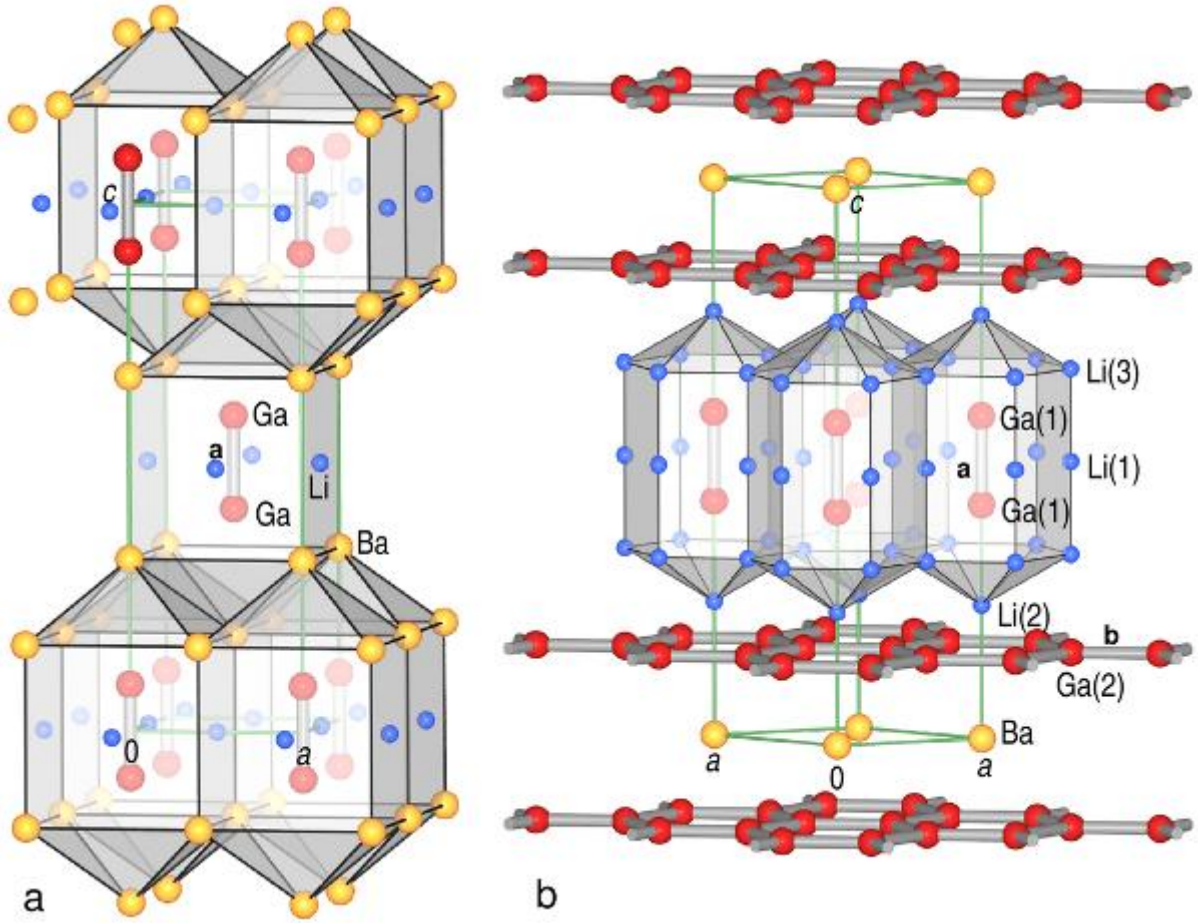
c
Ga
a
Ga
Li
Ba
0
a
a
Li(3)
Ga(1)
Li(1)
a
Ga(1)
Li(2)
b
Ga(2)
Ba
a
0
a
b

Fig. 2

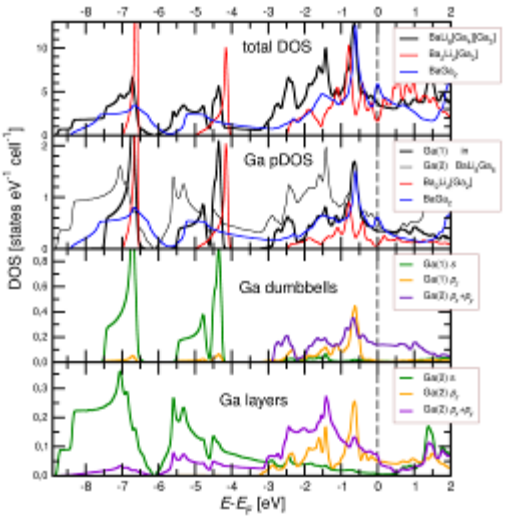
total DOS
Ga pDOS
Ga dumbbells
Ga layers
DOS [states eV^{-1} cell^{-1}]
E-E_F [eV]

PP-23

Novel Oxygen-Rich Phases in Alkali and Alkaline Earth Metal Oxides under Extreme Conditions

J. Lyu (Frankfurt a. M./DE), B. Winkler (Frankfurt a. M./DE), D. Spahr (Frankfurt a. M./DE), E. Bykova (Frankfurt a. M./DE), L. Brüning (Frankfurt a. M./DE), R. Akilli (Frankfurt a. M./DE), F. I. Akbar (Frankfurt a. M./DE), M. Bykov (Frankfurt a. M./DE)

Application of pressure in a chemical synthesis can allow to produce unique compounds, featuring various homonuclear polyanionic species. While extended polyanions are known for a variety of main-group elements, the chemistry of polyoxides is limited to dioxide anions having different formal charges (O2x-) or ozonides O3x-, despite many of more complex polyanions were predicted to be stable at high pressures.

In this work, we present the high-pressure study of the alkali/ alkaline earth metal–oxygen systems demonstrating the great diversity of accessible inorganic polyoxide compounds. In Na-O system, we discovered three novel compounds at 40 GPa: Na(O2)2, Na5(O3)2(O2) and Na3(O2)2. Among them, Na(O2)2 and Na3(O2)2 feature O2 dimers with non-integer charges of 1.5 and 0.5 in their crystal structures respectively. To the best of our knowledge, Na(O2)2 is the most oxygen-rich compound known among alkali metal oxides. Na12(O2)61.5−(O2)2−(O2)− features a mixture of charge-ordered superoxide O2−, peroxide O22−, and O21.5−, while Na5(O3)2(O2) compound contains two isolated V-shaped O32- and superoxide O2− anions. In the Sr-O system, we obtained four new polymorphs of Sr(O2)2 at 35 and 80 GPa, which crystallize in the space groups *P*-1, *I*2/*m*, *Fmmm* and *Ibam*. Another new compound Sr2(O2)3 contains a mixture of two independent O2 dimers: the peroxide and the superoxide anions. Furthermore, by calculating weighted average bond lengths for O2 dimers with different charges, we established the empirical relations between O–O distance and formal charge of the anion. The properties and crystal chemistry O-O dimers in solid state compounds are interesting not only from the point of view of fundamental chemistry, but also provide a deep understanding of the intermediate states of the anionic redox in oxide-based metal-ion batteries.

PP-24

$Tl_2Cu_2As_2S_5$, a new mineral with a unique 2D structure

S. Graeser (Kopenhagen/DK), D. Topa (Vienna/AT, Kopenhagen/DK), H. Effenberger (Vienna/AT), E. Makovicky (Copenhagen/DK), W. H. Paar (Bucharest/RO), G. Dincă (Bucharest/RO)

The crystal structure of the new mineral spaltiite, $Tl_2Cu_2As_2S_5$, exhibits a pronounced 2D-arrangement of the atoms. Spaltiite crystallizes in space group $P2_1/c$ (a = 15.791(8), b = 10.000(5), c = 6.323(3) Å, β = 99.25(2)°; single-crystal X-ray data, $R1$ = 12.1 % for 4748 data with $F_o > 4\sigma(F_o)$ and 101 variable parameters).

There are two chemically different sheets parallel to (100): (*i*) corner connected CuS_3 triangles, CuS_4 tetrahedra, and two topologically different AsS_3 pyramids form $CuAs_2S_5$ sheets that are separated by (*ii*) Tl^{1+} ions. Strong interconnections along [001] as well as prominent atomic arrangements at the boundaries of the $Cu_2As_2S_5$ layers are evident; they are polar and have layer symmetry pc. All tops of the AsS_3 pyramids point to the centre of the layers. Thus channels are formed which host the lone-electron pairs of the As atoms. Within the unit cell the $Cu_2As_2S_5$ layers are located in (1/4 *y z*) and (3/4 *y z*) and related by inversion symmetry. In (0 *y z*) and (1/2 *y z*) are topologically different Tl-layers formed by TlS_7 and TlS_8 coordination polyhedra, respectively. They exhibit layer-group symmetry $p2_1/c$. The atomic arrangement of spaltiite reflects its morphology with a platelet shape parallel to [100] and an elongation in [001].

Interestingly, the $Cu^{[3]}$ atom is shifted out of the S-atom plane by 0.497(4) Å towards to an As atom indicating some interaction ($Cu–As^{[3]}$ = 2.636 Å). This distance is longer than the sum of the radii of Cu and As atoms and longer than commonly observed for a $Cu^{[4]}$ atom in Cu-arsenides. Makovicky (2018) mentions the possibility of an interaction between the $Cu^{[3]}$ atom and the lone-electron pairs of the As atom.

Makovicky, E. (2018): Minerals 8, 478. https://doi: 103390/ min8110478

Fig. 1

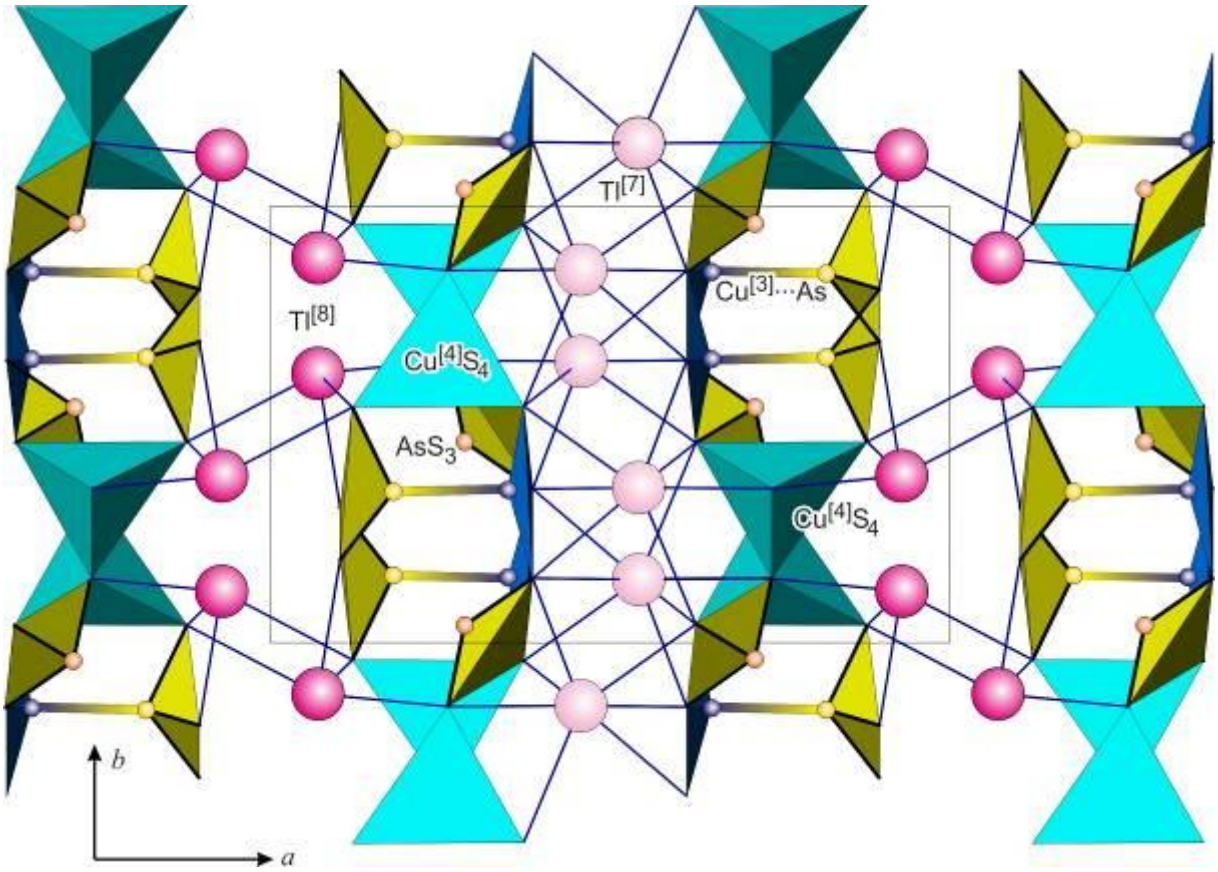

Poster Session 1: New Crystal Structures

PP-25

Design and synthesis of new photoluminescent coordination polymers employing a ligand derived from quinoline and pyridine

A. Kochel (Wrocław/PL), M. Hołyńska (Noordwijk/NL)

Application of organic aminocarboxylate ligand with N/O donor atoms enabled solvothermal synthesis of 1D to 3D Cu(II) coordination polymers. Condensed rings system of the applied ligand promotes formation of coordination polymers rather than mononuclear species. The resulting products may display interesting photochemical and/or magnetic properties, depending on the sort of employed metal ions.

Concerning the models of polymers, electron spin density distribution has been visualized and discussed.

PP-26

Synthesis and crystal structure of a new hydrous scandium carbonate $Sc[HCO_3][CO_3]$

J. Bungarten (Frankfurt a. M./DE), L. Bayarjargal (Frankfurt a. M./DE), D. Spahr (Frankfurt a. M./DE), N. Sharapova (Frankfurt a. M./DE), Y. Wang (Frankfurt a. M./DE), V. Milman (Cambridge/GB), B. Winkler (Frankfurt a. M./DE)

Rare-earth carbonates with trivalent metal cations (M^{3+}) typically occur in nature as water-, hydroxyl-containing or more complex carbonates [1]. Recently, an anhydrous M^{3+} rare-earth carbonate, $Y_3[CO_4]_2$, was synthesized under elevated pressure and temperature conditions [2]. To date, no scandium carbonate has been reported. Here, we studied the synthesis and and high-pressure behavior of $Sc[HCO_3][CO_3]$.

Sc_2O_3, CO_2 and H_2O were reacted at 35(2) GPa and 2800(200) K in a laser heated diamond anvil cell, resulting in the synthesis of $Sc[HCO_3][CO_3]$. New phases were identified by spatially resolved Raman spectroscopy. Subsequently, the structure was determined by single-crystal synchrotron X-ray diffraction experiments at beamline P02.2 at PETRA III. Raman and diffraction data were complemented with DFT calculations. $Sc[HCO_3][CO_3]$ crystallizes in the monoclinic space group $P2_1/c$ with Z = 4. The new hydrous carbonate features double layers of $[HCO_3]^-$ and $[CO_3]^{2-}$ groups arranged along the *a*-axis and contains 9-fold coordinated Sc^{3+}-cations.The structure and synthesis will be presented at the conference.

Financial support by DFG (DFG-Wi1232 to BW, DFG-BA4020 to LB) is gratefully acknowledged. BW is grateful for support by the Dassault Systèmes Science Ambassador program. We acknowledge DESY for the provision of experimental facilities and beam time. We thank N. Giordano for assistance at P02.2.

Fig. 1: a) Structure of $Sc[HCO_3][CO_3]$-$P2_1/c$ at ~35 GPa viewed along the *b*-axis. b) Enlargement of the $[HCO_3]^-$ and $[CO_3]^{2-}$ groups with bond lengths and angles.

References

[1] M. Back, The New IMA List of Minerals – A Work in Progress– Updated: September 2024, https://cnmnc.units.it/files/IMA_Master_List_(2024-09)-1.pdf.

[2] A. Aslandukova *et al.*, *Inorg. Chem.* 2025, 64, 10, 5098.

Fig. 1

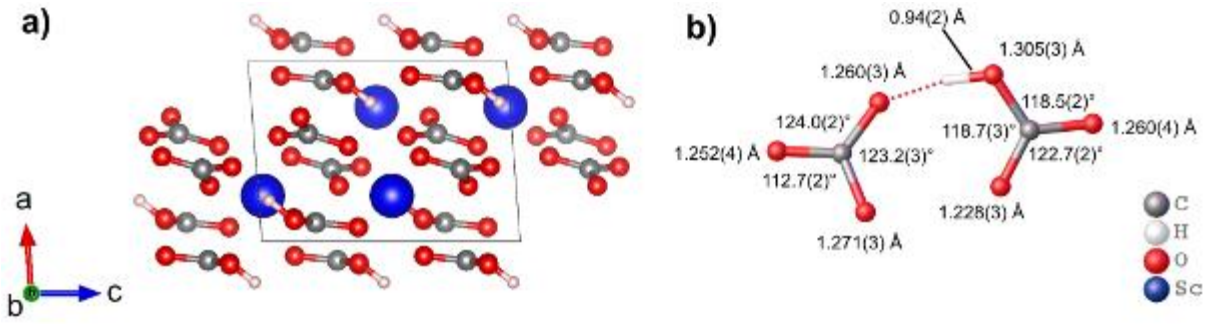

PP-27

Discovery of inorganic tricarbonate salt: high-pressure synthesis and structure of $K_2C_3O_7$

A. Aslandukov (Frankfurt a. M./DE)

The synthesis of carbonates with novel anionic species is significant for chemistry, geoscience, and materials science. Beyond common carbonates containing $[CO_3]^{2-}$ anions known at ambient conditions, high pressures can stabilize various sp^3-carbonates built of tetrahedral CO_4 units. At mild pressures, sp^2-pyrocarbonates with $[C_2O_5]^{2-}$ groups have also been reported. This suggests that the planar CO_3 unit, along with the tetrahedral CO_4 unit, can potentially also be a building block of exotic C-O anions at high pressure. This parallels borate chemistry, where diverse anions comprised of BO_3 and BO_4 building blocks exist. However, aside from the $[C_2O_5]^{2-}$ anion, no other species containing CO_3 units are known.

Here, we report the serendipitous discovery of $K_2C_3O_7$—the first inorganic tricarbonate salt—formed in a laser-heated diamond anvil cell at 55 GPa. The compound was unexpectedly formed during experiments exploring the high-pressure high-temperature behavior of potassium chlorate. Its presence was identified, and the crystal structure was solved and refined using synchrotron single-crystal X-ray diffraction data collected from a multigrain multiphase sample. The DAFi program was employed to efficiently sort reflections from individual crystallites.

The $K_2C_3O_7$ compound features non-planar $[C_3O_7]^{2-}$ anions built of three condensed planar CO_3 units rotated relative to one another. This anion extends the homologous series of sp^2-carbonates: $[CO_3]^{2-}$ - $[C_2O_5]^{2-}$ - $[C_3O_7]^{2-}$. Density functional theory (DFT) calculations corroborate the experimental results and suggest the thermodynamic stability of $K_2C_3O_7$ between 10 and 55 GPa. DFT calculations predict a phase transition between 80 and 90 GPa associated with a polymerization of the $[C_3O_7]^{2-}$ groups, accompanied by a change in the coordination polyhedra of two carbon atoms from triangles to tetrahedra. These results imply that other sp^2- and mixed sp^2/sp^3-carbonates might be stabilized at high pressure.

PP-28

Coinage metal complexes of a dehydrobenzo[16]annulene derivative: superstructures, diffuse scattering and intermolecular interactions

M. Koohgard (Brunswick/DE), M. Tamm (Brunswick/DE), D. Bockfeld (Brunswick/DE), C. Kleeberg (Brunswick/DE)

Figure: Structures of the dehydrobenzo[16]annulene (**1**) (left) and its silver complex [**1**(Ag)][BF4] (right).

Results & Conclusion: A substituted dehydrobenzo[16]annulene (**1**) was synthesised by alkyne metathesis. Crystals suitable for single crystal X-ray diffraction were obtained under different conditions resulting in different solvates exhibiting various intermolecular interactions. Complexation with coinage metal precursors resulted in complex cations of the type [**1**(M)]+ with counter ions such as [BF4]- or [SbF6]-. All crystals obtained exhibit their peculiar structural features may it be solvatisation, twinning, super structures or diffuse scattering.

The different crystal structures of **1** and coinage metal complexes thereof will be discussed regarding their challenging single crystal X-ray diffraction studies as well as their structural features in particular the intermolecular interactions.

Fig. 1

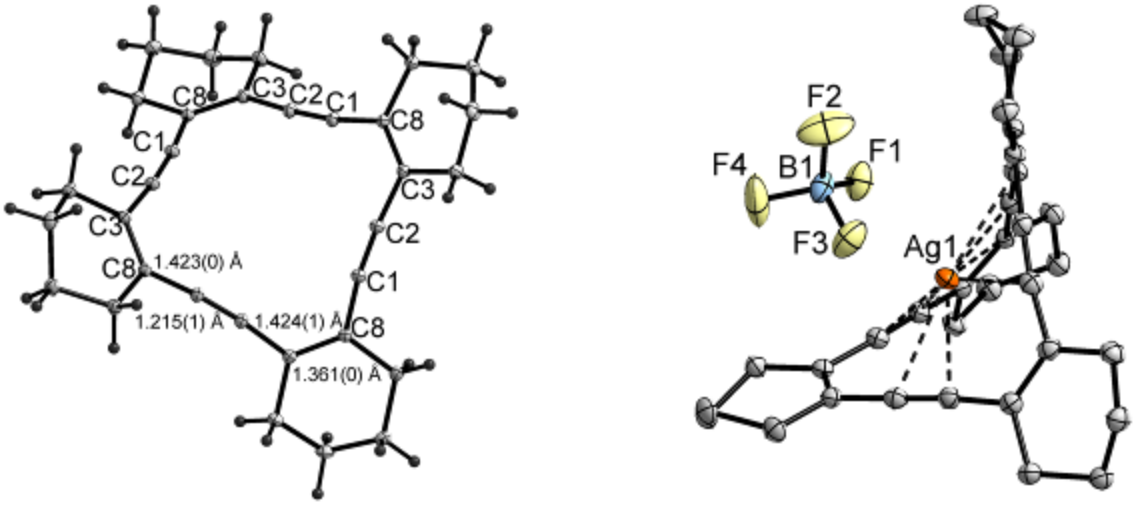

PP-29

$K_3Tm_7S_{12}$: Another Potassium Lanthanoid(III) Sulfide with $Cs_3Y_7Se_{12}$-Type Crystal Structure

K. Engel (Stuttgart/DE), T. Schleid (Stuttgart/DE)

In the systems of alkali-metal lanthanoid sulfides mainly three different compositions have been reported yet: $ALnS_2$[1] , ALn_7S_{11}[2] and $A_3Ln_7S_{12}$[3,4] (A = Li – Cs). The composition $A_3Ln_7Ch_{12}$ is well known for rubidium and cesium lanthanoid selenides[5], but for Ch = S just two erbium compounds, $K_3Er_7S_{12}$ and $Rb_3Er_7S_{12}$[4], have been published so far. The potassium thulium sulfide $K_3Tm_7S_{12}$ presented here adds a new representative to this series.

$K_3Tm_7S_{12}$ was synthesized from a mixture of Tm, K_2S_3, As_2S_3 and S in a molar ratio of 1:1:1:6 at 500 °C. Orange, transparent, needle-shaped crystals were obtained and characterized by single-crystal X-ray diffraction. $K_3Tm_7S_{12}$ crystallizes in the orthorhombic space group *Pnnm* with a = 1178.31(9) pm, b = 2443.25(19) pm, c = 391.72(3) pm for Z = 2, adapting the $Cs_3Y_7Se_{12}$-type crystal structure. It is built from four crystallographically unique $[TmS_6]^{9-}$ octahedra with edge-connectivity, forming a three-dimensional channel structure. These channels occur along [001] and can be described as rectangular with 6×4 $[TmS_6]^{9-}$ octahedra each. Charge balance of the 3D-$\{[Tm_7S_{12}]^{3-}\}$ framework is achieved by K^+ located within the channels. The crystal structure of $K_3Tm_7S_{12}$ is closely related to that of $RbTm_3S_5$, which can also be described as a channel structure with a fish-bone pattern of edge-connected $[TmS_6]^{9-}$ octahedra and a channel size defined by 5×4 octahedral units. So, the addition of another $[TmS_6]^{9-}$ octahedron within those 5×4 rectangles leads to the formation of a 6×4 pattern for the new composition $K_3Tm_7S_{12}$ with an additional half-occupied K^+-cation site for electroneutrality.

References

[1] R. Ballestracci, *Bull. Soc. Fr. Mineral. Cristallogr.* **1965**, *88*, 207.

[2] H. Lin, L.-H. Li, L. Chen, *Inorg. Chem.* **2012**, *51*, 4588.

[3] M. Folchnandt, Th. Schleid, *Z. Anorg. Allg. Chem.* **1997**, *623*, 1501.

[4] F. Lissner, I. Hartenbach, Th. Schleid, *Z. Anorg. Allg. Chem.* **2002**, *628*, 1552.

[5] M. Folchnandt, Th. Schleid, *Z. Anorg. Allg. Chem.* **1998**, *624*, 1595.

Fig. 1

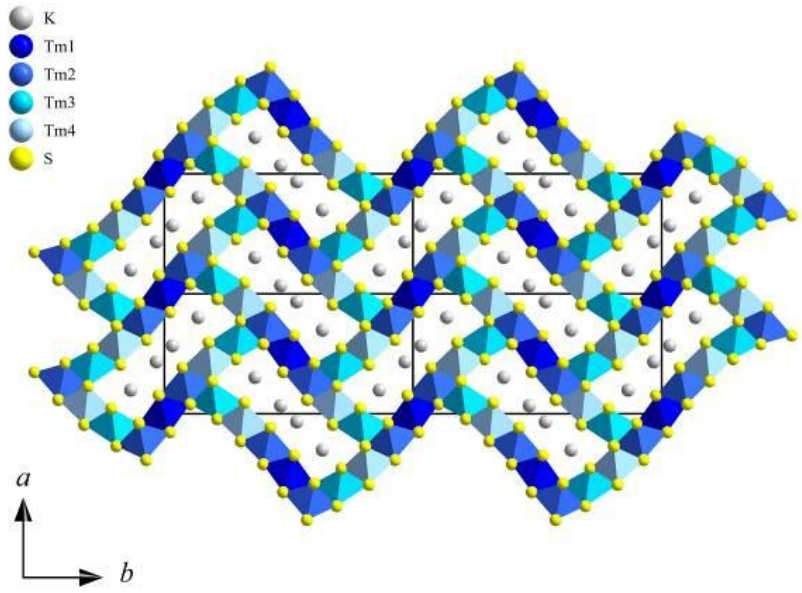

Figure 1: Crystal structure of $K_3Tm_7S_{12}$ built from edge-connected $[TmS_6]^{9-}$ octahedra with K^+ cations in empty channels along [001].

PP-30

{Yb[N(CN)$_2$]$_2$(H$_2$O)$_4$}Cl · H$_2$O: The First Mixed-Anionic Dicyanamide Hydrate

R. J. C. Locke (Stuttgart/DE), O. Reckeweg (Stuttgart/DE), T. Schleid (Stuttgart/DE)

When Yb^{3+} and $[N(CN)_2]^-$ ions meet in aqueous solution, Yb[N(CN)$_2$]$_3$ · 2 H$_2$O in analogy to other *Ln*[N(CN)$_2$]$_3$ · 2 H$_2$O representatives with *Ln* = Eu – Tb [1, 2] should result as hydrated product upon isothermal evaporation at room temperature. The presence of Cl^- anions alters the product palette, however, as colorless single crystals of Yb[N(CN)$_2$]$_2$Cl · 5 H$_2$O (triclinic, *P*-1; *a* = 926.56(1) pm, *b* = 1111.65(2) pm, *c* = 1252.08(2) pm, *α* = 97.239(1)°, *β* = 94.640(1)°, *γ* = 103.039(1)°, *Z* = 4) emerged from the corresponding brine. Its crystal structure consists of two crystallographically independent eightfold coordinated Yb^{3+} cations displaying four nitrogen atoms (*d*(Yb–N) = 237 – 241 pm) from four dicyanamide anions and four oxygen atoms (*d*(Yb–O) = 230 – 238 pm) from water molecules. Surprisingly, both have no contact to the Cl^- anions.

The $[N(CN)_2]^-$ anions exhibit their typical boomerang shape [N≡C–N–C≡N] with bond lengths and angles (*d*(C≡N) = 114 – 116 pm, *d*(C–N) = 130 – 132 pm, <(C–N–C) = 118 – 119°, <(N–C≡N) = 174 – 175°) in common ranges. They are part of a SiS_2-related chain 1D-{[(H$_2$O)$_4$(Yb1)[N(CN)$_2$]$_{8/2}$(Yb2)(H$_2$O)$_4$]$^{2+}$}, which suggests the more simple motif 1D-{[(H$_2$O)$_2$Yb[N(CN)$_2$]$_{4/2}$(H$_2$O)$_2$]$^+$} with a smaller unit cell. But the two crystallographically diverse Cl^- anions make the difference: one is far away from its inversion-symmetric counterpart, whereas the other one is connected via hydrogen bridges of two water molecules to its point-inverted one, forming a dimer [(Cl1)(H–O–H)$_2$(Cl1)]$^{2-}$ with an inversion center and $(Cl1)^-$–$(Cl1)^-$ distances like 481 pm. The second one $(Cl2)^-$ shows distances of about 580 pm to $(Cl1)^-$ and 670 pm to $(Cl2)^-$, and both reside in coordination spheres of water.

Fig. 1: Structural features of {Yb[N(CN)$_2$]$_2$(H$_2$O)$_4$}Cl · H$_2$O.

References

[1] A. Nag, W. Schnick, *Z. Anorg. Allg. Chem.* **2006**, *632*, 609–614.

[2] A. Nag, P. J. Schmidt, W. Schnick, *Chem. Mater.* **2006**, *18*, 5738–5745.

Fig. 1

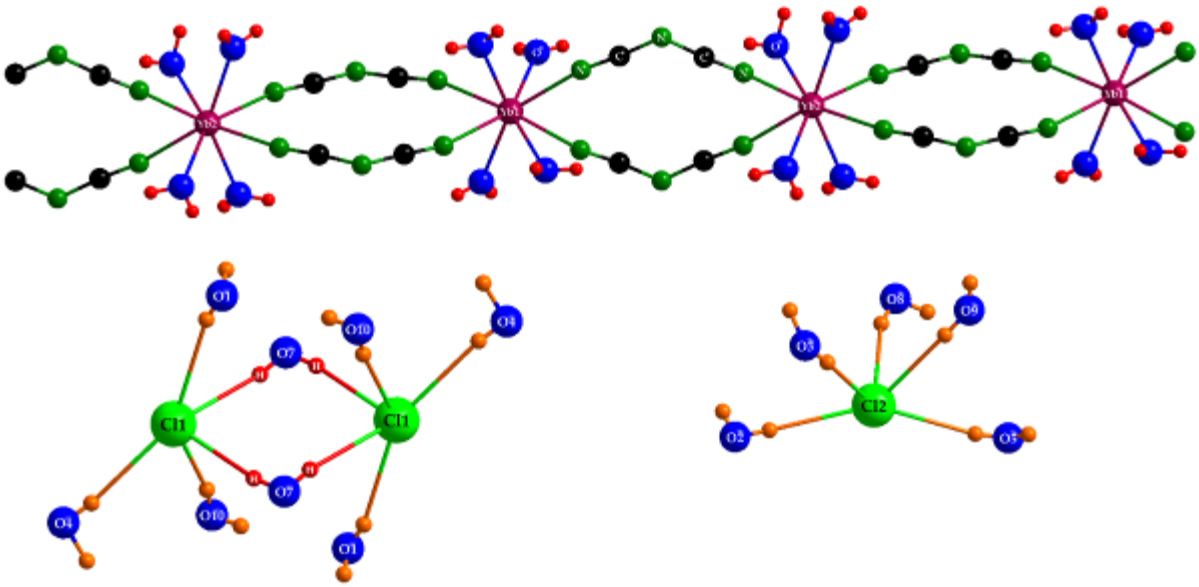

PP-31

Structure Elucidation of Liquids Using Organic Crystallization Chaperones

J. Hartenfels (Stuttgart/DE), T. Berking (Stuttgart/DE), G. L. Runge-Seither (Stuttgart/DE), W. Frey (Stuttgart/DE), C. Richert (Stuttgart/DE)

Determining the structure of a new compound, including its absolute configuration, can be challenging and time-consuming. The use of X-ray crystallography allows for reliable structure elucidation; however, single crystals of sufficient quality are required. If the analyte does not crystallize by itself, *i.e.* because it presents itself as a liquid or oil at room temperature, crystallography is inaccessible. Tetraaryladamantanes (TAAs) show a propensity to crystallize as solvates with liquid analytes.

Our work aims at 'co-crystallizing' analytes to elucidate their structure as solvates via SC-XRD. Here, we report on our investigation of the limits of the technique and the principles behind the chaperone effect.[1],[2],[3] Solvate single crystals are usually obtained within 24 h via thermal crystallization.[1]

A screen of 52 diverse compounds revealed a high inclusion rate of well-resolved analyte structures. Absolute configuration could be determined in most cases where chiral analytes were involved.[1] Various larger analytes up to squalene (411 g/mol) were successfully incorporated, though disorder is observed.[4] Other chaperone candidates mimicking established TAAs, such as tetraphenylporphyrins and spirobifluorenes, did not have the same broad application range.[5]

The crystallization protocols are easily performed, broadly applicable, and fast. The reduction of intermolecular forces between chaperone molecules and a "temperature jump protocol" allows for larger analytes to be encapsulated, at the cost of positional disorder.

References

[1] F. Krupp, C. Richert *et al.*, *Angew. Chem.* **2020**, *132*, 16009-16013; *Angew. Chem. Int. Ed.* **2020**, *59*, 15875-15879

[2] F. Rami, C. Richert *et al.*, *Beilstein J. Org. Chem.* **2021**, *17*, 1476-1480

[3] T. Berking, C. Richert *et al.*, *Synthesis* **2023**, *55*, 2473-2482

[4] T. Berking, C. Richert *et al.*, *Angew. Chem. Int. Ed.* **2024**, 63, e202402976

[5] J. Hartenfels, C. Richert *et al.*, *Chem. Eur. J.* **2025**, e01795

Fig. 1

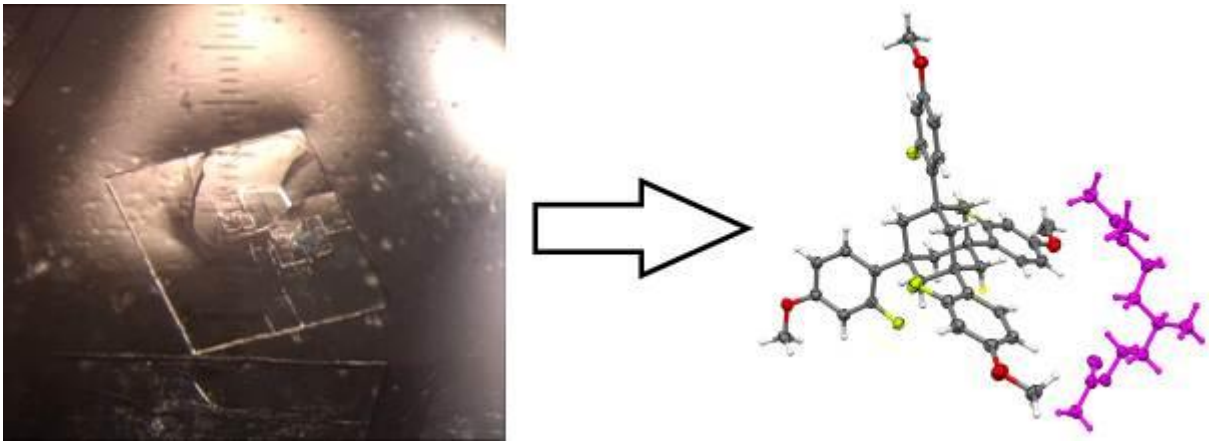

PP-32

Expanding the Coordination Mode Space of Calix[4]imidazolium[2]pyrazole

B. Bock (Neufahrn b. Freising/DE, Munich/DE), S. Deger (Munich/DE), T. Pickl (Munich/DE), J. Preinl (Munich/DE), S. Inoue (Munich/DE), A. Pöthig (Munich/DE)

In 2015, *A. Pöthig* and his research group synthesized the new macrocycle calix[4]imidazolium[2]pyrazole. This macrocycle has already demonstrated its potential in terms of structural diversity and flexibility in combination with different transition metals in organometallic complexes. The Pillarplexes **M8L2(X)4** (M = Ag, Au, Cu; X = counterion), which are octahedral metallocavitand structures can be modulated into Rotaxanes by incorporating various guest molecules.[1] The Capsoplexes (**M2L)2A(X)3** (M = Ni, Cu; A = Cl, Br) exhibit special host properties through the incorporation of halides by two macrocyclic dinuclear complexes.[2,3]

The limits of structural variability have recently been expanded using the cobalt group for complex synthesis. The reaction of **[RhCl2(Cp*)]2** with the **H6LMe(PF6)4** demonstrated the possibility of controlled synthesis of three dinuclear Rh(III) half-sandwich complexes (**C1**, **C2**, **C3**), including two isomers (**C2**, **C3**), by adjusting the pH value, temperature and time.

The successful syntheses of the three dinuclear Rh(III) half-sandwich complexes (**C1**, **C2**, **C3**) were validated by NMR spectroscopy, elemental analysis and HRESI-MS. The single crystal structures are determined by single crystal X-ray diffraction.

The two isomeric rhodium complexes demonstrate the high flexibility of the macrocycle **H6LMe(PF6)4** in combination with transition metals. This new structural class of chalice-shaped complexes provides insights into the possibilities of structural adaptability of the macrocycle calix[4]imidazolium[2]pyrazole controlled by the reactants and the general synthesis conditions.

References

[1] S. Guan, T. Pickl, C. Jandl, L. Schuchmann, X. Zhou, P. J. Altmann, A. Pöthig, *Org. Chem. Front.*, **2021**, *8*, 4061.

[2] T. Pickl, A. Pöthig, *Organometallics* **2021**, *40*, 3056-3065.

[3] P. J. Altmann, A. Pöthig, *Chem. Commun.* **2016**, *52*, 9089.

Fig. 1

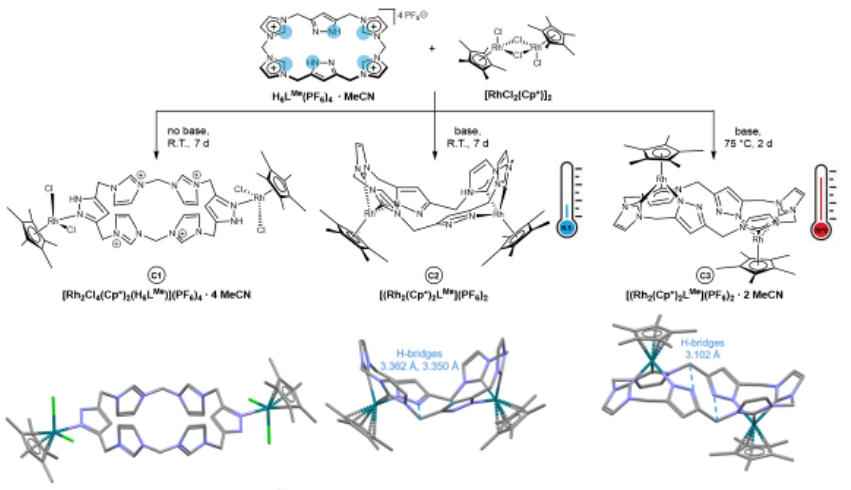

Figure 1: Reaction overview for the complexes **C1** - **C3** from the ligand $H_6L^{Me}(PF_6)_4$ and the Rh-precursor **[RhCl2(Cp*)]2**. Crystal structure of **C1** (left), **C2** (middle), **C3** (right). Hydrogen atoms are omitted for clarity.

PP-33

Beyond simple octahedral layers of Ruddlesden-Popper (RP) and Dion-Jacobson (DJ) phases: New mixed Ag^{+}/Bi^{3+} bromido metalates with organic ammonium cations

C. Schweinle (Freiburg i. Br./DE), M. Ade (Freiburg i. Br./DE), M. Daub (Freiburg i. Br./DE), C. Röhr (Freiburg i. Br./DE)

Based on our work on the crystal growth of the new X-ray detector material $Cs_2AgBrBi_6$ [1] we investigated the crystal chemistry of derivatives of this *cubic* double perowskite with bulky org. amines as counter cations. In an adapted synthetic protocol (i.e. half-conc. HBr, Bi_2O_3 and AgBr) substituting Cs by cations with a flexible org. ammonium function yielded a large number of RP/DJ-type salts [2]. These contain K_2NiF_4-analog layers $[AgBiBr_8]^{4-}$ of corner-sharing $[BiBr_6]$ and distorted $[AgBr_6]$ octahedra, CN(Ag) = 2+4. Herein the ammonium function nicely fits the voids inbetween the octahedra and stabilizes the anion via Br–H–N hydrogen bonds [3]. In contrast, cations with less flexible ammonium groups, e.g. protonated N-heterocyclic amines, form salts with more diverse Ag/Bi bromido anions.

With piperidine (Fig. 1c), we obtained $(H–Pip)_2[AgBiBr_6]$ (**I**), whose structure ($P2_1/c$, a = 735.5(3), b = 783.5(2), c = 1853.7(6) pm, β = 91.010(13)°; R_1 = 0.0236) is derived from that of *hexagonal* perovskites: Columns of face-sharing $[AgBr_{6/2}]$ and $[BiBr_{6/2}]$ octahedra are separated by the bulky piperidinium cations. The slight disorder of the Ag^+ ions also indicates a reduced coordination number, CN(Ag) = 2+(2+2); Fig. 1 b).

The variably protonatable 2,6-dimethylpyrazine (DMP) (Fig. 1f) yielded the mixed salt $(H–2,6–DMP)_2(H_2–2,6–DMP)_2[Ag_2Bi_4Br_{20}]·4H_2O$ (**II**, $P2_1/c$, a = 1557.5(5), b = 1001.5(3), c = 2340.3(10) pm, β = 119.449(11)°; R_1=0.0150), which contains novel flat hexamers $[Ag_2Bi_4Br_{20}]^{6-}$ embedded between the planar aromatic cations (Fig. 1d).

Fig. 1: Crystal structure of **I** / **II**. a/d: polyhedra representation of the unit cell; b/e: details of the polyanion, with selected bond lengths; c/f: organic amine with possible proton positions.

Reference

[1] V. Murgulov, C. Schweinle, M. Daub et al., *J Mater Sci* **2022**, *57*, 2758–2774. [2] H. A. Evans, L. Mao, R. Seshadri, A. K. Cheetham Annu. *Rev. Mater. Res.* **2021**, *51*, 1–33. [3] C. Schweinle, *Dissertation*, Freiburg im Breisgau **2025**.

Fig. 1

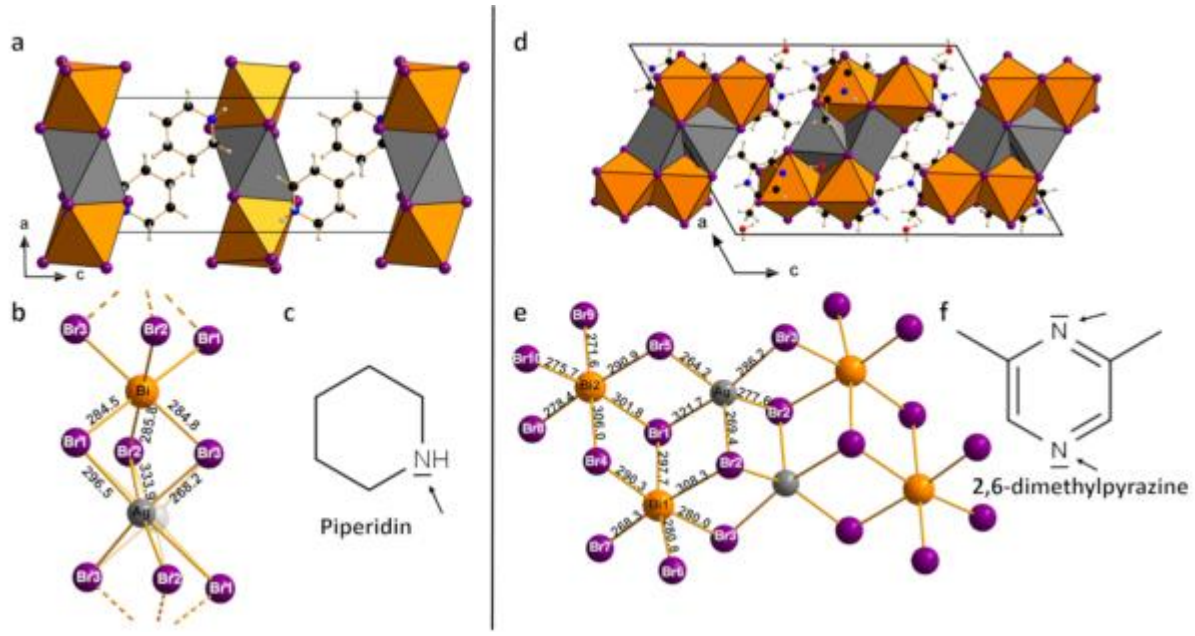

PP-34

Crystal structure, Hirshfeld surface analysis and three-dimensional frameworks and molecular docking studies: Derivatives of Norephedrine ; Part (I)

E. Şahin (Erzurum/TR), E. N. Ozkan (Erzurum/TR), Ö. Gundoğdu Aytaç (Erzurum/TR)

Generally acting on the central nervous system, caffeine and nicotine are among the most commonly used stimulants in the world (Johnson *et. al*. 2010). Stimulants are also used for medical purposes in the treatment of children with attention deficit and hyperactivity disorder (Santosh and Taylor 2000). The most common examples of stimulants of this type are amphetamine class substances. The active ingredient of commercially available drugs such as Dexedrine, Elvanse and Adderall in the treatment of attention deficit hyperactivity disorder is amphetamine (Dolder *et. al*. 2017). However, substances with stimulant effects also have undesirable side effects, both physically and psychologically. Amphetamine is used as an appetite suppressant in the treatment of various diseases such as asthma and narcolepsy (sleeping sickness), attention deficit and hyperactivity disorder, as well as in nutrition and weight control (Kramer 1969).

In this study, we synthesized new compounds that have drug potential Schiff bases (**15**-**18**), which are derivatives of Norephedrine. The structural description of Schiff bases (**16** and **17**) were confirmed by single crystal X-ray analysis. The relationships between molecules in the crystal structure were determined using Hirshfeld surface analysis (fingerprint maps by examining intramolecular and intermolecular interactions in the crystal). Furthermore, the affinity of ligands for dopamine receptors was determined using molecular docking.

Key words: Norephedrine, Schiff bases Single Crystal XRD, Hirshfeld surface analysis, Molecular Docking

References

[1] Dolder PC, Strajhar P, Vizeli P, Hammann F, Odermatt A, Liechti ME. Front Pharmacol. 2017 Sep 7; 8:617. doi: 10.3389/fphar.2017.00617. PMID: 28936175; PMCID: PMC5594082.

[2] Johnson, MW., Strain EC., and Griffiths RR., 2010. Experimental and Clinical Psychopharmacology. Vol. 18, No. 4, 305–31

[3] Kramer, J.C. (1969). Introduction to amphetamine abuse. J. Psychedelic Drugs 2 (2): 8

[4] Santosh, P.J. and Taylor, E. (2000). Stimulant drugs. Eur. Child Adolesc. Psychiatry 9: S27.

Fig. 1

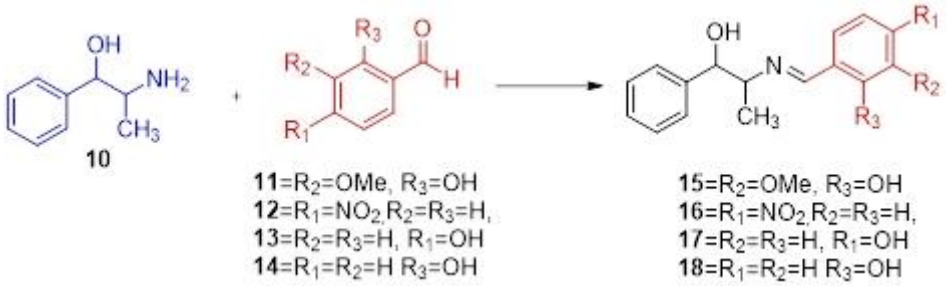

PP-35

Novel zwitterionic molecular structure of a barbiturate salt and DFT study (nnp-143)

A. Mahmoodi (Urmia/IR), E. Nemati-Kande (Urmia/IR), T. Tunç (Aksaray/TR), E. Şahin (Erzurum/TR), N. N. Pesyan (Orumiyeh/IR)

Barbituric acids and its derivatives are important compound from pharmaceutical and medicinal point of view [1]. These compounds e.g. pentobarbital is a short acting barbiturate has been used as hypnotic and epileptic drugs [2]. For example; phenobarbital (PB) is one of the known oldest antiseizure drugs, which is in clinical use since 1912 [3]. The sodium salt of pentobarbital is a short acting barbiturate is used as anticonvulsant drug [3]. Barbiturates include a broad family of central nervous system depressants derived from barbituric acid. They are used in the induction of general sedation, anesthesia and antiepileptic behaviour. Barbiturates act as allosteric modulators of γ-aminobutyric acid (GABA) channels, and they increase the passage of chlorine ions in these channels causing depression of neuronal activity and inhibition of actin potential . They are used in the induction of general sedation, anesthesia and antiepileptic behaviour. İn this study, A novel molecular structure of triethylammonium 5-bromo-2,4,6-trioxohexahydropyrimidin-5-ide (4aa") was obtained in the one-pot reaction of barbituric acid (BA) with cyanogen bromide (BrCN) and trimethylamine (TEA) in methanoland/or ethanol. The structure was characterized by FT IR, 1H, 13C NMR and X-ray crystallography techniques. 4aa" was solved and refined in the monoclinic space group P21/n.

Fig. 1: (a)H-bond geometry and (b) stacking motif of the ionic molecule 4aa" with the unit cell viewed down along the a-axis.

References

[1] M. Nematbakhsh, M. Abdollahi, Encyclopedia of Toxicology (Fourth Edition), Elsevier, 2024, 7, 331-337.

[2] P. S. García, M. K. Whalin, P. S. Sebel, Pharmacology and Physiology for Anesthesia Foundations and Clinical Application (Second Edition), Ed.: H. C. Hemmings, Jr., T. D. Egan, Chapt. 10, Elsevier, 2019, Pages 193-216.

[3] E. Trinka, Phenobarbital in Status epilepticus–Rediscovery of an effective drug. Epilepsy & Behavior, 2023, 141, 109104.

Fig. 1

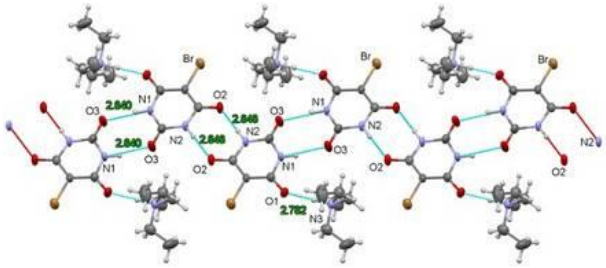

Fig. 2

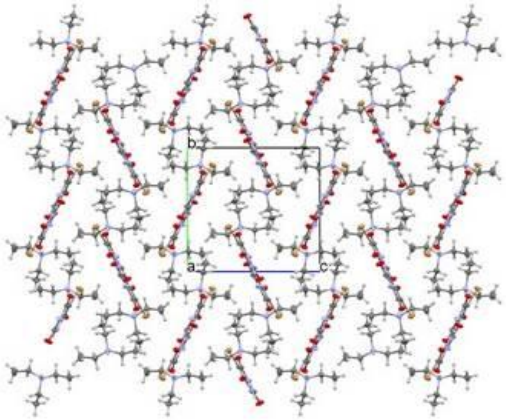

PP-36

Two novel Cu/Ce complexes: crystal structures and their properties

A. Koščíková (Košice/SK), M. Tomás (Zaragoza/ES), I. Ara (Zaragoza/ES), L. R. Falvello (Zaragoza/ES), J. Černák (Košice/SK)

Studies of the magnetic behaviour of molecular compounds including Single Molecule Magnets have generated increasing interest in recent years [1]. The bimetallic complexes are promising, because they combine the magnetic properties of both central atoms. For their preparation, the Schiff base type ligands are favoured thanks to their ability to form cavities with different sizes. The main objective of the present work was to prepare new Cu/Ce complexes with different halogenides and to compare their structures and properties. The method of horizontal diffusion [2] was used for the reaction of the [Cu(*o-van-en*)] metalloligand with $CeCl_3{\cdot}7H_2O$ or $CeBr_3{\cdot}xH_2O$ in ethanol. The syntheses afforded two new complexes - [Cu(H_2O)(*o-van-en*)$CeCl_3$(H_2O)] (**1**) and [Cu(*o-van-en*)Ce(H_2O)$_5$][Cu(*o-van-en*)Ce(H_2O)$_4$(EtOH)]$Br_6{\cdot}3H_2O$ (**2**). The X-ray data collection was done on a Bruker D8 VENTURE diffractometer. The products were characterized by IR spectroscopy, elemental analysis and by X-ray powder diffraction. The preparation method was similar to the one previously used for the [CuCl(*o-van-en*)LnCl(H_2O)$_3$]Cl·CH_3CH_2OH (Ln = Eu, Sm, Gd) [3], however the arrangement of ligands, corresponding anions and solvating molecules differ. The structure of **1** is molecular and Cu(II) atom creates tetragonal pyramid shape (donor set is N_2O_3) with the aqua ligand in the apical position. The Ce(III) atom exhibit coordination number 8 with donor set O_5Cl_3. On the other hand, the structure of **2** is ionic with two complex cations, six bromide anions and three solvate water molecules. Both Cu(II) atoms exhibit square coordination, while one Ce(III) atom is coordinated by four O-donor atoms from the (*o-van-en*)$^{2-}$ ligand and five aqua ligands. In the second Ce(III) atom one aqua ligand is replaced by an ethanol molecule.

References

[1] Costes J. P. et al., *Inorg. Chem.,* **2000**, 39, 165-168.

[2] Šterbinská S. et al., *Cryst. Growth Des*., **2023**, 23, 4357-4369.

[3] Koščíková A. et al., *Chem. Eur. J*., **2025**, 31, e202500376.

PP-89

"Hexagonal" Perovskites: From Stacking Sequence to Space Group Symmetry and New Opportunities

S. L. Kunz, M. Haefner, O. Clemens (Stuttgart/DE)

The term "hexagonal perovskite" has been widely used in literature to discuss the structure of perovskite-type compounds with composition ABX(3-y) with partial h-type stacking of AX(3) layers. Though the local surrounding of these AX 3 layers resembles a hexagonal close packing, the space group symmetries reported for some of these materials are not belonging to the hexagonal crystal system but are trigonal or orthorhombic instead. Though reports and books with lists of hexagonal perovskites exist which assign stacking sequences and list a corresponding space group, a concise guideline on how the maximum symmetry of the perovskite type material is related to the stacking sequence has not been reported. Clearly, such a systematization of space group symmetry and stacking notations would be desirable; for distortion or ordering variants of the cubic perovskite, the whole research community benefits from concepts of group-subgroup relations or classification of tilting via the Glazer notation. In this article, we derive a fully consistent guideline on how the aristotype space group symmetry can be determined for any stacking sequence (e.g., cchhchcch, ...) in the Jagodzinski notation and provide a computer program which can do this analysis. By this, one can narrow down the possible aristotype space group symmetries for any perovskite stacking sequence with h-type layers to seven space groups in total (R3m, P3m, P63/mmc, P6m2, R3m, P3m, and P6(3) mc). The space groups can be directly derived from the Jagodzinski sequence. Remarkably, the possibility to obtain polar perovskites with h-type layers by stacking has not been recognized in literature so far and provides the opportunity to develop new multiferroic materials by design of stacking.

References

[1] Chemistry of Materials 2024 Vol. 36 Issue 23 Pages 11341-11358

[2] Accession Number: WOS:001317083300001 DOI: 10.1021/acs.chemmater.4c01789

PP-90

Synthesis and Structural Characterisation of An Elusive, Organometallic Gallium Monofluoride Complex via Single-Crystal-Based Reactivity

J. Stephan, R. A. Fischer (Garching/DE)

In contrast to indium and thallium, the monohalides (EX) of boron, aluminium and gallium represent elusive gas-phase species, unstable at both room temperature and ambient conditions.[1] Despite their exotic nature, their potential for small molecules has already been recognised early on.[2] Although EX species are isolable as cryogenic, metastable solutions, their characterisation in the solid state still remains a "missing link".[3]

In this contribution, we present the first example of a complex, [(Cp*Ga)4Ni(GaF(NCtBu)2)](BArF24)2 (1), containing a gallium monofluoride moiety, that is stable at room temperature.[4] The GaF unit itself derives from C–F bond activation of a fluorinated, weakly coordinating anion at room temperature. The entire reaction cascade is largely based on the reactivity of single-crystalline compounds. Starting from a simple nickel(II) nitrile complex with weakly coordinating anions, the reaction is initiated by the addition of the gallium(I) compound GaCp* (Fig. *1*). This leads to the mixed GaCp*/nitrile-ligated [(Cp*Ga)4Ni(NCtBu)](BArF24)2 (2) as the key intermediate. Single-crystalline 2 slowly interconverts in fluorobenzene suspension to 1 over several weeks. Both structures show a variety of intramolecular interactions, like non-classical hydrogen bonding between protons and fluorinated residues.

References

[1] A. Haupt, in Organic and Inorganic Fluorine Chemistry - Methods and Applications, Walter de Gruyter GmbH, Berlin/Boston, 2021, pp. 64-65.

[2] P. L. Timms, Acc. Chem. Res. 1973, 6, 118-123.

[3] C. Dohmeier, D. Loos, H. Schnöckel, Angew. Chem., Int. Ed. Engl. 1996, 35, 129-149.

[4] J. Stephan, L. Gremmel, S. Kahlal, J.-Y. Saillard, C. Gemel, R. A. Fischer, manuscript in preparation

Fig. 1. Reaction sequence with the gallium monofluoride complex [(Cp*Ga)4Ni(GaF(NCtBu)2)](BArF24)2 (1) as the final product.

Fig. 1

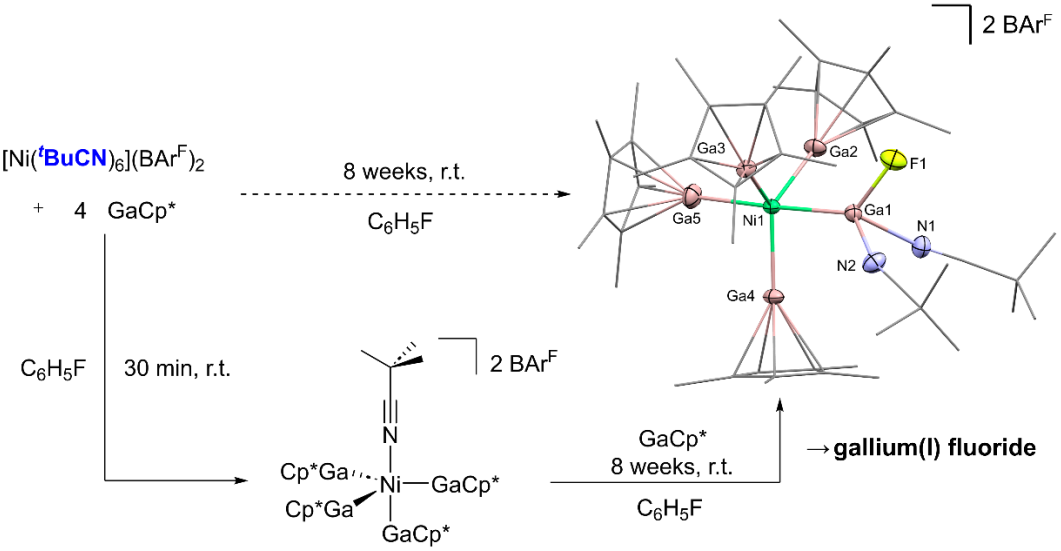

PP-93

U³ Unveiling the Unseen and Undetectable: Automated Electron Diffraction and its growing role in solid state characterization

G. Santiso-Quinones, C. Jandl, A. Berger, D. Braun (Allschwil/CH)

Following its Science Breakthrough of the Year nomination in 2018,1 electron diffraction (3D ED / MicroED, here referred to as ED) has emerged as a transformative method for solid-state characterization in both research and industry.2 ED addresses many of the same application areas as X-ray powder diffraction (XRPD) and single-crystal X-ray diffraction (SC-XRD), while offering a key advantage: the ability to determine structures from nanometer-sized crystals within minutes. The rapid growth3 in structures solved by ED is driven in part by the availability of dedicated commercial instrumentation, such as the ELDICO ED-1.4 Its instrument design and expanded sample environment enable automation, making ED increasingly accessible to non-specialist users.

This poster presents the discovery of a previously unknown polymorphic form of dapsone using automated ED. Although dapsone has been known for over a century and five polymorphic forms have been reported to date, analysis of a commercial sample by automated ED revealed a sixth polymorph. This form was not predicted by prior crystal structure prediction (CSP) studies, which were limited to Z′ = 1 and 2. Following its experimental identification by ED, CSP was subsequently able to locate this structure within the computed energy landscape, and its existence was independently confirmed by complementary experimental techniques after isolation via slurry experiments. 5 Overall, the poster highlights the power of automated ED workflows for unveiling the unseen and undetectable in solid-state chemistry.

Fig. 1

Automatic ED finds a NEW polymorph in a 100-year-old drug compound.

References

[1] T. Grüne, et. al., Angew. Chem. Int. Ed. 2018, 57, 16313-16317.
https://vis.sciencemag.org/breakthrough2018/finalists/#rapid-structure

[2] T. Grüne, E. Mugnaioli. Chem. Rev. 2021, 121, 11823-11834.

[3] CCDC, April-2025: number of published structures ~ 600. Exponential increase since 2018.
The total number, end 2025, should be close to ≥ 700.

[4] P. Simoncic, et. al., Acta Cryst., 2023, E79, 410-422.

[5] G. Santiso-Q, D. Stam, D. Braun. Manuscript submitted for publication.

Poster Session 1: Frontier molecular crystallography and supramolecular and framework structures

PP-37

Advanced crystallisation methods for SC-XRD

N. Nöthling (Mülheim an der Ruhr/DE), M. Turberg (Mülheim an der Ruhr/DE)

Single-crystal X-ray diffraction (SC-XRD) is a key technique in structural chemistry, enabling precise determination of atomic connectivity, molecular geometry, inter-/intramolecular interactions, absolute configurations, and charge densities. However, it requires high-quality crystals, and crystallisation often poses the main challenge. Alongside conventional solvent-based methods for small molecules, we report experiences with advanced crystal-growth techniques. Two such methods use pure melt crystallisation. Using a hot stage microscope, various small organic molecules have been crystallised; adding microcrystalline powders to the melt can trigger homogeneous nucleation, yielding high-quality single crystals [1]. The capillary method cools liquid compounds below melting point, then converts polycrystalline powders into large single crystals via zone melting. It applies to diverse substances, allows absolute configuration determination, and is suitable for air-sensitive compounds [2–4]. Other methods employ inclusion crystallisation, such as crystalline sponge, chaperone, and crystal mate techniques. Using crystalline sponges, we determined the structure and absolute configuration of a chiral silyl ether, though disorder and low occupancy caused diffuse electron density [5]. The chaperone method proved more effective, offering ease of use and high occupancy [6]. The crystal mate approach mixes functionalised coin-metal pyrazolates with analytes, forming stable phases via π-acidic interactions with metal centres, producing high-quality crystals [7]. Ongoing developments will make many previously inaccessible crystal structures achievable.

References

[1] Zimmer, A., Fürstner, A. *Chemistry Europe* **2024**, 2, e202400064.

[2] Bodach, A. et al., *Eur. J. Inorg. Chem.* **2021**.

[3] Luo, N. et al., *Nature* **2024**.

[4] Zheng, T. et al., *Science* **2024**.

[5] Zhou, H. et al., *J. Am. Chem. Soc.* **2022**.

[6] Berking, T. et al., *Angew. Chem. Int. Ed.* **2024**.

[7] Song, J. G. et al., *Chem* **2024**.

PP-38

Crystallography in Synergy: Updates on Rigaku Single-Crystal Instrumentation

C. J. Schürmann (Neu-Isenburg/DE), K. N. Truong (Neu-Isenburg/DE), J. Wojciechowski (Neu-Isenburg/DE), E. Buchsteiner (Neu-Isenburg/DE), F. White (Neu-Isenburg/DE)

Modern diffractometers are required to meet the ever-increasing demands of crystallographers who continue to expand the frontiers of structural science. Central to this progress is the development of advanced X-ray sources, which are critical to enhancing the performance and versatility of diffractometers across a wide range of research applications. The brightness and stability of an X-ray source often determine the success of a diffraction experiment by improving data quality, extending the diffraction limit, and reducing measurement time.

To meet these evolving challenges, Rigaku is dedicated to advancing in-house crystallography through the integration of high-brilliance radiation sources, state-of-the-art hybrid pixel detectors, and high-speed goniometers, all seamlessly controlled within the CrysAlisPro software environment. Among these components, rotating anode X-ray sources have emerged as a cornerstone technology, providing exceptional brightness, reliability, and efficiency for modern crystallographic laboratories.

This work presents an overview of Rigaku"s latest generation of single-crystal diffraction instrumentation, supported by experimental data that demonstrate substantial improvements in intensity, precision, and overall system performance. Special emphasis is placed on recent developments in rotating anode technology and its role in driving the next phase of synergy between source, detector, and software innovations in single-crystal crystallography.

Fig. 1

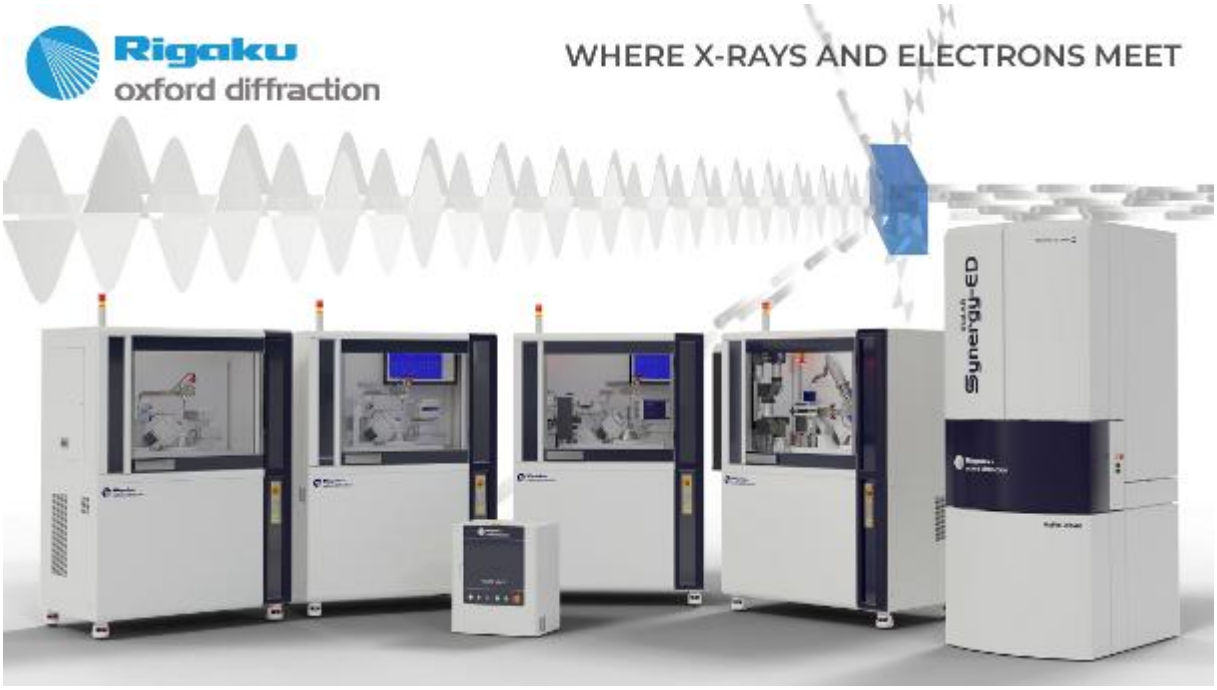

PP-39

The molecular und crystal structure of Durene: X-ray diffraction using a non-spherical approach and quantum chemical investigations of its weak intermolecular interactions

G. J. Reiss (Düsseldorf/DE), I. S. Konovalova (Düsseldorf/DE, Kharkiv/UA)

Durene is a basic chemical compound firstly reported in the 19th century [1]. The structure of Durene was one of the first organic crystal structures, which are reported in the 1930s, and classified early on with the *Strukturberichte* designation Type $O5_{10}$ [1,2], as part of an attempt to classify basic organic structures. To date, only one single crystalline polymorph of Durene has been reported. The crystal structure of Durene has been determined multiple times, and also the packing and its implications for the molecular geometry were discussed in the 1970s [3].

To analyze the intermolecular interactions in detail, we applied quantum chemical methods to identify the key forces connecting the molecules. The experimental structural model was obtained from non-sperical refinement of newly collected single crystal data. As shown in the right part of the figure, the most energetically significant interactions are C-H-π contacts, which link molecules into columns. These columns are further connected to neighboring ones, forming a layered structure. The packing scheme of solid Durene, as an archetype, is comparable to that of its derivative 1,4-bis(halogenomethyl)-2,5-dimethylbenzene (halogen = Cl, Br) [4]. In the second step, we analyzed the impact of intramolecular interactions on molecular geometry of Durene by comparing the experimental values with those obtained from quantum chemical calculations in the gas phase.

Fig. Left: Structure of durene based on X-ray diffraction data. Right: Columns of Durene molecules connected via C-H-π interactions.

References

[1] R. Fittig, Nachrichten von der Königl. Gesellschaft der Wissenschaften und der Georg-Augusts-Universität zu Göttingen, 1870, p. 66-70;

[2] Strukturberichte: *Suppl. of Z. Kristallogr.* (Eds.: P. P. Ewald and C. Herrmann), 1936, p. 863;

[3] E. S. Abovyan, R. M. Alyasnikova, A. I. Kitaigorodskii, *Zh.Strukt. Khim.* 1977, 18, 998; 4. J. Zhou, X. Zhang. *Z Kristallogr. - N. Cryst. Struct.*

doi.org/10.1515/ncrs-2025-0373

Fig. 1

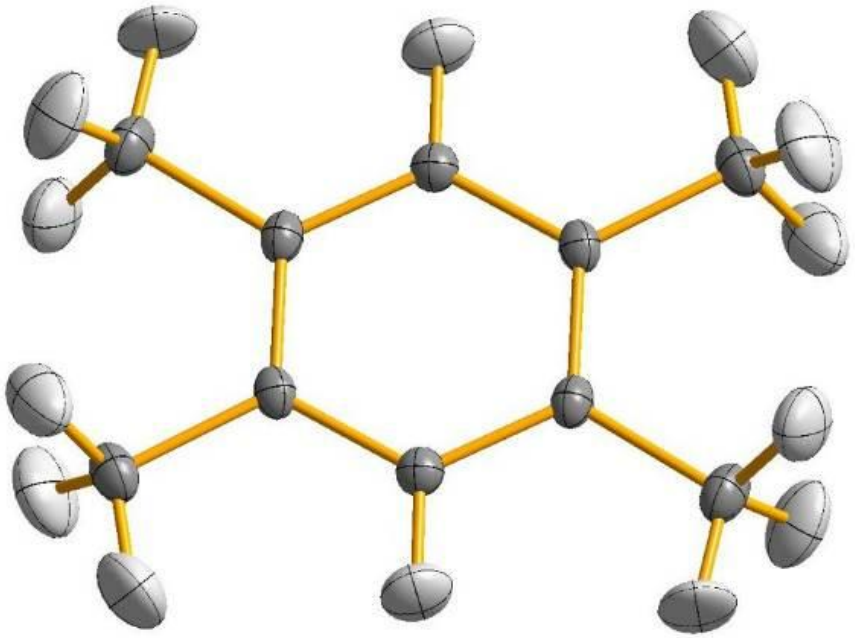

Fig. 2

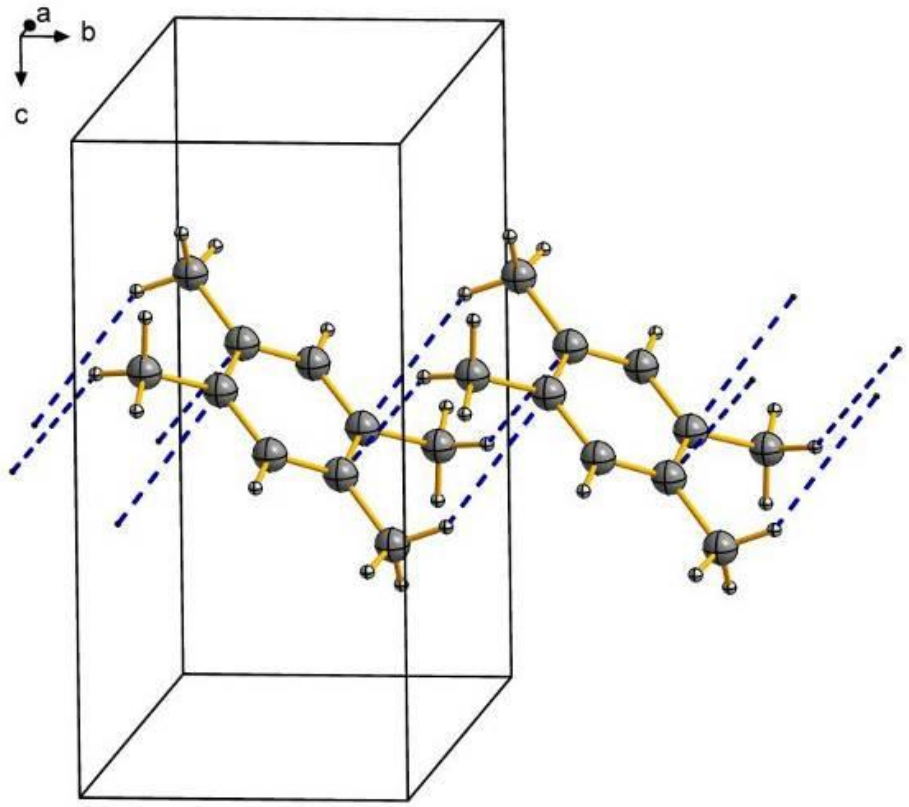

PP-40

Maximized Efficiency in MOF/COF Structure Analysis

C. Wolf (Karlsruhe/DE), T. Stürzer (Karlsruhe/DE), A. Lübben (Karlsruhe/DE), T. Dunaj (Karlsruhe/DE)

Metal-organic frameworks (MOFs) and covalent organic frameworks (COFS) have garnered significant attention since the early 2000s due to their exceptional porosity, modularity, and potential in applications such as gas storage, catalysis, sensing, separation, and electrochemical energy conversion. Their typically crystalline nature makes them candidates for single-crystal X-ray diffraction (SC-XRD), which provides essential structural insights into pore architecture, framework flexibility, and host–guest interactions. However, the structural elucidation of MOF/COFs is often hindered by intrinsic crystallographic challenges such as poor crystallization, presence of disordered, pore occupying solvents or unfavorable self-assembly of metal centers and linkers.

Advanced X-ray instrumentation can help to overcome these limitations. For example, the IμS DIAMOND II microfocus source delivers a highly focused, high-brilliance beam maximizing intensity on small or weakly diffracting crystal. The source features a patented Hybrid Diamond Anode technology and combines extraordinarily high uptime with a maintenance-free alignment. Paired with the PHOTON IV detector, researchers can capture strong and weak reflections with high dynamic range and excellent signal-to-noise ratios. Together, this hardware enables the collection of high-quality, high-multiplicity data even from challenging MOF/COF samples, significantly improving structural resolution and reliability.

High-quality data should be supported by robust, user-friendly software. Features such as an intuitive graphical user interface, advanced automation, and dependable computational engines empower researchers to efficiently address even the most complex questions.

By presenting selected sample cases, we will illustrate how state-of-the-art hardware and software help scientists maximize their efficiency in this dynamic area of research.

PP-41

Pillarplex SOCs: Rim-Functionalizations as Achor Points for Further Tailored Modifications

J. Preinl (Garching/DE)

Research in the field of *supramolecular coordination complexes* (SCCs) and *supramolecular organometallic complexes* (SOCs) has emerged as one of the most dynamic branches of modern chemistry,[1] particularly fueled by pioneering work published by M. Fujita,[2,3] P. J. Stang,[4] and K. N. Raymond.[5] The success of supramolecular coordination chemistry can be attributed primarily to the well-defined molecular design and modular architecture of the self-assembling aggregates. These structural characteristics allow, among other things, for the combination of different functionalities as well as stimuli-responsive behavior.[1]

A subclass of such SOCs is given by the so-called pillarplexes [M8L2]X4 (X = OAc, OTf, PF6), introduced by our group in 2016. These complexes can be described as tubular aggregates made from two macrocyclic ligands (**L**, Figure 1) sandwiching an "equatorial ring" of eight metal ions (M = Au, Ag) by means of an alternating coordination motif that comprises pyrazole and imidazole entities (heteroleptic coordination mode).[6] To expand the structural variability of L (i.e., structural change in the rim as well as modified interactions between counterions and the cationic complex) and to create additional coordination sites, enabling extended interactions beyond the limits of a structurally closed pillarplex entity, the pyrazole units were initially substituted with triazole entities (A, Figure 1).[7] In a next attempt, the pyrazoles" 4-positions were functionalized via bromination (B).[8] This modification paved the way for our most recent effort in regard of creating structurally more diverse pillarplexes. For the first time, a rim-functionalized pillarplex (Figure 2) was successfully synthesized through Suzuki cross-coupling utilizing an ethyl benzoate derivative as coupling partner (**C**).[9] The molecular structures of both this complex and the corresponding macrocycle, as well as their respective solid-state packings, are discussed.

Fig. 1

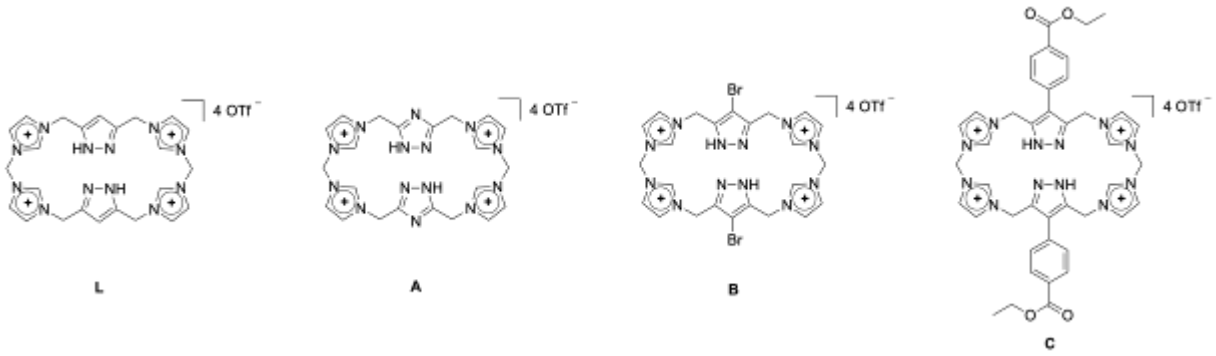

Fig. 2

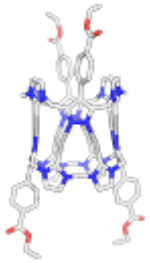

PP-42

Empirical electronic polarizabilities of iodine (I^-) and bromine (Br^-, Br^{7+}) for the prediction of refractive indices

S. Nezamabadi (Bremen/DE), R. X. Fischer (Bremen/DE)

Empirical electronic polarizabilities of I^-, Br^-, and Br^{7+} were determined to predict refractive indices of iodides, bromides, and perbromates at λ = 589.3 nm. Polarizabilities of the I and Br ions were derived from the total electronic polarizabilities of I or Br bearing compounds by subtracting the polarizabilities of the remaining ions yielding the contribution of the halogen ions to the total electronic polarizabilities calculated from the mean refractive indices. The anion polarizability parameters $\alpha\_^\circ$ and N_0 (in the equation $\alpha\_ = \alpha\_^\circ \cdot 10^{-N_0/V_{an}^{1.20}}$ Shannon & Fischer, 2016) for I^- and Br^- were determined by least-squares methods from compounds with known refractive indices, plus data from this study. Fig. 1a shows halogen anion polarizabilities versus the anion volume, and Fig. 1b shows their relationship to the cube of the ionic radii.

Fig. 1: a) Comparison of the anion polarizabilities for I^-, Br^-, Cl^-, and F^- versus the anion volume. b) The relationship between the cube of the ionic radii (Shannon, 1976) and polarizabilities for halogens.

Using polarizabilities of I and Br calculated here enable the prediction of refractive indices of minerals and inorganic compounds as shown in Fig. 2 where the resulting values are compared with the corresponding values calculated from the Gladstone-Dale approach according to Mandarino (1976).

Fig. 2: Predicted mean refractive indices of I (upper) and Br (lower) bearing compounds using the polarizability approach versus the Gladstone-Dale method.

Mandarino, J.A. (1976) The Gladstone-Dale relationship, Part I, Derivation of new constants, Can. Mineral, 14, 498-502

Shannon, R. D. (1976) Revised effective ionic radii and systematic studies of interatomic distances in halides and chalcogenides, Acta. Crystallogr, A32, 751-761

Shannon, R.D., Fischer, R.X. (2016) Empirical electronic polarizabilities of ions for the prediction and interpretation of refractive indices: oxides and oxysalts, Am. Mineral, 101, 2288-2300

Fig. 1

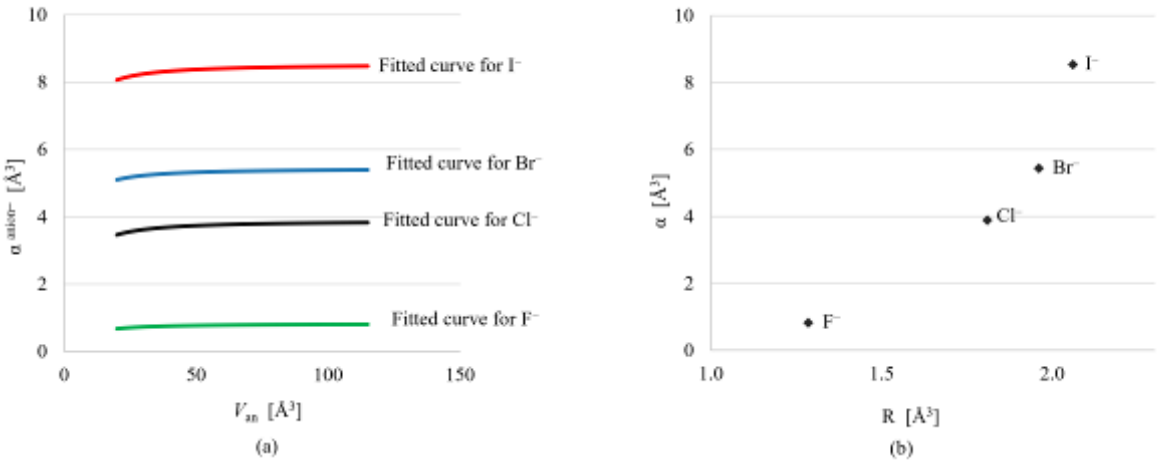

Fig. 2

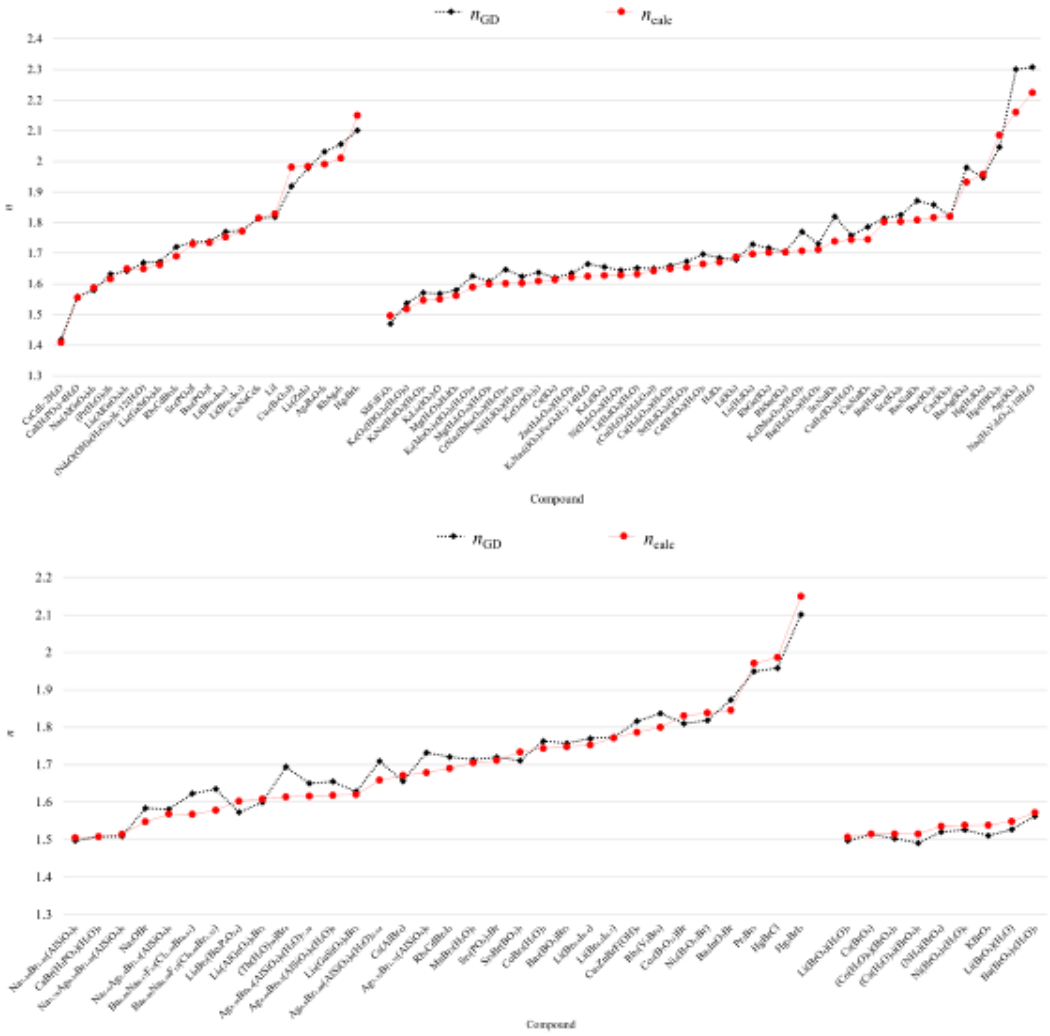

PP-43

High-pressure polymorphism in SnI_4

K. Fuchizaki (Matsuyama/JP), A. Suzuki (Sendai/JP), I. Rietveld (Rouen/FR)

SnI_4 has been known to exhibit pressure-induced solid-state amorphization (SSA) at approximately 15 GPa during room-temperature compression of the crystalline phase, CP-I, which is stable at ambient conditions, using a diamond anvil cell (DAC) [1]. Although another high-pressure modification, CP-II, has been known in the pressure region of SSA [2], no relationship between Am-I and CP-II has yet been established. The present project has begun addressing this issue by using in situ synchrotron X-ray diffraction measurements. However, multianvil apparatus compression, with better hydrostatic conditions than in the DAC, did not induce SSA. Instead of amorphization, we encountered a brand-new crystalline state, which we named "unknown," as reported in DGK 2025 [3]. The discovery of the "unknown," which we name CP-II' here, prompted a detailed re-examination of the diffraction patterns in the pressure region where SSA was initiated during DAC compression. To our surprise, a new crystalline phase, CP-IV, whose diffraction pattern is close to that of CP-II, exists at high temperatures. The slope of its melting curve is not deviated from CP-II's melting curve slope. Interestingly, a new metastable state, CP-IV', with a structure similar to CP-II', is associated with CP-IV. It is this CP-IV' that could be directly involved in amorphization. The boundaries between CP-II and CP-II' and CP-IV and CP-IV' are located at about 850 K independent of pressure, implying that they cross the boundary between CP-II and CP-IV. Because this situation is outside the phase rule, we speculate that SnI_4 is no longer a single component above the SSA pressure.

References

[1] Y. Fujii et al., J. Phys. C **18**, 789 (1985).

[2] M. Riggleman and H. G. Drickamer, J. Chem. Phys. **38**, 2721 (1963).

[3] K. Fuchizaki et al., High Press. Res. **45**, 90 (2025).

PP-44

Elastic and piezoelectric properties of $Bi_{12}GeO_{20}$ and $Bi_{12}TiO_{20}$ at high temperatures

D. Werner (Frankfurt a. M./DE), E. Haussühl (Frankfurt a. M./DE), B. Winkler (Frankfurt a. M./DE)

Materials with composition $Bi_{12}MO_{20}$ (M= Si, Ti and Ge) (BSO, BTO and BGO) crystallize in the sillenite structure type with space group *I*23 [1]. They have outstanding electrical and optical properties such as strong photoconductivity and a narrow bandgap [1-4]. Bismuth based materials are of interest due to their low toxicity and minimal environmental impact [3]. Potential applications include optical information processing, actuators, capacitors, dielectric materials, and photorefractive materials. [1-4]. In addition, BGO is a promising material for high-temperature piezoelectric applications and sensors. A thorough understanding of its elastic, thermoelastic and piezoelectric behavior over a broad temperature range is essential for developing and refining such applications. In previous studies the elastic and piezoelectric properties of BSO were determined in the temperature range of 100-773 K [5] and those of BTO in the range of 293-773 K [6]. The elastic and piezoelectric properties of BGO have only been measured at RT [7].

Resonance ultrasound spectroscopy (RUS) is one of the few techniques that enable the determination of piezoelectric properties when the dielectric coefficients of a material are known at high temperatures. Therefore, we performed RUS measurements between 293 K and 1073 K for BTO and between 293 K and 1123 K for BGO. Regions of strong acoustic attenuation were observed in BTO (433–673 K) and in BGO (693–1033 K), which were previously investigated by Haussühl et al. [5].

We acknowledge funding by the DFG (HA5137).

References

[1] Noh, T. H. et al., Ceram. Int., 43, (2017), 12102

[2] Foldvari, I. et al., J. Appl. Phys., 74, (1993), 13217

[3] Ruan, X. et al., Appl. Surf. Sci., 499, (2020), 143668

[4] Altunatas, G. et al., ACS Omega, 10, (2025), 25219

[5] Haussühl, E. et al., Mater. Res. Express, 7, (2020), 025701

[6] Shen, C. et al., Crystals, 4, (2014), 4020141

[7] Slobodnik, A. J. et al., J. Appl. Phys., 43, (1972), 247

PP-45

Coexisting antiferromagnetic phases on the frustrated pyrochlore sublattice of the mixed Jahn-Teller system $Ni_{1-x}Cu_xCr_2O_4$

M. Tovar (Berlin/DE), M. Reehuis (Berlin/DE), B. Klemke (Berlin/DE), D. M. Többens (Berlin/DE), J. U. Hoffmann (Berlin/DE), A. Hoser (Berlin/DE)

The ferri- and antiferromagnetic order in the normal spinel system $Ni_{1-x}Cu_xCr_2O_4$ was investigated using powder neutron and x-ray diffraction, complemented by magnetization measurements, to establish a comprehensive magnetic phase diagram [1–4]. For compositions with x(Cu) < 0.5, ferrimagnetic coupling between Cr and Cu spins occurs at the higher ordering temperature, followed by antiferromagnetic ordering within the Cr sublattice. Particularly noteworthy is the complex antiferromagnetic ordering of Cr ions on the orthorhombically distorted pyrochlore lattice for $0 \le x(Cu) \le 0.12$, where multiple magnetic phases coexist. In the magnetic ground state of $NiCr_2O_4$, two commensurate antiferromagnetic structures with propagation vectors $\boldsymbol{k}_{AF}$ = (0,0,1) and (½,½,½) coexist [2,4]. With increasing Cu content ($0 < x(Cu) \le 0.09$), these phases transform into a commensurate structure with $\boldsymbol{k}$ = 0 via two intermediate incommensurate phases, characterized by $\boldsymbol{k}_{IC1}$ = (0,0,k_z) and $\boldsymbol{k}_{IC2}$ = (0,k_y,k_z). The evolution of these magnetic structures and the associated magnetoelastic effects are discussed in terms of lattice distortions governed by the concentration ratio of the two Jahn–Teller ions at the tetrahedral *A* site, where Ni^{2+} induces elongated and Cu^{2+} compressed tetragonal distortions.

Fig. 1

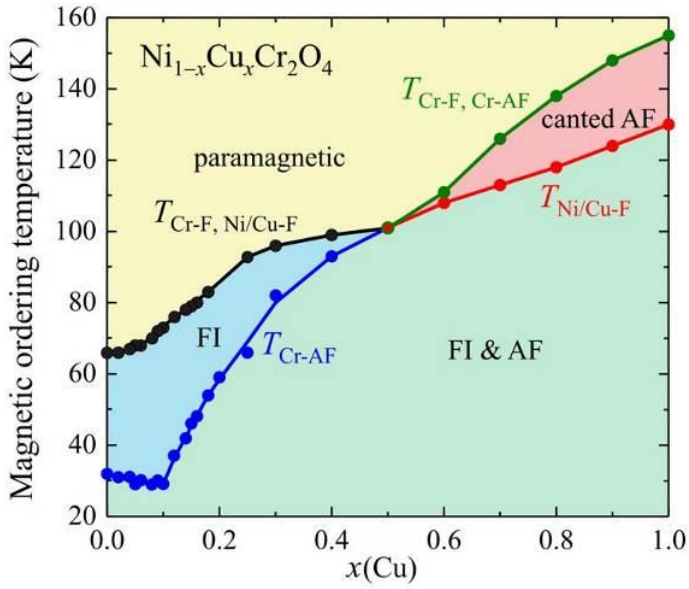

Fig. 2

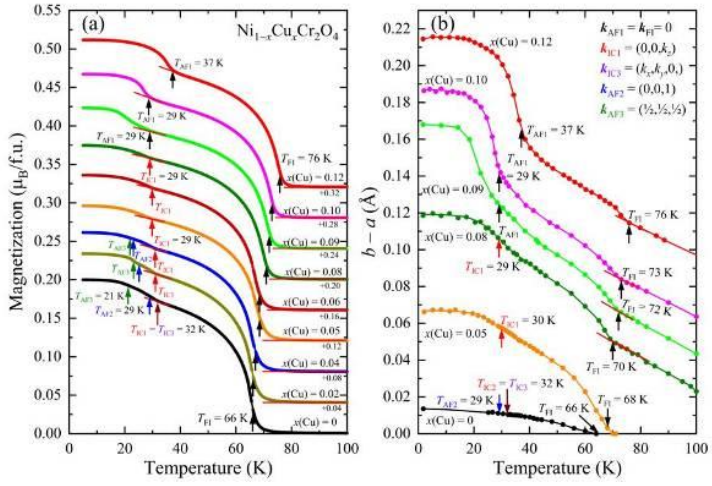

PP-46

High-Temperature Stability and the ~460 K Anomaly in Fresnoite probed by Resonant Ultrasound Spectroscopy and Dilatometry

E. Haussühl (Frankfurt a. M./DE)

Fresnoite ($Ba_2TiSi_2O_8$) is a ferroelectric silicate (space group *P*4*bm*) with moderate piezoelectricity but exceptional thermal stability, making it a benchmark for high-temperature piezoelectrics [1,2]. However, its elastic-electromechanical response near the reported incommensurate transition at about 460 K remains unexplained: pulse-echo measurements revealed anomalies in the elastic compliance coefficients s_{11}, s_{33}, s_{66}, and in the piezoelectric coefficients between ≈ 420–520 K, with inconsistent trends across the coefficients and no information on acoustic losses [3]. The central question, we address, is whether this anomaly is strongly coupled to the elastic tensor and dissipation, and how the elastic and piezoelectric coefficients behave over a very wide temperature range.

Resonant ultrasound spectroscopy (RUS) is ideally suited to address this question because it determines a set of normal modes for a single crystal with high sensitivity to symmetry breaking. From these modes, the complete elastic and piezoelectric tensors, as well as the internal friction, can be derived.

We performed resonant ultrasonic spectroscopy on a stoichiometric fresnoite single crystal [2] at 4.2–1450 K, complemented by high-resolution dilatometry at 100–1473 K. Several resonance modes show pronounced, reversible frequency shifts with a centre at ≈ 440 K, suggesting coupling to an incommensurate order parameter [3], as well as kinks in the thermal expansion curves at around 450 K. Above this temperature, the spectra develop uniformly up to 1450 K without further anomalies.

The authors would like to thank J. Schreuer (Ruhr University Bochum, Germany) for providing the RUSREF computer program and the DFG for financial support (HA 5137).

References

[1] C. Shen et al., J. Appl. Phys. 116 (2014) 044106.

[2] S. Haussühl et al., J. Cryst. Growth 40 (1977) 200–204.

[3] C. Jiang et al., Crystals 9 (2019) 1–12.

PP-47

CO2 sequestration using waste concrete in future building applications: unravelling elemental structural implications

C. Rüscher (Hanover/DE), S. J. Akinbodunse (Hanover/DE), S. Tome (Hanover/DE, Hanover/DE)

The production of portland cement (PC) is responsible for about 8% of the CO2 emission worldwide. Therefore, it is a core purpose to reduce or better avoid the use of PC. However, PC has been produced from the beginning of industrialization and is still used as the most men made material for building constructions world-wide. Therefore, it could be seen as a challenge, that CO2 could actively be re-sequestrated in waste concrete. It is "neustark AG" [1] advertising that at least 10 kg CO2 per ton concrete are save tied. The technology introduced by "neustark AG" is already applied in a number of concrete producing companies. And it seems still worthwhile to use "green cement" for concrete production in addition.

Unravelling elemental structural implications of accelerated re-sequestration requires key crystallographic methods. It is the gel-connectivity of CSH-binders (or more general N-ACSH: N = Na2O, A=Al2O3, C = CaO, S = SiO2, H = H2O), which becomes better and better understood from both sides, i.e. the alkali activation technology with ingredients of slag, fly ash , silica fume, metakaolin [2] and classical PC-technology with the same ingredients, in particular the addition of calcined clay [3]. Both applications reveal the same binder composed of Q1 and Q2 of relatively short Si-O-Si-O-Si Dreierketten type units, but only alkali-activated metakaolin, i.e. avaoiding CaO containing ingradients, forms a Q4 3-D geopolymer network. In any case the re-sequestration of CO2 is restricted to the CaO content in the materials which is observed with the CaCO3 formation (re-carbonation) and SiO2-gel formation. As a "clean model" the re-carbonation of artificial lime sand bricks could be discussed.

Fig. 1

[1] „neustark AG“, 2025: www.neustark.com/de
[2] Sankar, K.; Sutrisno, A.; Kriven, W. M., 2019: Slag-fly ash and slag-metakaolin binders: Part II-Properties of precursors and NMR study of poorly ordered phases. J Am Ceram Soc. 102, 3204-3227.
[3] Scrivener, K.; Martirena, F.; Bishnoi, S.; Maity, S., 2018: Calcined clay limestone cements (LC3). Cem. Concr. Res. 114, 49–56.
[4] Rüscher, C.H.; Lohaus, L.; Jirasit, F.; Tchakoute, H. K.: The effect of gel-type

PP-48

Crystal-chemical factors influencing Eu(II) luminescence in solid-state metal hydrides

H. Kohlmann (Leipzig/DE), A. Nain (Leipzig/DE), L. Millahn (Leipzig/DE), M. Gebauer (Leipzig/DE), L. Schmidt (Leipzig/DE)

Metal hydrides are compelling hosts for activator ions, as they enable tuning of emission wavelengths in luminescent materials. The strong nephelauxetic effect of the hydride ion lowers the barycenter of the d levels and thereby reduces the energy gap from the electronic ground state. However, general rules describing this influence are lacking due to the multitude of variables involved. Alkaline earth metal hydride halogenides MHX (M = Ca, Sr, Ba; X = Cl, Br, I) are particularly suitable for studying the impact of crystal chemical parameters on luminescence properties, as they crystallize isotypically in the tetragonal PbFCl structure type, which is relatively simple. MHX and Eu(II)-doped samples $M_{0.99}Eu_{0.01}HX$ were synthesized through solid-state reactions and structurally characterized by X-ray and neutron powder diffraction, confirming hydrogen atom positions. Refined crystal structure data for all nine compounds enable detailed analysis of crystal chemical trends. Across the series from BaHCl to CaHI, the coordination number of the cations decreases from nine to eight, the structure becomes more layered, and bonding character shifts toward lower ionicity. These structural changes are reflected in the luminescence spectra. For a given M, increasing the size of X has little effect on M–H distances but significantly increases the emission wavelength. This is most likely due to the increasing nephelauxetic effect of the halogen. Increasing the size of M while keeping X constant moderately increases M–H distances but markedly decreases the emission wavelength. Thus, Eu(II) luminescence in metal hydrides appears to be primarily influenced by M–H distances, with the nephelauxetic effect of the halogen atoms playing a secondary role. Combining these effects with partial substitution of fluorine for hydrogen or one metal for another presents significant opportunities for fine-tuning the luminescence properties of Eu(II) in metal hydride host compounds.

Fig. 1

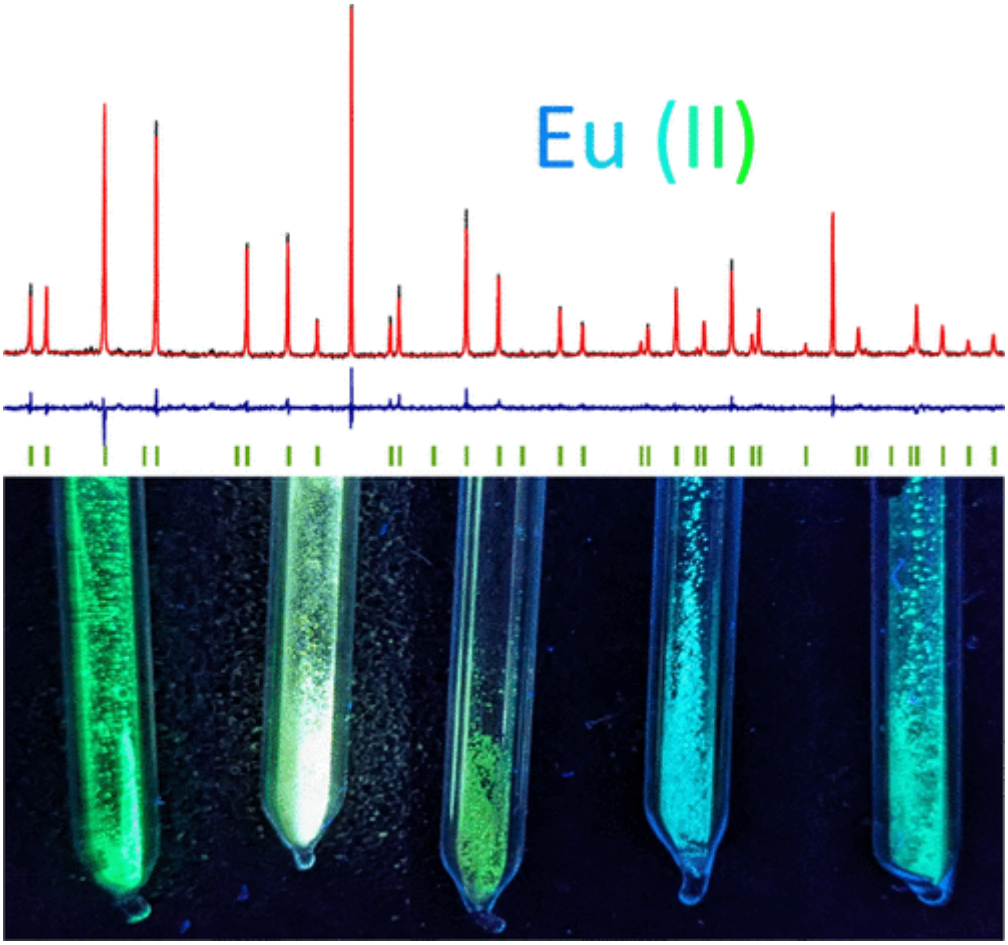

Poster Session 1: Functional materials 1

PP-58

Enhanced removal of hexavalent chromium using pine needle-derived activated carbon modified with NiO and $AlCl_3{\cdot}6H_2O$: Characterization and adsorption behavior

S. Kouvalakidou (Kavala/GR), A. A. Thysiadou (Kavala/GR), I. Konstantinou (Ioannina/GR), A. K. Tolkou (Kavala/GR), G. Z. Kyzas (Kavala/GR)

Heavy metal contamination of water poses serious environmental and health risks due to toxicity and bioaccumulation. Hexavalent chromium (Cr(VI)) is particularly hazardous because of its solubility, mobility, and carcinogenic effects, often originating from industries like electroplating, leather tanning, and textiles. Various removal methods, including chemical reduction, precipitation, membrane filtration, ion exchange, and adsorption, have been explored. Among these, adsorption is preferred for its simplicity, efficiency, cost-effectiveness, and low secondary pollution. In this study, pine needle-derived activated carbon (ACPN) was synthesized in a single-step phosphoric acid activation at 500 °C and used as a precursor to prepare modified adsorbents: ACPN@NiO and ACPN@Al, by adding NiO or $AlCl_3{\cdot}6H_2O$, respectively. These modifications introduce additional active sites, improve surface functionality, and enhance porosity, leading to higher adsorption capacity and faster Cr(VI) removal kinetics. The synthesized ACPN and its modified forms, ACPN@NiO and ACPN@Al, were thoroughly characterized to assess their adsorption potential. BET analysis showed increased surface area and porosity upon modification, while FTIR confirmed functional groups critical for Cr(VI) binding. XRD revealed the presence of NiO and Al-containing phases, and SEM-EDS demonstrated both the successful incorporation of Ni and Al into the ACPN structure and the subsequent adsorption of Cr(VI) onto the modified surfaces, as well as a uniform dispersion of the modifiers and the porous surface morphology. The adsorptive behavior was further investigated by optimizing key parameters, including pH, contact time, adsorbent dosage, and initial chromium concentration Together, these analyses highlight how structural and surface modifications enhance the adsorptive properties of the carbons, making them highly effective for hexavalent chromium removal from aqueous solutions.

Fig. 1

PP-59

Synthesis and characterization of hybrid modified activated carbons from olive stones for the removal of Cr(VI) from water

A. K. Tolkou (Kavala/GR), A. A. Thysiadou (Kavala/GR), K. N. Maroulas (Kavala/GR), I. Konstantinou (Ioannina/GR), G. Z. Kyzas (Kavala/GR)

Groundwater contamination with toxic metals remains a pressing global issue, with hexavalent chromium [Cr(VI)] being one of the most hazardous due to its high mobility and toxicity. Among the treatment strategies available, adsorption has gained prominence as a low-cost and efficient approach for removing trace metals from aqueous systems. In this study, activated carbon (AC) was prepared from olive stones (OS), an abundant agricultural byproduct, and was further functionalized with magnesium (Mg) oxide. Additionally, chitosan (Cs), a biodegradable biopolymer well known for its metal-binding capability, was incorporated to enhance adsorption characteristics. A major focus of the work was the structural and morphological characterization of the developed adsorbents. Surface area and pore distribution were quantified using Brunauer–Emmett–Teller (BET) analysis, which confirmed the increase in surface heterogeneity after metal oxide incorporation. X-ray diffraction (XRD) patterns provided evidence of the crystalline phases of Mg oxides. To investigate surface functionalities, Fourier-transform infrared spectroscopy (FTIR) was employed, identifying characteristic bands associated with hydroxyl, carbonyl, and amino groups from chitosan, as well as metal–oxygen vibrations indicative of successful impregnation. The morphological features and particle dispersion were further examined using scanning electron microscopy (SEM), which showed a highly porous architecture and the homogeneous distribution of chitosan and metal oxides across the AC surface. These structural insights supported the adsorption experiments, where the modified composites demonstrated exceptional Cr(VI) uptake—achieving almost complete removal (98.2%) at pH 3.0 ± 0.1 (<permissible limit of 50 μg/L).

Fig. 1

Acknowledgements: We acknowledge support of this work by the project "Hybrid technologies of smart membranes and novel materials for the removal of hexavalent chromium from water" (ΥΠ3ΤΑ-0560800) which is implemented under the action "SUB1.1: Clusters of Research Excellence" of the sub-action "Strategy for Excellence in Universities & Innovation" (ID 16289), Greece 2.0 – National Recovery and Resilience Fund and funded by European Union Next Generation EU.

Poster Session 2: Aperiodic and Complex Structures and Structue Property Relationships

PP-49

Competing Charge Density Waves in Pressurized $SmNiC_2$

A. Eich (Karlsruhe/DE), A. A. Haghighirad (Karlsruhe/DE), A. von Ungern-Sternberg Schwark (Karlsruhe/DE), M. von Westarp (Karlsruhe/DE), G. Garbarino (Grenoble/FR), M. Le Tacon (Karlsruhe/DE), M. Merz (Karlsruhe/DE), S. M. Souliou (Karlsruhe/DE)

In the family of rare-earth nickel dicarbides, RNiC$_2$ (R = rare earth), a large variety of charge density wave (CDW) and magnetic states is found depending on the incorporated R. The observed changes in the characteristic charge ordering and its interplay with magnetism upon substitution are in part attributed to the chemical pressure exerted throughout the rare-earth series. Hence, the investigation of the effect of hydrostatic pressure on the RNiC$_2$ compounds is of particular interest to elucidate the role of pressure in this system.

SmNiC$_2$ exhibits an incommensurate CDW-1 with propagation vector $q_{CDW\text{-}1}$ = (½, ½+η, 0), $\eta \approx 0.02$, below 148 K, evident from X-ray powder diffraction [1]. At T_C = 17.7 K, SmNiC$_2$ undergoes a first-order phase transition to a ferromagnetic state, coupled to an abrupt suppression of the CDW [1]. This strong interplay of the charge order and the magnetic order indicates a weakening of the Fermi surface nesting conditions responsible for the CDW formation in favor of the ferromagnetic ordering [2,3]. The existence of a second, commensurate CDW-2 with $q_{CDW\text{-}2}$ = (½, ½, ½) is implied by diffuse X-ray scattering up to room temperature [1].

To investigate the charge ordering in SmNiC$_2$, we have performed single-crystal X-ray diffraction experiments at simultaneously low temperatures and high pressures at the ESRF. Our findings show the suppression of CDW-1 at increased pressures and confirm the full formation of CDW-2 as shown in Figure 1. In addition, we observe a CDW with propagation vector $q_{CDW\text{-}3}$ = (½, ½, ξ), $\xi \approx 0.06$, coexisting with CDW-1 and CDW-2, that has not been reported in the system RNiC$_2$ until now.

Fig. 1: Pressure–temperature phase diagram of the CDWs in SmNiC$_2$; the stability fields of the different CDWs are indicated by colors.

References

[1] S. Shimomura *et al*., Phys. Rev. Lett. **102**, 076404, 2009

[2] J. Laverock *et al*., Phys. Rev. B **80**, 125111, 2009

[3] J.N. Kim, C. Lee & J.-H. Shim, New J. Phys. **15**, 123018, 2013

Fig. 1

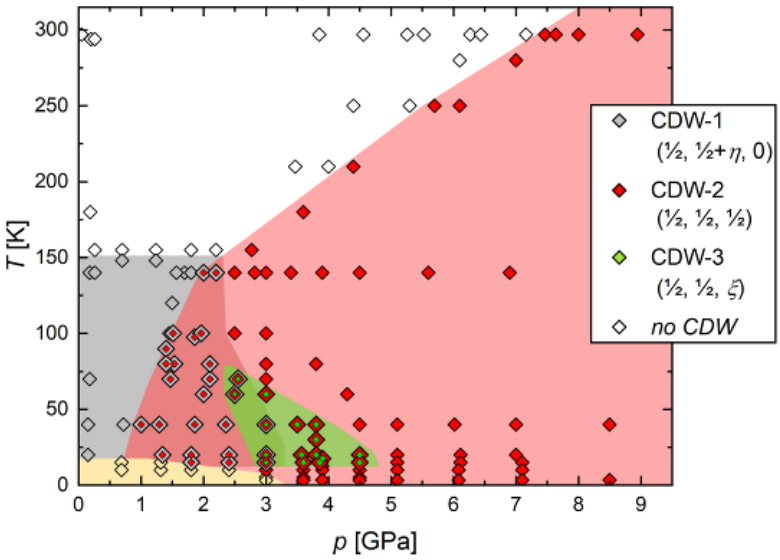
300
250
200
150
100
50
0
T [K]
0
1
2
3
4
5
6
7
8
9
p [GPa]
CDW-1
(½, ½+η, 0)
CDW-2
(½, ½, ½)
CDW-3
(½, ½, ζ)
no CDW

PP-50

$Na_{25}(Cd_xHg_{1-x})_{52}$ (x=0.252): A new complex sodium metallide at the pseudo-binary section '$NaCd_2$' – $NaHg_2$

I. Junker (Freiburg i. Br./DE), C. Röhr (Freiburg i. Br./DE)

Recently we extended our studies on the crystal chemistry and chemical bonding of binary and ternary alkali/alkaline-earth mercurides and cadmides [1] to the binary sections $NaHg_2$-'$NaZn_2$' [e.g. new structure type for Na_8M_{17}; M=Zn/Cd, 12.4% Zn, [2]) and $NaHg_2$-'$NaCd_2$' (this work) respectively. The latter case thus covers intermetallic compouds between the very simple dimercuride $NaHg_2$ [AlB_2-type, mainly covalent Hg-Hg bonding, CN(Hg)=3, [3]] and the extremly complex Laves-type mercuride '$NaCd_2$' [4]. Besides a small phase width of these two border compounds, the new, quite complex orthorhombic ternary title compound $Na_{25}[Cd_{13.1}Hg_{38.9}]$ was obtained. Despite the very similar metallic radii of Cd and Hg, and 33 (!) available crystallographically different *M* positions, of which no fewer than 23 are mixed Hg/Cd sites (cf. Fig. 1), the compound exhibits a very small phase width only. As expected, nearly all atoms in this new structure are centers of Frank-Kasper (FK) polyhedra: most Na atoms exhibit FK16 (12 *M* + 4 Na) polyhedra, most Cd/Hg atoms are icosahedrally coordinated by 6 M and 6 Na (FK12). These ideal coordination polyhedra of the classical Laves phases are dominating in sightly more Cd-rich regions of the structure, whereas the Hg-rich sections contain Johnson's J13 clusters (flat pentagonal bipyramids) and [Na(1)M_{15}] ccps with a pure *M* FK15 coordination (Fig. 2). Accordingly, the Cd/Hg polyanionic network exhibits six- to eight-fold *M* connectivity, with the shortest *M-M* bond length being 276 pm.

Fig. 1: Selected crystal data of $Na_{25}(Cd_xHg_{1-x})_{52}$ (x=0.252).

Fig. 2: Section of crystal structure of $Na_{25}M_{52}$. Appearance of *M* balls adapted to Cd:Hg ratio of the site; bond length ranges coded by stick radius.

References

[1] M. Schwarz, M. Wendorff, C. Röhr, *Z. Kristallogr.* **232**, 515-541 (2017).

[2] I. Junker, K. Köhler, C. Röhr, *Z. Kristallogr. Suppl.* **43**, s137-139 (2023).

[3] J. W. Nielson, N. C. Baenziger, *Acta Cryst.* **7**, 277 (1954).

[4] G. Bergman, *Acta Cryst.* **B52**, 54 (1996).

Fig. 1

Crystal system		orthorhombic	
Space group		*Pnma*, no. 62	
Pearson symbol		*oP*308	
Lattice parameters, pm	*a*	2139.05(13)	
	b	1540.05(9)	
	c	2184.54(12)	
V_a, c., 10^6 pm^3		7196.4(7)	
R Values [$I > 2\sigma(I)$]		0.0483	

Atoms	Wyckoff position	Cd [%]	*x*	*y*	*z*	CN
Na(1)	4c		0.0684(3)	1/4	0.4189(3)	15+0
Na(2)	4c		0.1585(3)	1/4	0.6706(3)	12+4
Na(3)	4c		0.2035(3)	1/4	0.8267(3)	14+2
Na(4)	4c		0.2941(3)	1/4	0.5763(3)	12+4
Na(5)	4c		0.3029(3)	1/4	0.0756(3)	12+2
Na(6)	4c		0.4338(3)	1/4	0.6693(3)	14+2
Na(7)	4c		0.5729(3)	1/4	0.5778(3)	12+4
Na(8)	8d		0.0686(2)	0.1321(3)	0.1698(2)	12+4
Na(9)	8d		0.0702(2)	0.6049(3)	0.4001(2)	11+2[+2]
Na(10)	8d		0.0714(2)	0.0614(3)	0.0162(2)	12+4
Na(11)	8d		0.0737(2)	0.0623(3)	0.6370(2)	11+4
Na(12)	8d		0.1836(2)	0.0498(3)	0.2472(2)	11+2(+1)
Na(13)	8d		0.2925(2)	0.0624(3)	0.4834(2)	12+4
Na(14)	8d		0.2973(2)	0.1333(3)	0.3279(2)	11+4
Na(15)	8d		0.3444(2)	0.0570(3)	0.0198(2)	12+4
Na(16)	8d		0.4350(2)	0.0607(3)	0.2635(2)	12+3
Hg(1)	8d		0.32219(3)	1/4	0.93306(3)	6+6
Hg(2)	8d		0.34872(3)	1/4	0.43981(3)	6(+1)+5
Hg(3)	8d		0.43680(3)	1/4	0.32720(3)	6+6
Hg(4)	8d		0.05263(2)	0.07592(3)	0.32431(2)	6+6
Hg(5)	8d		0.16085(2)	0.08113(3)	0.40149(2)	6+6

Atoms	W.p.	Cd [%]	*x*	*y*	*z*	CN
Hg(6)	8d		0.20453(2)	0.09104(3)	0.09686(2)	6+6
Hg(7)	8d		0.28998(2)	0.65037(3)	0.40958(2)	6+6
Hg(8)	8d		0.33372(2)	0.56209(3)	0.25255(2)	6+6
Hg(9)	8d		0.43177(2)	0.09428(3)	0.40882(2)	6+6
M(10)	4c	3.9(8)	0.43208(3)	1/4	0.00853(3)	6+6
M(11)	8d	4.2(5)	0.31849(2)	0.09114(3)	0.17295(2)	6+6
M(12)	4c	12.2(7)	0.04289(3)	1/4	0.56512(3)	6+6
Hg(9)	8d		0.43177(2)	0.09428(3)	0.40882(2)	6+6
M(10)	4c	3.9(8)	0.43208(3)	1/4	0.00853(3)	6+6
M(13)	4c	13.6(8)	0.15541(4)	1/4	0.30434(3)	6+6
M(14)	8d	17.2(5)	0.07106(2)	0.15492(3)	0.77934(2)	6+6
M(15)	8d	19.2(5)	0.06762(2)	0.65556(3)	0.03425(2)	6+6
M(16)	4c	19.9(7)	0.01371(4)	1/4	0.05801(3)	6(+1)+5
M(17)	8d	22.5(5)	0.43833(3)	0.14476(3)	0.11961(2)	7+5
M(18)	8d	25.0(5)	0.15502(3)	0.15164(3)	0.52825(2)	6+6
M(19)	8d	25.3(5)	0.13345(3)	0.58093(3)	0.12804(2)	6+6
M(20)	8d	28.1(6)	0.20149(3)	0.65796(4)	0.21993(3)	7+5
M(21)	4c	28.5(7)	0.00020(4)	1/4	0.68689(4)	8+6
M(22)	8d	30.7(6)	0.02838(3)	0.07634(4)	0.47974(3)	7+5(+2)
M(23)	4c	42.0(7)	0.01540(4)	1/4	0.28073(4)	7+5
M(24)	8d	42.1(5)	0.35841(3)	0.55792(4)	0.37848(3)	6+6
M(25)	8d	43.3(5)	0.50196(3)	0.06078(4)	0.62533(3)	6+6
M(26)	8d	43.5(5)	0.05907(3)	0.57826(4)	0.25159(3)	7+3(+3)
M(27)	8d	45.9(5)	0.27411(3)	0.57305(4)	0.11989(3)	6+6
M(28)	4c	52.4(8)	0.21670(5)	1/4	0.19158(4)	7+7
M(29)	4c	53.9(8)	0.36765(5)	1/4	0.81184(5)	8+4
M(30)	4c	59.0(7)	0.36369(5)	1/4	0.21980(4)	7+5
M(31)	4c	64.0(7)	0.14229(5)	1/4	0.09711(4)	6+6
M(32)	4c	64.0(7)	0.21962(5)	1/4	0.42857(4)	6+6
Cd(33)	8d		0.23828(4)	0.57790(6)	0.36165(4)	7+6

Fig. 2

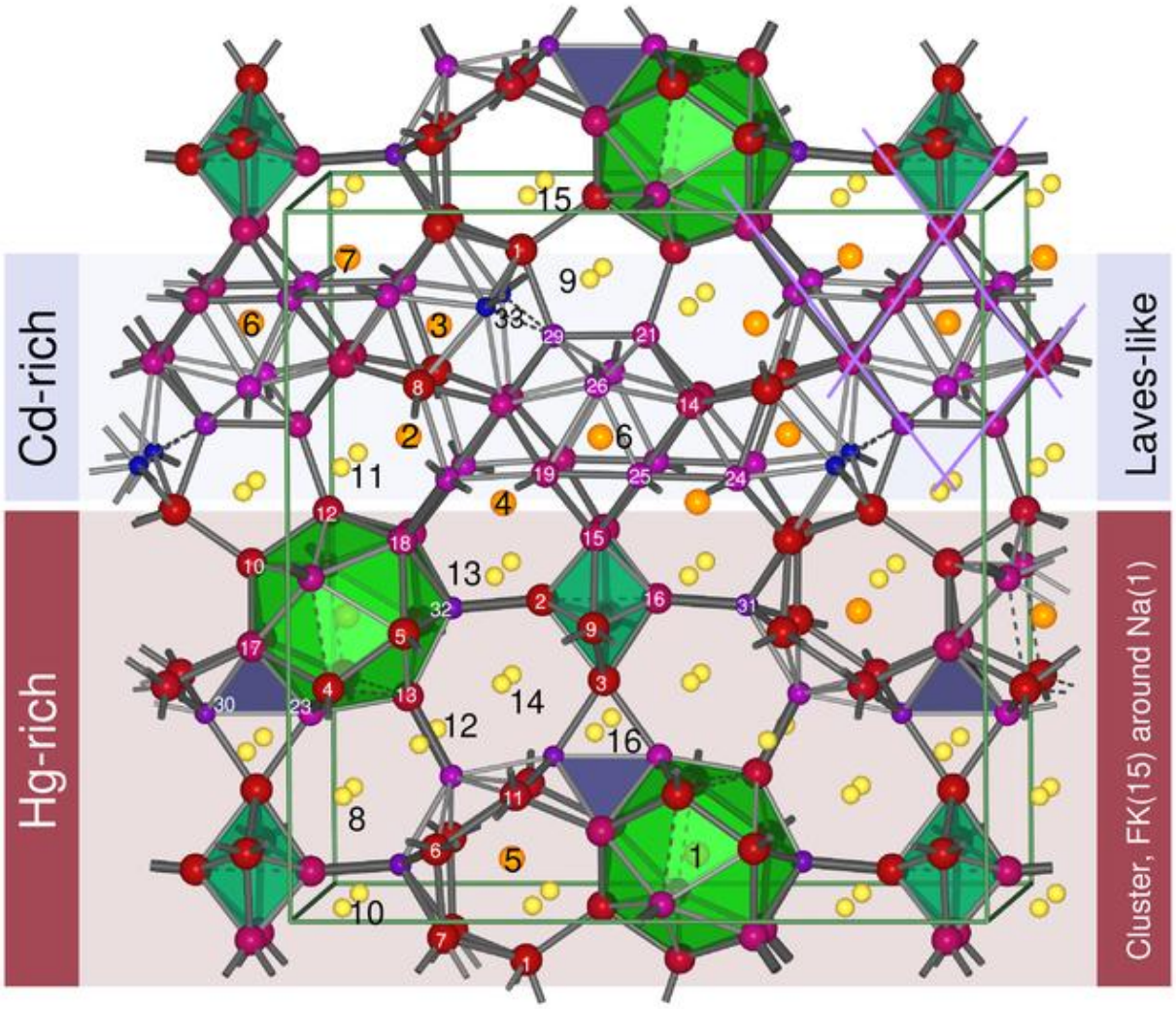

PP-52

Combining single crystal diffuse scattering and* ab initio *molecular dynamics simulations to understand framework dynamics in $AlPO_4$-5

E. M. Schmidt (Bremen/DE), M. Fischer (Bremen/DE)

Zeolites and zeotypes, including the aluminium phosphate framework materials $AlPO_4$-5, exhibit an inherent structural flexibility due to the unique way their rigid building blocks are connected via shared oxygen atoms (Fig. 1(a)). The general framework structure of $AlPO_4$-5 is typically described as a structure where the Al-O2-P bond angle approaches 180° - see Fig. 1(a). This configuration is considered energetically unfavourable and unrealistic, creating a form of bond frustration [1,2]. To experimentally probe this distortion, we use synchrotron single crystal diffuse scattering (ESRF, ID28 dedicated diffuse scattering side station) on a calcinated $AlPO_4$-5 sample. In addition to structured diffuse scattering, we observe weak, but resolution-limited sharp satellite reflections at **q** = (0,0,0.37) – see Fig.1(b). *Ab initio* molecular dynamics (AIMD) simulations performed on 3x3x6 supercells of the parent *P6cc* structure qualitatively reproduce these features. These simulations identify the observed phenomena as dynamic distortions that establish a persistent three-fold superstructure along the *c*-axis, offering new insights into the complex structural dynamics of $AlPO_4$-5 [3].

Fig. 1. (a) Average structure of $AlPO_4$-5. Al in blue, P in purple, O in red. (b) *h*0*l*-layer of the experimentally measured diffuse scattering compared to the AIMD simulation.

References

[1] Liu, Y., Withers, R. L. & Norén, L. (2003). *Solid State Sciences*. **5**, 427–434.

[2] Cortie, D. *et al.* (2017) *J. Phys. Chem. C* **121** 18762–18770.

[3] Fischer, M. *et al.* (2025) *Microporous and Mesoporous Materials* 4**01**, 113912.

EMS greatly acknowledges the support of D.A. Chaney (ESRF) for support during beam time. MF acknowledges financial support by the Deutsche Forschungsgemeinschaft (German Research Foundation, DFG) through a Heisenberg fellowship (project no. 455871835).

Fig. 1

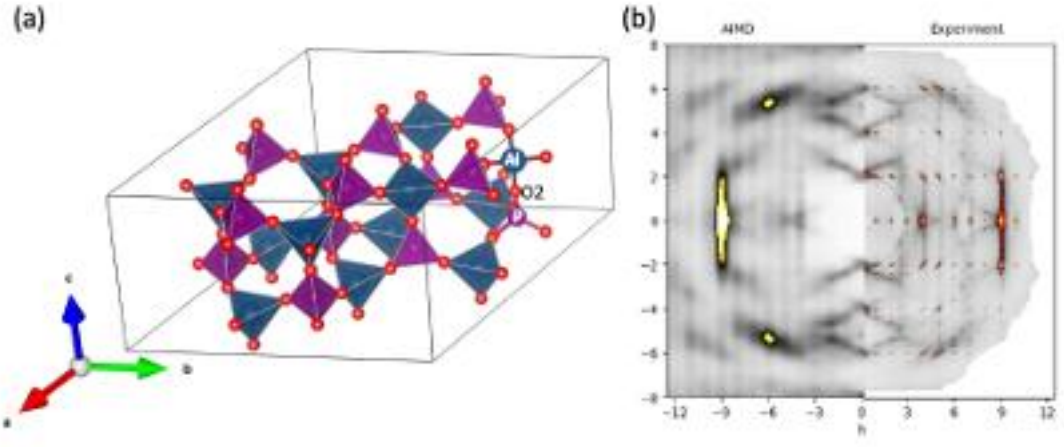

PP-54

Single-crystal growth and characterisation of the kagome material $CeFe_6Ge_6$

M. Schulze (Dresden/DE), E. Carrillo-Aravena (Dresden/DE), T. Doert (Dresden/DE), M. Ruck (Dresden/DE)

Materials with transition-metal (*TM*) kagome nets can host exotic quantum phenomena arising from geometric frustration and topological band structures.[1] Ternary rare-earth (*RE*) germanides *RE* TM_6Ge_6 combine such *TM* kagome nets with the magnetic moments of the localised *RE* 4*f* electrons, enabling a complex interplay between topology and magnetism.

$CeFe_6Ge_6$ was previously reported as a microcrystalline powder[2] but received no further attention. In this work, we report the growth of mm-sized single-crystals of $CeFe_6Ge_6$ using a Sn flux method. X-ray diffraction on a single-crystal suggests that $CeFe_6Ge_6$ crystallises as a superstructure of the hexagonal $Y_{0.5}Co_3Ge_3$ structure type. Kagome nets of Fe atoms and honeycomb nets of Ge atoms alternate along the *c*-axis. Their hexagons form channels where Ce and Ge atoms are located. The stacking order of the Ce and Ge atoms varies between the channels (Figure 1a,b), and strong diffuse scattering features indicate disorder among these hexagonal channels (Figure 1c,d).

Both the kagome and honeycomb nets are known to exhibit magnetic frustration. Combining them adds an additional level of complexity to magnetic interactions. Further investigations will focus on the interactions of magnetic, electronic, and topological phenomena

Figure 1 a) Crystal structure of $CeFe_6Ge_6$ projected approximately perpendicular to, and b) along the *c*-axis. The ellipsoids enclose a space where 95% probability of the electron density of the atoms can be found at 298(1) K. c) Reconstructed (3*kl*) and d) reconstructed (*hk*6) plane of the diffraction pattern of a $CeFe_6Ge_6$ crystal.

References

[1] M. Jovanovic, L. M. Schoop, *J. Am. Chem. Soc.* 2022, 144, 10978–10991.

[2] D. Berthebaud, *Dissertation*, Université de Rennes, France, 2007.

Fig. 1

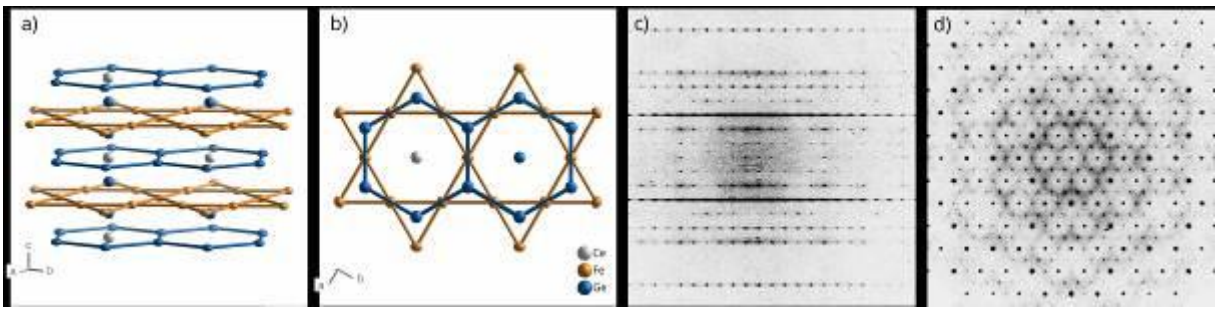

PP-55

Structural and spectroscopic characterizations of mullite-type $PbAl_{1-x}Fe_xBO4$

M. M. Murshed (Bremen/DE), T. M. Gesing (Bremen/DE)

We report detailed structural and spectroscopic characterizations of mullite-type Pb(Al1-xFex)BO4 using X-ray powder diffraction, and Raman, FTIR and 57Fe Mössbauer spectroscopy. Each member of the solid solution was produced by conventional solid-state reaction. The endmember PbAlBO4 appears to be light yellow which successively changes over light orange to dark brown for PbFeBO4. The crystal structure of each member has been analyzed by X-ray power diffraction data Rietveld refinements. The average crystallite size sharply drops for $0.1 \leq x \leq 0.9$ while the microstrain can be described with a gaussian peak shape with the highest value at $x = 0.5$. Metric and geometric parameters (bond length, angle, polyhedral distortion) have been followed with respect to the chemical composition. A slight deviation of the *a*-lattice parameter from the Vegard"s line of the endmember PbFeBO4 indicates the sample most probably crystallizes with a low-spin configuration while all other iron containing members follow a high-spin configuration. The Wang-Liebau eccentricity parameter mainly representing the strength of the stereochemical activity for this 08 mullite-type phases, has been found to be associated with the overbonding nature of the Pb2+ cations. The frequencies red-shift observed by both Raman and FTIR spectra clearly supports the quasi-harmonic nature of the vibrational modes. The main doublet in the center part of the 57Fe Mössbauer spectra at room temperature demonstrates the lack of any magnetic interactions. The substitution of Al by Fe ($0.1 \leq x \leq 1.0$) does not change the number of sub-spectra, supporting complete miscibility. The isomer shift values are characteristics of octahedrally coordinated Fe3+, which linearly increase with increasing Fe content. The non-zero quadrupolar splitting indicates the non-cubic symmetry at the Fe site. These values successively decrease with increasing Fe content in the solid solution.

PP-56

Crystallography and mechanical properties of τ_2-Al_3FeSi

L. Richter (Freiberg/DE), A. Leineweber (Freiberg/DE)

Question: To contribute to the understanding of Al/steel joints prepared by hybrid casting, we (re)investigate fundamental properties of Al-Fe-Si phases. This involves crystal structure, microstuctures and mechanical properties studied by nanoindentation. In this contribution we focus on the τ_2 phase of approximate formula Al_3FeSi. Its rhombohedral crystal structure has been reported in two apparent independent works [2, 3], agreeing about an unusual Fe site partially occupied by Al and about the preferential location of Si atoms.

Methods: Samples of various compositions of τ_2 have been produced by arc melting and subsequent heat treatments. After quenching, PXRD was carried out for the reassessment of crystal structure models indicating the mixed occupancy of iron sites by Al and Si [2, 3]. As prerequisite to the planned and to be presented nanoindentation studies, the microstructure of cross-sections was analysed in the SEM by EBSD and EDS.

Results: PXRD analysis as outlined in Fig. 1 confirmed presence of a rhombohedral crystal, consistent with reported literature data of τ_2. Rietveld refinement indicates nearly complete occupation of iron Wyckoff sites, suggesting a highly ordered atomic arrangement in the sample.

EBSD measurements on the same alloy as shown in Fig. 1 allowed for evaluating the microstructure and texture of the phases, revealing a non-textured orientation distribution being a good starting point to study orientation-dependent indentation properties.

Fig. 1: PXRD pattern (Co-Kα_1) of an alloy containing τ_2-Al_3FeSi, lesser amounts of t_4-Al_3FeSi_2 and Al solid solution: Red observed data points, blue calculated intensity (Rietveld) and grey difference.

Fig. 2: EBSD IPF map of cross-sectioned alloy also investigated in Fig. 1. Only orientations of τ_2 are colored.

References

[1] Martin et al, Intermetallics **2022**, *151*, 107712.

[2] Rogeret et al, Z. Kristallogr. **2011**, *226,* 805-813.

[3] Sugiyama et al, J. Alloys Compd. **2004**, *368*, 251-255

Fig. 1

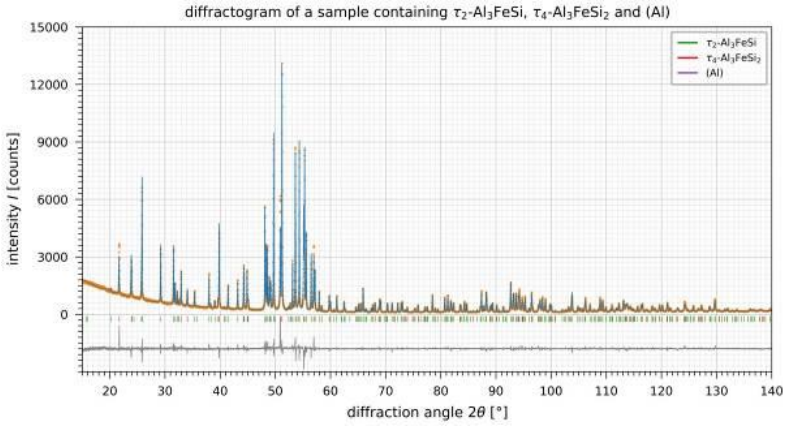

Fig. 2

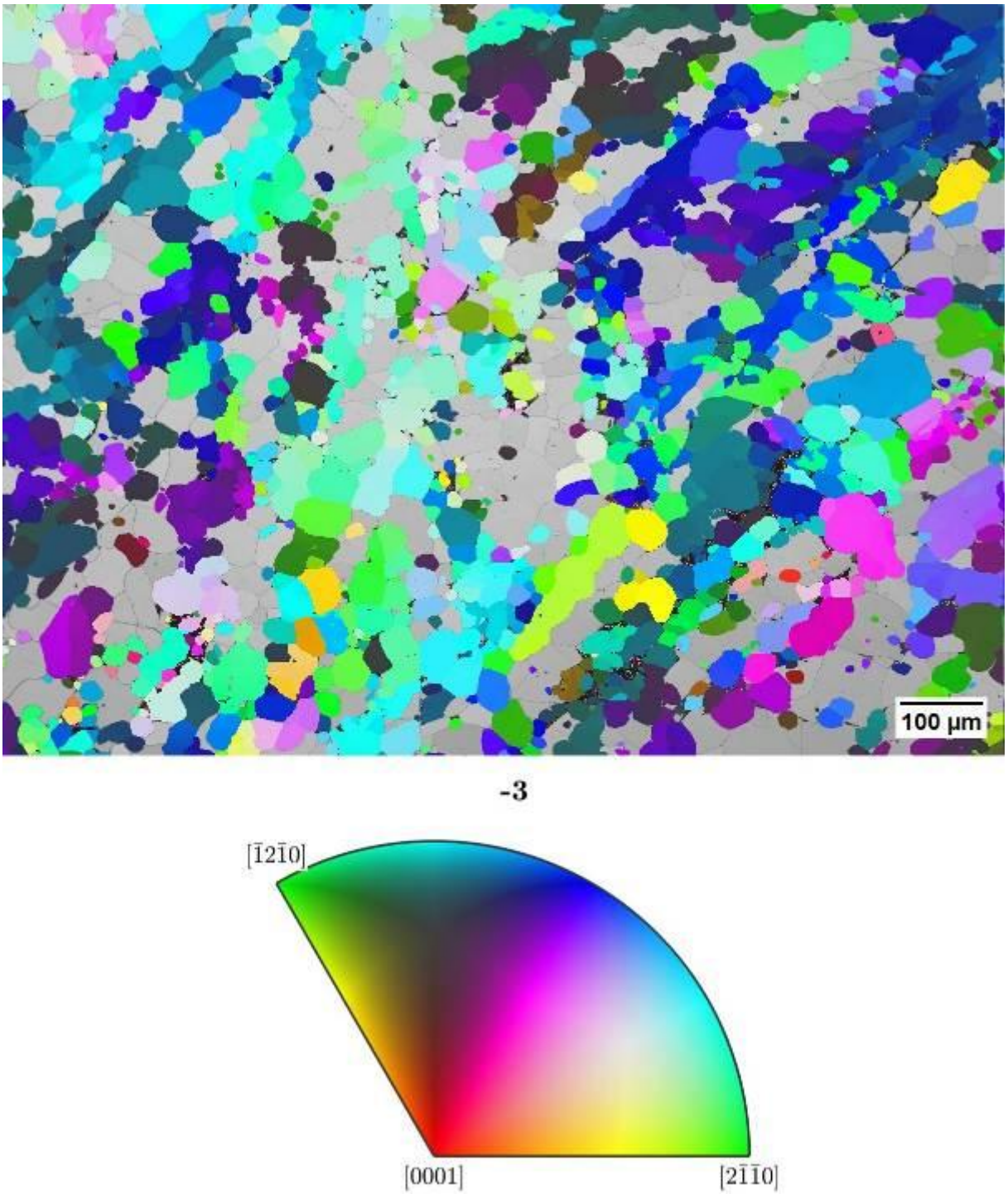

PP-57

Cation mutation in chalcogenide semiconductors as a path towards CRM-free top absorber layer for tandem solar cells

G. Gurieva (Berlin/DE), D. M. Többens (Berlin/DE), M. Pilvet (Tallinn/EE), A. Manjon Sanz (Oak Ridge, TN/US), M. Avdeev (Lucas Heights/AU), M. Kauk-Kuusik (Tallinn/EE), S. Schorr (Berlin/DE)

The search for sustainable, efficient, and cost-effective photovoltaic materials continues to be a challenge in the field of solar energy production. In particular, the development of critical raw material free top absorber layers for tandem solar cells is crucial in the effort to transition away from fossil fuels and towards a greener energy future. The emergence of compound semiconductors has provided an opening into low-cost fabrication of thin-film solar cells, made possible a reduction in absorber layer thickness, and therefore lead to a decrease in production costs.

In this work, we explore the potential of divalent and tetravalent cation mutations in compound semiconductors with the aim of finding a material with increased bandgap (ideally around 1.7eV) and reduced structural disorder. We studied the structural phase transition in both Cu2(Zn1-xCdx)SnS4 and Cu2Zn(SixGe1-x)Se4 mixed crystals by neutron diffraction. It was found that the re-distribution process in Cu2(Zn,Cd)SnS4 is different from the process in Cu2(Zn,Fe)SnS4 obtained before, and in the Cu2Zn(Ge,Si)Se4 transition is distortion driven and is going via a region where two phases with different crystal structures co-exist.

The results of this study highlight the importance of considering alternative materials beyond the known chalcopyrites or kesterites and demonstrate that cation mutation in quaternary chalcogenides is a promising path towards the development of highly efficient tandem solar cells.

A portion of this research used resources at the Spallation Neutron Source, a DOE Office of Science User Facility operated by the ORNL. We thank HZB for the allocation of neutron diffraction beamtime. A portion of this research used resources at the Australia's Nuclear Science and Technology Organisation (ANSTO) at the ECHIDNA end station.

Poster Session 2: Functional Materials 2

PP-60

Influence of electrolyte solvents on the intercalation reaction of Na^+ into ZrS_2 and HfS_2 host structures

L. Liers (Kiel/DE), S. Mangelsen (Kiel/DE), M. Behrens (Kiel/DE)

Group IV transition metal disulfides (TMDS) are well known as intercalation hosts for alkali metal ions what makes them suitable candidates as electrode materials in batteries.[1–4] The underlying intercalation reaction of Na^+ into ZrS_2 and HfS_2 was investigated by combining electrochemical experiments, X-ray powder diffraction and Rietveld analysis. The intercalation ability is influenced by the use of electrolyte solvents. The use of coordinating solvents leads to co-intercalation in any case, while weakly coordinating solvents are not co-intercalated into the interlayers of ZrS_2.[1] For HfS_2, we found co-intercalation in gradations for a carbonate mixture, but not for tetrahydrofuran. While for the use of diglyme the co-intercalation results in the loss of long-range order, the co-intercalation of carbonates into HfS_2 leads to expansion of the interlayer distances, but it has less of an effect on the crystallinity of the initial phase and the intercalated states than diglyme. Rather, there are coexisting structures of co-intercalated HfS_2 and non-co-intercalated HfS_2. Whether co-intercalation occurs or not, the intercalation of Na^+ leads in all cases to a phase transition from the 1T-TMS_2 to the 3R-$NaTMS_2$ structure (TM= Zr, Hf). In conclusion, the intercalation reaction of Na^+ into group IV TMDS is different for all of the materials which makes it even more important to investigate the intercalation reactions of battery materials for better cycle life and efficiency.

References

[1] L. Liers, L. Mereacre, H. Li, J. Mickenbecker, M. Knapp, S. Indris, M. Behrens, S. Mangelsen, *Inorg. Chem.* **2025**, *64*, 18045–18061.

[2] G. Alvarez Ferrero, G. Åvall, K. A. Mazzio, Y. Son, K. Janßen, S. Risse, P. Adelhelm, *Adv. Energy Mater.* **2022**, *12*, 2202377.

[3] J. Park, S. J. Kim, K. Lim, J. Cho, K. Kang, *ACS Energy Lett.* **2022**, *7*, 3718–3726.

[4] M. H. Whangbo, J. Rouxel, L. Trichet, Inorganic Chemistry **1985**, *24*, 1824–1827.

PP-61

Synthesis and characterization of spinel-type compounds AM_2O_4 (A: Zn^{2+}, Cu^{2+}, M: Fe^{3+}, Ga^{3+}) with different average crystallite sizes (ACS) as tailored visible-light photocatalysts

M. Lovino Nocetti (Bremen/DE), A. Wollbrink (Essen/DE, Bremen/DE), T. M. Gesing (Bremen/DE)

Photocatalytic reactions driven by oxidic semiconductor materials can play an important role in waste water purification by the degradation of persistent organic pollutants (POP's) [1]. The performance of photocatalytic materials is due to their band-gap energy that depends on the materials used, e.g., crystal structure, composition, average crystallite and particle size as well as their respective morphology. Promising candidates are spinel-type AM_2O_4 compounds (sg: Fd3m), cf. Fig. 1 [2], due to the high number of possible element combinations for tailored band-gap transitions in the visible light range.

In the search for effective materials with respect to photocatalytic properties for water treatment, the four phase-pure spinel-type phases $ZnFe_2O_4$ (ZFO), $ZnGa_2O_4$ (ZGO) $CuFe_2O_4$ (CFO), and $CuGa_2O_4$ (CGO) were synthesized using an adapted "glycerin method" [3] at different synthesis temperatures (T_S) and times (t_S) resulting in spinel-type compounds with different ACS, particle size and compositions, analyzed by XRPD-Rietveld, SEM/EDX, UV/Vis spectroscopy, DLS, and photocatalytic degradations tests.

The results revealed that i) the composition defines the band-gap energy, showing 1.99(3) eV (ZFO), 4.91(9) eV (ZGO), 1.50(1) eV (CFO) and 3.50(2) eV (CGO), and ii) preliminary photocatalytic studies on ZFO showed that a decrease in the average crystallite size (ACS) slightly increases the corresponding band-gap energy by about 5–6% and enhances the photocatalytic degradation of methyl orange (MO) in aqueous solution from 60 to 468 nmol L^{-1} h^{-1}. iii) in contrast to the ACS trend, larger ZFO particles exhibited the highest degradation rates.

The results show that the glycerin method is a versatile and effective method for the synthesis of such spinel-type compounds.

References

[1] Mashuri et. al., Catalysts 10.11 (2020) 1260

[2] Granone et. al., Phys. Chem. Phys. (2018) 28267

[3] Hoffmann et. al., Z. Kristallogr. (2014) 699.

We acknowledge support by DFG (GE1981/13-1).

Fig. 1

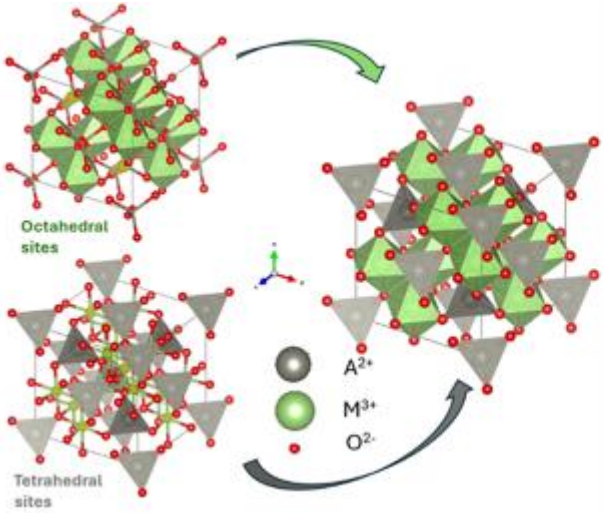

Figure 1: View of the tetrahedral sites (in grey, occupied by A^{2+}) and octahedral sites (in green, occupied by M^{3+}) in spinel-type compounds AM_2O_4 (SG: $Fd\bar{3}m$).

PP-62

Phase segregation of end-of-life nickel-rich layered lithium transition metal oxide cathodes: implications for direct regeneration

C. Zamparas (Karlsruhe/DE), E. Eiche (Karlsruhe/DE), J. Kolb (Karlsruhe/DE)

Environmentally friendly methods and direct recycling of anodes and cathodes of lithium-ion batteries dominate academic and industrial efforts. A crucial objective is nickel-rich cathode recycling, i.e., of layered lithium nickel cobalt manganese oxides, nominally $Li(Ni_{1-x-y}Mn_xCo_y)O_2$ (NMC), which serve as major replacement for $LiCoO_2$.

The present contribution focuses on understanding the fate of the crystal structure of end-of-life (EoL) NMC cathodes. The samples are characterized by X-ray diffractometry (XRD) coupled with Rietveld refinement, scanning electron microscopy (SEM) and microanalysis.

Transition metal molar ratios agree with NMC111 chemistry, with Ni/Mn and Co/Mn at 1.049±0.023 and 1.029±0.017, respectively. However, Ni/Mn ratios up to 1.923 and as low as 0.600 are linked to battery cycling. Evaluation of the diffractograms shows two distinct features for the NMC cathode, i.e., diffraction peak broadening and peak splitting. In the first case, crystal refinement suggests that the EoL NMC is overlithiated with structural formula $Li_{1.436}Ni_{0.333}Mn_{0.333}Co_{0.333}O_2$, c/a=4.973, and space group R-3m. Peak broadening is assumed to be related to overlithiation and is refined by Lorentzian anisotropic micro-strain and size. Peak splitting is compatible with phase segregation of the NMC cathode material into two varieties. Structural refinement of the two phases derived $Li_{1.163}Ni_{0.244}Mn_{0.378}Co_{0.378}O_2$, c/a=4.978, and $Li_{1.486}Ni_{0.536}Mn_{0.232}Co_{0.232}O_2$, c/a=4.973, as supercell formulas and space group R-3m for both. Additionally, XRD shows trace to minor xNiO·yCoO mixed oxide compounds and potential NMC crystallized in the C2/m space group.

Our analytical and crystal refinement results indicate that recycling, regeneration or repurposing processes need to consider the transition metal diffusion and over- or delithiation of the EoL cathode material. Cathode resetting is important for shaping materials for high-end applications and following safety prerequisites.

PP-63

Synthesis and Optical Characterization of (Nd,Pr):$LiYF_4$ Crystals

N. Tuvjargal (Ulaanbaatar/MN), U. Nergui (Ulaanbaatar/MN), D. Unurbileg (Ulaanbaatar/MN), N. Tsogbadrakh (Ulaanbaatar/MN), B. Chunfeng (Hohhot/CN), J. Davaasambuu (Ulaanbaatar/MN, Ulaanbaatar/MN)

Recent advances in laser technology and photonics research have stimulated extensive research on the use of laser generators for a wide range of applications. Trivalent rare earth (RE^{3+}) ions, which have multi-level emission levels characterized by 4f-4f transitions in the visible and near-infrared regions, have been adopted as novel pump sources to obtain visible lasers. The $LiYF_4$ compound, co-doped with rare-earth Pr^{3+} and Nd^{3+} ions, were successfully synthesized using a solid-state reaction method. The crystal structures of the samples were analyzed using the Rietveld refinement method, and the XRD results were compared to the JCPDS 01-077-0816 standard database. The lattice parameters are a=b=5.168Å, c=10.747Å. The optical absorption spectrum was measured using a Shimadzu UV-2550 spectrometer in the range 200 to 900nm, and the emission spectrum was measured in the 400 to 900 nm range using a F-4600 FL spectrophotometer. The optical absorption spectra of the samples prepared in this experiment are shown in Figure 1. The (Nd:Pr)$LiYF_4$ crystal combines the strengths of the two ions to produce a broad absorption spectrum from 400 to 800nm. This enhanced spectral coverage makes the material highly suitable for a broad range of optical applications.

Fig. 1

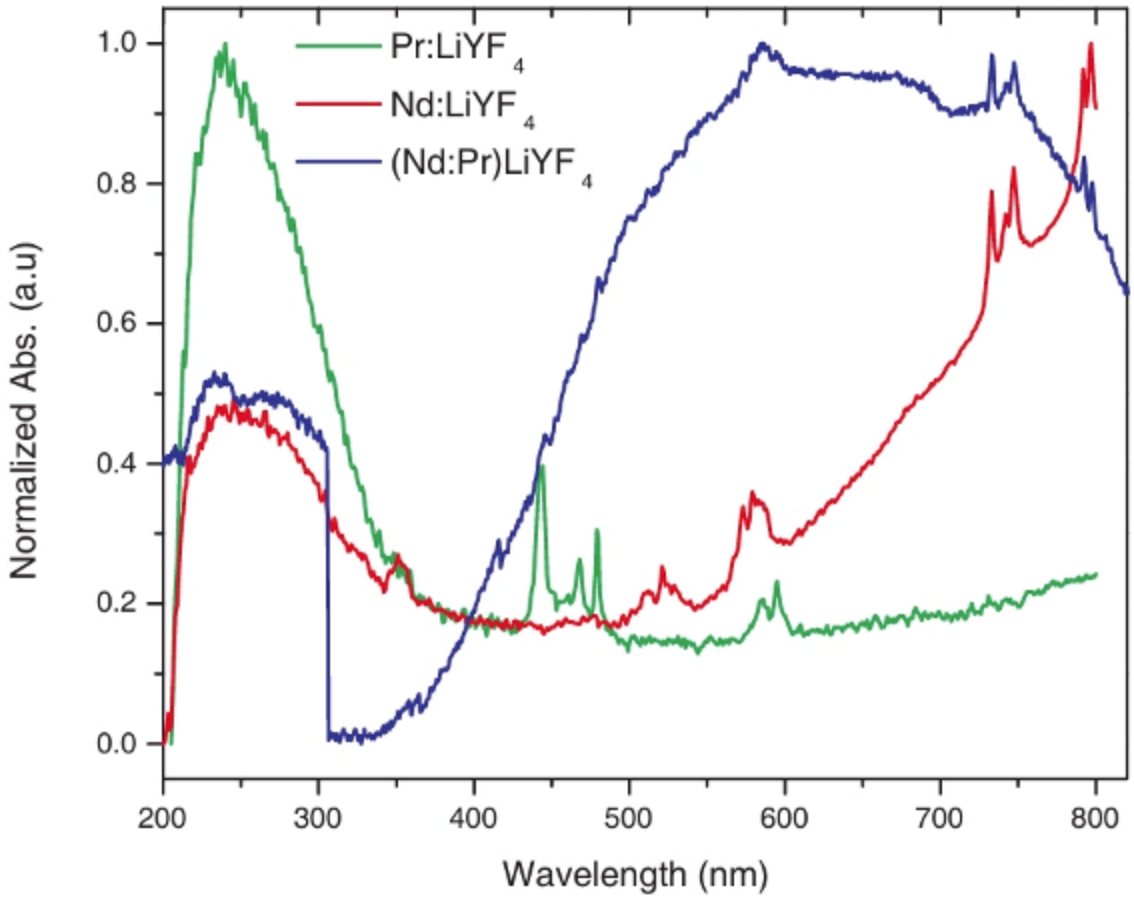

PP-64

Lithium Makes the Difference – Phase Transitions of the Lithium-Ion Conductor Li_4SnS_4

L. G. Balzat (Stuttgart/DE, Munich/DE), S. Bette (Stuttgart/DE), J. Blahusch (Stuttgart/DE, Munich/DE), C. Schneider (Stuttgart/DE), I. Moudrakovski (Stuttgart/DE), K. Gjorgjevikj (Stuttgart/DE), S. Krause (Stuttgart/DE, Ulm/DE), B. V. Lotsch (Stuttgart/DE, Munich/DE)

Lithium-ion solid electrolytes (Li-SEs) are essential for solid-state batteries, offering higher power and energy densities than conventional Li-ion cells. Among Li-SEs, sulfide-based SEs stand out for their high ionic conductivities, but they are typically moisture-sensitive. [1] Li_4SnS_4 has recently attracted scientific interest because it is more resistant towards humidity than most sulfide electrolytes. [2] Two orthorhombic Li_4SnS_4 polymorphs (α and β) are known, but their temperature-dependent behavior has not been investigated yet. [3, 4]

We performed temperature-dependent powder X-ray diffraction to map the phase diagram of Li_4SnS_4 (Fig. 1). In addition to the transition from α-Li_4SnS_4 to β-Li_4SnS_4 at ~100 °C we identified a second, previously unknown transition from β-Li_4SnS_4 to a new γ-polymorph at ~200°C. Differential scanning calorimetry showed no other transitions between –150 °C and 1000 °C.

All polymorphs crystallize in space group *Pnma* (no. 62) and feature the same zig-zag-like arrangement of SnS_4 tetrahedra. The main differences of the crystal structures lie in the ordering of the lithium substructure. Using neutron diffraction, we show that Li_4SnS_4 transitions from the Lithium-vacancy-disordered α-phase to the ordered β-phase and then to another disordered γ-Li_4SnS_4 . The structures of the polymorphs were further confirmed by using temperature-dependent ^{7}Li and ^{119}Sn NMR, and Raman spectroscopy.

Lastly, using electrochemical impedance spectroscopy, we measured ionic conductivities from 10^{-6} to 10^{-1} S cm^{-1} between 25–220 °C. Conductivity changes are gradual, which is attributed to the small structural variations among all polymorphs.

References

[1] J. Janek, W. G. Zeier, *Nat. Energy* **2023**, *8*, 230-240.

[2] Y. Morino *et al.*, *ACS Omega* **2024**, *9*, 38523.

[3] T. Kaib *et al.*, *Chem. Mater.* **2012**, *24*, 2211-2219.

[4] J. H. MacNeil *et al.*, *J. Alloys Compd.* **2014**, *586*, 736-744.

Figure 1: Contour plot of temperature-dependent *in situ* PXRD data of Li4SnS4.

Fig. 1

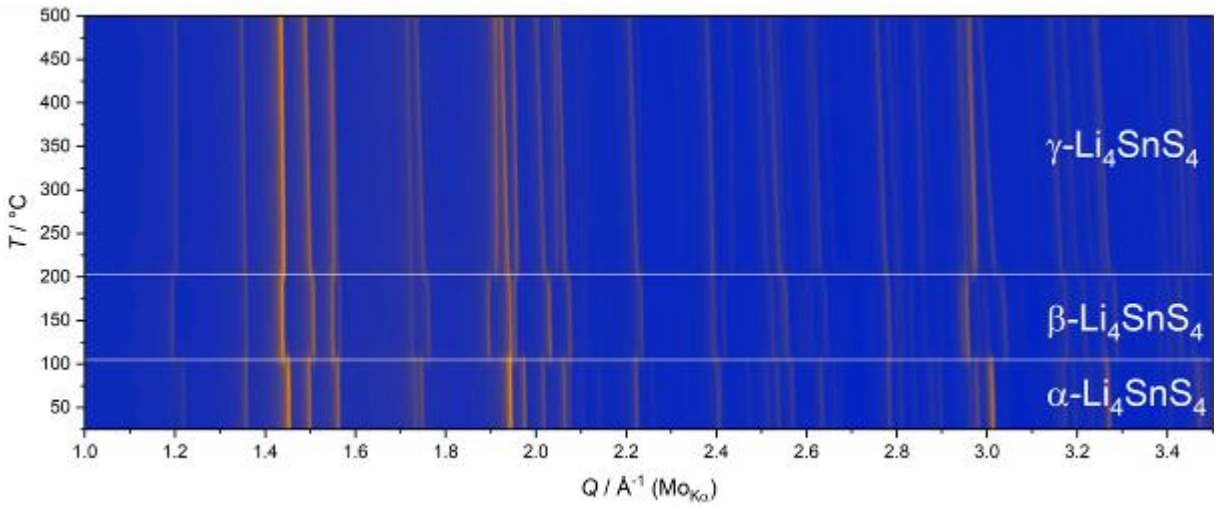

PP-65

Microstructural, Electrochemical and Mechanical Behavior of Cold-Worked and Heat-Treated AISI 316Ti Stainless Steel in Aggressive Acidic Media

H. Kaddour (Alger/DZ, Bab ezzouar/DZ)

This study examines the microstructural, electrochimical and mechanical behavior of AISI 316Ti austenitic stainless steel subjected to heat treatment at 1100 °C for 3 hours, followed by 40% cold plastic deformation in an acidic environment. Microstructural analysis by X-ray diffraction (XRD) revealed that the heat treatment stabilizes the austenitic phase, while subsequent cold deformation introduces crystalline defects. The formation and volume fraction of strain-induced α′- martensite were found to be closely linked to the stability of the austenite phase achieved through heat treatment. These crystalline defects contribute to increased hardness but adversely affect the electrochemical stability. Corrosion testing indicated a weakened passive film and greater susceptibility to localized corrosion in cold-worked specimens. Overall, the findings highlight a clear trade-off between enhanced mechanical strength and reduced corrosion resistance, underscoring the need to carefully optimize thermal.

Key words: AISI 316Ti, heat treatment, plastic deformation, crystalline defect, micrustructural behavior, X-ray diffraction (XRD) analysis

PP-66

Understanding the nature of Cu- and Mg-oxides in Cu/MgO catalyst systems

B. Taetz (Kiel/DE), S. Mangelsen (Kiel/DE), M. Behrens (Kiel/DE)

The interface of the active phase and the support material often plays an important role in the performance of in heterogenous catalysts.[1] For that reason it is crucial to know about the structure of not only the active phase but also the support. During the characterization of Cu/MgO catalyst systems for CO hydrogenation, differences, for example in TPR experiments (Fig. 1), between a material derived from a malachite and an amorphous precursor became apparent after calcination at 450 °C. Further investigations are now applied to understand the different Cu- and Mg-containing oxide species present in the samples. Two catalyst precursors were prepared by coprecipitation, from $Cu(NO_3)_2$ and $Mg(NO_3)_2$ as well as Na_2CO_3 as a precipitation agent. The slurry was aged hydrothermally or under atmospheric pressure to obtain a malachite or amorphous precursor respectively. The precursors were calcined at 450 °C. XRPD patterns of both samples display CuO with pronounced line broadening due to size effects (Fig. 2), with the crystalline precursor leading to smaller domains for CuO. Further, a difference in the measured diffraction patterns can be observed in regard to shifts in peak positions and anisotropic line broadening of the $(\bar{1}14)$ and (002) reflections for CM-mal-450 which could be indicative of a slight magnesium uptake in the CuO phase. Apart of that, no MgO phase can be observed, which gives rise to the additional question about the nature of the MgO phase. This is addressed using PDF analysis, yielding hints for a distorted rock salt–like structure. Since knowledge of the whole catalyst structure is relevant to understand the differences in catalytic activity, XRPD and PDF analysis were employed to unravel the nature of MgO in Cu/MgO catalyst systems.

Fig.1 TPR, Fig.2 XRD

References

[1] M. Behrens et al., *Science*, **2000**, 336, 893-897.

[2] H. Yamada et al., *Trans. Mat. Res.* Soc. Japan., **2000**, 25, 1199-1202.

[3] S. Sasakil, et al., *Proc. Jpn. Acad.*, Ser. B, **1979**, 55, 2, 43-48.

Fig. 1

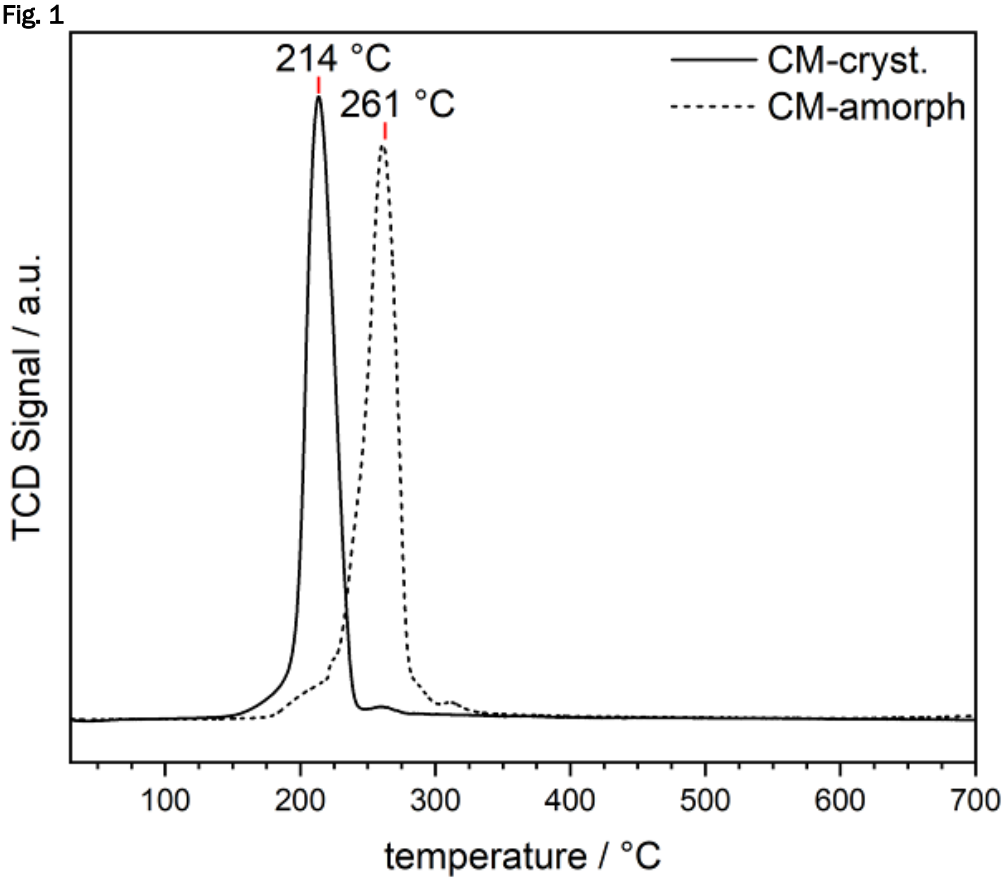

Fig. 2

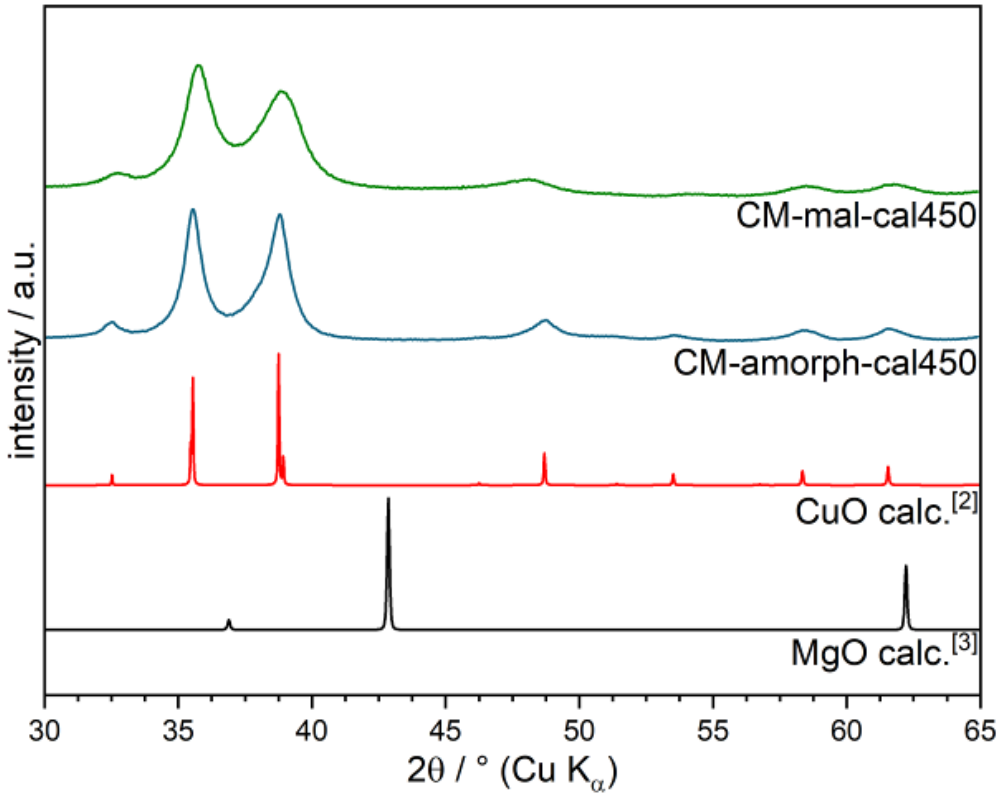
CM-mal-cal450
CM-amorph-cal450
CuO calc.[2]
MgO calc.[3]
intensity / a.u.
30
35
40
45
50
55
60
65
2θ / ° (Cu Kα)

PP-67

Mesoscale architecture of gadolinium and cobalt doped cerium oxide hierarchical catalyst

P. Woźniak (Wrocław/PL)

Structural hierarchy refers to materials that consists of building blocks organized into multi-scale structures [1]. Such materials show increased catalytic activity due to increased availability of active sites and facilitated mass transport. Due to repetitive arrangement of building blocks within the macroparticles volume, the stability of hierarchical catalysts is increased when compared to unorganized nano-sized particles or bulk counterparts. While introduction of dopants may improve catalytic activity, it may also greatly affect material architecture. In this study, the influence of synthetic parameters – (a) the composition of reaction mixture, (b) dopant type, (c) thermolysis conditions – on the development of Ce1-xCoxGdy O2-x/2 (x = 0- 0.15, y=0.1) catalyst architecture was thoroughly investigated. TEM and SEM imaging, electron diffraction, electron tomography, and crystallographic modelling were used to elucidate mesoscale architecture of hierarchical CeO2 sample. In particular, formation of specific texture that relates to ordering of CeO2 nanocrystals within macroparticles of hierarchical catalyst – obtained after thermolysis of Ce(HCOO)3 precursor – was ascribed to certain similarity between structural elements of cerium formate (R3m) and cerium oxide ($Fm\bar{3}m$). While similarity along [001] (formate) and [110] (oxide) crystallographic directions is the reason for the ordering of nanocrystals formed in thermolysis process, the areas of structural elements dissimilarity is behind formation of channels for rapid diffusion of gaseous thermolysis products. This effects in formation of highly porous macroparticles composed of nanocrystals showing defined habit and preferential 3D spatial orientation (Fig. 1). The architecture-related properties were correlated with propane oxidation activity. While Co2+ dopant improves catalyst activity, Gd3+ increases particles stability. Fig. 1. CeO2 hierarchical catalyst, (A) TEM image, (B) ET reconstruction, (C) model showing spatial arrangement of CeO2 nanocrystals. [1] R. Lakes, Nature 361 (1993) 511–515.

Fig. 1

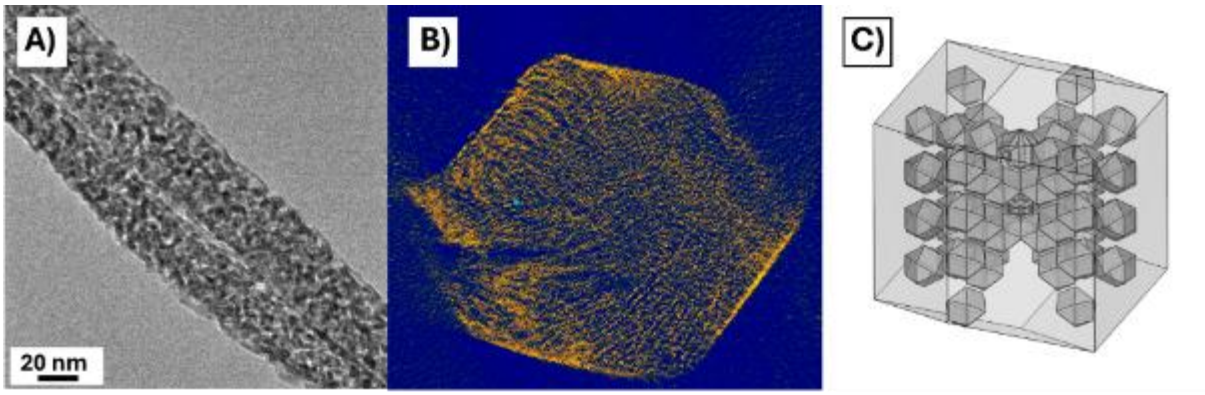

PP-68

Structural Studies of Substituted Polycrystalline $Na_3Co_{2-x}Ni_xSbO_6$ Antimonates

M. Gorbunov (Eggenstein-Leopoldshafen/DE), B. Schwarz (Eggenstein-Leopoldshafen/DE), D. Mikhailova (Eggenstein-Leopoldshafen/DE)

Layered alkali- and 3*d* metal oxides with a honeycomb-type lattice are examples of model structures for Kitaev magnetism[1]. Typical stoichiometries are: A_2MO_3 with two metals (A_2RuO_3, A_2IrO_3)[2] or $A_3M_2M'O_6$ with three metals, where M is a magnetic, and M' – usually, a non-magnetic cation[3].

Often, the synthesis defines the structural type for the $A_3M_2M'O_6$ oxides. The ordered honeycomb lattice has a higher Gibbs free energy ($\Delta G_T = \Delta H - T\Delta S$) than the disordered one with a random distribution of M and M' cations. In case of powder samples, formation of both structures as a mixture is probable. Overlooking it might lead to an incorrect interpretation of the XRD data. This might be an issue for magnetism studies as well as for battery research[4].

Syntheses of the target structural types with a singular magnetic cation are well-established. Mixing two different magnetic cations, as we did for the $Na_3Co_{2-x}Ni_xSbO_6$ series, complicates the task. For example, we might consider a crystal containing separate ordered and disordered domains with a random distribution of Co and Ni within the magnetic layers. One can implement this into the Rietveld fit.

In our work, we applied this approach to the synthesised $Na_3Co_{2-x}Ni_xSbO_6$ series, to define the fractions of the ordered (monoclinic, *C/2m*)[5] the disordered (trigonal, *R-3m*)[6] phases in the samples (Figure 1). The fit gets significantly better, as the differences in M'–O distances for the two structures are considered. This was followed by electrochemical desodiation of the samples combined with *operando* XRD and XAS to track the changes in crystal and electronic structures of the materials.

References

[1] A. Kitaev. *Annals of Physics*, **2006**, 321, 2–111.

[2] B. Mortemard de Boisse, et. al, *Nature Comm*., **2019**, 10, 2185.

[3] D. K. Yadav, et. al, *Dalton Trans*., **2019**, 48, 8955–8965.

[4] D. Yuan, et. al, *Adv. Mater*., **2014**, 26, 6301–6306.

[5] E. Vavilova et. al, *Phys. Rev. B*, **2023**, 107, 054411.

[6] M. I. Stratan, et. al, *New J. Chem*., **2019**, 43, 13545–13553.

Fig. 1

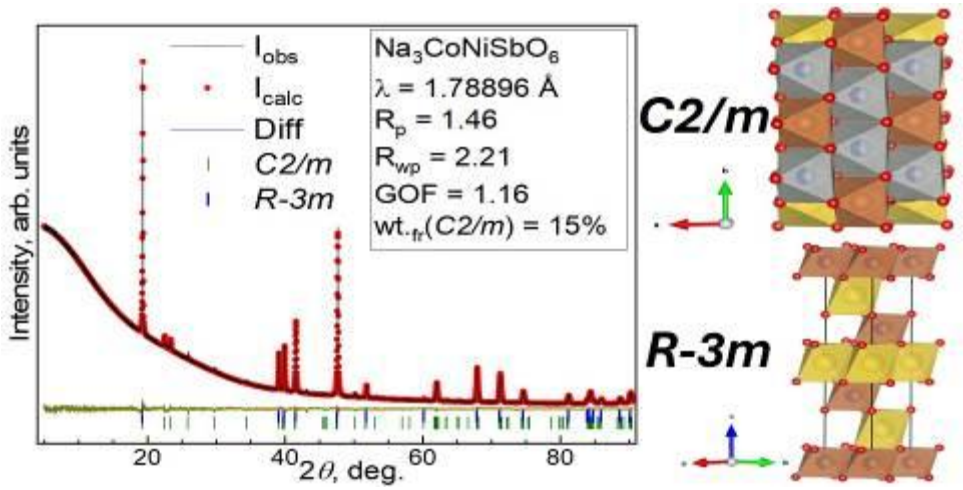

PP-69

Modelling stacking disorder in $Fe(C_2O_4)\cdot 2H_2O$

S. Mangelsen (Kiel/DE), M. Chumakovski (Kiel/DE), M. Behrens (Kiel/DE)

Oxalates appear as minerals but also in various biological processes and are further interesting in synthetic form e.g. as catalyst precursor due to their ease of preparation. In contrast, interpreting their powder diffraction patterns poses challenges, as many of these compounds are prone to structural disorder. The problem is long known[1] but typically treated by the application of an averaged structure model[2] to refine experimental data. For $Fe(C_2O_4)\cdot 2H_2O$ (FeOx) two distinct polymorphs are known, an orthorhombic form and a monoclinic one[3], while for the latter several somewhat varying reports exist. All forms are built from chains that are linked to layers, their connection in different stacking patterns leads to the distinct polymorphs. We prepared FeOx under various conditions, changing in particular the pH for precipitation and found that none of the respective powder patterns matches the reported structure data (Fig. 1). The local structure was studied by pair distribution function and is identical for all samples and matches calculated data. Differences occur for inter chain distances, underscoring that modelling of the stacking pattern is required. Further, the PDF data reveals closer resemblance to the orthorhombic form compared to the monoclinic. This was used as starting point to model the real structure according to different faulting scenarios conveying the stacking vectors and sequences according to the different polymorphs. Some of these modellings will be presented in the contribution.

Fig. 1: Comparison of observed and calculated diffraction patterns for different polymorphs and samples prepared at select pH values.

References

[1] H. Fichtner-Schmittler, *Krist. Tech.*, 1979, **14**, 1079–1088.

[2] A. N. Puzan, V. N. Baumer, D. V. Lisovytskiy and P. V. Mateychenko, *J. Solid State Chem.*, 2018, **260**, 87–94.

[3] R. Deyrieux and A. Péneloux, *Bull. Soc. Chim. Fr.*, 1969, 2675–2681.

Fig. 1

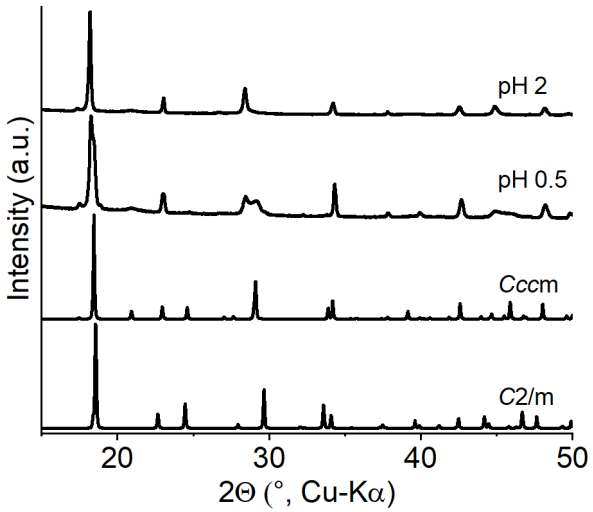

PP-70

Structure of a deep eutectic solvent, a mixture of proline and glycerol, from X-ray and neutron diffraction

C. Garvey (Garching/DE), B. Becks (Garching/DE), G. Bryant (Melbourne/AU), S. Bryant (Melbourne/AU), S. Rouziere (Orsay/FR), T. Hughs (Chilton/GB), Y. Zhang (Chilton/GB)

Introduction: Deep eutectic solvents (DES) provide alternative physicochemical properties and replacements for solvents in a range of scenarios. Here we investigate the structure of a mixture of 1:3 proline and glycerol which is used to replace water during the cryopreservation of biological cells. The mixture avoids the detrimental expansion of water during freezing and shows enhanced viability of cells.[1]

Objectives: The H-bond network structure of the DES is an important consideration to preserve the activity of tissue and avoid large volumetric changes during freezing. In this study we aim to characterize the network structure at 25oC. We will use this as a basis to understand the replacement of water during freezing/cryopreservation with a combined experimental/computation approach.

Materials & methods: The bulk solvent has been characterized by high resolution densitometry measurements to provide the packing density of proline and glycerol in a representative volume. The configuration of the molecules and the H-bonding network formed by the mixture has been elucidated from laboratory based X-ray scattering and neutron diffraction with isotopic substitution from the instrument SANDALS using the program DISSOLVE.

Results: We have determined partial structure factors of the binary mixture constrained by densitometry and diffraction measurements.

Conclusions: The model of packing of glycerol and proline into a representative volume is consistent with the perspective of glycerol as a H-bonding donor and proline as an acceptor.

Reference

[1] S.J. Bryant, M.N. Awad, A. Elbourne, A.J. Christofferson, A.V. Martin, N. Meftahi, C.J. Drummond, T.L. Greaves, G. Bryant, Deep eutectic solvents as cryoprotective agents for mammalian cells, Journal of Materials Chemistry B 10(24) (2022) 4546-4560.

PP-71

Sintered diamond and wBN alloy using a combination of shock and static high pressure

M. Araki (Handa/JP)

The sintering method for diamond grains was first reported by Bundy et al.1) However, residual cobalt within the diamond structure degrades its properties. A mixture of statically synthesized diamond and shock-synthesized wurtzite boron nitride (hereafter wBN) was sintered under static high pressure, using few intermetallic compound as a binder A similar approach has been used to produce diamond–cubic boron nitride (hereafter cBN) composites2 resulting compacts have been reported as universal cutting tools capable of machining ferrous alloys.

Experiment

A mixture of 74 wt% diamond, 18 wt% wBN, and 8 wt% TiAl3 was sintered under a pressure of 5.6 GPa, at a temperature of 1550 °C, for 2200 seconds. The average grain sizes of the diamond, wBN, and TiAl3 were 25, 5,and 5 μm respectively. The Knoop hardness (Hk) of the compact was measured 58.2 GPa (average of six points). Figure 1. Diamond–wBN sintered body views Figure 2. Optical microscope image

Discussion

While the measured hardness was satisfactory, some diamond grains were observed to have detached. Optimizing the dispersion of the binder may allow the formation of carbides or nitrides through reactions with the matrix, thus eliminating the presence of free metal. In this study, no transformation from wBN to cBN was observed. However, applying higher sintering pressure and temperature may yield a significantly harder structure.

References

[1] F.P.Bundy et. al. Carbon Vol.34, No.2 pp141, 1996

[2] Pei Wang et. al. Appl. Phy. Let. 107, 101901 (2015); doi:10.1063/1.4929728

[3] T.Akashi et. al. The Chemical Society of Japan pp1416, (9) in Japanese

Fig. 1

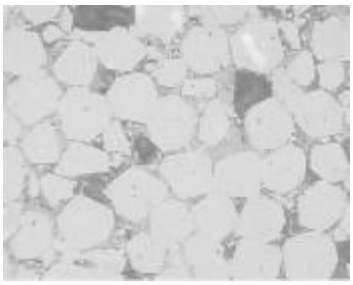

Fig. 2

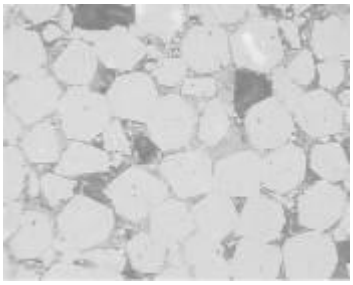

PP-91

Advancing PDF Analysis: Fast and High-Quality Local Structure Insights with XRDynamic 500

Marius Kremer (Graz / AT), Tom Faske, Praveen Vir, Benedikt Schrode

Pair distribution function (PDF) analysis is a powerful technique for investigating the local structure of materials, regardless of their state—crystalline, amorphous, or liquid. It provides critical insights into how atoms or molecules are arranged at the atomic scale.

PDF measurements are typically performed at synchrotron facilities, which offer rapid data collection. In contrast, conventional laboratory X-ray diffractometers (XRD) require significantly longer acquisition times to achieve comparable results. However, Anton Paar's XRDynamic 500 overcomes this limitation with cutting-edge hardware automation, enabling faster measurements without compromising data quality. A key factor in accelerating PDF data acquisition is the use of high-quantum-efficiency detectors optimized for hard X-ray radiation, such as Mo or Ag Kα sources. For instance, just one hour of measurement on the XRDynamic 500 can produce high-quality PDF data from a quartz sample.

In this presentation, we will showcase Anton Paar's state-of-the-art solutions for PDF analysis, introduce groundbreaking hardware advancements, and highlight real-world application examples that push the boundaries of what's possible in PDF data acquisition.

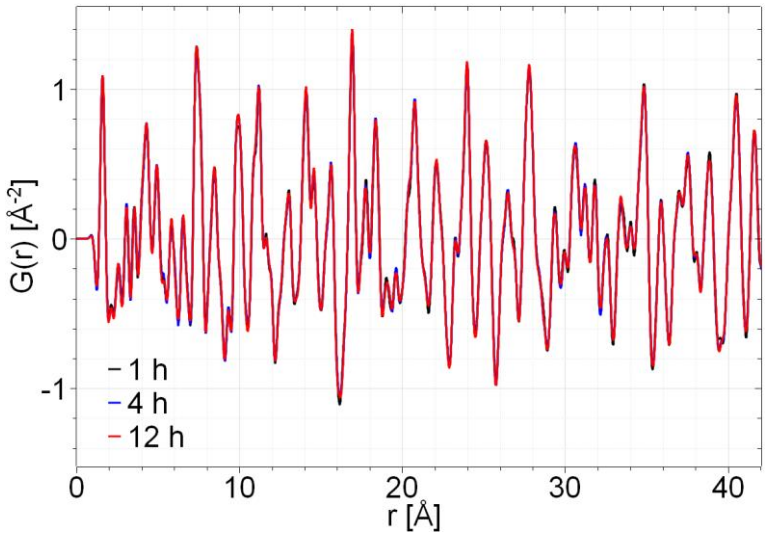

No abstract available / Talks cancelled:

LT-05 | PP-76, OP-37, KL-09, PP-21, PP-51